

https://dspace.org/

Waste to energy via the plasma gasification of biomass

Ncwane, Simphiwe

2022
https://hdl.handle.net/10539/34928

Downloaded from a DSpace repository. https://dspace.org/



UNIVERSITY OF THE
WITWATERSRAND,
JOHANNESBURG

WASTE TO ENERGY VIA THE PLASMA GASIFICATION OF BIOMASS

MSc Eng. (Chemical) by Research

Final Submission

Simphiwe Ncwane (832 359)

Master of Science in Engineering by research:
"A dissertation submitted to the Faculty of Engineering and Built Environment, University of the Witwatersrand, Johannesburg, in fulfilment of the requirements for the degree of Master of Science in Engineering.''

Supervised by

Dr Isabella L. Greeff and Dr Jaco van der Walt

August 2022

Declaration

I declare that this dissertation is my own unaided work. It is being submitted for a Degree of Master of Science in Chemical Engineering to the University of the Witwatersrand, Johannesburg. It has not been submitted before for any degree or Examination to any other University.

S.F. Ncwane

Signature of Candidate

30 day of August year 2022

Acknowledgements

I would like to thank the Council for Scientific and Industrial Research (CSIR) for funding this project and for all the support they have provided. I thank Dr Isabella Greeff for all her guidance and support in the research period. For constantly pushing me and wanting nothing but the best out of me. Dr Jaco van der Walt for all the input and data he injected into this project. My family for all the emotional support and encouragement they have given me over the years throughout this difficult journey.

Finally, I would like to thank the University of the Witwatersrand, School of Chemical and Metallurgical Engineering for allowing me to use their facilities.

Synopsis

The plasma gasification reactor was considered for the thermal reforming of biomass and organic feedstock in the production of electricity and biofuels. The presence of a plasma torch, a highly reliable heat source, makes the process substantially effective in the production of synthesis gas with low quantities of impurities. In small scale applications of the plasma gasification process, the content of impurities is so low that the cleaning process of the synthesis gas does not even have to be as rigorous. With process simulation software such as Aspen Plus, a small-scale plasma gasification process aimed at generating electricity can be easily investigated and this is what was done in this research study.

In this research study, Aspen Plus models for the plasma gasification reactor and power cycles were presented in the exploration of a small-scale system, aimed at assessing the feasibility of electricity generation. The nature of the model for the plasma gasification reactor aims to understand the equilibrium behaviour of this process, with one biomass feedstock and thereafter replicating this for other biomass and organic feedstocks. The small-scale nature of the plasma gasification reactor through a 20 kW plasma torch was the point of focus for this study. Understanding the small-scale behaviour of the plasma gasification reactor can assist in the advancements of this technology for electricity generation on larger scales. Advancements can be brought about by understanding every facet of the plasma gasification reactor and finding ways of improving the thermodynamic performance. An energy analysis performed on this model of the plasma gasification reactor would help in understanding the flow of heat through this reactor and the percentage of the heat dedicated to the reforming of biomass.

On the power cycle side of the project, there was an investigation to assess the feasibility of small-scale power cycles in generating electricity, and the use of synthesis gas as compared to conventional fossil fuels such as natural gas and coal. The power cycles of focus in this research study were, i) the Brayton power cycle, ii) the Rankine power cycle and iii) the combined power cycle. With the power cycles, there was a number of different configurations in their arrangement which are explored in this project. The different configurations explored for the power cycles, assist in understanding how the thermal efficiency for the overall process can be improved. The changes in the configuration of the power cycles were centred on different aspects such as a varying number of expansion stages, different pre-treatment processes for the hot synthesis gas effluent of the plasma gasification reactor and incorporation of waste heat

recovery mechanisms. The thermodynamic performance of these power cycles was analysed through the 1st and 2nd laws of thermodynamics i.e., energy and exergy analysis.

In developing a model for the plasma gasification reactor, firstly literature data was used to develop a base case model, thereafter this model was consolidated with data from a NECSA demonstration plasma gasification reactor plant model. There are some correlations between the composition of the synthesis gas generated by the current model and that from the plant's models. There are some slight deviations associated with the differing equilibrium behaviours between the NECSA model and the model for this study. The Gibbs free energy minimization approach is followed in modelling the plasma gasification reactor. The Gibbs free energy minimization approach presents a broader view of the equilibrium behaviour of the reactor model and can be used in the development of any reactor. The kinetic modelling approach on the other hand presents the thermodynamic behaviour of a particular reactor, with the design of that reactor being critical.

After the simulation of the plasma gasification reactor model, the thermal efficiency of the reactor was calculated to be 67%, which is within the range of typical efficiencies for commercial gasification reactor systems. The thermal efficiency in this case was defined by the cold gas efficiency, which analyses the amount of heat input to the process which goes towards reforming the feedstock into the synthesis gas product. This thermal efficiency indicated that this reactor model successfully converted biomass into synthesis gas. The generated synthesis gas had a good calorific value and could present opportunities for use in power cycles for the generation of electricity.

In the models developed for the Brayton cycle, there was a number of findings made, with the simple Brayton cycle model being the least effective in producing power from synthesis gas. This model designated as **Case 3b** achieved a thermal efficiency of 22.05% which was far below that of a typical commercial gas turbine at 33.3%. A better performing model was that of the direct fired synthesis gas power cycle without any prior pre-treatment, **Case 3c**. This cycle achieved a thermal efficiency of 27.89% and a net power output of 5.77 kW, which was a significant improvement from that of **Case 3b** at 0.22 kW. Critical findings for the Brayton cycle case studies were that the models which integrated the sensible heat from the hot synthesis gas effluent into the power cycle, tend to have higher thermal efficiencies and power production capabilities. The models for the Brayton power cycle were all severely underperforming as none of them reached the benchmark commercial efficiency of 33.3%,

meaning that small scale production of electricity using the Brayton cycle might not be the best option.

For the Rankine cycle models, **Case 4b** which was the simple Rankine cycle achieved a thermal efficiency of 36.39%, while producing a net power output of 7.53 kW. This was well within the typical commercial thermal efficiency of 36–40% for steam turbines, proving the effectiveness of the steam turbine model in generating power. The model for a directly fired hot synthesis gas without any quenching and cleaning, **Case 4c** achieved a similar thermal efficiency of 36.39% while generating a net power output of 12.1kW. The comparison of **Case 4c** to **Case 4b** indicated that the simple Rankine cycle outperformed the modified version of this power cycle. The best performing cycle was **Case 4f**, which is a two-stage expansion steam turbine system achieving a thermal efficiency of 37.66% and a net power output of 8.62 kW. The use of steam turbines for the generation of electricity is thermodynamically feasible and the only problem might be with the investment costs of small-scale steam turbines.

For the combined power cycle models, **Case 5b** the simple combined power cycle model achieved a thermal efficiency of 37.08% and generated a net power output of 14.5 kW. The thermal efficiency for the combined power cycle was far below the typical thermal efficiency for a commercial system at 50–60%. **Case 5d** involving the direct firing of the synthesis gas in the power cycle without quenching or cleaning achieved a thermal efficiency of 44.14% and generated a net power output of 20.64 kW. Some improvements were noted in the combined cycle when compared to the Brayton cycle, showing the effectiveness of the waste heat recovery system through the bottoming Rankine cycle. Even though the thermal efficiencies were below the commercial standard for these models, the combined power cycle shown power generating potential as **Case 5d** generated a net power output of 20.64 kW which was 33% of the total power generated.

All of these case studies for the different power cycles were using a similar fuel source which was synthesis gas at a mass flowrate of 30.862 kg/hr. An energy analysis of all of these case studies indicated that the combined power cycle had the best heat to power conversion. The effectiveness of the combined power cycles relied on the use of two different turbine systems using a single fuel source. Between the small-scale gas and steam turbine, the latter had a better heat to power conversion and had a thermodynamic behaviour in accordance to commercial systems.

The exergy analysis performed on selected case studies of the Brayton cycle, Rankine cycle and combined cycle, indicated that the combustion chamber case studies had the highest exergy destruction rates of 150−154 kW. There was a slight variation in the exergy destruction rates in between the case studies, however they are all the highest. The boiler case studies closely followed with exergy destruction rates of 130−150 kW. The boiler was noted to have a better combustion mechanism and heat transfer regimen when compared to the combustion chamber as shown by the exergy destruction rates. The HRSG in the case of combined cycle case studies had the second highest exergy destruction rates of 13−18 kW. The quench probe, however presented the biggest challenge with an exergy destruction rate of 8.21 kW. Considering the scale of operation for the quench probe compared to the other process units with high exergy destruction rates, some improvements can be made to the quench probe's operation.

The recommendation for a project of this nature was that it could be applied through a co-generation system, which could be used in a hospital for the generation of power and steam. With this system a small amount of power can be generated for the less energy intensive activities such as lighting. The waste heat can be used to generate steam which is required for a number of different operations in a hospital such as sterilization of surgical equipment and rooms. Another alternative would be an increase of the scale of the process for better power production.

Table of Contents

Declaration i
Acknowledgements ii
Synopsis iii
List of Figures x
List of Tables xiii
Nomenclature xvi
Chapter 1 Introduction 1-1
1.1 Background 1-1
1.2 Motivation 1-6
1.3 Problem Statement 1-8
1.4 Hypothesis 1-8
1.5 Aim 1-8
1.6 Objectives 1-8
1.7 Structure 1-9
1.8 References 1-9
Chapter 2 Literature Review 2-1
2.1 Introduction 2-1
2.2 Fossil Fuel Based Energy Production 2-1
2.3 Biomass Feedstocks and Beneficiation Processes 2-4
2.3.1 Lignocellulose Biomass 2-5
2.3.2 Other Waste Feedstock 2-6
2.3.3 Advantages and Disadvantages of Biomass for Energy Production 2-10
2.3.4 Waste and Biomass Preparation 2-13
2.4 Pyrolysis and Gasification 2-15
2.5 Plasma Gasification 2-17
2.6 Syngas Quenching System and Heat Recovery System 2-22
2.7 Syngas Cleaning Process 2-25
2.8 Pressurized Gasification Reactors 2-26
2.9 Power Generation 2-28
2.9.1 Open Brayton Cycle 2-28
2.9.2 Steam Rankine Cycle 2-30
2.9.3 Combined Power Cycle 2-31
2.9.4 Waste Heat Recovery 2-33
2.10 Small Scale Power Production Systems 2-34

2.11 Industrial Scale Plasma Gasification Reactor 2-36
2.12 Aspen Plus Modelling 2-36
2.13 References 2-38
Chapter 3 Methodology 3-1
3.1 Introduction 3-1
3.2 Plasma Gasification Reactor 3-1
3.2.1 Assumptions 3-1
3.2.2 Flowsheet Description of the Demonstration Unit 3-2
3.2.3 Plasma Gasification Reactor 3-3
3.2.4 Plasma Gasification Reactor Aspen plus Model 3-6
3.2.5 Hypothetical Pressurized Plasma Gasification Reactor 3-7
3.2.6 Synthesis Gas Pre-treatment Process 3-7
3.2.7 Biomass Characteristics and Reactor Specifications 3-8
3.3 Power Cycles 3-10
3.3.1 Assumptions 3-10
3.3.2 Process Flowsheet Development 3-10
3.3.3 Flowsheet Modelling and Analysis 3-16
3.4 Energy Analysis 3-26
3.5 Exergy Analysis 3-28
3.6 Economic Analysis 3-31
3.7 References 3-32
Chapter 4 Results and Discussion 4-1
4.1 Introduction 4-1
4.2 Model Validation 4-1
4.3 Energy Balance 4-4
4.3.1 Brayton Cycle 4-4
4.3.2 Rankine Cycle 4-9
4.3.3 Combined Power Cycle 4-15
4.3.4 Real Synthesis Gas Composition from the NECSA Reactor 4-19
4.4 Sensitivity Analysis of the Experimental Synthesis Gas Turbine 4-21
4.5 Exergy Analysis 4-23
4.6 Economic Analysis 4-29
4.7 Co-generation System Producing Steam for a Hospital 4-30
4.8 References 4-34
Chapter 5 Recommendations and Conclusion 5-1

5.1 Recommendations 5-1
5.2 Conclusion 5-1
5.3 References 5-3
Appendix 1
Appendix A.1 Plasma Gasification Reactor 1
Appendix A.2 Power cycle Models and Mass Balance 8
Appendix A.2.1 Brayton cycle Mass Balance 8
Appendix A.2.2 Rankine cycle Mass Balance 19
Appendix A.2.3 Combined power cycle Mass balance 31
Appendix A.2.4 Brayton cycle for the experimental synthesis gas results 44
Appendix A.3 Energy Analysis 46
Appendix A.3.1 Brayton cycle Energy Balance 46
Appendix A.3.2 Rankine cycle Energy balance 47
Appendix A.3.3 Combined power cycle energy balance 47
Appendix A.3.4 Brayton cycle for the experimental synthesis gas product 49
Appendix A.4 Exergy Analysis 49
Appendix A.5 Alternative Power cycles 61
Appendix A.5.1 co-generation cycle 61

List of Figures

Figure 2-1: Fossil Fuel Usage per Capita (Ritchie & Roser, 2020) 2-2
Figure 2-2: Breakdown of energy consumption in South Africa (Ritchie & Roser, 2020) ... 2-3
Figure 2-3: Summary of waste production in South Africa from 2018 (Department of Environmental Affairs, 2018). 2-7
Figure 2-4: Classification of hazardous waste 2-10
Figure 2-5: Carbon cycle 2-12
Figure 2-6: PFD of plasma gasification process 2-18
Figure 2-7: Block diagram of the biomass power generation system 2-21
Figure 2-8: Turbine expander power production mechanism 2-24
Figure 2-9: Direct synthesis gas firing power production mechanism 2-25
Figure 2-10: Brayton cycle process mass, heat and power flow system 2-29
Figure 2-11: Rankine cycle process mass, heat and power flow system 2-30
Figure 2-12: Combined power cycle process mass, heat and power flow system 2-32
Figure 3-1: Plasma Gasification Demonstration Plant Diagram (Ncwane, et al., 2021) 3-2
Figure 3-2: Theoretical Plasma Gasification Reactor Model (Minutillo, et al., 2009) 3-4
Figure 3-3: Consolidated Plasma Gasification Reactor Model 3-6
Figure 3-4: Hypothetical Pressurized Plasma Gasification Reactor 3-7
Figure 3-5: Pre-treatment Phase of the Synthesis Gas 3-8
Figure 3-6: Brayton Cycle (Moran & Shapiro, 2006) 3-11
Figure 3-7: Reheat Brayton Cycle 3-12
Figure 3-8: Steam Rankine Cycle 3-13
Figure 3-9: Reheat Rankine Cycle (Moran & Shapiro, 2006) 3-13
Figure 3-10: Combined Power Cycle 3-15
Figure 3-11: Syngas Preparation Section of the Model 3-17
Figure 3-12: Brayton Power Cycle Model 3-18
Figure 3-13: Turbine Expander and Preparation of the Syngas in Case 3d 3-19
Figure 3-14: Two-stage Expansion with Inter-heating in Case 3e 3-20
Figure 3-15: Syngas Preparation and Combustion Process in Rankine Cycle 3-22
Figure 3-16: Direct Syngas Feeding Rankine Cycle Process Without Preparation Stages . 3-22
Figure 3-17: Two-stage Expansion Process 3-23
Figure 3-18: Exergy Analysis Process System Boundary for the Brayton Power Cycle 3-28
Figure 3-19: Exergy Analysis Process System Boundaries for the Rankine Power Cycle . 3-29

Figure 3-20: Exergy Analysis Process System Boundaries for the Combined Power Cycle .. 3-30
Figure 4-1: Brayton cycle thermal efficiencies for the various cases 4-8
Figure 4-2: Rankine cycle thermal efficiency 4-11
Figure 4-3: Temperature Entropy Diagram for Case 4b 4-12
Figure 4-4: Temperature Entropy Diagram for Case 4c 4-13
Figure 4-5: Temperature Entropy Diagram for Case 4f 4-14
Figure 4-6: Temperature Entropy Diagram for Case 4e 4-15
Figure 4-7: Combined cycle thermal efficiency 4-17
Figure 4-8: Overall integrated plasma gasification combined cycle thermal efficiency 4-18
Figure 4-9: Pressure Ratio sensitivity analysis on the gas turbine at T=1 000 °C 4-22
Figure 4-10: Temperature sensitivity analysis on the gas turbine at P_{ratio}=15 4-22
Figure 4-11: Brayton cycle and steam co-generation model 4-32
Figure A-1: NECSA Demonstration Plasma Gasification Reactor Plant Model 1
Figure A-2: Aspen Plus model flow diagram for the Minutillo (2009) reactor validation case 4
Figure A-3: Plasma Gasification Reactor Model 6
Figure A-4: Aspen Plus model flow diagram for Case 3a 8
Figure A-5: Aspen Plus model flow diagram for Case 3b 10
Figure A-6: Aspen Plus model flow diagram for Case 3c 12
Figure A-7: Aspen Plus model flow diagram for Case 3d 14
Figure A-8: Aspen Plus Flow diagram for Case 3e 16
Figure A-9: Aspen Plus Flow diagram for Case 3f 18
Figure A-10: Aspen Plus model flow diagram for Case 4a 20
Figure A-11: Aspen Plus model flow diagram for Case 4b 22
Figure A-12: Aspen Plus model Flow diagram for Case 4c 24
Figure A-13: Aspen Plus model flow diagram for Case 4d 26
Figure A-14: Aspen Plus model flow diagram for Case 4e 28
Figure A-15: Aspen Plus model flow diagram for Case 4f 30
Figure A-16: Aspen Plus model flow diagram for Case 5a 32
Figure A-17: Aspen Plus model flow diagram for Case 5b 34
Figure A-18: Aspen Plus model flow diagram for Case 5c 36
Figure A-19: Aspen Plus model flow diagram for Case 5d 38
Figure A-20: Aspen Plus model flow diagram for case 5e 40

Figure A-21: Aspen Plus model flow diagram for Case 5f 42
Figure A-22: Brayton cycle model processing the experimental synthesis gas from the demonstration plant 44
Figure A-23: Exergy analysis boundary for the gas turbine 50
Figure A-24: Exergy analysis boundary for the steam turbine 53
Figure A-25: Exergy analysis boundary for the combined power cycle 57
Figure A-26: Aspen Plus Model Flow Diagram for the co-generation cycle 62

List of Tables

Table 2-1: Reactions in a pyrolysis and gasification process 2-17
Table 3-1: Biomass Feedstock Properties 3-9
Table 3-2: Experimental Data for the Plasma Gasification Reactor Demonstration Plant 3-9
Table 3-3: Process Descriptions for the Open Brayton Cycle Cases 3-17
Table 3-4: Process Description for the Rankine Cycle Cases 3-21
Table 3-5: Process Description for the Combined Power Cycle Cases 3-24
Table 3-6: Process Operating Conditions 3-25
Table 4-1: Plasma gasification model operational assumptions 4-2
Table 4-2: Syngas model validation results 4-2
Table 4-3: Demonstration Model Results Validation 4-3
Table 4-4: Cold Gas Efficiency 4-4
Table 4-5: Gas Turbine cases Energy Balances 4-5
Table 4-6: Air to Fuel Ratio for the Gas Turbine Case studies 4-6
Table 4-7: Steam Turbine cases energy balances 4-10
Table 4-8: Lower Heating Value Efficiencies of Case 4b and Case 4c 4-13
Table 4-9: Combined Power cycle cases energy balances 4-16
Table 4-10: Experimental synthesis gas composition 4-20
Table 4-11: Energy Analysis of the gas turbine 4-20
Table 4-12: Air to Fuel Ratio 4-21
Table 4-13: Brayton cycle exergy analysis for case 3b and case 3c 4-24
Table 4-14: Rankine cycle exergy analysis for case 4b and case 4c 4-25
Table 4-15: Combined Power cycle exergy analysis for Case 5b and Case 5d 4-25
Table 4-16: Exergy Analysis for an externally heated combined power cycle 4-27
Table 4-17: Quench Probe exergy analysis 4-28
Table 4-18: Small scale gas turbine cost calculations 4-29
Table 4-19: United States CPI 4-29
Table 4-20: Operational Maintenance Cost of Small-scale gas turbine 4-30
Table 4-21: Power balance for the co-generation cycle 4-33
Table A-1: Mass Balance for the demonstration plasma gasification plant model 2
Table A-2: Mass Balance for the Minutillo (2009) reactor validation case 5
Table A-3: Mass balance for the plasma gasification Reactor Model 7
Table A-4: Mass balance for Case 3a 9
Table A-5: Mass balance for Case 3b 11

Table A-6: Mass balance for Case 3c 13
Table A-7: Mass balance for Case 3d 15
Table A-8: Mass balance for Case 3e 17
Table A-9: Mass balance for Case 3f 19
Table A-10: Mass Balance for Case 4a 21
Table A-11: Mass balance for Case 4b 23
Table A-12: Mass balance for Case 4c 25
Table A-13: Mass Balance for Case 4d 27
Table A-14: Mass balance for Case 4e 29
Table A-15: Mass balance for Case 4f 31
Table A-16: Mass balance for Case 5a 33
Table A-17: Mass balance for Case 5b 35
Table A-18: Mass balance for Case 5c 37
Table A-19: Mass balance for Case 5d 39
Table A-20: Mass balance for Case 5e 41
Table A-21: Mass balance for Case 5f 43
Table A-22: Mass balance for the Brayton cycle model processing the experimental synthesis gas product 45
Table A-23: Brayton cycle energy balance for the various case studies 46
Table A-24: Rankine cycle energy balance for the various case studies 47
Table A-25: Combined power cycle energy balance for the various case studies 48
Table A-26: Energy balance for the Brayton cycle processing the experimental synthesis gas product 49
Table A-27: Atmospheric Specific molar exergy values 49
Table A-28: Exergy Analysis for the Model of Case 3b 50
Table A-29: Exergy Analysis for the synthesis gas quench probe 51
Table A-30: Combustion chamber chemical exergy analysis for Case 3b 51
Table A-31: Exergy Analysis for the model of Case 3c 52
Table A-32: Combustion chamber chemical exergy analysis for Case 3c 52
Table A-33: Exergy analysis for the model of Case 4b 53
Table A-34: Boiler exergy analysis for the model of Case 4b 53
Table A-35: Combustion chamber chemical exergy analysis for Case 4b 54
Table A-36: Exergy analysis for the model of Case 4c 55
Table A-37: Boiler exergy analysis for the model of Case 4c 55

Table A-38: Combustion chamber chemical exergy analysis for Case 4c 56
Table A-39: Exergy analysis for Case 5b 58
Table A-40: Exergy Analysis for the pump of Case 5b 58
Table A-41: Exergy Analysis for the HRSG of Case 5b 58
Table A-42: Combustion chamber chemical exergy analysis for Case 5b 59
Table A-43: Exergy Analysis for the combustion chamber of Case 5b 59
Table A-44: Exergy Analysis for Case 5d 60
Table A-45: Exergy Analysis for the HRSG of Case 5d 60
Table A-46: Combustion chamber chemical exergy analysis for Case 5d 61
Table A-47: Mass balance for the co-generation power cycle 63

Nomenclature

Nomenclature

A	– activity	out	– Outlet
C_p	– Specific heat, kJ/(kg·°C) or kJ/(kg·K)	net	– Balance value
e	– Specific exergy, kJ/kg	j	– Control volume boundary
E_d	– Exergy destruction, kJ/hr	cv	– Control Volume
E_i	– Exergy Input, kJ/hr	d	– destruction
E_o	– Exergy Output, kJ/hr	i	– inlet
ε_{chem}	– Specific chemical exergy, kJ/kmol	e	– exit
H	– Enthalpy, kJ/kmol or kJ/kg	mix	– mixture
M	– Mass flowrate, kg/hr	chem	– Chemical
N	– Molar flowrate, kmol/hr		
P	– Pressure, kPa or bar	**Abbreviations**	
Q	– Heat flow, kJ/s or kW	C.E	– Chemical Exergy
s	– entropy, kJ	CGE	– Cold Gas Efficiency
T	– Temperature, °C or K	CW	– Cooling Water
		HRSG	– Heat Recovery Steam
W	– Work, kW or kJ/s		Generator
X	– Molar fraction	HTR	– High Temperature Region
		IGCC	– Integrated Gasification
η	– Efficiency, %		Combined Cycle
η_{CGE}	– Cold Gas Efficiency, %		
η_{LHV}	– Efficiency (Lower Heating Value Energy basis)	IPGCC	– Integrated Plasma Gasification Combined Cycle
		LHV	– Lower Heating Value
Subscripts		LTR	– Low Temperature Region
		NECSA	– Nuclear Energy
0-9	– Character Points		Corporation of South Africa
in	– Inlet	ORC	– Organic Rankine cycle
		P. E	– Physical Exergy
		REIPPPP	– Renewable Energy Independent Power Producer Procurement Programme

Chapter 1 Introduction

1.1 Background

With the inception of the annual Conference of Parties (COP) international treaty, a general shift in the production of electricity using fossil fuels to renewable energy was initiated. Most of the developed countries have managed to successfully adopt renewable energy sources into their energy production sector, whilst for the African continent, there has been a slow application of renewable energy resources. It is estimated that by 2030 only 10 % of electricity will be coming from renewable energy sources, excluding hydro power, with fossil fuel-based energy sources still dominating the energy sector (McGrath, 2021). Solar has been the most dominantly applied form of renewable energy, with its application span ranging from regular household to the industrial sector. South Africa is the biggest solar market in the African continent, with an installed solar PV capacity of 2.5 GW (Hendriks, 2020).

The rising interest in renewable energy has opened the market for biomass, and organic feedstock such as municipal solid waste (MSW) as potential fuels in the production of power and biofuels. There is a large availability of biomass globally and this includes wood, and wood waste, municipal solid waste, forestry, agricultural and livestock waste (Ahmad, et al., 2016 & Shahabuddin, et al., 2020). The potential use of biomass as a renewable source of energy has broadened the scale of available biomass resources beyond just woody material, but waste generated from the various economic sectors. Biomass is not only plant and animal matter generated in the various industries such as forestry, agricultural and animal waste industries, but also waste generated amongst households and the commercial sectors.

Waste landfilled in various sites across South Africa has been viewed as a potential fuel source due to the shortage of land space and the energy value it possesses. In South Africa about 108 million tonnes of waste is generated and 59 million of this comes from Gauteng, which is running out of landfilling space, and it is estimated that by 2022 there will be no landfilling space available (Dada & Mbohwa, 2016). Waste generated in South Africa as of 2016 had an estimated monetary value of R17 billion which is why it cannot just be destroyed, means of generating monetary revenue from this waste must be discovered (Dada & Mbohwa, 2016). Although there are numerous ways of handling waste such as thermochemical treatment and biochemical digestion, landfilling has been the most convenient waste management technique.

In an African perspective, an interesting example of waste to energy biofuels is the successful application of a Kenyan plant using biogas. This plant is known to produce electricity, and the supply of heat required by the farmers for their greenhouses in the predominantly farming area where this project was initiated (Kamadi, 2021). The biogas plant is in the Gorge Farm Energy Park in Naivasha Kenya with a power production capability of 2 MW, which is enough for the cultivation of the crops on the farm (about 706 hectares), and to supply about 5 000 – 6 000 rural households with electricity (Kamadi, 2021). In South Africa, the introduction of biomass driven power plants has been slow through the initiative in the Ngodwana Energy Biomass Project which is expected to produce 25 MW of power under the South African Renewable Energy Independent Power Producer Procurement Programme (REIPPPP) (Stephens-Borg, 2018). With construction of the project having begun in April of 2018, the expectation was for the construction of the project to be complete in 27 months, however the project is still under construction towards the end of 2021.

Developments in thermochemical processes have altered the use of biomass for primitive reasons, such as cooking and heat provision, to more ground-breaking systems aimed at a more efficient use of the heat value present in the biomass. Through the thermochemical treatment of biomass, the organic matter in the waste has the potential to be reformed into a synthesis gas that is more convenient for use in the energy sector. This synthesis gas product is a mixture of mainly H_2 and CO, along with other small quantities of gases such as CH_4, CO_2, H_2O, and other chlorine and sulphur impurities. The synthesis gas can be applied for a whole lot of different uses such as the provision of biofuels, and the generation of electricity in large scale applications. The thermochemical treatment of the biomass will be investigated in this study, more specifically the plasma gasification of the biomass.

Thermochemical treatment of the waste involves processes such as torrefaction, incineration, pyrolysis, gasification and plasma gasification for the enhancement of the organic matter in the biomass, and other organic feedstocks. The high temperatures at which these processes occur ensures the thermal decomposition of the biomass, and the reactions responsible for the formation of the synthesis gas product. Biomass has been noted to begin the disintegration process at temperatures of 200°C and upwards (Okoroigwe, et al., 2016). The high operational temperature of the reactor for these different processes ensures the good compositional quality of the synthesis gas formed. Some of the factors that influence the quality of the synthesis gas produced include the types of feedstocks and their fuel value, the moisture content, the plasma

gas or oxidising agent in gasification reactors and the temperature of the heat from the plasma torch into the process (Shahabuddin, et al., 2020).

Plasma gasification is the stoichiometric combustion of organic matter at high temperatures (>1000°C) to produce a synthesis gas product, with the inclusion of plasma technology for the provision of heat required by the process. A large amount of energy is required for the gasification reaction due to the endothermic nature of the reaction and the addition of the plasma gas through the plasma torch has been found to successfully provide the required heat to maintain the reaction. The integration of plasma technologies into the gasification reactor offers several operational advantages such as the improvement of the synthesis gas concentration. With the inclusion of plasma technologies to the gasification process an improvement of the carbon conversion efficiency from 50% to 100% has been noted (Muvhiiwa, et al., 2018). The plasma technology does however require substantial amounts of electricity and in IPGCC power production processes a substantial amount of the power produced is used by the plasma torch (Shahabuddin, et al., 2020).

The energy demand of the plasma torch system has a negative impact on the thermodynamic performance of the plasma gasification reactor and the cold gas efficiency of the plasma gasification reactors. The higher energy demand results in lower efficiencies of the plasma gasification reactors when compared to conventional thermal gasification reactors. The cold gas efficiency is defined as the ratio of the heat energy output of the reactor to the heat energy input of the reactor. The heat energy output comprises of the potential heat energy stored in the produced synthesis gas. The heat energy input consists of the potential heat energy of the biomass and the heat generated by the plasma torch. There is no way of working around this high energy demand of the plasma torch, thus other processes in the plant must be optimized to operate at better conditions to improve the overall thermal efficiency.

The plasma gasification of biomass and organic feedstocks has achieved the potential of these feedstocks being fuel sources for electricity generation, due to the quality of the synthesis gas produced from this process. The use of waste in these plasma gasification processes has other benefits besides the production of electricity such as a reduction of the waste volume in landfills, reduction in the emission of toxins associated with the combustion of fossil fuels, preservation of land for more important purposes and prevents pollution of the soil which can contaminate underground water sources (Hameed, et al., 2021). The plasma gasification

process can change the act of landfilling waste from a long-term solution to rather a short-term solution for the pre-treatment of waste before being fed into the reactors.

This study will be based on results from a demonstration plasma gasification reactor plant mass and energy balances by the Nuclear Energy Corporation of South Africa (NECSA). The data provided was based on using wood chips as a feedstock, but the plant can generate synthesis gas from a range of other organic feedstocks such as municipal solid waste and refuse derived fuel. This plant uses a nitrogen plasma torch which is highly efficient when compared to the other plasma torches. The differentiating factor for the nitrogen plasma torch is the power consumption which is much lower than that of a steam, argon, or air plasma torch (Agon, et al., 2016). A steam plasma used by Agon et al, (2016) can be noted to have a power consumption of 120 kW for a mass capacity of 29 kg/hr, while the model for the demonstration plant uses a plasma torch with a power consumption of 20 kW for a mass capacity of 20 kg/hr. The design of the plasma gasification demonstration plant supports its adaptability as it is a mobile unit and can thus be used in a range of settings using different biomass and organic feedstocks. For instance, it can be used to process waste from a landfill, waste from a hospital or biomass from remote locations in the event of land clearing.

This project involved the development of an Aspen Plus model for a small-scale plasma gasification reactor system in conjunction with data received from the demonstration reactor plant model developed at NECSA. There have been other small gasification systems which have been successfully applied for use in rural areas as means of electrification, as proven in a study by Indrawan, et al. (2020) investigating the economic possibilities of using a 60 kW downdraft gasifier coupled to an internal combustion engine for the provision of electricity in a rural environment. The application of the downdraft gasifier coupled to the internal combustion engine was found to be extremely economical for application in a rural setting, as a payback period of 7.7 years is found, while the internal rate of return, modified internal rate of return and net present value are found to be 10.9%, 7.7% and $84 550, respectively. In terms of the economic success of this biomass gasification process for electricity generation in any area, the local economy and technological advancements in that country, city or town play a crucial role (Indrawan, et al., 2020). The success of this electricity generation process should be assessed on a case-by-case basis rather than a universal measure with all variables considered.

In the world currently there is a lot more focus on large scale operations of processes for economic reasons, with the industrial revolution built around the large-scale operation of processes. Small scale operations can however be the building block to much larger operations, as they are easier to manage, lower cost to maintain and can help in understanding how production can be pushed to larger scales. With the plasma gasification reactor, operations through small scale offers the advantage of mobility, which can assist in testing the thermodynamic capability of this system at different conditions i.e., using biomass in different locations, developing a power generation system that can be moved around as per demand. This is proven by the 20 kW nitrogen plasma torch gasification reactor at NECSA which has been designed to fit into a container. The nitrogen plasma torch can achieve much higher temperatures when compared to other plasma torches since less heat is required to heat up N_2 compared to air, steam or argon.

In the operation of a gas turbine powered system integrated with the plasma gasification process, depending on the quality of the synthesis gas fuel produced, the combustion mechanism (internal or external) is a potentially far-reaching factor in the power generation capacity and thermodynamic performance for the power cycles. The clean-up process to ensure the synthesis gas is suitable for firing in an internal combustion gas turbine can be eliminated by incorporation of externally fired gas turbines. The gas turbines with internal combustion have the thermodynamic advantage of achieving much higher thermal efficiencies than the externally fired gas turbines and steam turbines. The inhibitor in the thermal performance of externally fired turbine systems is the transfer of heat between the combustion gas product and the working fluid of the power cycle, substantial irreversibility's occur during this process leading to the loss of heat quality. The internally combusted gas turbine uses the combustion gas product directly as the working fluid of the cycle and can extract work during the expansion process in the gas turbine at the maximum possible temperature.

The application of Brayton cycles and Rankine cycles in the generation of electricity using synthesis gas offers many possibilities. A couple of IGCC power production systems have been developed around the idea of a biomass gasification system coupled to a turbine system. The basic structure of the power generation system does not change, when burning synthesis gas versus natural gas. With synthesis gas having significantly lower LHV (Lower Heating Value) than coal and natural gas, the combustion process for the turbines is the most affected by a change in fuel type. Lower LHV significantly decreases the rate at which the combustion reaction progresses, meaning more synthesis gas will have to be fired for the same heat value

derived from natural gas (Axelsson, et al., 2014). In a similar amount of time, a gas turbine firing natural gas can generate a higher amount of power than the one firing synthesis gas. In the technical thermodynamic operations of the gas turbines, natural gas offers superior behaviours, however synthesis gas derived from biomass offers other advantages such as the lower compression power being required for the synthesis gas. The lower internal power demand by the synthesis gas turbine firing system ensures the thermodynamically feasibility of the process.

With the heat value from the synthesis gas being quite low, alternative means of deriving this heat value can be employed. A cycle such as the co-generation power cycle is a possibility. This cycle involves the effluent of the gas turbine being used to generate low pressure steam. This type of power cycle has been considered for application in hospital or clinic, where waste generate in the hospital could be treated through this system. The generated steam which has a heat value can be used for a number of different purposes in the hospital such as sterilization, humidification, heat and the provision of hot water in the taps. The power generated from this system can be used for other low power duty activities such as lighting and running computers. The potential of this type of technology can be fully achieved in this type of setting as the repurposing of the waste can be vital to the operation of an establishment of this nature. This process bears similarities to the biogas project in Kenya which supplies electricity and heat required by the farmers in their greenhouses. These types of power cycles tend to be more effective as they found multiple ways of using the heat value from the synthesis gas derived from biomass. In the small-scale capacities under investigation in this study, only generating electricity might not be the most effective application of such a technology.

For small scale synthesis gas driven systems there has been industrial application of power cycles such as gas turbines and steam turbines being used for electricity production. This project will aim to investigate the various power cycles that can be coupled to a small-scale plasma gasification system to produce electricity while exploring how the process and economic conditions can affect the feasibility of such an initiative.

1.2 Motivation

This project considered the plasma gasification of biomass through a small-scale reactor system and the potential for the generation of electricity from this system. The small plasma gasification reactor system provides a lot of advantages especially in an experimental study as different kinds of scenarios can be tested at minimal costs.

A smaller system is better to manage compared to a large system where one small defect on the process can have a ripple effect throughout the entire system. The evaluation of a small-scale plasma gasification reactor coupled to an energy generation system is the building block in how the technology can be applied in a larger scale or rather small units spread out over numerous locations for big energy users. With big energy users generating their own power, some of the municipalities can follow suit and have their own power generation facilities to reduce the strain on the national energy supplier. Energy decentralisation has been proven to reduce energy poverty as a result of more competition in the energy sector which makes it easy to regulate the electricity tariffs and creates transparency in the operational and financial aspect of these organisations (Lawrence, 2020).

The mathematical modelling of an energy production process in software packages such as Aspen Plus assists in developing a scope of how applicable any initiative can be in real life conditions. The results obtained can be correlated with those generated from real life systems and adjustments can be done accordingly for a clearer illustration. The flowsheet model development for the plasma gasification reactor along with the different power cycles i.e., gas turbines and steam turbine, can map the development of an actual energy generation system of this nature. With increases in scale clear outcomes must be defined for the successful application of the technology i.e., waste management, biofuels generation or electricity generation.

The City of Johannesburg in the Gauteng province of South Africa is a prime example of how the plasma gasification process can assist in developing a more efficient waste management system. The current waste management system not only in Johannesburg but the country is landfilling, which has certain restrictions with regards to land and it is projected that the landfill space in the City of Johannesburg is to be depleted by the end of the year 2022 (Dlamini, et al., 2019). With the city of Johannesburg contributing about 17% to the growth of the national economy, it is bound to generate a lot of waste due to the commercial activities and urbanisation as the citizens of the country seek employment opportunities and better standards of living (Dlamini, et al., 2019). To test the feasibility of applying plasma gasification technology in waste management, small scale plasma gasification system can be assessed using process simulation models. The proven success of the integrated plasma gasification combined cycle in places such as a Semarang, Indonesia for the treatment of waste in the Jatibarang landfill, supports the application in other landfills as waste in landfills tends to have striking similarities throughout the world.

1.3 Problem Statement

Plasma technology has been a marvel in the field of waste to energy in the reforming of the biomass and organic feedstocks, however the power requirements by the plasma torch have been a major disadvantage in the case of biomass being designated for power generation. This project will consider how much electricity can be generated through the plasma gasification of biomass and whether this is promising from a mostly thermodynamic and economic perspective.

1.4 Hypothesis

The goal for this research work involves testing the feasibility of a small-scale plasma gasification system towards the production of power. This plasma gasification system will be coupled to three different power systems such as a Brayton cycle, Rankine cycle and a combined power cycle. The expectation is that the plasma gasification system coupled to the combined power cycle will produce the most power at the best thermal efficiency. The implementation of waste heat recovery to system such as the Brayton cycle and Rankine cycle can be expected to improve their thermal performance.

1.5 Aim

The aim of the project was to assess the feasibility extent to which biomass can be reformed to produce electricity using plasma gasification and turbine technology.

1.6 Objectives

The objectives to be achieved for the development of this research project are as follows:

- Analyse literature to find the suitable thermodynamic properties that can be used in the development of the models for the plasma gasification reactor and power generation through power cycles using the Aspen plus software.
- Develop the models for the plasma gasification reactor and the power cycles i.e., Brayton cycles, Rankine cycles, combined cycles, externally fired cycles, co-generation cycles and other relevant power cycles.
- Consolidate the model for the plasma gasification reactor with data acquired from NECSA for the demonstration plasma gasification model.
- Organise the generated results and perform qualitative and quantitative analysis on these results through the first and second laws of thermodynamics (energy and exergy analysis)

- Perform an economic feasibility analysis into the availability of the power cycle equipment such as the small-scale gas turbines and small-scale steam turbines.
- Analyse different scenarios through which the plasma gasification technology aimed at power generation could be applied i.e., a gas turbine and steam production co-generation systems.

1.7 Structure

The dissertation comprises the following chapters:

- Chapter 1 is the introduction which presents a background into the work done and the motivation for why the work was done.
- Chapter 2 is a wide-ranging literature review through which influential literature on plasma gasification processes and power generation cycles are presented. The literature is set to cover mathematical modelling using the Aspen plus software and prominent work in the field of thermochemical processes and power generation.
- Chapter 3 deals with the methodology and is split over two sections being the plasma gasification plant and the power generation system section of the project. This chapter will present the procedure in the development of the model.
- Chapter 4 presents the results obtained and formulate a discussion into the significance of these results.
- Chapter 5 recommendations and conclusion presents ways in which the research could have been improved and a conclusion is drawn for the research project along with highlighting what has been achieved

1.8 References

Agon, N. et al., 2016. Plasma gasification of refuse derived fuel in a single-stage system using different gasifying agents. *Waste Management,* Volume 47, pp. 246 - 255.

Axelsson, L. U., Beran, M. & Bouten, T., 2014. *Technical challenges and opportunities for utilizing syngas in gas turbines,* Hengelo, Netherlands: OPRA Turbines.

Dada, O. R. & Mbohwa, C., 2016. *Municipal Solid Waste from Landfills a Solution to Energy Crisis in South Africa,* Auckland Park: City of Johannesburg.

Dlamini, S., Simatele, M. D. & Kubanza, N. S., 2019. Municipal solid waste management in South Africa: from waste to energy recovery through waste-to-energy technologies in Johannesburg. *Local Environment,* 24(3), pp. 249-257.

Hameed, Z. et al., 2021. Gasification of municipal solid waste blends with biomass for energy production and resources recovery: Current status, hybrid technologies and innovative prospects. *Renewable and Sustainable Energy Reviews 136 (2021) 110375,* Volume 136, pp. 1-18.

Hendriks, T., 2020. Op-ed: The future of solar energy in the South African context. *ESI AFRICA,* 06 October, p. Online.

Indrawan, N., Simkins, B., Kumar, A. & Huhnke, R. L., 2020. Economics of Distributed Power Generation via Gasification of Biomass and Municipal Solid Waste. *Energies,* 18 July, 13(3703), pp. 1-18 (Online).

Kamadi, G., 2021. Africa's first grid-connected biogas plant powers up. *Reuters,* 10 January, p. Online.

Lawrence, A., 2020. Energy decentralization in South Africa: Why past failure points to future success. *Renewable and Sustainable Energy Reviews 120 (2020) 109659,* 120(109659), pp. 1-8 (Online).

McGrath, M., 2021. Climate change: Africa's green energy transition 'unlikely' this decade. *BBC NEWS,* 11 January, p. Online.

Muvhiiwa, R. F., Sempuga, B., Hildebrandt, D. & Van der Walt, J., 2018. Study of the effects of temperature on syngas composition from pyrolysis of wood pellets using a nitrogen plasma torch reactor. *Journal of Analytical and Applied Pyrolysis,* 13 January, Volume 130, pp. 159-168.

Okoroigwe, E. C., Enibe, S. O. & Onyegegbu, S. O., 2016. Determination of oxidation characteristics and decomposition kinetics of some Nigerian biomass. *Journal of Energy in Southern Africa,* August, 27(3), pp. 39-49.

Shahabuddin, M. et al., 2020. A review on the production of renewable aviation fuels from the gasification of biomass and residual wastes. *Bioresource Technology 312 (2020) 123596,* 28 May, Volume 312, pp. 1-15 (Online).

Stephens-Borg, D., 2018. Progress for first biomass plant under South African energy scheme. *Bioenergy Insight,* 13 April, p. Online.

Chapter 2 Literature Review

2.1 Introduction

The focus of this dissertation is on the modelling of power generation systems based on a plasma gasification reactor aimed at assessing how thermodynamically feasible a small system could be in the production of electricity. A background into the application of biomass and organic feedstock for the purposes of producing electricity will be brought about in this review. This will serve as motivation for the small-scale plasma gasification in this research study and will show the vital need of such a project and the different sectors where it could apply depending on the scale.

Modelling of the plasma gasification reactor will be guided by experimental data acquired from NECSA for a demonstration DC arc plasma gasification reactor plant. The synthesis gas effluent to be generated from the plasma gasification reactor will be combusted through various power cycles such as gas turbines, steam turbines, and combined power cycle. The focus on the plasma gasification reactor will be on the various biomass feedstock that are available for use in the reactor, and the modelling of the reactor will be strongly influenced by the behaviour of the experimental plasma gasification reactor.

To better understand the different types of biomasses available in South Africa and the different types of processes through which the energetic value of the biomass can be enhanced, a literature survey is conducted. The literature survey will cover the different thermodynamic processes in the beneficiation of biomass and the technologies availability to acquire electricity from the synthesis gas produced through the biomass. More focus will be brought into the plasma gasification reactor as means of thermally reforming the biomass into synthesis gas. Beyond understanding the behaviour of the different thermochemical processes such as the plasma gasification process, techniques for the mathematical modelling of this process will also be explored.

2.2 Fossil Fuel Based Energy Production

Fossil fuel-based energy has been a dominant resource in the energy sector for centuries and was the driving factor in the industrialization of the world. For years facilities have been developed for harnessing the potential of these resources such as coal, oil and gas. These resources have been particularly fruit-full in the energy sector which has relied on them for years in the development of countries throughout the world. The electrification of the world

could not have been possible without the discovery of these resources and many countries throughout the world are still heavily invested in these resources. A lot of the infrastructure in the energy sector was built to use such resources as coal, oil and gas. Even as the world tries to adopt renewable energy resources to curb the toxic emissions associated with the use of fossil fuels, the reality is that most of the developing countries are far from implementing renewable energy as fossil fuels are the more realistic and convenient option at their disposal.

South Africa is amongst one of the developing countries that are heavily reliant and invested in fossil energy such as coal, with the coal still providing 77% of the country's electricity (Mdhluli & Harding, 2021). Although more developed countries have been applying renewable energy resources, more scrutinized research shows that they may still have a long way to go. The consumption of the three different energy resources is shown per capita in several developed and developing countries in **Figure 2-1**.

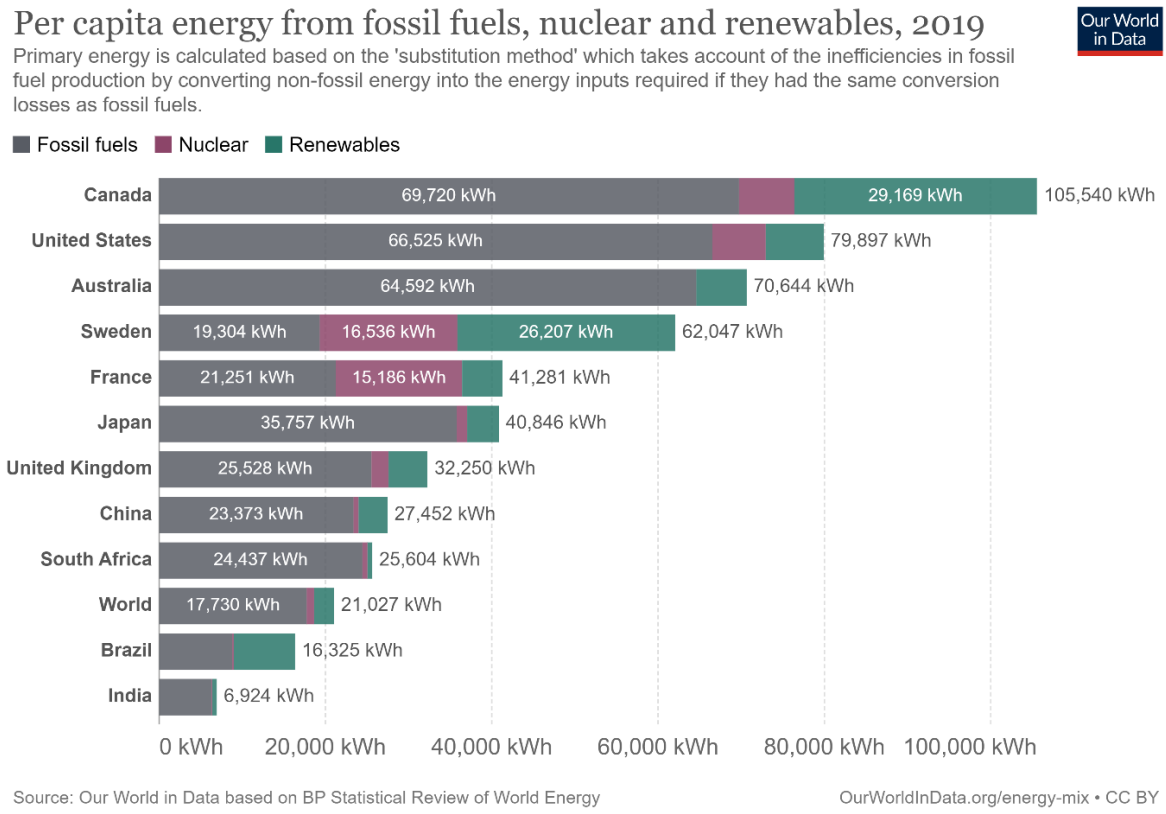


Figure 2-1: Fossil Fuel Usage per Capita (Ritchie & Roser, 2020)

It can be seen from **Figure 2-1** that more developed countries have a better per capita application of renewable energy resources than the developing countries, with Sweden having the healthiest balance between the application of fossil fuel, nuclear and renewable energy resources. South Africa is shown to have a huge dependency on fossil fuel energy resources,

with the per capita application of nuclear and renewable energy being less than 5%. Evaluation of the energy consumption in South Africa from the year 1965 to 2020 shows a better picture into the fossil fuel market of this country as seen in **Figure 2-2**.

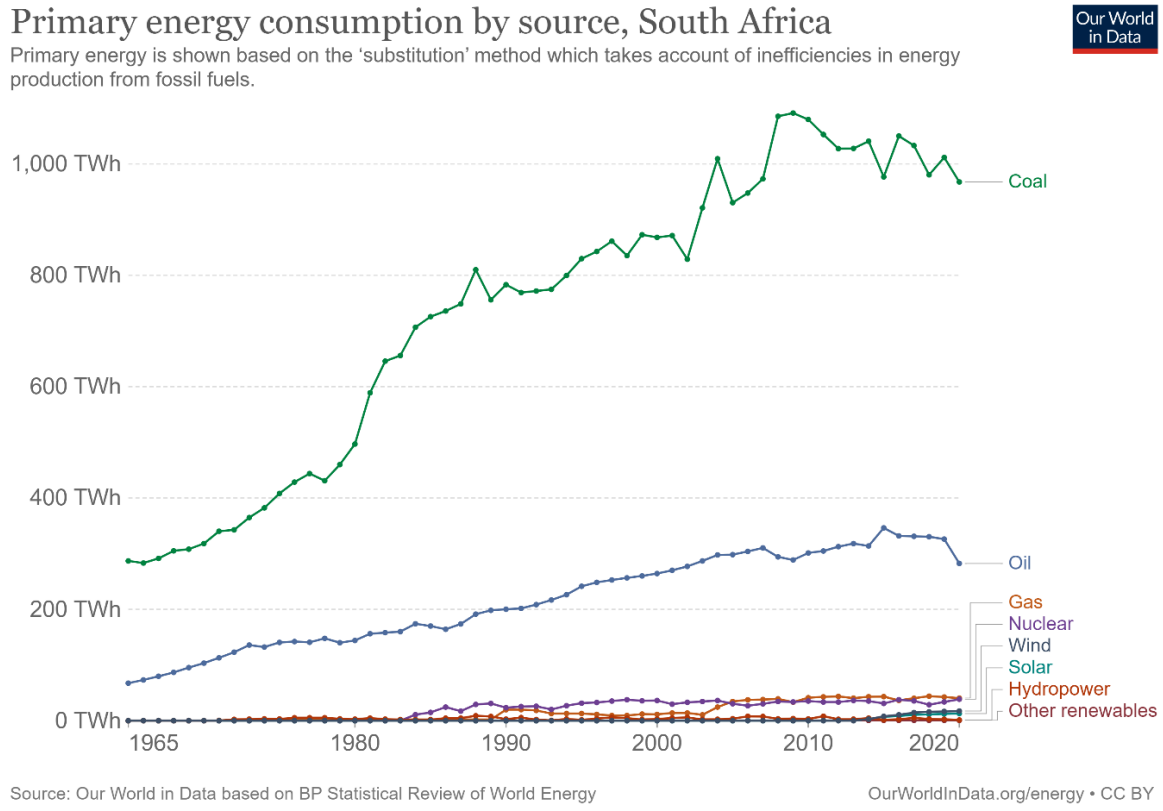


Figure 2-2: Breakdown of energy consumption in South Africa (Ritchie & Roser, 2020)

A minor spark in the solar slope shows that although the implementation process maybe slow, the South African energy market is responding better to the implementation of solar energy. The minor rise in solar and other renewable energy sources is due to the Renewable Energy Independent Power Producer Procurement Programme (REIPPPP) which has seen the government empower companies in the country to build power producing facilities using renewable energy resources such as solar, wind, biomass and other renewable energy sources (Fraser, 2021). Solar being the most abundant renewable energy source, can be harvested with ease for household use through a photovoltaic (PV) panel. Biomass is the other renewable resources that offers a lot of potential and have an enormous impact on the environment through its application in the energy sector.

2.3 Biomass Feedstocks and Beneficiation Processes

Biomass has been generally considered to be a low-grade fuel source that has been mostly used in underdeveloped areas of the world such as rural settlements who are heavily dependent on fuelwood. Fuelwood which is the most common biomass resource that has been used throughout the world for cooking and heating purposes on very small scales and the growing desirability of renewable energy sources sees investigations centred towards the large-scale application of biomass. In the year 2013 it was found that more than 70% of the Sub-Saharan population in Africa were still using fuelwood as their primary source of energy (Matsika, et al., 2013). With the growing population and decline in economic activities in these developing countries, the demand for fuel wood will continue to be high, except if the government of these countries can implement electrification that will have similar costs to fuel wood (Matsika, et al., 2013). The high costs of electricity propagate the use of firewood for the more energy demanding activities such as cooking and heating, while the electricity may be used for lights and other less demanding activities.

Developments in research assessed how the use of biomass can be shifted from domestic activities to a broader range for the provision of electricity and biofuels. Biomass is an energy source that is derived from living organisms such as plant and animal matter. The organic matter found in these feedstocks contains the energetic value that can be manipulated into more convenient fuel sources. The organic matter in the biomass feedstock is made of oxygen, carbon, hydrogen, water and nitrogen and trace elements such as sulphur and chlorine (Muvhiiwa, et al., 2018). There is a varying number of biomass resources that are available for use in the production of biofuels and electricity through several processes ranging from biochemical to thermochemical.

In using biomass as an energy source there must not be any competition between food production and energy feedstock production. This can present challenges in a country like South Africa, as biomass feedstocks require water to be produced and food production also requires water (Lundqvist, 2020). The water scarcity in parts of South Africa means that the biomass feedstock to be used in the energy production process must require minimal amounts of water or none. Compared to fossil fuel resources such as coal, gas and oil, biomass feedstocks usually require land and water for their production, i.e., plant matter requires fertile land & water while animal matter also requires water and land, along with municipal solid waste that requires land for its storage. The extent to which biomass can be implemented as an energy source, thus has severe consequences on both sides of the equation, a compromise must

be made between food security, sectors requiring land the most and the environmental impacts associated with deforestation.

These biomass resources are often referred to as feedstocks and include agricultural waste, forest residue, wood processing facility residue, refuse derived waste, dedicated energy crops, aquatic plants, food waste and other types (Energy, n.d.) (Zafar, 2021). Amongst the available biomass resources, fuelwood has the highest rate of use especially among rural settlements where there is no electricity. In 2007 it was found that about 20% of the world's population was heavily reliant on fuelwood which is lower than the 27% of the population in 1996 (Prasad, 2010). The decline in the users of fuelwood is primarily due to the introduction of electricity in such settlements which were previously reliant on fuelwood.

Fuel wood is still the most abundant form of biomass followed by municipal solid waste which has a high yearly accumulation. The extent to which biomass can be realistically applied towards electricity production and biofuels is limited by a variety of factors, but a study by Dias, et al., (2021) estimated that energy acquired from biomass can only contribute 5-17.7% to the global energy matrix. With a future energy grid solely dependent on renewable energy sources, this fraction of biomass power is a significant amount, and the continuing growth of energy dedicated crops will improve this percentage.

2.3.1 Lignocellulose Biomass

Lignocellulose biomass accounts for a major fraction of the available biomass and it's mostly found in plant materials which are composed of cellulose, hemicellulose and lignin (Lundqvist, 2020), (Anwar, et al., 2014) & (Basu, 2018). A considerate amount of this biomass is an agricultural waste product and common examples of materials containing this form of biomass includes hardwood, softwood and grass to name a few (Lundqvist, 2020) & (Anwar, et al., 2014). Lignocellulose biomass is among the top misused energy sources and a major portion of this biomass is often disposed of by burning it, especially in the agricultural sector. Lignocellulose biomass is mostly in the field of biofuels and in countries like the United States of America, annually about 1.3 million tons of lignocellulose biomass is used in producing biofuels (Fatma, et al., 2018).

Available lignocellulose biomass varies according to their composition with regards to the cellulose, hemicellulose and lignin content. In the enrichment of the different lignocellulose biomass feedstocks, the composition is a determining factor on the quality of the product, often the synthesis gas which can be derived. A study by Gulec, et al., (2021) performed an

investigation on the hydrothermal reforming of 5 different types of lignocellulose biomass into hydro-char. From the study it was proven that a higher hemicellulose content produces a higher hydro-char content while a higher cellulose content tends to result in a lower quantity of hydro-char being produced. The importance of this study is in the enrichment of the char present in the biomass and how it can be enriched to produce a synthesis gas product with a desired composition. The study can further assist in knowing the components of lignocellulose biomass that results in the production of synthesis gas with a desired composition.

2.3.2 Other Waste Feedstock

The generation of waste across the different economic sectors of any country can be split according to two categories which determine the handling of the waste, and these categories are 1) non-hazardous waste and 2) hazardous waste. In the non-hazardous waste categories, there is mostly municipal solid waste which is generated by different economic sectors and this waste type does not pose any threat to the environment. Hazardous waste includes waste generated from mostly industrial processes and this waste is often toxic to living organisms and the environment. Hazardous waste would include waste such as fly ash produced from coal power plants, chemical waste from laboratory activities and other waste types from other processes involving toxic materials.

The waste generated in South Africa for the year 2018 according to the state of waste report supplied by the Department of Environmental affairs has been summarized in **Figure 2-3**.

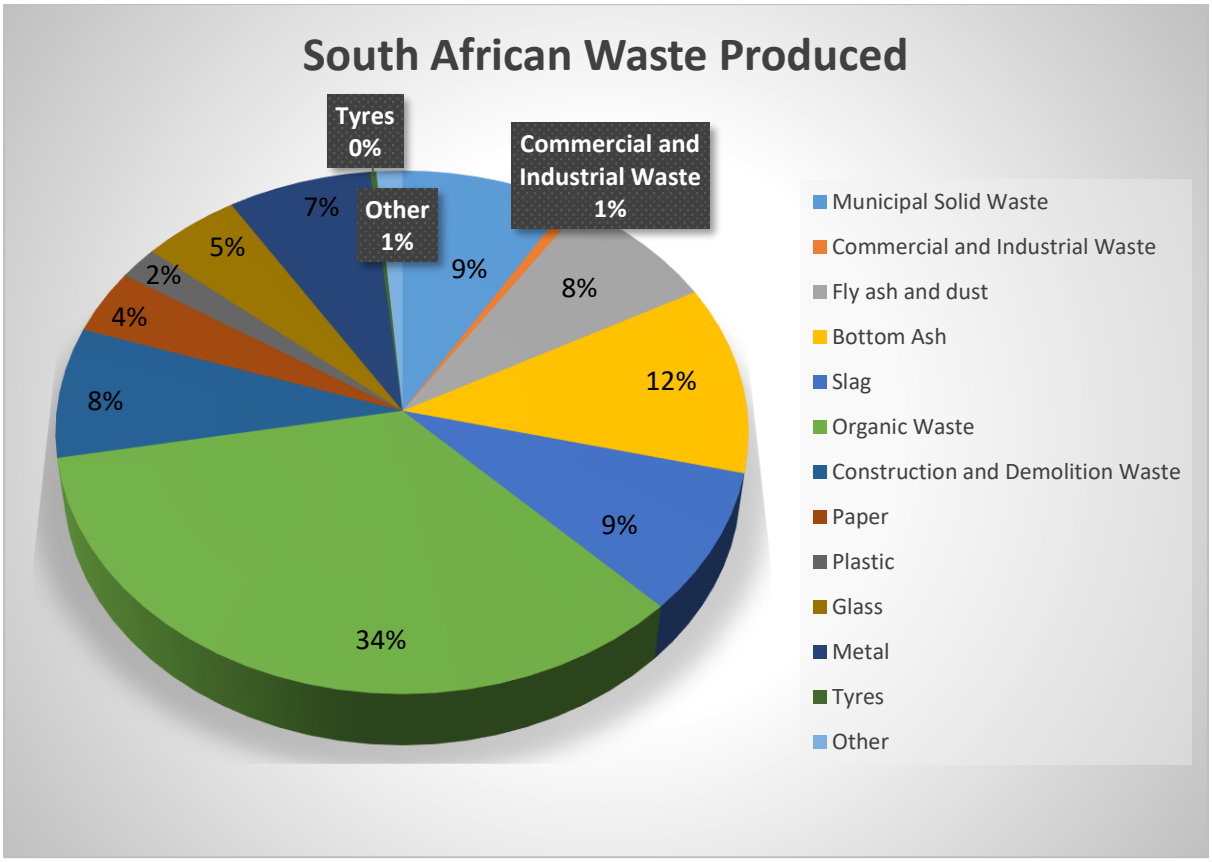


Figure 2-3: Summary of waste production in South Africa from 2018 (Department of Environmental Affairs, 2018).

2.3.2.1 Municipal Solid Waste

Waste management is a major environmental problem in developing countries such as South Africa, along with other African countries. A solution to the management of municipal solid waste has been landfilling which involves collecting the waste generated by the household and commercial sector & storing it in a designated space. The constant dumping of the waste in these designated places leads to an accumulation of waste and eventually space runs out. The issue of waste management and disposal sees waste landfills getting filled over capacity, leading to more space being required for disposal. To demonstrate the importance of waste management in South Africa, it's estimated that out of the 57 million citizens, each citizen generates about 2.5 kg of waste per day depending on the income level of the citizen (Alive2green, 2019) & (Department of Environmental Affairs, 2018). In a year, about 54.2 million tons of municipal, commercial and industrial waste is generated, out of this about 10% of the waste is recycled while the other 90% is dumped in landfills (Alive2green, 2019) & (Department of Environmental Affairs, 2018). The state of the waste landfills also comes into question as the 90% accumulation of yearly waste leads to them filling up in a short space of

time. In some Metropolitan municipalities in Gauteng, there have not been any new landfill space acquired in over 24 years, while the remaining landfills are filling up at a rapid rate (Alive2green, 2019) & (Department of Environmental Affairs, 2018). Even the newly acquired landfills will be filled up in a short space of time which leads to the topic of researching new ways of managing waste other than the traditional landfilling method which is no longer sustainable.

A major flaw in the current waste management system is that it is more for storage rather than dealing with the waste. Only recycling and other means of repurposing the waste are viable in the management of the waste. The other potential waste management processes include incineration which is already in place for a small portion of the waste, and thermochemical processes which seeks to extract the heat potential (calorific value) of the waste and use it in the energy sector. These thermochemical processes include pyrolysis, gasification and plasma gasification, & through these processes a value-added gas can be derived and used as an energy source.

2.3.2.2 Hazardous Waste

The disposal of hazardous waste is another critical issue in the scope of South African waste management. As reported by Department of Environmental Affairs, (2018), in the 66.9 million tonnes of hazardous waste generated in 2017 approximately 6% of the waste was re-used or recycled while the other 94% was treated and/or landfilled. Most of the hazardous waste generated was 74% in the form of fly ash and bottom ash from coal-fired power plants which dominate the South African energy sector. In the case of fly ash and bottom ash being the highest hazardous waste produced in South Africa about 93.4% and 91.7% respectively were landfilled (Department of Environmental Affairs, 2018). Although ash does not have any chemical value whatsoever, it has many applications in the construction industry to produce cement and bricks (Department of Environmental Affairs, 2018), thus the fact that above 90% of the waste was landfilled indicates the inadequacy of the current waste management system in South Africa. The landfilling of hazardous waste is troublesome as this waste contain substances that are known to have harmful effects to the environment and the living organisms present in the region where such a landfill exists.

Hazardous waste usually refers to waste containing mercury, lead, arsenic, cyanide and sulphur, if not properly managed these chemicals found in the waste can either pollute the water or the air which can be harmful to humans, animals and the ecosystem through which all living

organisms exist in a particular region (Akpan & Olukanni, 2020). Lead poisoning or exposure of any kind has been proven to cause a fluctuation in blood pressure, sleep disorder, kidney damage and nerve disorder, and lead poisoning is a major contributor to the child mortality rate in countries like Nigeria including the death of 28 children due to a gold mine contaminating a local drinking stream in the previous years (Akpan & Olukanni, 2020), (Payne & Pitchford, 2015) & (Olukanni, et al., 2017). In African nations such as Nigeria the mishandling of hazardous waste as a result of the technological advancements in the country and medical waste has seen an influx in the deterioration of human health leading to birth deficiencies, cancer and infectious diseases such as HIV, hepatitis B and C (Akpan & Olukanni, 2020).

The advancements in medical studies throughout the world has been a blessing to people suffering from chronic illnesses, however these advancements come with a price of more medical waste being generated. Medical waste can either be non-hazardous or hazardous, with the hazardous waste being more of a threat to society and the environment at large. The hazardous waste falls under a range of categories such as sharps, infectious, pharmaceutical, cytotoxic, pathological, radioactive and chemical waste (Chartier, et al., 2014) & (Olaniyi, et al., 2018). Medical waste poses a variety of injuries to living organisms and the environment ranging from physical injuries in the case of sharps and indirect injuries and illness from the waste that can pollute the air, water and the land (Olaniyi, et al., 2018).

Prior to the landfilling of hazardous waste, it must be classified using the parameters shown in **Figure 2-4**. The design of the waste landfill heavily relies on these parameters and waste that is explosive in nature cannot be store in landfills as the ambient temperature in the landfill could cause them to explode resulting in damage at the landfill and the environment.

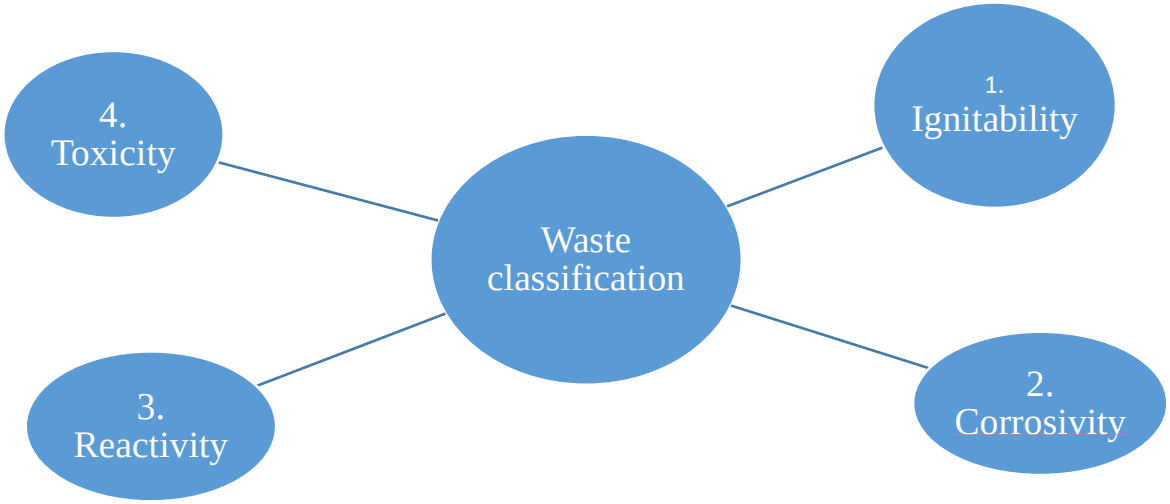


Figure 2-4: Classification of hazardous waste

In terms of hazardous waste landfills, the Averda's Vlakfontein Class A hazardous waste landfill in Gauteng is the best of its kind due to it being built on top of a previous brick-making facility, which prevents the waste from affecting the soil and the environment around it due to the dense clay layer on the surface (Averda Editor, 2018). This hazardous waste landfill is the first of its kind to meet the South African hazardous waste landfilling regulations, mostly due to the 1.2 metres of geotextiles, compacted clay, high density polyethylene and gravel (Averda Editor, 2018). Hazardous waste landfilling does not however accommodate all types of waste streams as flammable, explosive and corrosive types of waste streams do not meet the standards for disposal in such a hazardous waste landfill. The hazardous waste streams that do not meet the standards for disposal in a landfill must first be destabilized before disposal and can only be disposed once they meet the acceptable criteria for that waste disposal facility.

A more common method of hazardous waste disposal is incineration which uses heat to reduce the volume of the waste. In the medical waste management industry, the use of incinerators is on the decline as incinerators are known to release toxins to the environment, which has led to a trend of illegal dumping of the toxic medical waste (Olaniyi, et al., 2018). Better means of managing the medical waste are required and processes such as plasma gasification can be instrumental in the management of medical waste whilst also getting thermal value from this waste.

2.3.3 Advantages and Disadvantages of Biomass for Energy Production

One of the most positive things about the use of biomass as an energy source is that it is generated everyday either through waste generated by people, waste generated by animal or plant waste from the daily agricultural activities. Most of this waste is accumulated in landfills

for years, which is an irresponsible use of landfill space since this waste could be easily recycled or repurposed for energy. Developing the necessary infrastructure to re-use the waste will be another challenge though as this will require a lot of capital compared to landfilling. A cost benefit analysis between the values of landfilling the waste versus the thermal re-use of the waste can determine the economic value in re-use of the waste.

Large scale use of biomass as an energy feedstock comes at the expense of extremely underdeveloped countries who have relied on biomass feedstocks such as firewood, and crop residue as fuel for cooking. In countries like Malawi where over 90% of the population is heavily reliant on biomass and with investigations pointing out that there is diminishing forestry cover (Schuenemann, et al., 2018), large scale use of the biomass can threaten the survival of ordinary citizens. Several socio-economic factors are influential in the design of large-scale biomass power plants, although feasible in some parts of the world, other parts must weigh their options before investing in this technology.

One of the main reasons why biomass has been favoured over the diminishing fossil fuels is due to its carbon neutrality. Biomass is considered carbon neutral due to the balance between the carbon it releases and the carbon it absorbs. According to the carbon cycle shown in **Figure 2-5** the quantities of carbon absorbed by the biomass are like those released, thus during the combustion process a similar amount of carbon dioxide is released (Bracmort, 2016). The carbon neutrality of the biomass means that any product derived from it can be carbon neutral, i.e., production of electricity or biofuels generated from biomass. The carbon neutrality of the biomass mostly applies to the naturally growing biomass and not the biomass whose growth might be enhanced due to time limitations.

Biomass that is grown under the influence of fertilizers cannot be carbon neutral as the greenhouse gases absorbed and released in preparing the fertilizers are not accounted for (Bracmort, 2016). Most of the biofuel dedicated crops grown under agricultural practices tend to have a high nitrous oxide emission as compared to other biomass feedstock sources. Replenishment of the biomass feedstock harvested is another factor affecting the carbon neutrality of the biomass, more specifically the time it takes to regrow the biomass. The growth process of the biomass determines the extent of its carbon neutrality, and the goal is for the growth of biomass that is carbon neutral.

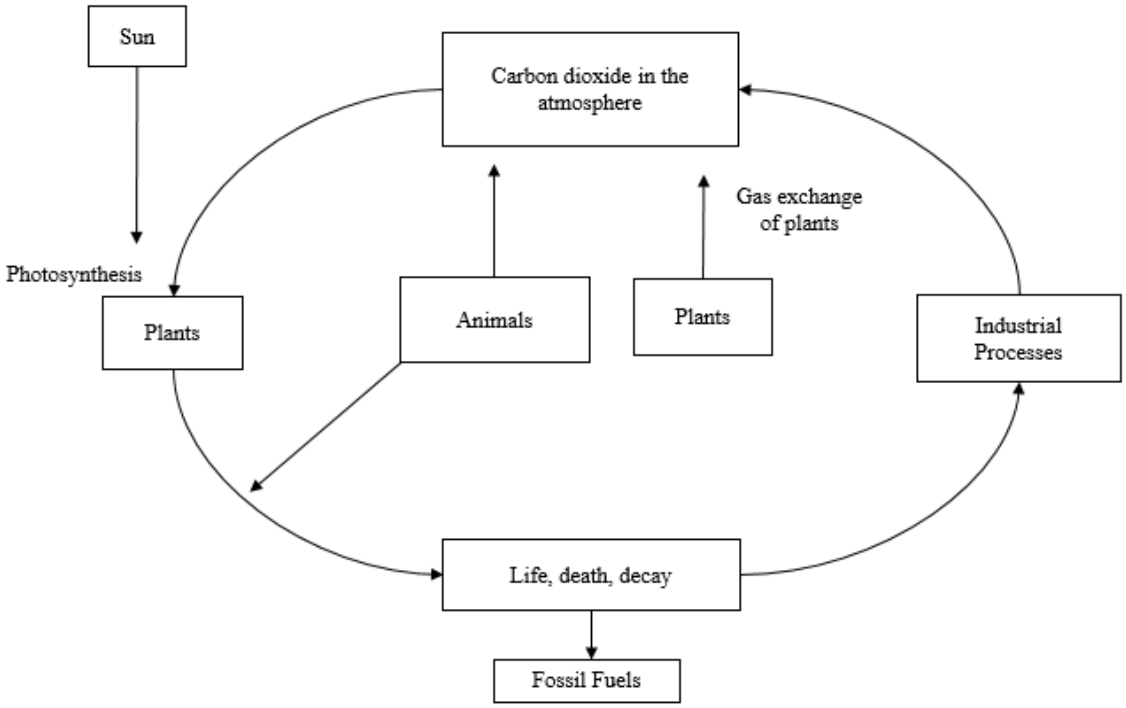


Figure 2-5: Carbon cycle

There are plenty of challenges that may be associated with the use of plant material as a feedstock in the operation of a power plant or biofuel generating plant such as the time frame before harvesting. The cultivation of such biomass as energy dedicated crops should be such that there is a constant availability throughout the year. Most crops are seasonal thus in the operation of a power plant, the biomass feedstock growth must not have any seasonal effects and must require a minimal amount of water. Energy dedicated crops which are specifically grown for use in generating biofuels are amongst the biomass resources that can be grown at any point of the year and in short space of times.

The biggest obstacle with using biomass as a fuel resource is the requirement of land space and the time constraints in their growth contributes to more land being required. With more land space the biomass can be planted and cultivated at different stages of the year leading to the time frame no longer being an issue. The dedication of more land into growing biomass takes away land from people for the building of houses and other shelters. In a country like South Africa where there are land issues, the initiation of a project of this nature has a lot of socio-economic implications. Weighing all the pros and cons associated with the use of biomass resources as energy sources will determine the extent of their application in any context.

2.3.4 Waste and Biomass Preparation

The pre-treatment of biomass and waste is used as a tool for altering the structural, physiochemical and compositional characteristics of the material that presents a challenge in their anaerobic or thermochemical treatment (Bhagwat, et al., 2015). Depending on the product required from the biomass or waste, the pre-treatment processes vary, for biofuels and biogas production the process is more rigid than that where the biomass is aimed for the production of electricity. In the production of biofuels using lignocellulose, the pre-treatment process would involves de-polymerization of the hemicellulose, de-crystallization of the cellulose and preservation of the structures (Bhagwat, et al., 2015), while if the lignocellulose biomass was for electricity production depending on the water content it would require drying and crushing prior to being fed in a thermochemical reactor. With the focus of the project being on electricity generation, pre-treatment processes aimed at enhancing the biomass and waste for this purpose will be considered.

A common biomass pre-treatment process is torrefaction which is a thermochemical process operating at low temperatures to reform the biomass structure for better combustion or gasification. This mild pyrolysis process often occurs at temperatures between 200 °C – 300 °C in atmospheric conditions and usually changes the structure of the biomass into a homogenous fuel with lower moisture and oxygen content (Xu, et al., 2021). The torrefaction process also improves the calorific value of the biomass and potentially makes it easier to crush the biomass. A higher calorific value of the biomass increases the calorific value of the synthesis gas that can be generated from this biomass feedstock. The torrefaction process is a perfect example of the de-polymerization of the hemicellulose found in the lignocellulose biomass, through the condensation of lignin in the wood by heating up the biomass which breaks down carbon molecules in polymers (Cheah, et al., 2016 & Kacik, et al., 2016). The effect of the torrefaction process on the lower heating value of the synthesis gas produced was investigated by Yong & Rasid (2021), along with the effects on the cold gas efficiency of the gasification reactor used for this study. The pre-treatment torrefaction of the biomass proves to be futile in reforming the composition of the synthesis gas generated specifically the hydrogen in synthesis gas primarily as a result of the dehydrating nature of the torrefaction process.

The pre-treatment process in the case of the biomass used as feedstock in a gasification reactor or an incinerator will be less complex, and the investment costs will be far lower. For biomass such woody materials, crushing it before it can be charged to a thermochemical reactor, increases the surface area in contact with the flame and propels the reaction to reach

equilibrium much faster than it would if chunks of wood were to be fed to the reactor. The pre-treatment processes for the preparation of the biomass and organic waste feedstock prior to being gasified involves crushing, drying, reforming and other means of ensuring the biomass is up to standards before being fed to the reactor. For woody biomass such as lignocellulose and other forestry derived biomass, the common pre-treatment methods include drying of wet biomass, torrefaction of biomass, flash pyrolysis and dissolution of woody biomass in organic solvents (Svoboda, et al., 2009).

For organic waste feedstock the pelletization process is a means of classifying the waste and controlling the composition of the waste. Pelletization involves the compression of waste or biomass with a dedicated apparatus, thereafter the compressed ball of waste is held together with an electric heat tape operating at mild temperatures of 80 °C – 100 °C preventing the waste pellet from disintegrating (Rezaei, et al., 2020). In the pelletization of waste materials with components such as paper, plastic, wood, and organic matter, it is found that the waste material with plastics tend to form more durable pellets compared to materials with paper, while plastics requires more heating energy to soften for the formation of pellets compared to paper (Rezaei, et al., 2020).

To some level the ability to pre-treat the biomass for use in a pyrolysis process or gasification process contributes to the output synthesis gas product that can be generated from that biomass. In assessing pre-treatment of biomass through three different processes which are 1) the pelletization of the oak to increase surface area, 2) Drying the oak at 180 °C and 3) Torrefaction of the biomass at 270 °C in nitrogen. Cheah et al, (2016) was able to prove that the pre-treatment process influences the thermodynamic operation of a reactor and the synthesis gas product generated from said reactor. The biomass torrefied at 270 °C was found to improve the ratio of the hydrogen to carbon monoxide for the synthesis gas in favour of hydrogen and lower methane quantities were produced. The other processes such as drying of the biomass and pelletization are more effective in assisting the thermodynamic performance of the plasma gasification reactor. Drying of the biomass helps the thermochemical reactions of the biomass reach equilibrium at a much faster rate compared to the wet biomass. The pelletization of the biomass bears similarities to crushing of the biomass which increases surface area in contact with the heat source.

2.4 Pyrolysis and Gasification

Pyrolysis is the process of converting solid and liquid matter into a value-added gas product through heating which prompts the decomposition process in the absence of air. The pyrolysis process tends to operate at temperatures from 300 °C – 600 °C to produce a gas product with energetic value (Gadek, et al., 2016). The pyrolysis process still operates at lower temperatures than the gasification process, which resulted in the value-added gas produced from this process being of low quality and containing a significant amount of tar which makes it difficult to use in power cycles and gas engines. The low temperatures of operation for this process makes it undesirable in the conversion of biomass to electricity, which is why the process is mostly applicable for the synthesis of biofuels and biogas.

The pyrolysis process operates at similar temperatures to the coal-fired heaters used in fossil fuel-based power plants and the emission in operating the pyrolysis process is lower than that in combustion-based boilers. In assessing the feasibility of a co-pyrolysis reactor system, Yao et al, (2021) considers biomass, plastic waste and bituminous coal as feedstock for the process. Through this study the author can prove that the pyrolysis of a mixture of bituminous coal along with biomass and plastic waste yields better results than the sole combustion of the low-grade coal. The pyrolysis process offers the advantage of using a mixture of fuel feedstock making it desirable in the use of low-grade fuel sources. The pyrolysis reactor used for this scenario operates at a temperature of about 550 °C and a reaction pressure of 20 kPa, while in an actual steam boiler co-firing coal with biomass studied by Gu et al, (2013) the operational temperature was found to be 800 °C and the steam was generated at a temperature of 400 °C and a pressure of 12.5 bar. The co-fired actual boiler does not negatively influence the efficiency of the process compared to the standard coal-only boiler and it reduces the emission of CO_2 and SO_x. The results of these studies create a landscape for not only low-grade fuel sources but systems that can use a mixture of these fuel sources to derive more value out of them.

The pyrolysis process has been contrasted with the gasification process which operates at much higher temperature than the pyrolysis process and uses a gasifying agent to aid in the reaction of converting biomass into synthesis gas. The gasification process similarly to the pyrolysis process involves the thermochemical conversion of solid and liquid matter into a synthesis gas product with energetic value, however unlike the pyrolysis process, a gasifying agent is added to assist the reaction. The addition of the gasifying agent into the process is stoichiometric and the equivalence ratio which is the determining factor for how much of the gasifying agent is

required is limited in the range of 0.2 – 0.4, a significant improvement to the temperature is also witnessed as this process operates at temperatures in the range of 700 °C – 1 200 °C (Gadek, et al., 2016).

Most typical gasification reactors operate at temperatures from 600 °C – 800 °C and the gasifying agent used has been known to influence the extent to which the gasification reaction proceeds. Operation of a gasification reactor is assessed by Bandara et al, (2021) in an air fluidized bed gasification reactor that operates at temperatures between 650 °C and 800 °C, using three types of biomasses in wood chips, wood pellets and grass pellets. The temperature at which the gasification reactor operates is important for the carbon conversion efficiency and in most cases the higher the temperature, the better the conversion of the carbon in the organic matter of the biomass will be. The gasification temperature of 650 °C had its limitations in the conversion of carbon while the temperature of 800 °C is found to have reasonable conversion efficiencies of about 75.8% and 70.6% for the wood chips and wood pellets, respectively (Bandara, et al., 2021).

The types of gasifying agents used for the gasification process have been seen as means of controlling the path of the gasification reaction. Some of the most common gasifying agents in industrial and experimental gasification reactor systems includes air, oxygen and steam to name a few. The selection of gasifying agents to be used in any gasification process should consider the end use of the synthesis gas to be generated from this process. For synthesis gas with a higher hydrogen content which is often used in the biogas and biofuels industry, steam is the best gasifying agent to use due to the water gas shift reaction occurring in favour of H_2 production as seen in **Table 2-1**. A study by Shayan et al, (2018) assessed the effects of different gasification agents in a biomass gasification process aimed at producing synthesis gas with a better H_2 composition. Steam gasification produces the best synthesis gas composition of H_2=48.92% & CO=35.27% closely followed by oxygen gasification with a product more suitable for combustion in gas turbines with a composition of H_2=34.13% & CO=41.51%. In the interest of the synthesis gas generated towards electricity production, gasifying agents such as air, oxygen and steam are all applicable, air and oxygen though have the advantage of producing a CO enriched synthesis gas product.

In both the pyrolysis and gasification reactor there are several reactions occurring and they can be summarized by **Table 2-1**.

Table 2-1: Reactions in a pyrolysis and gasification process

Name of reaction	Chemical reaction	$\Delta H_0 r(298K)$ (kJ/mol)	$\Delta G_0 r(298K)$ (kJ/mol)
Pyrolysis	$C_xH_yO_z \rightarrow aCO_2 + bH_2O + cCH_4 + dCO + eH_2 + fC_2 + char + tar$		
Partial oxidation	$C + 0.5\ O_2 \rightarrow CO$	-111	
Complete oxidation	$C + O_2 \rightarrow CO_2$	-394	
Steam-tar reforming	$C_nH_m + 2NH_2O \rightarrow (2n + m/2)\ H_2 + nCO_2$		
Hydrogenating gasification	$C + 2H_2 \rightleftharpoons CH_4$	123.7	168.6
Boudouard equilibrium	$C + CO_2 \rightleftharpoons 2CO$	205.3	140.1
Water-gas shift (WGS)	$CO + H_2O \rightleftharpoons CO_2 + H_2$	-41.47	-28.5
Heterogeneous WGS	$C + H_2O \rightleftharpoons CO + H_2$	130.4	89.8
Steam reforming of methane	$CH_4 + H_2O \rightleftharpoons CO + 3H_2$	172.6	118.4
Dry reforming of methane	$CH_4 + CO_2 \rightleftharpoons 2CO + 2H_2$	-74.9	-50.3
H2S formation	$S + H_2 \rightleftharpoons H_2S$		
H2S-COS equilibrium	$H_2S + CO \rightleftharpoons COS + H_2$		

Source: (Koido & Iwasaki, 2018)

The thermodynamic parameters of the gasification process are heavily dependent on the costs of operating such a system, for instance steam may be the best gasifying agent but its acquisition incurs far higher costs than those of air as an oxidising agent, in the long term continuous operation of the process, the costs required to operate a steam gasification reactor might outweigh the thermodynamic performance of such a system and the quality of the value added gas produced through this process.

2.5 Plasma Gasification

The gasification process involves an extremely endothermic reaction, and it has been proven that conventional gasification processes don't have enough heat energy for the optimum reforming of the solid biomass and waste into synthesis gas. The shortage of heat often leads to higher chain hydrocarbons in the synthesis gas accumulating as tar and pyrolysis oils. The limitations of the conventional gasification reactor can be overcome by integrating plasma technology into the gasification reactor. Using electricity with sufficient power, a gaseous medium is ionized between the electrodes of a plasma torch and the continued supply of power ensures it remains in that state (Surma, 2010). The gas in the ionized state is the plasma gas

and this gas is used to supply heat to the gasification process. Even though plasma is generated at temperatures of 17 727 ℃, the temperature suitable for the gasification of the biomass and waste is usually around 1 200 ℃ – 1 400 ℃ (Hlina, et al., 2014).

Figure 2-6 shows the input and output analysis of the plasma gasification reactor in terms of the process streams.

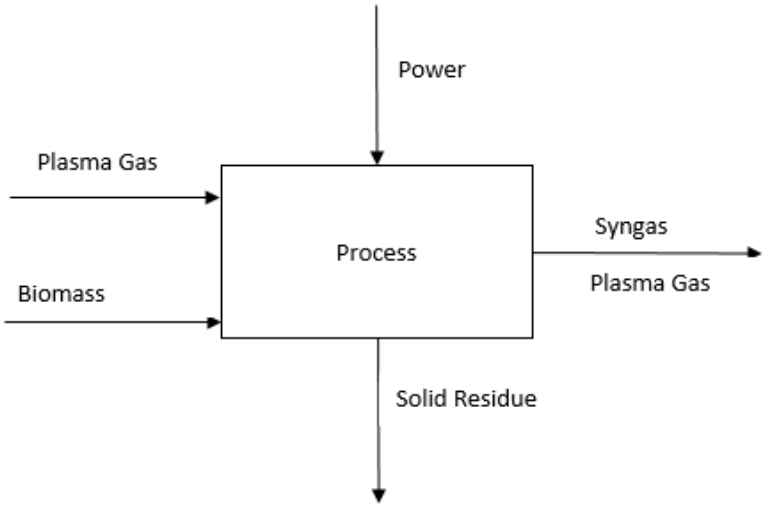


Figure 2-6: PFD of plasma gasification process

Conversional gasification reactor would have a gasifying agent rather than the plasma gas stream and the gasifying agent reacts with the biomass in the reactor under stoichiometric conditions to supply the heat responsible for the gasification of biomass. The plasma gas on the other hand is a heat stream on itself which is why in most cases an inert gas is used as a plasma gas. The plasma arc gasification reactor has an operational temperature ranging from 1 000 ℃ – 1 500 ℃. The most important attribute of the plasma gasification reactor relates to the temperature of operation which is higher than that of conventional gasification reactors.

A direct correlation between the temperature and the conversion of carbon matter has been proven, typical gasification reactors have been found to convert about 75% of the carbon to synthesis gas materials leaving the remaining carbon as char and tars. In an experimental study by Kibret et al, (2021) on the gasification of spent coffee grounds, a carbon conversion efficiency of about 95% is achieved by a semi-fluidized bed using a mixture of two gasification agents in the form of steam and carbon dioxide. The carbon conversion efficiency achieved in this research study can be attributed to the presence of two different gasifying agents which leads up to a reaction temperature of 900 ℃ which is uncommon for typical gasification reactors. For plasma gasification reactors which tend to operate at temperatures above 1 000

°C, the carbon conversion efficiency achieved is mostly 100% leading to a more favourable composition of the synthesis gas being generated.

The operational temperature influences other parameters beyond the carbon conversion efficiency and some of these as highlighted by Muvhiiwa et al, (2018) are:

- Biomass conversion efficiency,
- Syngas yield,
- Decomposition of tar and other higher chain hydrocarbons,
- Cold gas efficiency of the plasma gasification reactor, and
- Exergy efficiency of the reactor.

The synthesis gas generated in conventional gasification reactors has been known to contain a lot of tar which necessitates an intensive clean-up process before it can be combusted in gas turbines or gas engines. The conversion of the tar goes hand in hand with the carbon conversion efficiency, tar can only be eliminated if the conversion of carbon is at 100%. Several studies investigating the performance of a plasma gasification reactor conclude that tar is completely decomposed at temperatures above 1 000 °C. In investigating a small scale 15 kW nitrogen torch plasma gasification reaction, Muvhiiwa et al, (2018) found that tar particles began decomposing at a temperature of 800 °C and were completely decomposed at temperatures around 1 000 °C. The temperature of operation for a plasma gasification reactor thus plays a critical part in not only the thermodynamic operation of the reactor but also the synthesis gas generated from this reactor. In the interest of the synthesis gas generated there are some factors that influence the quality and some of these factors can be seen below, with a strong link noted between the type of plasma gas used and the temperature.

Factors contributing to the quality of the synthesis gas in a plasma gasification reactor:

- Temperature,
- Content of the biomass, and
- Type of plasma gas used

The type of plasma gas used has strong effects on the composition of the synthesis gas generated and some plasma gas types determine the state of the equilibrium. Common plasma gases include air, nitrogen, argon, steam, and oxygen. These plasma gases often determine the equilibrium state of the synthesis gas with regards to the H_2 and CO formed through the gasification of a particular biomass feedstock.

The use of oxygen as a plasma gas has been noted to result in a combustion process occurring alongside the gasification process meaning that more oxides are formed. The formation of CO can be expected to be high along with water as some of the generated H_2 will be converted to water through a combustion reaction. The operation of plasma gasification reactor with a plasma gas enriched in oxygen, has the added benefits of the biomass reacting with the oxygen to supply additional heat to the gasification process. An oxygen plasma can thus be used to reduce the heat required from the plasma torch and the work potential required to operate the plasma arc torch (Muvhiiwa, et al., 2021). The use of steam as a plasma gas differs from oxygen as the steam favours the formation of the hydrogen through the water shift gas reaction as previously mentioned for the gasification reactor. Researcher such as Pang et al, (2018) who investigated a thermal gasification process and a plasma gasification process both using steam as the gasifying agent/plasma gas for the gasification of wood powder and char powder were able to prove this theory. The dissociation of the water into elemental constituents of hydrogen and oxygen are attributed for the equilibrium composition of the synthesis gas that is generated.

The simulation model to be developed are for the demonstration plasma gasification reactor plant at NECSA using a nitrogen plasma. This reactor is supplied with a stoichiometric oxygen quantity for the progression of the gasification reaction and to ensure a suitable synthesis gas product is generated. In the start-up of the reactor, argon is used and is gradually changed into nitrogen before the feeding of the biomass commences. Upon completion of the plasma gasification process, the produced synthesis gas product undergoes several downstream processes as shown in **Figure 2-7**.

The work to be done in this study involves a small-scale plasma gasification reactor plant geared towards the production of power. **Figure 2-7** gives an indication of the model to be developed for the entire process, following the plasma gasification of the biomass.

A plasma gasification plant can be represented by **Figure 2-7** which shows the different process stages involved in the conversion of biomass to electricity.

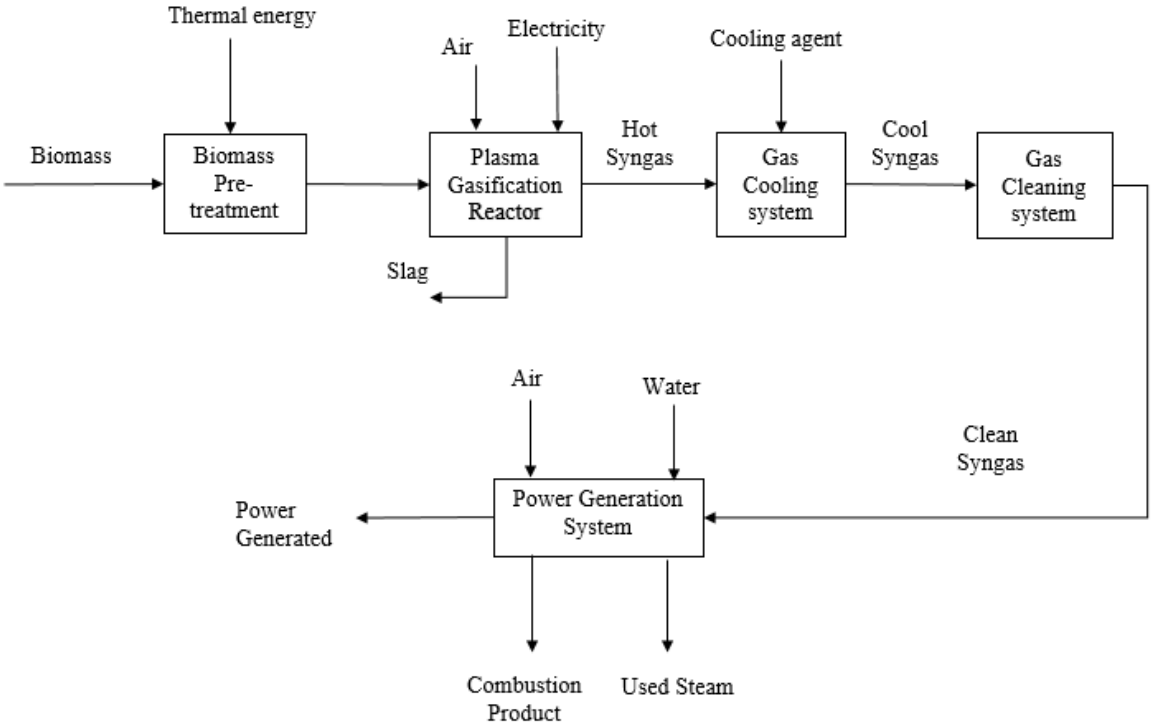


Figure 2-7: Block diagram of the biomass power generation system

The different process models to be simulated will revolve around the process flow diagram in **Figure 2-7**, with different modifications being adopted and the response studied through the energy and exergy analysis of the process. The initial investigation of the process will be according to **Figure 2-7**, some of the modifications will involve elimination of the gas cooling system along with the gas cleaning system. In the modification scenario, the synthesis gas produced through the plasma gasification reactor will be fed directly to the power generation system without any cooling or cleaning. The process to be carried out can be associated with some of the investigations done by van der Walt et al, (2017), in the investigation of three different processes through which the synthesis gas generated from the plasma reactor can be used.

The first scenario which resembles **Figure 2-7** features an internal combustion gas engine at the power generation centre of the process. This internal combustion engine is assumed to have a generator efficiency of 35%. The second scenario quenches and scrubs the hot crude synthesis gas before it can be fired in a boiler to generate steam. In the final scenario, the sensible from the exhaust synthesis gas product of the reactor is fed directly to a boiler with the goal of producing steam. In the final scenario, the quench probe and the scrubber are bypassed to derive the heat present in the hot crude synthesis gas.

Similar assessment with be done in the current investigation, with regards to the different ways through which the synthesis gas can be used, the results achieved in the above study create a foundation for the investigation to follow.

2.6 Syngas Quenching System and Heat Recovery System

The synthesis gas produced from the plasma gasification reactor is usually at extremely high temperatures and must be cooled down, as downstream processes such synthesis gas cleaners operate at low temperatures. A synthesis gas cooling mechanism that has been developed to fulfil this task is the quenching system, which involves the rapid cooling of the synthesis gas effluent to ambient temperatures through some different cooling processes. Some of these quenching processes include 1) water quench, 2) chemical quench, 3) gas quench and 4) radiant quench (Liu, et al., 2010).

The quenching process can be seen as a heat exchanger which cools the hot synthesis gas through a cooling agent which absorbs this heat. In some of the quenching probes the cooling agent is directly mixed with the hot synthesis gas and in others different tubes are used for the synthesis gas and the cooling medium with the heat transfer being convective. The model for the demonstration plant under consideration from NECSA uses a total water quench system which sprays water over the quenching chamber to cool down the synthesis gas. The aim of this system is primarily the cooling of the synthesis gas, resulting in the thermal heat present in this stream being lost. The loss of this thermal heat negatively impacts the thermal efficiency of the entire process and Liu et al, (2010) notes that amongst the four quenching mechanisms highlighted, the water quench system has the highest exergy destruction.

The radiant quench system has been viewed as a better quenching mechanism in terms of preserving some of the heat in the synthesis gas effluent of the reactor. The radiant quench process investigated in a study done by Botros & Brisson, (2013) offers the advantage of recovering rather than destroying the sensible heat in the synthesis gas, with this heat being recovered to generate power through high pressure steam. The material of design for the radiant quench heat exchanger and the working fluids (mostly water but also molten salt and liquid metals) used for heat recovery are proven to be important factors in minimizing the temperature difference between the synthesis gas and the generated high-pressure steam which strongly influences the destruction of exergy in the process. An investment into this radiant heat exchanger system with a secondary heat exchanger using molten salt has been proven to be economically feasible with a payback period of one year. In comparing the water quench and

the radiant quench, Liu et al, (2010) notes that the radiant quench consumes 1/3 of the exergy consumed in a water quench. Considering that the radiant quench has prospects of recovering heat from the synthesis gas whilst performing the cooling, it appears to be far more desirable than the water quench.

Even though the primarily goal of the quenching system is the cooling of the hot synthesis gas to prepare it for the clean-up process, some additional benefits are noted in controlling the presence of undesirable materials in the synthesis gas. The quenching of the synthesis gas has been linked with the control of tar material and can assist other tar removal processes such as filters. Thapa et al, (2017) investigated the effectiveness of a water quench process in conjunction with a biomass filter medium. Three tar removal techniques are investigated, with 1) wood shavings filter, 2) Wood shavings filter with heat exchanger and 3) wood shavings filter with oil bubbler. The filter was more effective when coupled with another tar removal process, with the oil bubbling system being more effective due to the ability of the oil to absorb tar particles rather than the quenching/cooling system, which only condenses the tar particles for capture in the filter.

There has been a surge in research studies that try to use a turbine expander as means of cooling the synthesis gas and reducing the exergy destruction associated with the quench probe. The sensible heat present in the synthesis gas is used to drive a power cycle without any need for combusting this fuel source in these power cycles. This concept of using a turbine expander to cool down the synthesis gas in chemical processes has been extensively investigated by Greeff et al, (2001), Greeff et al, (2002), Greeff et al, (2003), Greeff et al, (2003), Greeff et al, (2004), Greeff et al, (2004), Greeff (2021) & Perold et al, (2001) in different publications. It was proven effective in most of the publications, with significant energy savings being realised for several well-known chemical processes such as methanol production, ammonia production, ethylene oxide production, and phthalic anhydride and synthesis gas production. This proves that the turbine expander can be successfully adopted into the power cycles as another means of cooling the synthesis gas while obtaining some of power in lieu of destroying the exergy in a quench probe. Using synthesis gas as a working in turbine expansion is not without changes as it may pose risks to rotating machinery. Greeff (2022) recently proposed another way to cool synthesis gas, which overcomes this problem. It is proposed to integrate the hot synthesis gas stream with an externally fired gas power cycle, wherein the synthesis gas heat is directed into this cycle by heating a working fluid further against the hot synthesis gas. In so doing the synthesis gas is cooling and the heat converted to work via the externally fired cycle.

In the current study some of the cases will bypass the quenching mechanism to observe the effects of the hot synthesis gas streams sensible heat on the thermal efficiency of the power cycles. This will be achieved through two different mechanisms, where in one case this sensible heat stream will be expanded in a gas turbine expander, while in the second mechanism the hot synthesis gas heat stream will be directly fed into the combustion chamber or boiler in these different power cycles. These two power production schemes excluding the quench probe are represented by **Figure 2-8** and **Figure 2-9**, respectively. The supporting research as conducted by Greeff (2022) & van der Walt et al, (2017) indicates that the addition of this heat stream drastically improves the thermal efficiency of the power cycles under considerations. The simulation of the two quench probe bypass systems will determine which one offers the best thermal efficiency while minimizing the costs associated with this improvement in the thermal efficiency.

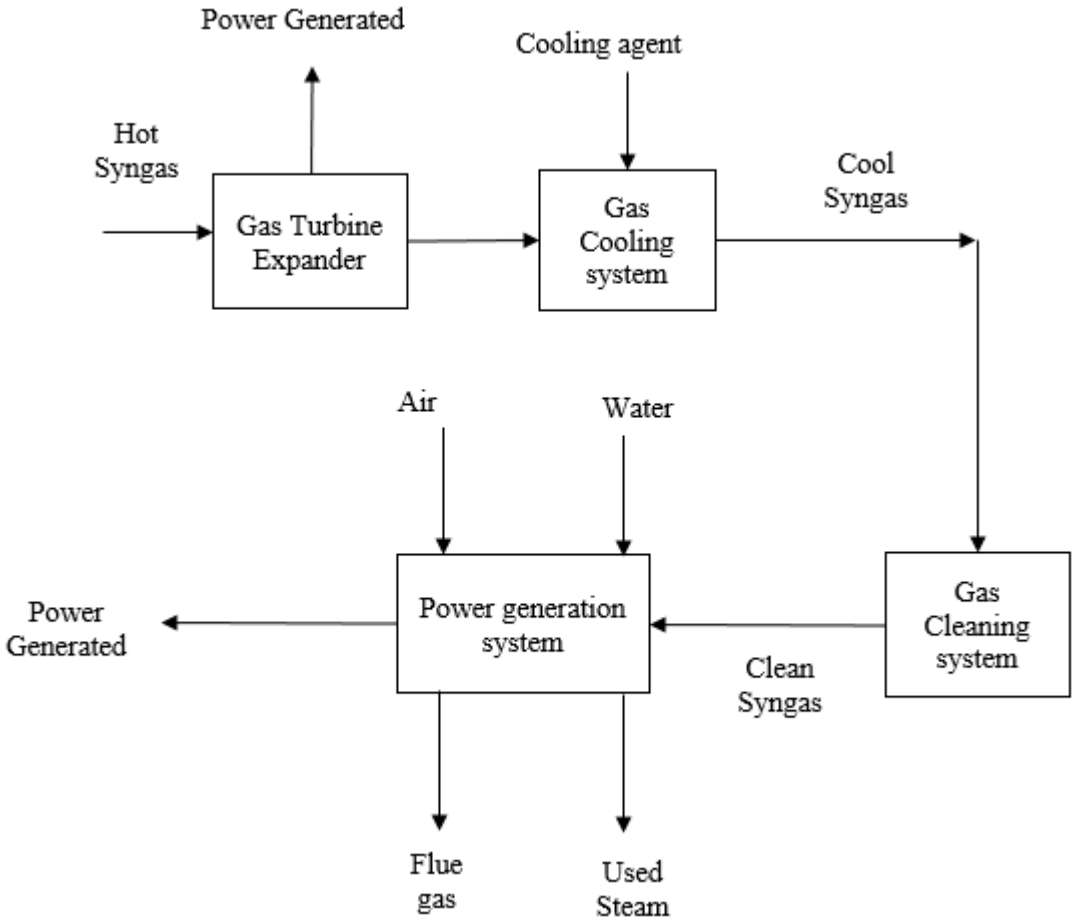


Figure 2-8: Turbine expander power production mechanism

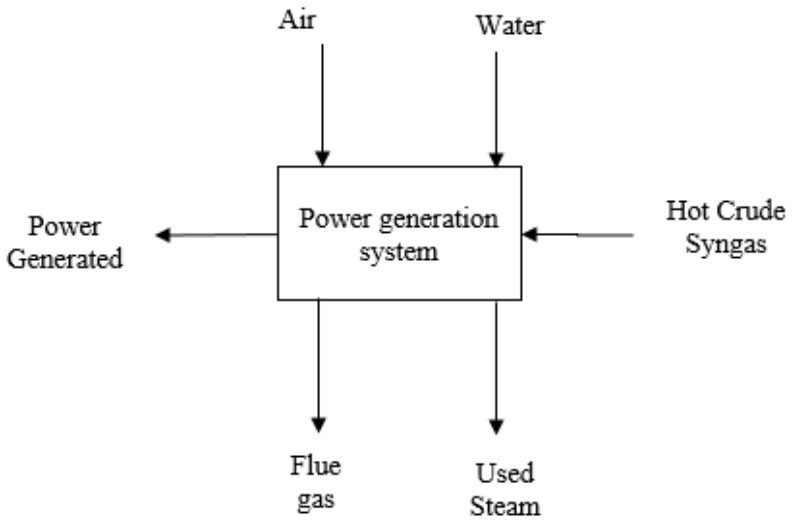


Figure 2-9: Direct synthesis gas firing power production mechanism

In the process where synthesis gas is combusted to generate electricity, the aim will be to use a quenching system that recovers the heat from the synthesis gas effluent of the reactor to be integrated to the power generation process.

2.7 Syngas Cleaning Process

The thermochemical treatment of biomass has been known to produce crude synthesis gas, which contains a variety of impurities posing a threat to not only the environment, but the infrastructure of the plant producing this synthesis gas. The potential damages posed by these impurities include corrosion of the pipelines resulting in leakages of the synthesis gas, damaging infrastructure for the storage and transportation of the synthesis gas, tar particles which affecting the operation of gas turbines leading to potential for severe accidents (Balas, et al., 2014). A few of these impurities of note are nitrogen oxides and sulphur oxides which are highly toxic to the environment, any damages to the facilities infrastructure can cause a leakage of these species.

The synthesis gas clean-up process usually occurs in a scrubber which could be wet or dry, with the former being favoured. The wet scrubber has been observed to be cost-effective in small scale systems involving small amount of sulphur impurities (H_2S) (Argonul, et al., 2021). Some of the scrubbing agents used in this process include water, and sodium hydroxide, which are the most common and have been noted to be effective in the removal of sulphur and chlorine impurities. In the case that the synthesis gas being scrubbed is a feed material for a gas turbine, the amount of particles present should be below 15 mg/m^3 while for gas engines such as internal

combustion engines particles are tolerated to a concentration of 50 mg/m^3. This shows that there is little room for error in the case of a scrubber producing fuel for a turbine, the goal is to use a scrubbing agent that is the most effective.

A wet scrubber is one of the most common equipment used in the clean-up of synthesis gas and its effectiveness using different fluids is investigated in an experimental study done by Balas et al, (2014). The investigation assesses which fluid between water or an organic fluid in the scrubber best cleans up the synthesis gas. Water was found to be highly ineffective in the scrubbing of tar in the synthesis gas, as most of the tar particles are not soluble in water, while the tar particles were highly soluble in the organic fluid with the only disadvantage being the high costs associated with acquiring these organic fluids.

In an investigation into a wet scrubber performed by Arnif et al, (2018) the performance of a water equipped wet scrubber is analysed by studying the characteristics of the product wastewater. The wastewater composition indicates the extent to which the synthesis gas is cleaned up with regards to impurities such as sulphur and carbon dioxide. The wastewater characteristics with the most attention paid to them are i) the turbidity of the water, ii) pH and iii) the phenol concentration. This is deduced from a study of two synthesis gas products derived from the gasification of coconut shells and palm shells.

In a small-scale plasma gasification reactor system, the concentrations of sulphur, nitrogen oxides and chlorine impurities are often low, meaning that the design of the scrubber doesn't have to be as rigorous as it would be for a large-scale system. For the synthesis gas generated by the NECSA demonstration plant model, the presence of sulphur and chlorine impurities can be noted to be very low, meaning the scrubbing process can be bypassed in the development of the Aspen Plus model for this plant.

2.8 Pressurized Gasification Reactors

The plasma gasification reactor is extremely efficient in producing the desired synthesis gas quality and in a process aimed at producing electricity, a design flaw of most plasma gasification reactors systems is the synthesis gas leaving the reactor at low pressures and high temperatures requiring the synthesis gas to be cooled down before it can be compressed. The incorporation of a pressurized plasma gasification reactor could lead to the production of synthesis gas that can be directly fed to a heat engine without any prior pre-treatment processes. In the investigation developed for this project, a hypothetical case study is developed where a

pressurized synthesis gas product is fed directly to a gas turbine and a boiler for the Rankine cycle.

In investigating a pressurized gasification reactor system, Kitzler et al, (2011) assessed the operation of a reactor varying pressure and temperature in a range of 1-5 bar and 700 °C-900 °C, respectively. The author finds that the synthesis gas can leave the gasifier at a temperature of 850 °C and an optimum pressure which for a small-scale integrated gasification combined cycle would be 5 bar. A challenge with the pressurized gasification reactor system is that operating beyond the atmospheric pressure leads to higher investment costs, which might not be worth the cost should there not be any thermodynamic benefits acquired from this system.

The operation of a pressurized gasification reactor in most instance does not improve the concentration of the synthesis gas generated in the process or has minor improvements. Szul et al, (2021) investigated the influence of pressure variation of a fluidized bed reactor from 1-2 bar in the biomass gasification of lignin and bark. The author notes that the variation in pressure had the most influence on the methane content of the synthesis gas product and decreased the overall flowrate of the synthesis gas produced. The influence of the pressure on the system can be explained by the Le Chatelier's principle which notes that an increase in pressure shifts the equilibrium of a reaction to the side with the lower molecule production. For the steam reforming of methane reaction in **Table 2-1**, this will be to the side of methane and water.

In another research study by Mahapatro & Mahanta, (2020) performed on a circulating bed gasifier varying pressure from 1 to 4 bars using a mixture of coal and biomass, a similar behaviour was noted where only the methane content of the synthesis gas is affected by the variation in pressure. The author further proves that an increase in pressure compliments the thermodynamic performance of the reactor, as the calorific value of the synthesis gas is improved along with the cold gas efficiency. An increase in the cold gas efficiency shows that the heat fed to the reactor is effectively used in reforming the feedstock to synthesis gas.

For the plasma gasification reactor not a lot of work has been done on the effects of pressurization and thus this study will assess the potential for the pressurization of the reactor. Specifically, the effects a pressurized synthesis gas product will have on the thermal efficiency and power produced for the power cycles. Various studies have proven that pressure has no effect on the synthesis gas composition besides the methane present in the synthesis gas, thus this aspect will not be considered. The synthesis gas generated from the NECSA demonstration

plant model does not contain any methane, which supports the assumption of increasing the pressure of the synthesis gas product stream without any changes to the composition.

2.9 Power Generation

2.9.1 Open Brayton Cycle

The Brayton cycle is a thermodynamic process that represents how a heat engine can directly combust a fuel source to produce heat and further extract that heat to generate mechanical work (Moran & Shapiro, 2006)**.** The Brayton cycle systems features a compressor, combustion chamber and a gas turbine. In this system air is continuously being drawn from the environment into the compressor which discharges it into the combustion chamber where it mixes with the fuel leading to the combustion of the fuel. The combustion of the fuel causes the temperature to escalate in the combustion chamber and this temperature is limited by the addition of air until a feasible temperature for the operation of a combustion chamber can be reached. Gas turbines were traditionally developed to combust natural gas, however the rising interest in biomass as an alternative fuel source has seen structural modification being made in the interest of synthesis gas combustion. Synthesis gas is a fuel with a low calorific value when compared to natural gas, thus the operational parameters in a synthesis gas firing gas turbine often differ, parameters such as temperature, pressure, air to fuel ratio, pressure ratio's, turbine inlet temperature, and isentropic efficiencies. These thermodynamic parameters affect the performance of the gas turbines along with the power production capability of the gas turbines.

Figure 2-10 represents the flow diagram of an open gas turbine along with the heat and power flow into the process.

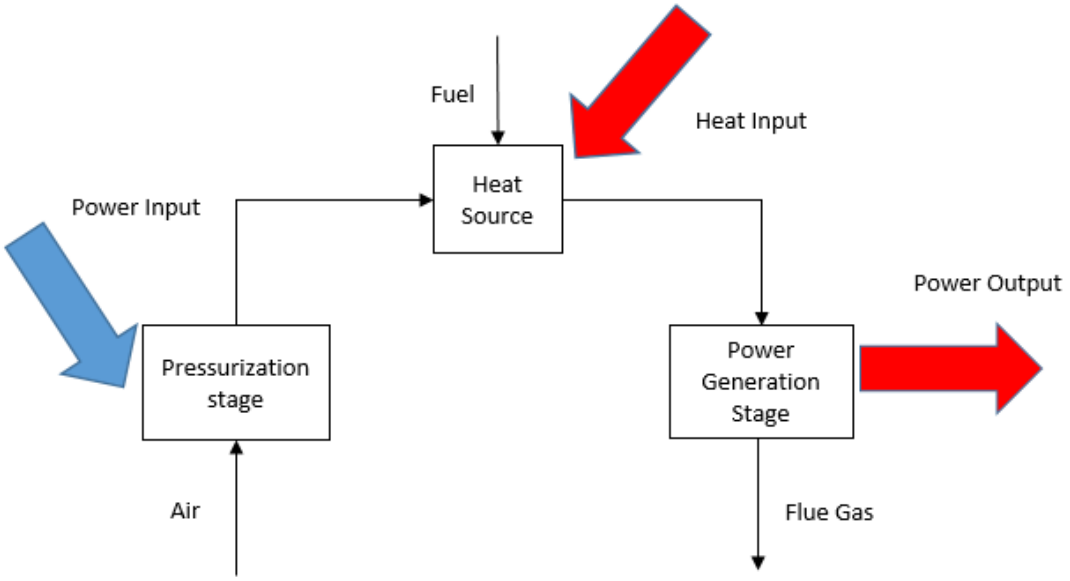


Figure 2-10: Brayton cycle process mass, heat and power flow system

Synthesis gas offers a number of variations to natural gas, since synthesis gas can be generated from a variety of biomass, fossil fuels and waste feedstock it often has varying compositions. The performance of a gas turbine driven by synthesis gas thus differs from case to case, owing to variations in the hydrogen and carbon monoxide content present in the synthesis gas.

Beyond the mechanical performance of the gas turbine system, there are similarities in the thermodynamic behaviour of gas turbines firing synthesis gas, natural gas or any other gaseous fuel. Parameters such as compression ratio, turbine inlet temperature, air to fuel ratio, isentropic efficiency of the turbine and compressor and the ambient temperature of the surroundings define the performance of the turbine (Rahman, et al., 2011). In the thermodynamic investigation of a gas turbine plant, Rahman et al, (2011) notes that parameters such as compression ratio, ambient temperature, air to fuel ratio and isentropic efficiency exhibit the strongest influence on the thermal efficiency of the gas turbine. An increase in the ambient temperature and air to fuel ratio can be noted to negatively impact the power output and the thermal efficiency of the gas turbine system.

There is no means of regulating parameters such as the air to fuel ratio as it varies from case study to case study, however in the design of Aspen Plus model for a gas turbine system such a parameter is used to control the turbine inlet temperature of a gas turbine. Depending on the size of a gas turbine and the temperature tolerance of the metal used, the operator of such a system has limited control on such parameters. Several of the parameters of influence on the

gas turbine are out of the user control as they are affected by the size of the gas turbine and the material of make, thus in the development of the Aspen Plus model, literature sources with similar operational dynamics will be consulted.

2.9.2 Steam Rankine Cycle

The Rankine power cycle can be categorized as a closed power cycle where a fuel source is combusted through a boiler and the heat from the hot combustion product is used to superheat the working fluid of the power cycle. The boiler is the heat source of the cycle through combustion of the fuel source in the presence of the air, and this heat is transfer to the pressurized working fluid before it can be expanded in the steam turbine designated as the power generation stage in **Figure 2-11**. The working fluid of this power cycle for various commercially available turbine systems is water due to its availability and thermodynamic behaviour.

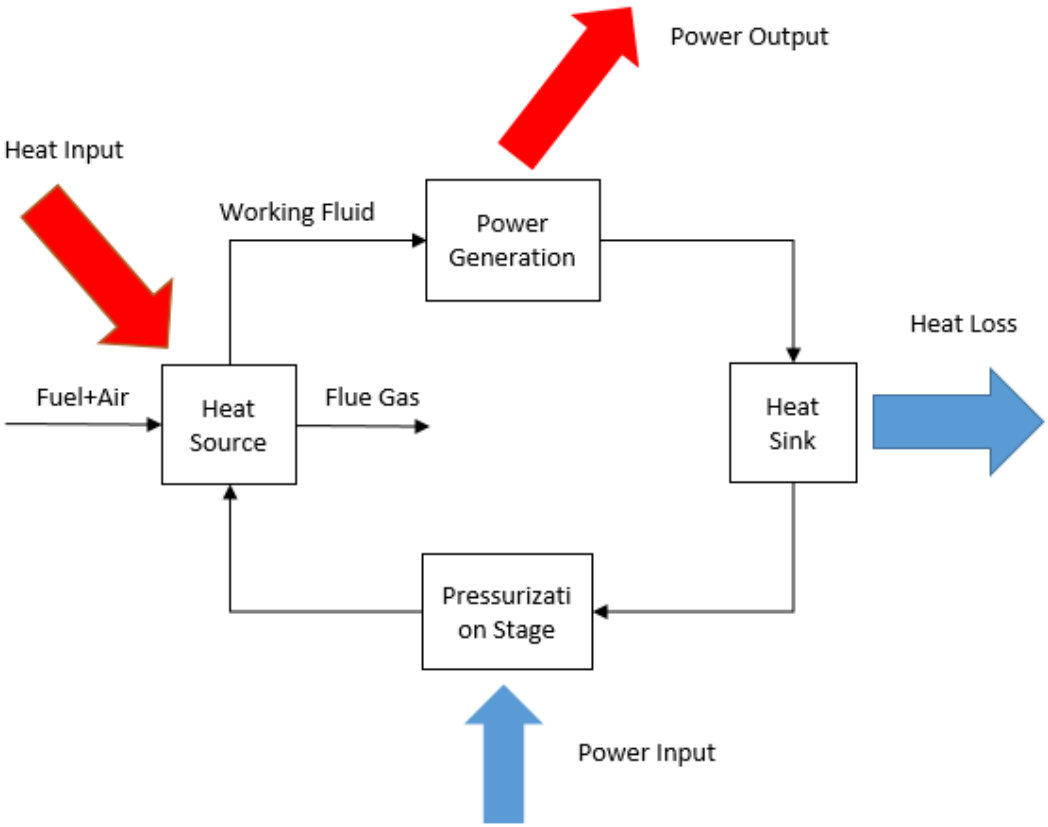


Figure 2-11: Rankine cycle process mass, heat and power flow system

The flow of heat in and out of this power cycle system can be seen in **Figure 2-11** with the heat sink representing the condenser while the heat source is representing the fuel-fired boiler of the power cycle.

In the use of biomass in Rankine cycles due to the low calorific value of the synthesis gas fuel, most studies often applied these cycles as means of recovering the waste heat from gas turbines in a combined power cycle. The power generation stage in the **Figure 2-11** is the most significant section of the cycle with the steam turbine being used in the expansion of the superheated working fluid to generate power.

There is a variety of heat recovery systems ranging from recuperating heat exchangers, economizers, heat recovery steam generators, steam turbines for the conversion of waste heat to power, etc. An investigative study performed by Andreasen et al, (2017) considers two heat recovery systems in the form of a steam Rankine cycle and an Organic Rankine cycle for the recovery of waste heat, with these two systems compared to each other to find which heat cycle is the better alternative and under which conditions. Two fuel sources are considered, with the first fuel source having a high sulphur content and the other a low sulphur content.

The results indicate that at large scale operations the steam Rankine cycle has a better net power production while at small scale operations the Organic Rankine cycle is found to have a better net power production. For the thermal efficiencies of the two different cycles, designs of the turbines indicate that the Organic Rankine cycle can reach a better efficiency than the steam Rankine cycle. The above can be assumed to indicate that low temperatures and small-scale operation of the Rankine cycle offer better results than the larger scale operations in terms of thermal efficiency. The performance of the Organic Rankine cycle can be accredited to the efficient design of the axial turbine for low power outputs.

Some crucial parameters in the thermodynamic performance of a steam turbine include the mass flowrate of steam into the turbine, turbine inlet temperature, pressure, steam turbine pressure ratio, isentropic efficiency, and material of design (not applicable for this study).

2.9.3 Combined Power Cycle

One of the biggest flaws for gas turbines is the exhaust process which usually features the spent hot gas stream at temperatures above 500 °C being cooled down and discarded to the environment without any form of waste heat recovery being applied. This flaw in the design restricts the thermal efficiency that can be achieved for this cycle as a substantial amount of thermal heat in this cycle is discharged to the environment. Means of remedying this shortfall

have been successfully implemented through the combined power cycle which recovers the waste heat from the exhaust of the gas turbine and seeks to use this heat to generate more power. This heat is usually extracted through a heat recovery steam generator in the combined power cycle which is the connecting block between the topping Brayton cycle and the bottoming Rankine cycle. The combined cycle typically has a Brayton cycle system as the main cycle or top cycle coupled to a Rankine cycle as the bottoming cycle which is the means of recovering the waste heat from the expanded flue gas product stream.

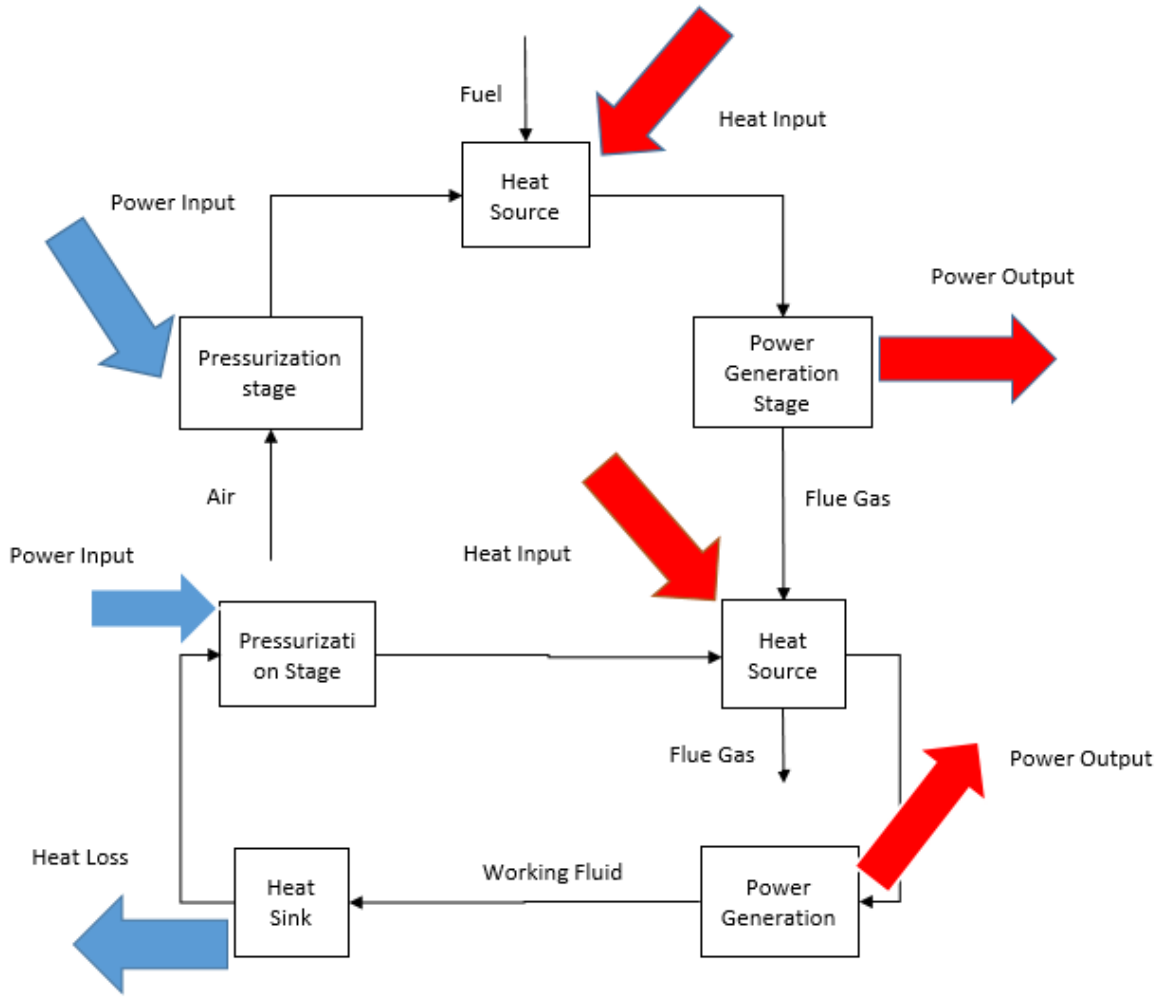


Figure 2-12: Combined power cycle process mass, heat and power flow system

The coupling of the Rankine cycle to the primary Brayton cycle has been proven to improve the thermal efficiency of the process. One of the benefits of operating the combined power cycle as depicted in **Figure 2-12** is that two power cycles being the Brayton cycle and the Rankine cycle can be operated using a singular heat source through the combustion of the fuel source in the presence of the air.

The driving force of this cycle is the topping Brayton cycle and the power generation capacity for this setup depend on the operational parameters of this cycle such as the mass capacity of the fuel, pressure of the cycle, turbine inlet temperature at which the cycle can operate, pressure ratio of the gas turbine and the compression ratio. These factors are the driving forces for the entire combined cycle as they determine the amount of waste heat in the exhaust stream of the gas turbine which is the heat source of the bottoming Rankine cycle.

2.9.4 Waste Heat Recovery

Waste heat refers to the heat from process streams that are rejected to the environmental without any means of recovering the sensible heat present in these streams. It has been estimated by Reddy et al, (2013) that about 20% to 50% of the energy used in industrial processes ends up as waste heat. The discharge of waste heat to the environment can be associated with the costs for the acquisition of cooling towers, fin-fan coolers and tall stacks for the fuel gas discarded from thermal processes (Reddy, et al., 2013). Waste heat is often low temperature heat that is discarded to the environment as recovery methods might be financially infeasible. The economic feasibility of a waste heat recovery system is influence by the quantity of the waste heat and the temperature possessed by the waste heat source (Reddy, et al., 2013). For heat engines some of the common waste heat recovery technologies includes the use of recuperation heat exchangers (economizers), using an organic Rankine cycle as the bottom cycle to recover the waste heat, and heat pumps used to reduce the fuel combusted & the waste heat temperature (Reddy, et al., 2013).

For a gas turbine power plant, Eveloy et al, (2016) investigated a heat recovery option using an organic Rankine cycle powered by the effluent flue gas stream of the gas turbine, with 1,1,1,3,3-pentafluoropropane (R245fa) being the working fluid of the ORC. The system is designed to ensure that the flame temperature or boiling point of the organic working fluid is not reached by using an intermediate fluid between the effluent flue gas from the turbine and the organic fluid of the ORC. The Organic Rankine cycle using R245fa is found to be highly effective in the recovery of heat, with a thermal efficiency of 12%. The use of an intermediate heat recovery system is found to have a negative influence on the overall thermal efficiency of the system, as the heat exchanger for this cycle has the second highest exergy destruction rate (Eveloy, et al., 2016).

Reshid et al, (2016) investigated the transient model of a waste heat recovery system (HRSG), recovering heat from the exhaust of a 5.2 MW gas turbine, and designed using the TRNSYS

simulation environment. The transient nature of the model presents some challenges in the study of heat recovery, two parameters were found to have substantial influence on the power generation output of the turbine and these parameters are i) the ambient temperature and ii) the mass flowrate of the fuel. An increase in the ambient temperature is found to negatively affect the power generation of the gas turbine with a 20% change in ambient temperature having a 0.7% impact on the power output of the gas turbine. A similar change has a 1.7% positive influence on steam generation through the HRSG. A change in the mass flowrate of the fuel has a proportional effect to the steam generation capacity and the power output of the gas turbine.

2.10 Small Scale Power Production Systems

One of the ways in which the energetic efficiency of power production systems can be improved, is using small-scale power production systems which create the opportunity for the decentralization of the power generation system. Having several small-scale power production units in different locations can reduce the need for transmission which causes the loss of several units of power (Tocci, et al., 2017). The decentralisation of the power generation unit empowers big energy users and municipalities to generate their own power, eliminating transmission losses and administrative redundancies. Currently a large amount of the South Africa's electricity is generated through 18 coal fired power plants which are in different provinces of the country, with 12 of these facilities located in the Mpumalanga Province, 3 facilities in Gauteng, 2 in Limpopo and 1 in the Free State Province. The other five provinces of the country have other means of power generation; however, most of their power comes from the coal fired power plants, meaning there is a lot of electricity transmission involved.

The centralised electricity grid in South Africa has its fair share of problems such as the ripple effect caused by malfunctions and damages to some of these coal power facilities. A minor incident such as a malfunction with the coal feeding system of one of the coal fired power plants has been met with rolling power blackouts in the whole country. Besides the malfunctions of some process units, other challenges include the maintenance of the infrastructure as some of these facilities are well beyond their estimated useful life. With there already being a severe strain on the power grid, maintaining portions of these power plants becomes a nightmare and can lead to power outages for some parts of the country.

Small-scale systems can open the market to other fuel sources such as solar, wind, biomass, hydro energy, geothermal and many others. With renewable energy sources, there is a potential

to develop power system with multiple fuel sources. The use of multiple energy sources in power generation facilities was firstly noted through the augmentation of coal-fired power plants with solar energy. Similar process setups can be adapted with biomass and solar energy as fuel sources of a small scale or even large-scale power generation facility. This can improve the economy of the country as most of these renewable energy sources are natural resources with no costs for their acquisition i.e., solar, geothermal, hydro and biomass. The costs involved in using these energy resources is through their extraction, i.e., solar panels and solar collectors for solar energy. Other energy resources such as biomass have the distinct advantage of being adaptable to current coal-fired power plants without drastic changes to the infrastructure.

The plasma gasification of biomass and waste feedstocks allows for the creation of smaller and more manageable power generation systems. The availability of biomass as a renewable energy source makes it's a great prospect in the operation of small-scale power generation facilities. There are already stockpiles of waste feedstocks across the world in landfills and the organic matter found in these feedstock supports their use as fuel sources. With the research that has been done in smaller plasma gasification reactors, designing an effective plasma gasification reactor is no longer a challenge. Adding the technological advances that have been achieved with small scale gas turbines specifically designed for the combustion of synthesis gas broadens the possibilities. The biggest obstacle associated with small scale power production systems is the high investment cost for these systems. Competing with large scale systems that have already been well established in the market, makes it difficult for small scale power production systems to be successfully applied.

Some of the factors reviewed that affect the application of a decentralized electricity grid or micro electricity grid are social, technical, economic, and environmental and policy related in nature (Akinyele, et al., 2018). Therefore, several small-scale power generation systems are currently developed to use fuel sources which are environmentally friendly, especially with regards to the low carbon emissions. Social factors include provision of affordable electricity to rural and low-income areas. The technical and economic factors include thermodynamic challenges of small-scale systems compared to macro systems, and economic operational challenges through the investments and construction of these systems.

This project will focus on the technical and economic aspect, which presents challenges to the application of small-scale systems for power generation using a theoretical means through the Aspen Plus software. The technical aspects will assess the thermodynamic feasibility of an

integrated plasma gasification combined cycle towards the generation of power from a plasma gasification reactor with a biomass feed capacity of 20 kg/hr. The power cycles investigated will not be limited to the combined power cycle, as the Brayton cycle and Rankine cycle will also be considered.

2.11 Industrial Scale Plasma Gasification Reactor

There are different industrial plasma gasification plants that are already well established and operating at larger capacities compared to the NECSA demonstration plasma gasification reactor plant. These plants operate at sizes ranging from 10 times that of the current plant up to 1 000 times, the capacity of the current plant.

The smallest plasma gasification reactor plant is a 5 ton/day research pilot plant processing municipal solid waste and other unspecified feedstock operating in Castellgali in Spain (vd Walt & Jansen, 2014). This plant has an operational capacity which is 10 times that of the NECSA demonstration plant.

Another plasma gasification reactor plant operating in Mihama-Mikata, Japan commissioned in 2002 operates at a capacity of 20 tons/day for Municipal solid waste and an additional capacity of 4 tons/day for sewage sludge. This plant produces heat for the waste drying process and is operated by the AlterNRG Company (vd Walt & Jansen, 2014). The AlterNRG Company operates another plant at the Westinghouse Plasma Centre in Madison USA processing 100 different types of feedstocks at a capacity of 48 tons/day to generate synthesis gas for various applications (vd Walt & Jansen, 2014).

The largest plant operates at a capacity of 1 000 tons/day through a joint venture between three different companies in Air Products/AlterNRG/Westinghouse in Teesside, United Kingdom (vd Walt & Jansen, 2014).

Many of these industrial plasma gasification reactor plants are designed to produce biofuels. Some of these plants have encounter some difficulties in operation due to the costs associated with the plasma technology.

2.12 Aspen Plus Modelling

Amongst some of the computer software's used for the modelling of different process systems, Aspen Plus has been a vital tool in the investigations of chemical, and thermal processes. With challenges such as shortage of funds, as is always the case in most research and development projects, the Aspen Plus software creates a platform for research to be conducted. The models

developed can be validated using experimental data from literature studies that had the financial capacity to design actual process systems.

There are several processes that can be modelled using the Aspen Plus software and these processes tend to have different thermodynamic and physical behaviours. The different processes that can be simulated using the Aspen Plus software include air separation, chemical processes, electrolytic processes, gas processing, and metallurgical processes to name a few. The simulations of these processes are driven by the physical properties which determine the results obtained in the process with regards to the mass and energy balances. Inadequate physical properties can have a severe impact on the accuracy of the results generated through a model for a particular process.

The studies conducted in Aspen Plus for the modelling of the plasma gasification reactor were broad and considered a variety of parameters that have an influence on the performance of the reactor. Some of the parameters include:

1. Different biomass feedstock compositions,
2. A range of plasma gases,
3. Various heat ranges the plasma torches can operate in,
4. Different equivalent ratios, and
5. Different fuel to air ratios.

In the development of most models, two approaches were used for the reactor with i) the equilibrium approach using the minimization of the Gibbs free energy and ii) the kinetic approach which involves the use of a kinetic model found in previous literature studies (Tan, 2018). The equilibrium approach is the one mostly preferred in the numerous literature studies that have been conducted using Aspen Plus, as it forms a broad picture into the behaviour of the reactor without focus on the performance of specific sections within the reactor (Tan, 2018). The kinetic model approach is a more detailed means of developing a model and often relies on scientific data from an actual plasma gasification reactor. This system offers the advantage of producing more accurate results with regards to the reactor being modelled. Different reactions under different conditions tend to have differing kinetics, which presents a limitation with the use of the kinetic model.

The Gibbs free energy minimization approach of developing a plasma gasification reactor model is a more universal approach. This approach presents a more holistic view into the operation of the plasma gasification reactor by focusing on the equilibrium behaviour of the

reactor rather than steps it took to reach the equilibrium state. The results generated from this model approach will have some degree of variation to experimental results. In a study by Cekovic et al, (2019) these variations are attributed to the model parameters not being versatile enough to account for the differences between the model and the actual reactor. There will always be differences between theoretical systems and actual systems, as theoretical systems can't fully account for all the behaviours of experimental systems, as a result of some assumptions made in their development. In the investigation to be performed, the Gibbs free energy minimization approach will be applied to model the reactor and to improve the accuracy of the results, data generated in the model of a demonstration plant will be used.

The modelling of the power cycles is less detailed than that of the plasma gasification reactor, the power cycles in most instances emulates the theoretical behaviour presented by various literature sources studied over the decades. The approach for developing the model of these power generation systems depends on the type of power cycle used i.e., Brayton power cycle, Rankine power cycle and the combined power cycle.

2.13 References

Akinyele, D., Belikov, J. & Levron, Y., 2018. Challenges of Microgrids in Remote Communities: A STEEP Model Application. *Energies,* 14 February.11(432).

Akpan, V. E. & Olukanni, D. O., 2020. Hazardous Waste Management: An African Overview. *Recycling,* 5(15), pp. 1-24.

Alive2green, 2019. *South Africa is drowning in its own waste – are our regulators taking this crisis seriously?*. [Online]
Available at: https://alive2green.com/south-africa-is-drowning-in-its-own-waste-are-our-regulators-taking-this-crisis-seriously/
[Accessed 26 September 2020].

Andreasen, J. G., Meroni, A. & Haglind, F., 2017. A Comparison of Organic and Steam Rankine Cycle Power Systems for Waste Heat Recovery on Large Ships. *Energies,* 10(547).

Anwar, Z., Gulfraz, M. & Irshad, M., 2014. Agro-industrial lignocellulosic biomass a key to unlock the future bio-energy: A brief review. *Journal of Radiation Research and Applied Sciences,* Volume 7, pp. 163 - 173.

Argonul, A. et al., 2021. Syngas cleaning for coal to methanol demo plant – H2S and COS removal. *Chemical Engineering Communications,* 208(7), pp. 950-964.

Arnif, I., Indartono, Y. S., Susanto, H. & Adriansyah, W., 2018. *Experimental Study of Gas Cleaning System on Biomass Gasification.* Bandung, AIP Publishing, pp. 030004-1 - 030004-8.

Averda Editor, 2018. *Averda.* [Online]
Available at: https://averda.co.za/news/averdas-class-hazardous-waste-landfill/
[Accessed 30 September 2020].

Balas, M., Lisy, M., Skala, Z. & Pospisil, J., 2014. Wet scrubber for cleaning of syngas from biomass gasification. *Advances in Environmental Sciences, Development and Chemistry,* 17 July.pp. 195-201.

Bandara, J. C. et al., 2021. Air gasification of wood chips, wood pellets and grass pellets in a bubbling fluidized bed reactor. *Energy 233 (2021)*, 12 June, 233(121149), pp. 1-13 (Online).

Basu, P., 2018. Biomass Gasification, Pyrolysis and Torrefaction: Practical Design and Theory. 3rd ed. Nova Scotia: Elsevier Academic Press.

Bhagwat, S., Ratnaparkhe, S. & Kumar, A., 2015. Biomass Pre-treatment Methods and Their Economic Viability for Efficient Production of Biofuels. *British Biotechnology Journal,* 8(2), pp. 1-17.

Botros, B. B. & Brisson, J. G., 2013. Improving high temperature heat capture for power generation in gasification plants. *International Journal of Heat and Mass Transfer,* 26 February, Volume 61, pp. 129-137.

Bracmort, K., 2016. *Is Biopower Carbon Neutral?,* Washington DC: Congressional Research Service.

Cekovic, I. et al., 2019. Modelling of Wood chips gasification process in Aspen Plus with multiple validation approach. *Chemical Industry & Chemical Engineering Quarterly,* 25(3), pp. 217-228.

Chartier, Y. et al., 2014. *Safe management of wastes from health-care activities.* 2nd ed. Geneva, Switzerland: World Health Organisation.

Cheah, S. et al., 2016. Effects of thermal pretreatment and catalyst on biomass gasification efficiency and syngas composition. *Green Chemistry,* 16 September, 18(23), pp. 6291-6304.

Department of Environmental Affairs. 2018. South Africa State of Waste. A report on the state of the environment. Final draft report. Department of Environmental Affairs, Pretoria. 112 pp.

Dias, T. A. d. C., Lora, E. E. S., Maya, D. M. Y. & Olmo, O. A. d., 2021. Global potential assessment of available land for bioenergy projects in 2050 within food security limits. *Land Use Policy,* 26 March, Volume 105, pp. 1-15 (Online).

Energy, U. D. o., n.d. *Energy.gov.* [Online]
Available at: https://www.energy.gov/eere/bioenergy/biomass-resources
[Accessed 12 February 2021].

Eveloy, V. et al., 2016. Waste Heat Recovery from Gas Turbine Flue Gases for Power Generation Enhancement in a Process Plant. *International Journal of Thermal and Environmental Engineering* , 12(1), pp. 53-60.

Fatma, S. et al., 2018. Lignocellulosic Biomass: A Sustainable Bioenergy Source for the Future. *Protein & Peptide Letters,* 25(2), pp. 1-16.

Fraser, T., 2021. Does social capital boost or block renewable energy siting? South African solar politics in comparison. *Energy Research & Social Science,* 71(101845).

Gadek, W. et al., 2016. Gasification and pyrolysis of different biomasses in lab scale system: A Comparative Study. Gliwice, EDP Sciences.

Greeff, I., 2022. Using synthesis gas heat to produce work via an externally fired gas power cycle. *Energy,* 239(122132).

Greeff, I. L., 2004. *Recovery of work from exothermic chemical reaction systems by means of turbine expansion,* Eindhoven: PhD of Engineering Thesis, Eindhoven University of Technology.

Greeff, I. L., 2021. Integration of an externally fired gas power cycle with a synthesis gas production process, Johannesburg: University of the Witwatersrand.

Greeff, I. L., Ptasinski, K. J. & Janssen, F. J., 2001. Integration of a turbine expander with an exothermic reactor for the combined production of power and ammonia. *Proceedings of ECOS 2001,* Volume 1, pp. 369-375.

Greeff, I. L., Visser, J. A., Ptasinski, K. J. & Janssen, F. J., 2002. Utilisation of reactor heat in methanol synthesis to reduce compressor duty – application of power cycle principles and simulation tools. *Applied Thermal Engineering*, Volume 22, pp. 549-558.

Greeff, I. L., Visser, J. A., Ptasinski, K. J. & Janssen, F. J., 2003. Integration of a turbine expander with an exothermic reactor loop – flow sheet development and application to ammonia production. *Energy – The International Journal*, 28(14), pp. 1495-1509.

Greeff, I. L., Visser, J. A., Ptasinski, K. J. & Janssen, F. J., 2003. *Mathematical modelling of a process gas power cycle for the direct recovery of exothermic reaction heat.* Sun City Johannesburg, SAIChE Congress.

Gu, H. et al., 2013. Waste biomass from production process co-firing with coal in a steam boiler to reduce fossil fuel consumption: A case study. *Journal of Energy Chemistry*, Volume 22, pp. 413-419.

Gulec, F. et al., 2021. Hydrothermal conversion of different lignocellulosic biomass feedstocks – Effect of the process conditions on hydrochar structures. *Fuel,* 15 June, Volume 302, pp. 1-11 (Online).

Hlina, M., Hrabovsky, M., Kavka, T. & Konrad, M., 2014. Production of high quality syngas from argon/water plasma gasification of biomass and waste. *Waste Management,* Volume 34, pp. 63-66.

Kacik, F. et al., 2016. Chemical Alterations of Pine Wood Lignin during Heat Sterilization. *BioResources,* 11(2), pp. 3442-3452.

Kibret, H. A., Kuo, Y.-L., Ke, T.-Y. & Tseng, Y.-H., 2021. Gasification of spent coffee grounds in a semi-fluidized bed reactor using steam and CO2 gasification medium. *Journal of the Taiwan Institute of Chemical Engineers,* Volume 119, pp. 115-127.

Kitzler, H., Pfeifer, C. & Hofbauer, H., 2011. Pressurized gasification of woody biomass—Variation of parameter. *Fuel Processing Technology*, 8 January, Volume 92, pp. 908-914.

Koido, K. & Iwasaki, T., 2018. Biomass Gasification: A Review of Its Technology, Gas Cleaning Applications, and Total System Life Cycle Analysis. In: M. Poletto, ed. *Lignin - Trends and Applications.* s.l.:IntechOpen.

Liu, Y. H., Chen, W., Che, D. F. & Cao, Z. D., 2010. *Comparisons of four quench methods for high temperature Syngas-Exergy Analyses.* China, AIP Publishing, pp. 674-679.

Lundqvist, A., 2020. Future development of bioenergy in South Africa: A study of increased use of available biomass for the future development of renewable energy in South Africa, Vasteras: Malardalen University.

Mahapatro, A. & Mahanta, P., 2020. Gasification studies of low-grade Indian coal and biomass in a lab-scale pressurized circulatingfluidized bed. *Renewable Energy,* Volume 150, pp. 1151-1159.

Matsika, R., Erasmus, B. F. N. & Twine, W. C., 2013. Double jeopardy: The dichotomy of fuelwood use in rural South Africa. *Energy Policy,* Volume 52, pp. 716-725.

Mdhluli, F. T. & Harding, K. G., 2021. Comparative life-cycle assessment of maize cobs, maize stover and wheat talks for the production of electricity through gasification vs traditional coal power electricity in South Africa. *Cleaner Environmental Systems,* 3(100046).

Moran, M. J. & Shapiro, H. N., 2006. *Fundamentals of Engineering Therrmodynamics.* 5th ed. Chichester: John Wiley & Sons.

Muvhiiwa, R. F., Sempuga, B., Hildebrandt, D. & Van der Walt, J., 2018. Study of the effects of temperature on syngas composition from pyrolysis of wood pellets using a nitrogen plasma torch reactor. *Journal of Analytical and Applied Pyrolysis,* 13 January, Volume 130, pp. 159-168.

Muvhiiwa, R., Sempuga, B. & Hildebrandt, D., 2021. Using the G-H space to show heat and work efficiencies associated with nitrogen plasma gasification of wood. *Chemical Engineering Science 243 (2021) 116793,* 2021(116793), pp. 1-16 (Online).

Olaniyi, F. C., Ogola, J. S. & Tshitangano, T. G., 2018. A Review of Medical Waste Management in South Africa. *Open Environmental Sciences,* Volume 10, pp. 34-45.

Olukanni, D. O., Olujide, J. A. & Kehinde, E. O., 2017. Evaluation of the Impact of Dumpsite Leachate on Groundwater Quality in a Residential Institution in Ota, Nigeria. *Covenant Journal of Engineering Technology (CJET),* 1(1), pp. 1-16.

Pang, Y. et al., 2018. Plasma-Assisted Biomass Gasification with Focus on Carbon Conversion and Reaction Kinetics Compared to Thermal Gasification. *Energies,* 20 May, Volume 11, pp. 1-24.

Payne, J. & Pitchford, R., 2015. *Reuters.* [Online]
Available at: https://www.reuters.com/article/us-nigeria-lead-casualties/at-least-28-children-

killed-by-lead-poisoning-in-nigeria-idUSKBN0O013I20150515
[Accessed 02 October 2020].

Perold, J., Greeff, I. L., Ptasinski, K. J. & Janssen, F. J., 2001. Using a turbine expander to recover exothermic reaction heat – a case study on a phthalic anhydride process. *South African Journal of Chemical Engineering,* 13(2), pp. 1-14.

Prasad, G., 2010. *Bioenergy, rural development and poverty alleviation in Southern Africa,* Cape Town: University of Cape Town Energy Research Centre.

Rahman, M. M., Ibrahim, T. K. & Abdalla, A. N., 2011. Thermodynamic performance analysis of gas-turbine power-plant. *International Journal of the Physical Sciences,* 6(14), pp. 3539-3550.

Reddy, C. C., Naidu, S. V. & Rangalah, G. P., 2013. *Waste Heat Recovery Methods and Technologies,* Visakhapatnam: ChemEngOnline.

Reshid, M. N., Muhamad, W. M. W. & Majid, M. A. A., 2016. Transient Simulation of a Waste Heat Recovery from Gas Turbine Exhaust. *Journal of Applied Sciences,* 15 December, Volume 17, pp. 22-31.

Rezaei, H., Panah, F. Y., Lim, C. J. & Sokhansanj, . S., 2020. Pelletization of Refuse-Derived Fuel with Varying Compositions of Plastic, Paper, Organic and Wood. *sustainibility,* 6 June, Volume 12, pp. 1-11.

Ritchie, H. & Roser, M., 2020. *Energy,* s.l.: OurWorldInData.org.

Schuenemann, F., Msangi, S. & Zeller, M., 2018. Policies for a Sustainable Biomass Energy Sector in Malawi: Enhancing Energy and Food Security Simultaneously. *World Development,* Volume 103, pp. 14-26.

Shayan, E., Zare, V. & Mirzaee, I., 2018. Hydrogen production from biomass gasification: a theoretical comparison of using different gasifying agents. *Energy Conversion and Management,* 11 January, Volume 159, pp. 30-41.

Surma, J. E., 2010. Why Plasma?. *Cogeneration and Distributed Generation Journal,* 25(2), pp. 18-32.

Svoboda, K., Pohořelý, M., Hartman, M. & Martinec, J., 2009. Pretreatment and feeding of biomass for pressurized entrainedflow gasification. *Fuel Processing Technology,* Volume 90, pp. 629-635.

Szul, M., Głód, K. & Iluk, T., 2021. Influence of pressure and CO2 in fluidized bed gasification of waste biomasses. *Biomass Conversion and Biorefinery,* Volume 11, pp. 69-81.

Tan, B. H., 2018. *Process Simulation of Plasma Gasification for Landfill Waste,* Stockholm: kTH Royal Institute of Technology.

Thapa, S., Bhoi, P. R., Kumar, A. & Huhnke, R. L., 2017. Effects of Syngas Cooling and Biomass Filter Medium on Tar Removal. *Energies,* 11 March, 10(349), pp. 1-12.

Tocci, L., Pal, T., Pesmaz, I. & Franchetti, B., 2017. Small Scale Organic Rankine Cycle (ORC): A Techno-Economic Review. *Energies,* 10(413), pp. 1-26.

van der Walt, I. J., Jansen, A. A. & Crouse, P. L., 2017. Plasma-Assisted Treatment of Municipal Solid Waste: A Scenario Analysis. *Plasma Chem Plasma Process,* 28 January, Volume 37, pp. 763-782.

vd Walt, I. J. & Jansen, A. A., 2014. *A very small plasma gasification system.* Marrakech, Morocco, 4th International Round Table on Thermal Plasmas for Industrial Applications: Challenges and Opportunities.

Xu, J. et al., 2021. Prediction and modeling of the basic properties of biomass after torrefaction pretreatment. *Journal of Analytical and Applied Pyrolysis,* 159(105287).

Yao, Z. et al., 2021. Demonstration and multi-perspective analysis of industrial-scale co-pyrolysis of biomass, waste agricultural film, and bituminous coal. *Journal of Cleaner Production,* 4 January, Volume 290, p. 125819.

Yong, Y. S. & Rasid, R. A., 2021. Process simulation of hydrogen production through biomass gasification: Introduction of torrefaction pre-treatment. *International Journal of Hydrogen Energy,* 27 July, Volume In Press, Corrected Proof, pp. 1-12 (Online).

Zafar, S., 2021. *BioEnergy Consult.* [Online]
Available at: https://www.bioenergyconsult.com/biomass-energy-introduction/
[Accessed 06 March 2021].

Chapter 3 Methodology

3.1 Introduction

This chapter will present the thought process behind the development of the Aspen Plus models for the plasma gasification reactor and the power cycles. This model development process was split into two sections namely the plasma gasification reactor and the power cycles such as gas turbines, steam turbines, and combined power cycles for the conversion of synthesis gas to power. A detailed model and validation phase is carried out for the plasma gasification reactor due to the availability of data generated for a demonstration plant reactor model previously developed by NECSA. For the power cycles the development of the model involve simple power cycles and a range of variations of these models to assess how their thermodynamic performance will differ. A simple economic analysis will also be done to present the investment costs, maintenance and operational costs associated with these small-scale power generation systems.

3.2 Plasma Gasification Reactor

3.2.1 Assumptions

Several assumptions made for this study relate to the development of the Aspen Plus models for the plasma gasification reactor and these can be seen below.

- The Peng-Robinsons equations of state with the Boston-Mathias modification property will be the physical property method used in the simulation of the process. This physical property method is used in gas processing, petrochemical and refinery applications, the behaviour of the gases involved in this process fit into this thermodynamic physical property method.
- All of the processes being modelled are at steady state conditions.
- The effect of the synthesis gas cleaning process in the form of a scrubber is negligible due to the low content of toxic materials such as NO_x, HCl and H_2S.
- For non-conventional solids such as the feedstock and ash, the HCoalgen and DCoalligt property method is used in the estimation of the biomass formation enthalpy, specific heat capacity in constant pressure and chemical density based on the proximate and ultimate analysis.
- The biomass stream (FEED) and ASH is classified as a non-conventional stream

- A pressurized synthesis gas stream (5 bar and 5.5 bar) is produced for some of the cases with the assumption that the plasma gasification reactor can operate at pressurized conditions without severe impact on the composition of the produced synthesis gas.

3.2.2 Flowsheet Description of the Demonstration Unit

The process under analysis for this study is a synthesis gas generation system that features a 15 kW DC Arc Nitrogen torch plasma gasification reactor system. A diagram of the NECSA demonstration system is shown in **Figure 3-1** featuring the preparing stages of the biomass and the cleaning process for the crude synthesis gas produced.

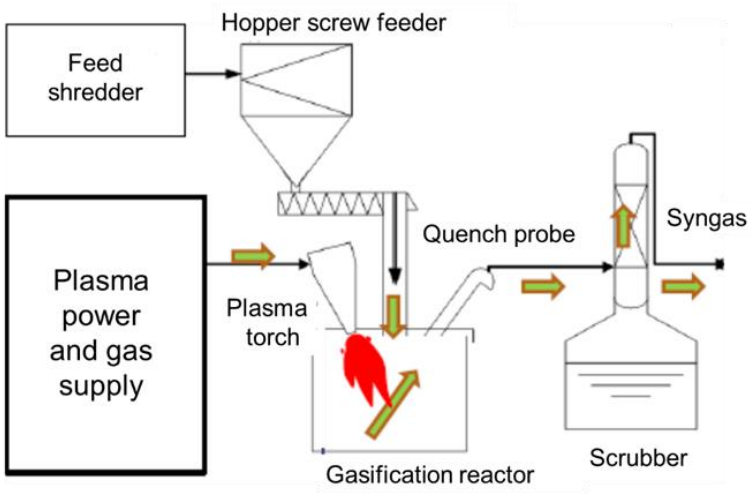


Figure 3-1: Plasma Gasification Demonstration Plant Diagram (Ncwane, et al., 2021)

The process features a feeding system as can be seen in **Figure 3-1**, this system is responsible for preparing the biomass and feeding it into the reactor. The biomass must meet reactor requirements such as size, organic matter content, moisture content and other plant parameters to assess its suitability prior to the gasification process. Biomass material is charged to the feed shredder where it is shredded to a size of +/- 5 mm (Motau, et al., 2017) and thereafter passes through the feed hoppers which regulates the flowrate of the biomass being fed into the reactor. The hopper screw feeder has a series of valves and a fan for controlling the flowrate of the feedstock to be gasified in the reactor.

The gasification process in this demonstration plant takes place in the plasma reactor which operates at a temperature of 1 000 °C and a pressure of 84 kPa (Motau, et al., 2017). The reactor is well insulated and assists in minimizing the loss of heat to the surroundings, the heat

required for the reaction is supplied by a DC arc plasma torch. The plasma torch is driven by nitrogen as the plasma gas however, to ensure a suitable composition of the synthesis gas with regards to H_2 and CO, the torch allows for an additional stoichiometric stream of oxygen to be added as plasma. The oxygen supply of the process is tightly regulated to avoid the conversion of the CO into CO_2 which not only increases the greenhouse emission content of the process but also dilutes the synthesis gas reducing its calorific value. Depending on the feedstock used for the process i.e., in the case of wood chips, the main products of the synthesis gas are hydrogen (H_2) and carbon monoxide (CO), along with small quantities of CO_2, H_2S, H_2O, HCl and other impurities. A large presence of the plasma gas is expected in the synthesis gas product from the reactor due to the plasma gas being in direct contact with the biomass and synthesis gas produced from the biomass.

The synthesis gas product leaving the reactor is usually at a high temperature of 1 000 °C and passes through a quench probe aimed at cooling down the synthesis gas in preparation for its cleaning in the scrubber. The quench probe used for this process is a water quenching system and it has a rapid cooling mechanism that reduces the temperature of the synthesis gas quickly to final temperatures of 50 °C to 60 °C (Motau, et al., 2017). The scrubber is responsible for the removal of impurities such as H_2S and HCl, the solvent used for the scrubber is water through a packed bed scrubber with three spray nozzles (Motau, et al., 2017). The synthesis gas from the quench probe enters the scrubber at a temperature of 50 °C and after the scrubbing process exits at a temperature of 42 °C.

The operation of the plasma gasification reactor can be further scrutinized for a better understanding of the process, and this will be done in the section 3.2.3.

3.2.3 Plasma Gasification Reactor

A model was set up in Aspen Plus and validated against data found in literature. This model which was developed in a study by Minutillo et al, (2009) can be broken down into different units operates as shown in **Figure 3-2**.

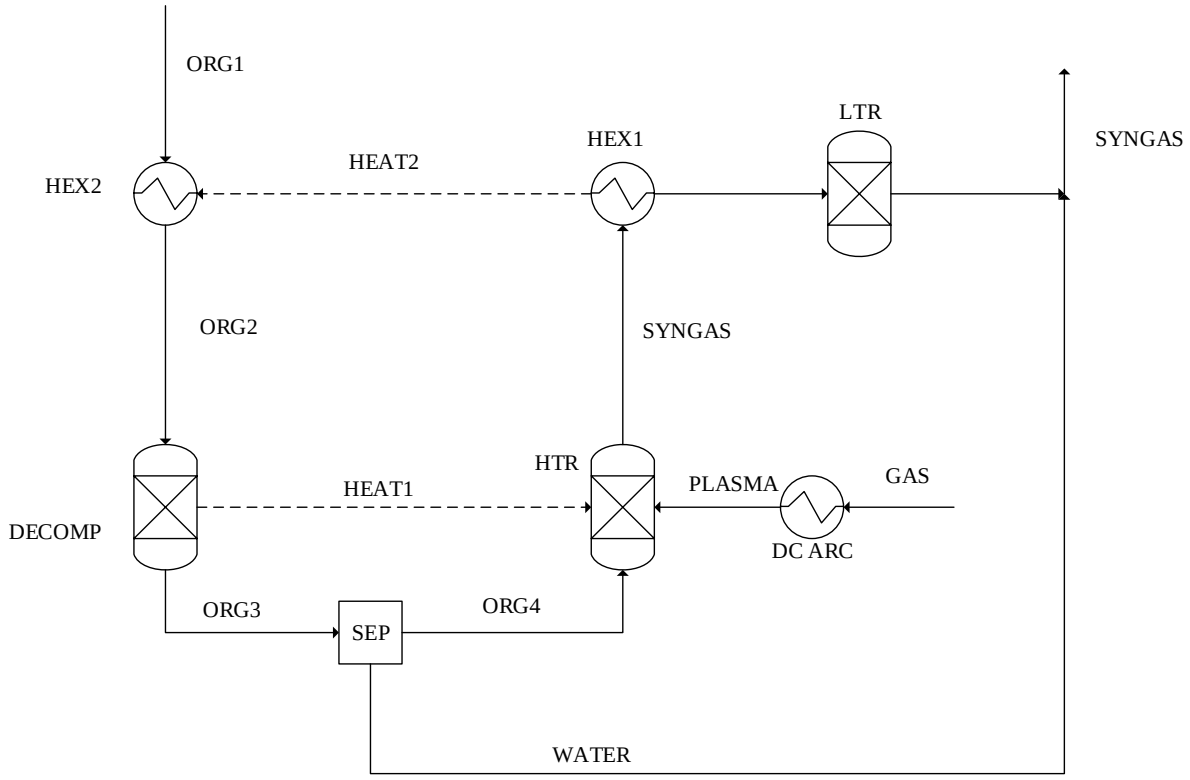


Figure 3-2: Theoretical Plasma Gasification Reactor Model (Minutillo, et al., 2009)

Figure 3-2 shows the stages involved in the gasification of biomass, from the instance it enters the reactor, to the moment where the product synthesis gas leaves the reactor. The pre-treated biomass represented by the stream ORG1 enters the reactor and some of the heat from the synthesis gas product along with the plasma gas inside the reactor (HEX1), heats up the biomass through HEX2 driving the decomposition of the biomass into its elemental constituents. The structural decomposition of the biomass has been observed to occur at temperatures between 200 °C and 600 °C (Okoroigwe, et al., 2016 & Babinszki, et al., 2021) depending on moisture content and type of biomass feedstock used. Lignocellulose biomass is the most difficult biomass to decompose due to the presence of the various layers which decompose at various temperatures. The hemicellulose layer decomposes at a temperature range of 150 – 350 °C, the cellulose layer at a temperature range of 275 – 350 °C and lastly the lignin a temperature range of 250 – 500 °C (Saddawi, et al., 2010 & Rao Pala, et al., 2017). The decomposition of the biomass is according to the ultimate and proximate analysis of the feedstock used for the process, and these feedstocks tend to vary in moisture, ash, carbon, hydrogen and oxygen contents to name a few.

The water present in the decomposed biomass is evaporated and leaves the reactor with the effluent synthesis gas product, while the organic matter (solid and gas) undergoes gasification

in the high temperature region (HTR) of the reactor directly fired by the plasma gas. The HTR is responsible for the gasification of the decomposed biomass, through an equilibrium model following the Gibbs free energy minimization principles (Minutillo, et al., 2009). The HTR tends to operate at high temperatures which have been approximated to an average of 2 500 °C (Minutillo, et al., 2009) to account for heat losses in the development of models. A DC plasma arc supplies the heat for the gasification process by generating plasma at temperatures around 13 000 °C, however the temperature of the plasma usually drops as it flows and by the time it comes to contact with the biomass it is between 2 700 °C and 4 500 °C (Sesotyo, et al., 2019).

The lower temperature region (LTR) of the plasma gasification reactor is responsible for reforming the crude synthesis gas product generated in the HTR, where reactions such as the water shift reaction, hydrogen sulphide synthesis reaction and other side product reactions occur. This part of the reactor operates at temperatures in the range of 800 °C – 1 200 °C (Minutillo, et al., 2009 & Sesotyo, et al., 2019). The thoroughly reformed synthesis gas product combined with the evaporated water than leaves the reactor flowing to other sections of the plant.

In reviewing the data obtained from NECSA the literature model can be updated to fit the NECSA model data according to the properties of the synthesis gas product. The performance parameters of note in consolidating the plasma gasification reactor model from literature with the data from the demonstration plant model include the temperature (°C) of operation, the pressure (bar), the heat duty (kW) of the plasma torch, the heat loss (kW) from the quench probe, the flow of heat (kW) in the process and lastly the mass flowrate (kg/hr) of the synthesis gas product.

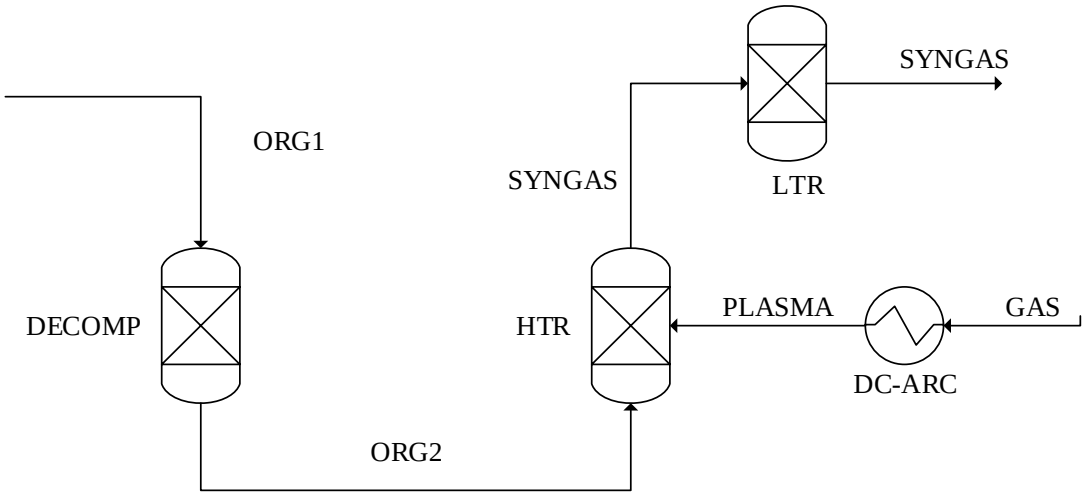


Figure 3-3: Consolidated Plasma Gasification Reactor Model

Figure 3-3 presents the consolidated model for the plasma gasification reactor in the demonstration plant from NECSA with regards to the flow of heat and other operational conditions like there being no evaporation of the water from the decomposed biomass stream as previously shown in **Figure 3-2** and therefore HEX1 and HEX2 blocks were removed. The flow of the feedstock throughout the different stages of the decomposition process is still similar for **Figure 3-2** and **3-3**. Replicating the behaviour of the demonstration reactor from NECSA helps in formulating other studies on this reactor system using different fuel feedstocks under similar mass flow capacities. In understanding the behaviour of the wood chips plasma gasification system at equilibrium, extrapolations can be done to fit this behaviour into a potential system using other organic feedstocks such as refuse derived fuel (RDF), and municipal solid waste.

3.2.4 Plasma Gasification Reactor Aspen plus Model

The Aspen plus model for the gasification reactor involves a 15 kW Nitrogen plasma reactor mainly using woodchips as a feedstock but, can test other feedstock such as municipal solid waste and refuse derived waste. The Aspen model for the reactor is provided in **Appendix A.1** featuring an RYIELD block for the decomposition chamber.

The HTR and LTR are modelled using the RGIBBS block which simulates the equilibrium nature of the gasification reaction through the Gibbs minimization energy principles. The DC-ARC block which features the HEATER block operates at a heat duty of 20.72 kW and a pressure of 84.5 kPa. The ash and other residues are deposited to the bottom of the plasma gasification reactor upon completion of the gasification process, and these are separate from the synthesis gas using the SEP block in Aspen Plus.

3.2.5 Hypothetical Pressurized Plasma Gasification Reactor

Several case studies assessed in this study involve a hypothetical scenario where the synthesis gas product from the plasma gasification reactor is pressurized without changes to the temperature (°C) or mass flowrate (kg/hr). A potential model for this hypothesized reactor system can be seen in **Figure 3-4** with a pressurized plasma gas entering the reactor.

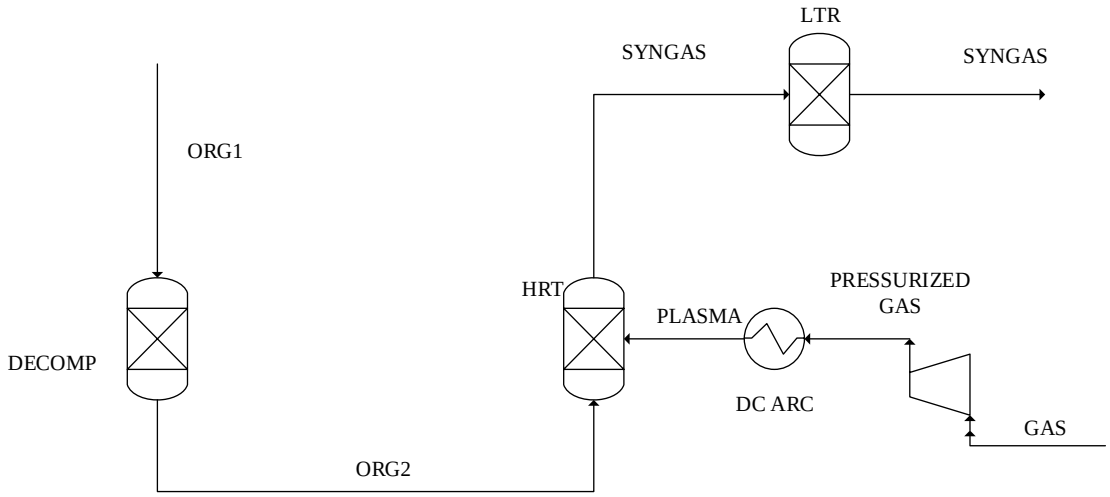


Figure 3-4: Hypothetical Pressurized Plasma Gasification Reactor

The hypothesized modelled case studies only involve the pressure (bar) changing in the synthesis gas product stream without any changes to the temperature or mass flowrate or the calorific value of the generated synthesis gas product.

The purpose of this hypothetical case study would be to investigate the effect of a pressurized synthesis gas product on downstream processes such as the different power cycles. This scenario will allow the synthesis gas to be fed to a turbine expander for generating power with the sensible heat found from this product. It's further assumed that the expanded syngas can be directly fed to a combustion chamber in the gas turbine without any cleaning being required. The purpose of this case study is to assess the possibility of extracting work from the high temperature heat.

3.2.6 Synthesis Gas Pre-treatment Process

The synthesis gas generated from the plasma gasification reactor passes through a phase of treatment processes before it can be suitable for use in the power cycles. This pre-treatment process includes a quench probe, a scrubber vessel which for this model has been converted to a synthesis gas dryer as a result of the low impurities content in the synthesis gas from the demonstration plant. Lastly a blower is used to pressurize and remove any water still present

in the synthesis gas product. This three-phase pre-treatment process can be seen in **Figure 3-5** as adapted from the demonstration plant.

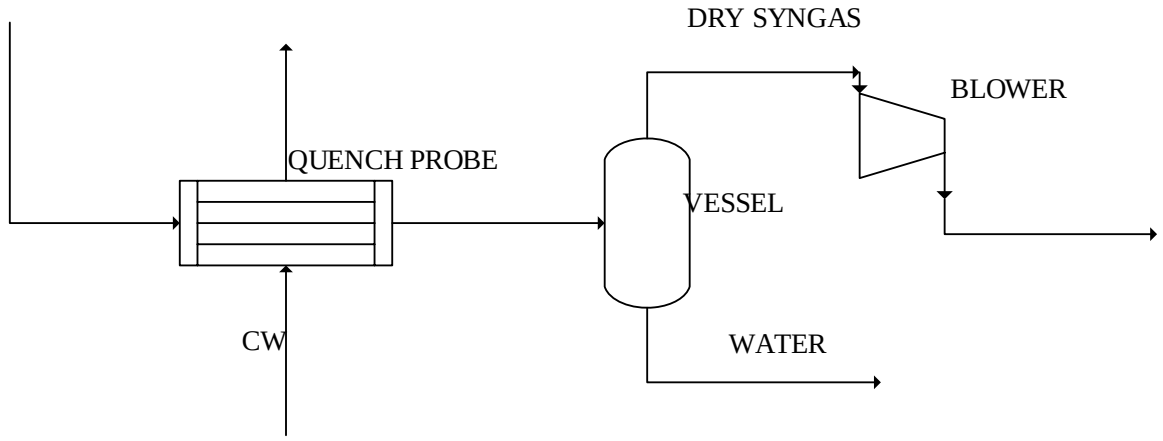


Figure 3-5: Pre-treatment Phase of the Synthesis Gas

The quench probe is a water quench system which rapidly cools the hot synthesis gas effluent of the plasma gasification reactor from a temperature of 1 000 °C, to a temperature ranging from 40 °C to 30 °C as the clean-up process for the synthesis gas operates at low temperatures. Following the quenching of the synthesis gas, the water present in this product stream is condensed due to the sub 100 °C temperature at which this stream exits the quench probe. The water is removed from this synthesis gas stream using the VESSEL block shown in the **Figure 3-5** which is the equivalent of a scrubber system for the demonstration plant shown in **Figure 3-1**. The final stage of this process is a blower used to pressurize the synthesis gas stream and remove any water that may still be present. The pressure changes from 84 kPa to 200 kPa over this blower, a secondary blower system is employed for some of the power cycle models, depending on the pressure at which the synthesis gas is fed into the combustion chamber of the power cycle.

3.2.7 Biomass Characteristics and Reactor Specifications

Table 3-1 presents the ultimate and proximate analysis of the two biomass feedstocks to be used in the plasma gasification reactor models. The ultimate and proximate analysis is used as an estimate of the content of the different types of substances that make up the biomass feedstocks along with other solid fuel sources such as coal. The ultimate and proximate analysis of the wood chips and refuse derived fuel (RDF) is shown in **Table 3-1**.

Table 3-1: Biomass Feedstock Properties

Feedstock & composition	**Wood Chips (%)**	**RDF (%)**
Moisture	20	20
Ultimate analysis (wt.%, dry)		
C	51.19	48.23
H	6.08	6.37
O	41.3	28.48
N	0.2	1.22
S	0.02	0.76
Cl	0.05	1.13
Ash	1.16	13.81
Proximate analysis (wt.%, dry)		
Volatile Matter	80	75.95
Fixed Carbon	18.84	10.23
Ash	1.16	13.81

Source: (Rao Pala, et al., 2017 & Minutillo, et al., 2009)

The process conditions used in the model for the plasma gasification reactor and the pre-treatment process is shown in **Table 3-2** as adapted from the data of the plasma gasification reactor demonstration plant model.

Table 3-2: Experimental Data for the Plasma Gasification Reactor Demonstration Plant

Plasma Gasification Reactor	
Temperature (°C)	1000
Pressure(kPa)	84
Heat Loss from the Quench heat exchanger (kW)	16.548
Blower Pressure (kPa)	200
Blower Isentropic efficiency (%)	85
Blower 2 Output Pressure (kPa)	500
Blower 2 Isentropic efficiency (%)	85
Plasma torch heat duty (kW)	20.72
Nitrogen plasma gas mass flowrate (kg/hr)	3.832

3.3 Power Cycles

3.3.1 Assumptions

- The power cycles operate under steady state conditions.
- There are actual gas and steam turbines that can be designed to operate under these conditions.
- The mechanical operation of equipment such as the pumps, compressors and turbines are negligible for the context of this study.
- As a result of the size of operation for the gas turbine, it can only accommodate an inlet temperature of 1 000 °C.

3.3.2 Process Flowsheet Development

3.3.2.1 Brayton Cycle

The Brayton cycle is a thermodynamic process that represents how a power cycle can directly combust a fuel source to produce heat and further extract that heat to produce mechanical work. The Brayton cycle system features a compressor, combustion chamber and a turbine. In this system air is continuously being drawn into the compressor which discharges it into the combustion chamber where it mixes with the fuel sources leading to combustion of the fuel. The combustion of the fuel causes the temperature to increase in the combustion chamber and this temperature is limited by the addition of air until a feasible temperature for the operation of a combustion chamber can be reached. Before the production of electricity with the power from the gas turbine, a portion of this work is used to drive the mechanical equipment of the process and the rest goes through an electrical generator. The combustion products then expand in the gas turbine to produce power before being discharged into the environment. This process can be seen in **Figure 3-6** which shows a Brayton cycle.

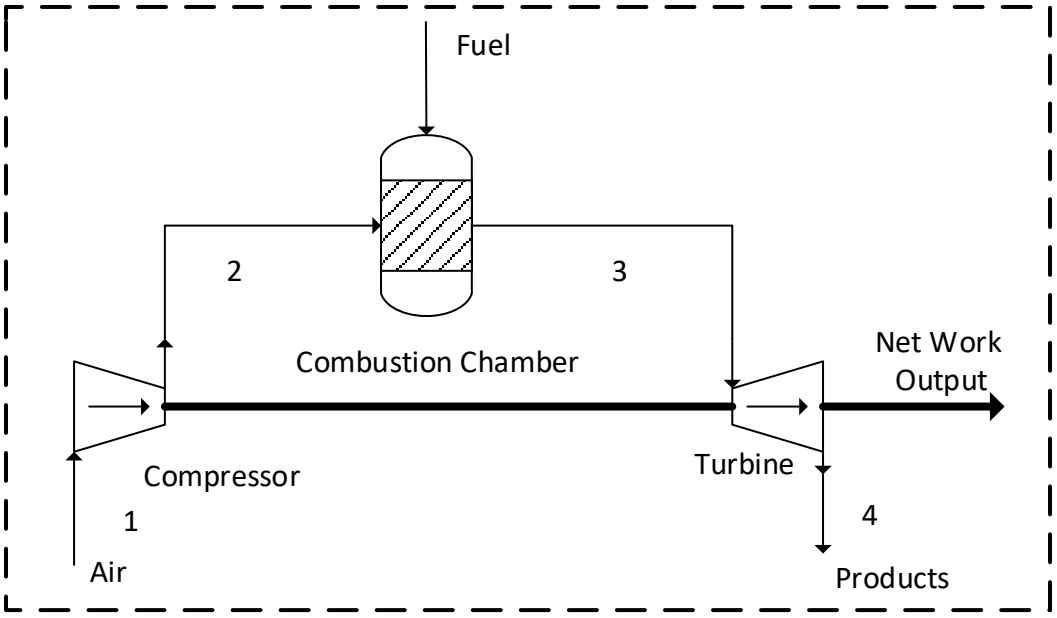


Figure 3-6: Brayton Cycle (Moran & Shapiro, 2006)

The developed models for the Brayton cycle will be representative of a small-scale gas turbine system which has a lot of performance restrictions when compared to the much larger gas turbines. These restrictions on small scale Brayton cycles can be presented through the air standard Brayton cycle. The equations for the air standard Brayton cycle can be used as a guide to show the important parameters in the performance of the Brayton cycle. The thermal efficiency of the air standard Brayton cycle can be expressed according to equation 3.1 (Greeff, 2021).

$$\eta = 1 - \left(\frac{P_{out}}{P_{in}}\right)^{\frac{1-k}{k}} \tag{3.1}$$

The analysis of equation 3.1 shows the direct proportional relationship between the thermal efficiency and the pressure ratio of the Brayton cycle. The work produced from the air standard Brayton cycle can provide further information of the parameters to control in the model to operate at optimum conditions.

$$W = \frac{nkRT_{in}}{k-1}\left[\left(\frac{P_{out}}{P_{in}}\right)^{\frac{k-1}{k}} - 1\right] \tag{3.2}$$

In equation 3.2 (Greeff, 2021) three process conditions can be seen to influence the power produced in the molar flow of the gas, the turbine inlet temperature and the pressure ratio in the gas turbine.

The inlet turbine temperature for this power cycle will be 1 000 °C while the pressure is 5 bar, with these process conditions deemed suitable for the small-scale gas turbine.

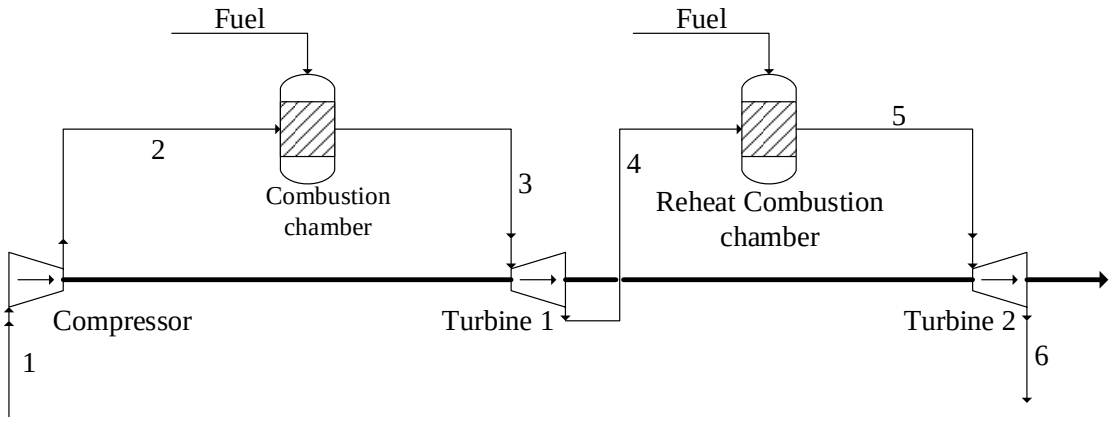


Figure 3-7: Reheat Brayton Cycle

The reheat Brayton cycle shown in **Figure 3-7** is a two-stage expansion system with a reheater between the expansion stages of the hot pressurized gas. This system reheats the initial effluent stream of the first turbine to the initial turbine inlet temperature of the first turbine which is 1 000 °C. In terms of pressure changes this system finds an intermediate between the initial and final pressure, where the first turbine exhaust stream can be.

3.3.2.2 Rankine Cycle

A Rankine cycle is a thermodynamic cycle of an idealized process representing how certain power cycles such as steam turbine power plants, use fluids moving between heat sources and heat users to extract mechanical work. The Rankine cycle is shown in **Figure 3-8** with the working fluid of the cycle being water in actual coal-fired power plants.

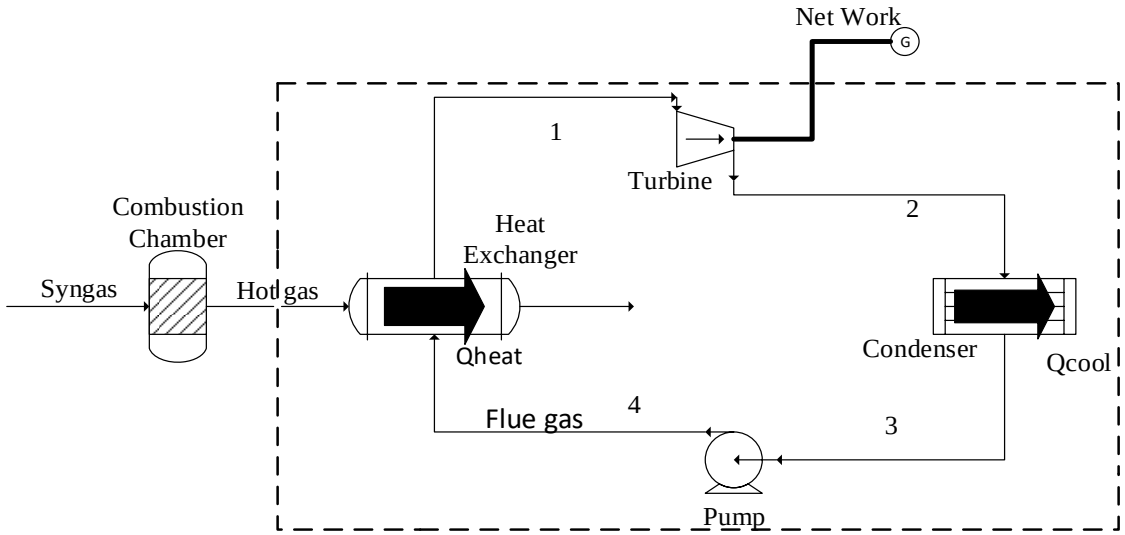


Figure 3-8: Steam Rankine Cycle

These power cycle models will be under small scale conditions meaning that only sub critical conditions are viable for their operation. This is mostly a result of the low calorific value of the synthesis gas fuel used along with the low quantity available for combustion in the boiler at a mass flowrate of 30.864 kg/hr.

The Reheat Rankine cycle

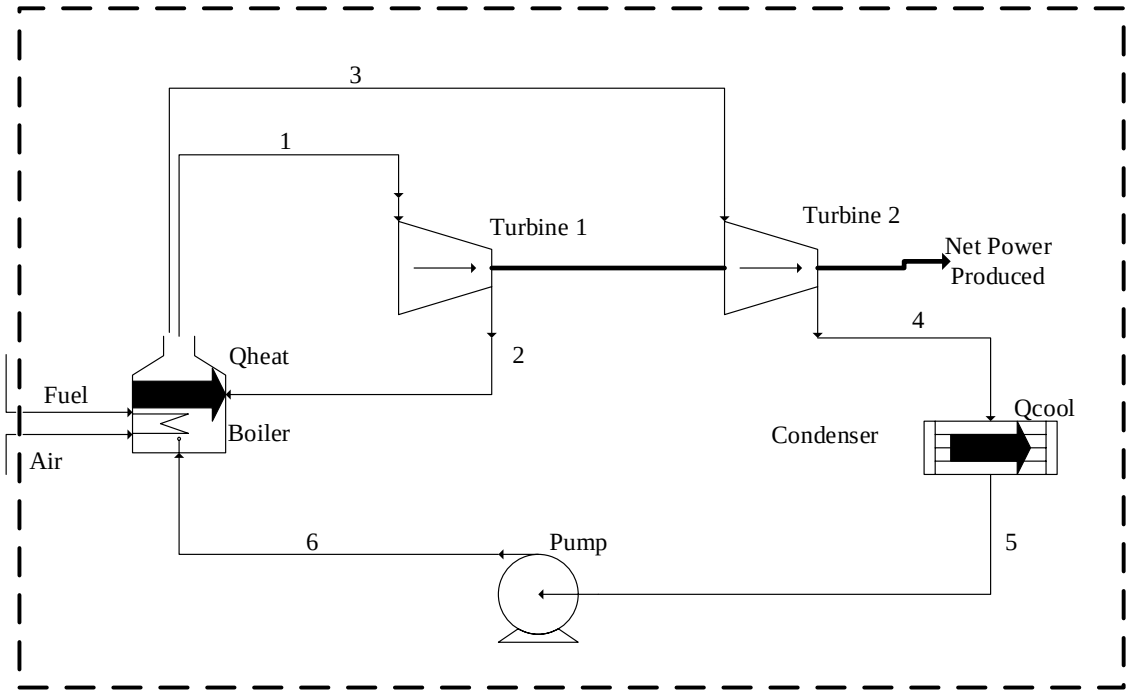


Figure 3-9: Reheat Rankine Cycle (Moran & Shapiro, 2006)

Even though an increase to the boiler pressure is known to increase the thermal efficiency of the Rankine cycle, it also increases the moisture content of the steam at the turbine outlet to unacceptable levels (Cengel & Boles, 2015). This increase in the moisture content of the steam might have some detrimental effects to the operation of the steam turbine. To overcome this limitation the use of a reheat two stage Rankine cycle was developed. In this system the high-pressure expansion of the steam occurs in the first steam turbine and the effluent of this turbine is reheated to a temperature close to the temperature at which the steam enters the first turbine. The steam then expands in the second turbine to a pressure close to that at which the condenser operates. The reheat of the steam in-between the turbines prevent the increase in the moisture content of the steam at the turbine outlet.

3.3.2.3 Combined Power Cycle

In the operation of an open Brayton cycle, the effluent flue gas usually leaves the cycle at high temperatures and must be discarded to the environment, thus leading to a loss of a high quantity of waste heat. The combined cycle was implemented with the aim of recovering the heat from the Brayton cycle effluent stream, by incorporating a bottom cycle that can extract this heat and use it for generating more power before the spent flue gas stream can be discarded.

For this power generation system, the waste heat from the effluent of the gas turbines with be recovered in a heat recovery steam generator (HRSG), with the steam generated from this block being expanded in a steam turbine with the aim of generating power. The topping cycle in the form of the Brayton cycle commonly being the internal combustion power gas turbine is the driving force for this power cycle and the amount of power that can be generated in the bottoming steam Rankine cycle is determined by the amount of heat that can be recovered from the spent flue gas exiting the gas turbine.

The operation of a combined power cycle is shown in **Figure 3-10**.

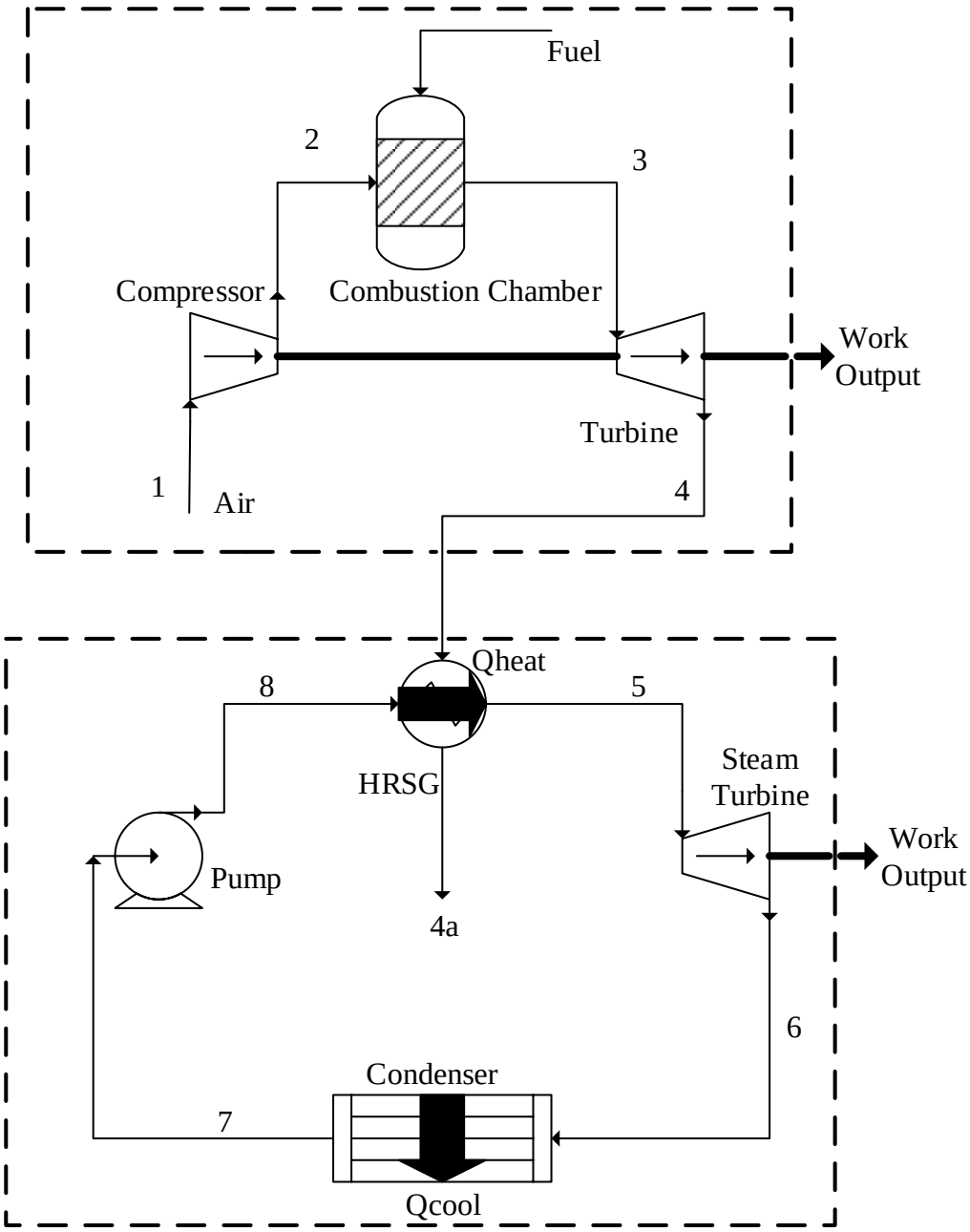


Figure 3-10: Combined Power Cycle

The operation of the bottoming cycle in most of these cases is under subcritical condition in terms of the pressure, which in most cases is far below the subcritical pressure of 124 bar (Salazar-Pereyra, et al., 2016). For a small-scale system such as in **Figure 3-6** with the pressure and temperature of operation for the gas turbine being around 5 bar and 1 000 °C. The pressure in the bottoming cycle is limited by the pressure of the main cycle and the waste heat available. A reasonable pressure must be used for this power cycle, and this has been found to be below 10 bar.

3.3.3 Flowsheet Modelling and Analysis

Simulation models for the plasma gasification unit along with the potential power generation systems that can be coupled with this unit will be developed on Aspen Plus. The Aspen Plus software enables for the assessment of different scenarios to determine which of these systems have the potential to materialize. The Peng-Robinson equations of state with Boston-Mathias modification is used as the property method in the model due to the presence of hydrocarbons, and the steam tables are used for water & steam (Doherty, et al., 2013). Literature sources will be used in estimating the feasible physical conditions at which the compressors, pumps, and turbines in these power cycles can operate.

Using previous literature studies of a similar nature to the current study the temperatures, pressures, chemical composition, heat duties, mechanical work consumed or produced, isentropic efficiencies, and other physical parameters are obtained to be used in the Aspen plus blocks used for developing the model. The developed model presents an approximated mass and energy balance of the plasma gasification process along with the power cycles under consideration for the study.

3.3.3.1 Gas Turbines

Several different gas turbine models have been generated in order to assess their effectiveness in generating power using the same synthesis gas stream. Some of the models feature the pre-treatment system in **Figure 3-5** before the combustion of the synthesis gas in the gas turbine, while others do not. The pre-treatment system involves a quench probe modelled through the HEATER block and a SEP block to remove the condensed water present in the synthesis gas. A series of two blowers, with the first blower using the COMPR block increasing the pressure from 1 bar to 2 bar and the second COMPR block increases the pressure from 2 bar to 5.5 bar. The compressed synthesis gas is then introduced to the combustion chamber of the gas turbine using the RSTOIC block.

The Brayton cycle features in all the gas turbine models, an air stream is drawn onto the air compressor using the COMPR block. The compressed air stream along with the compressed synthesis gas stream are fed into the combustion chamber, where they are combusted in the RSTOIC block to form a hot gas product to be expanded in the gas TURBINE block, shown as the COMPR block resulting in the generation of power.

The different power cycle cases modelled for this part of the study can be summarized according to **Table 3-3**.

Table 3-3: Process Descriptions for the Open Brayton Cycle Cases

Case 3	Description
Case 3a	A simple ideal Brayton cycle using an isentropic efficiency of 100%.
Case 3b	A simple real Brayton cycle using an isentropic efficiency of 85%.
Case 3c	A Brayton cycle system where the syngas is directly combusted in the combustion chamber without any prior compression. (Isentropic efficiency of 85%)
Case 3d	A Brayton cycle system using a turbine expander before the introduction of the syngas into the Brayton cycle (Isentropic efficiency of 85%)
Case 3e	A Brayton cycle with a two-stage turbine system with inter-heating between the two different gas turbines (Isentropic efficiency of 85%).

Case 3a and **Case 3b** represent the model of a simple Brayton power cycle, featuring the synthesis gas preparation section of the process under ideal and realistic condition, with regards to the isentropic efficiency used. The synthesis gas preparation phase of the power cycle can be seen in **Figure 3-11** featuring the quench probe, water removal vessel and the two-stage blower system. The first blower changes the pressure of the synthesis gas from 84 kPa to 200 kPa while the second blower changes the pressure from 200 kPa to 550 kPa. A difference in the pressure of the SYNGAS stream and AIR stream entering the combustion chamber of the Brayton power cycle is maintained, with that of the fuel stream being higher. **Figure 3-12** shows the Brayton cycle models showing the production of power in **Case 3a** and **Case 3b**.

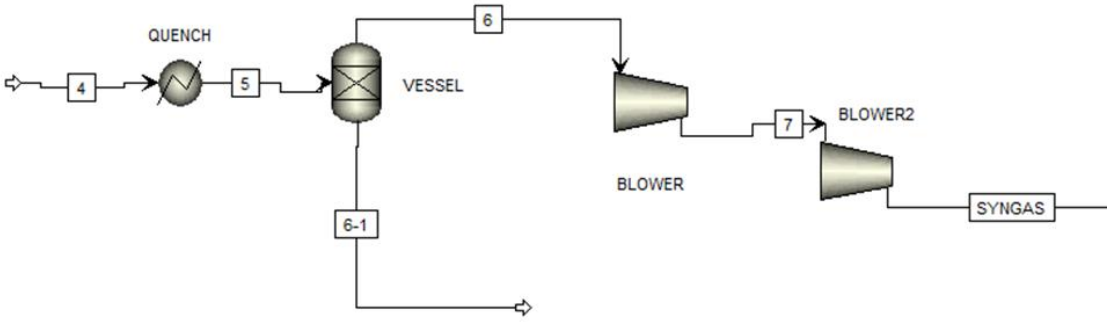


Figure 3-11: Syngas Preparation Section of the Model

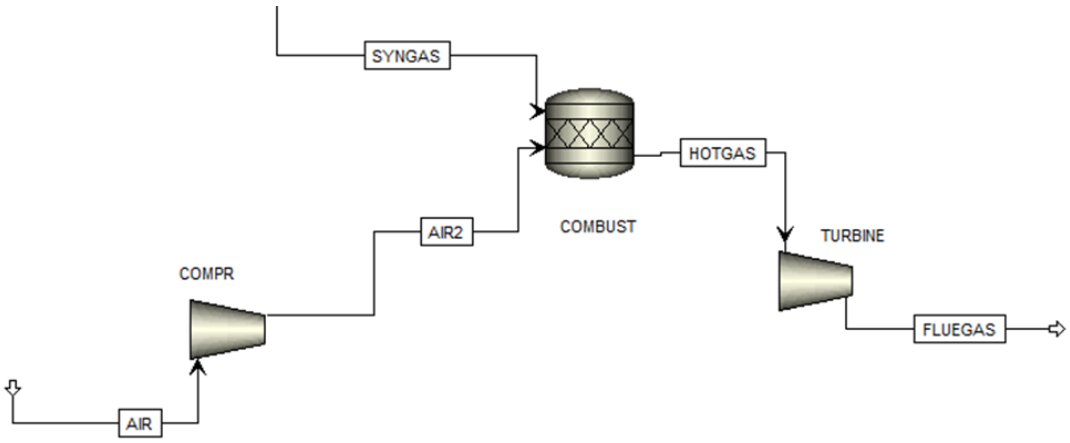


Figure 3-12: Brayton Power Cycle Model

Case 3c represent the model of a hypothesized power cycle system where the synthesis gas does not flow through the pre-treatment process but is rather directly fed into the combustion chamber of the power cycle as shown in **Figure 3-12**. This case assumes that the synthesis gas exhaust of the plasma gasification reactor exits at a pressure of 550 kPa. This case is developed to assess how the thermal efficiency of the power cycle will be influenced if the heat from the synthesis gas is not lost through the quench probe, but rather added into the power production process. Literature studies conducted by several researchers has shown that the quench probe is responsible for the loss of a large amount of high-quality heat, which might have improved the performance of the power cycle if it had not been lost through the quench probe. This power cycle will thus aim to quantity the influence of omitting the quench probe from power cycle and the potential of designing a pressurized plasma gasification reactor system.

In **Case 3d** the synthesis gas from the plasma gasification reactor model is pressurized to 5 bar and expanded in a turbine expander before it can be cooled and pressurized prior to being fed to the power cycle. In this model the sensible heat from the pressurized effluent of the plasma gasification reactor is used in a turbine expander rather than being quenched. The exhaust stream of the turbine expander is cooled, and water is removed before compression and introduction into the power cycle depicted by **Figure 3-12**. This cycle aims to analyse the thermodynamic value of the turbine expander in lieu of the quench probe. The flow of the synthesis gas prior to being introduced in the power cycle can be seen in **Figure 3-13**.

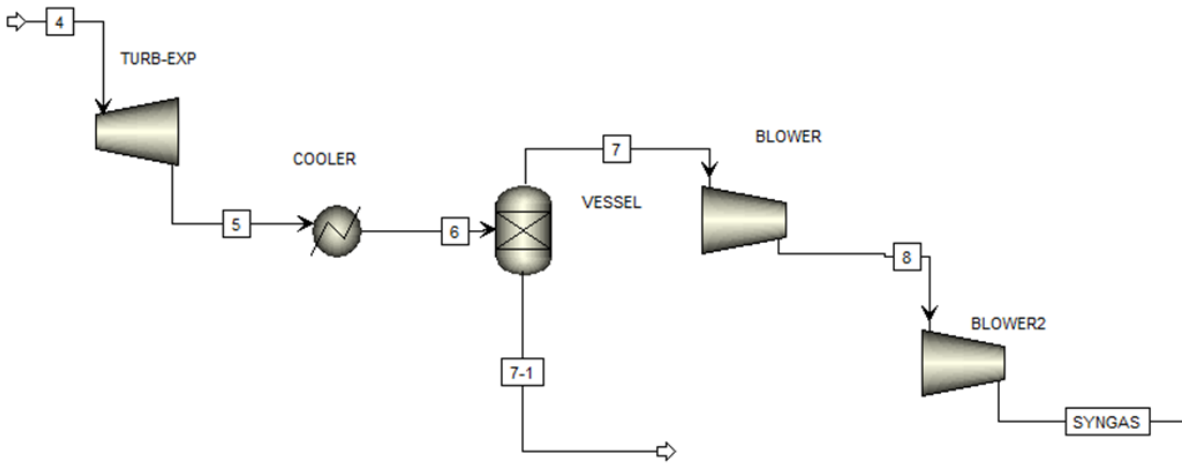


Figure 3-13: Turbine Expander and Preparation of the Syngas in Case 3d

The model for **Case 3e** is built around the concept of a reheat Brayton cycle with inter-heating between the two turbines. This model features the synthesis gas preparation process depicted by **Figure 3-11**, before the introduction of the synthesis gas into the combustion chamber of the power cycle. **Case 3a and Case 3e** have a lot of similarities except for a two-stage expansion system with an inter-heater for **Case 3e**, while **Case 3a** has a single expansion system. The inter-heater is responsible for increasing the sensible heat available for expansion in the second gas turbine and an assessment will be done to observe this effect. The inter-heater unfortunately requires that more fuel be combusted so that the heat can be added into the process, making this process costly as an additional combustion chamber is required. The two-stage expansion with inter-heating for this process can be seen in **Figure 3-14**.

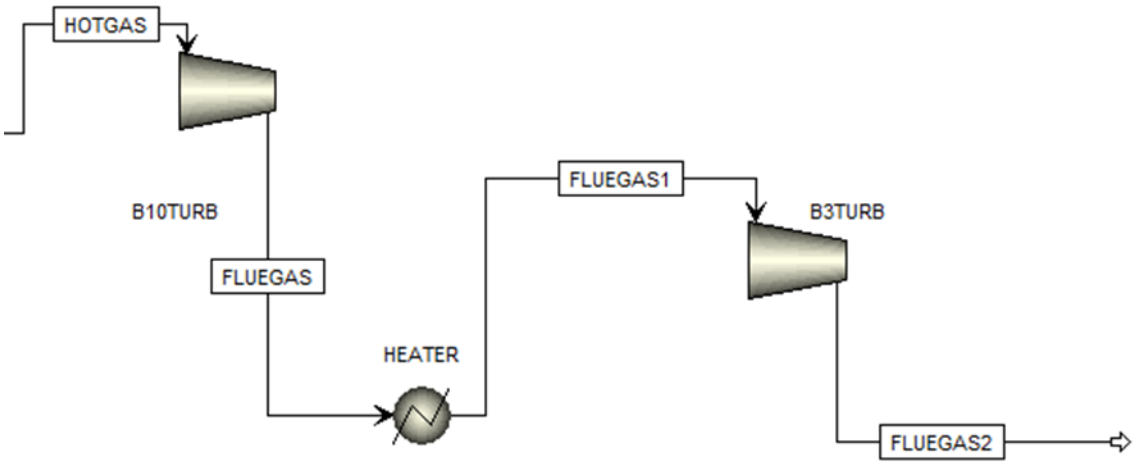


Figure 3-14: Two-stage Expansion with Inter-heating in Case 3e

3.3.3.2 Steam Turbines

Like the gas turbine models generated in the study, varying steam turbine cases are considered. A similar pre-treatment process is adopted to the one featured for the gas turbine models, except for only one blower being used for these cases.

In these Rankine cycle cases, an air compressor using the COMPR block draws air onto the combustion chamber, which is the RSTOIC block, where synthesis gas is combusted in the presence of this air. The flue gas product in the boiler is used to heat up the boiler feed water which has been pressurized in the PUMP block. The pressurized water is superheated to generate a steam product to be expanded in the steam turbine block ST-TURB in order to produce power. The expanded steam is condensed in the HEATER block before it can continue the cycle.

The models feature ideal and real versions of the power cycles, with the isentropic efficiency being the difference between these two cycles. The ideal cycles operate under perfect conditions and thus the isentropic efficiency is 100%. The real cycles operate under more realistic conditions and accounts for the loss of entropy during expansion and compression of the working gas.

Table 3-4: Process Description for the Rankine Cycle Cases

Case 4	Process Description
Case 4a	A simple ideal Rankine cycle using an isentropic efficiency of 100%.
Case 4b	A simple real Rankine cycle using an isentropic efficiency of 86%.
Case 4c	A real Rankine cycle system where the syngas is directly combusted in the combustion chamber without any prior compression. (Isentropic efficiency of 86%)
Case 4d	An ideal Rankine cycle system where the syngas is directly combusted in the combustion chamber without any prior compression. (Isentropic efficiency of 100%)
Case 4e	An ideal Reheat Rankine cycle (Isentropic efficiency of 100%)
Case 4f	A real Reheat Rankine cycle (Isentropic efficiency of 86%)

Case 4a and **Case 4b** represent the model of a simple steam Rankine cycle process, with the synthesis gas preparation process included prior to the boiler under ideal and realistic conditions. Like the gas turbine case studies, these cases feature a synthesis gas preparation stage with one blower rather than two for the Brayton cycle cases. The blower pressurises the synthesis gas from 84 kPa to 200 kPa and combusted in the presence of air from the air compressor in the boiler. Upon combustion of the synthesis gas, the heat released is transferred to the working fluid (water) of the cycle in the heater of the boiler as shown in **Figure 3-15**. These ideal and real versions are modelled to analyse the thermal performance of the small-scale steam turbine system generating power under the simplest setup of the Rankine cycle process.

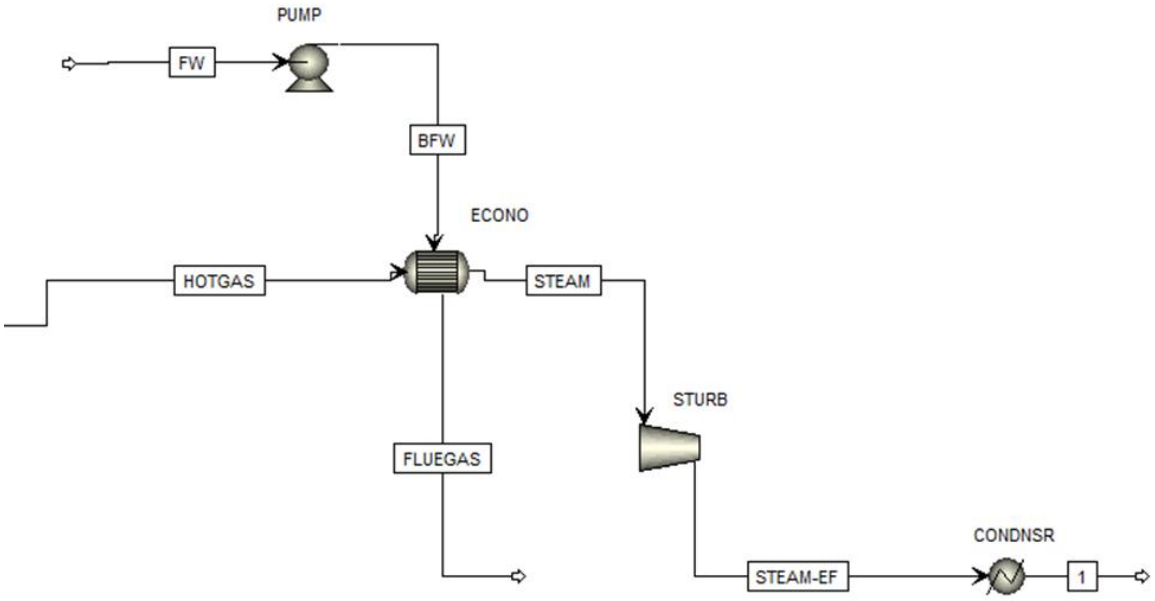


Figure 3-15: Syngas Preparation and Combustion Process in Rankine Cycle

Case 4c and **Case 4d** present the steam Rankine cycle model that does not have the synthesis gas preparation phase as the synthesis gas leaving the reactor is assumed to be pressurized to a pressure of 2 bar and the sensible heat from this stream is not destroyed using the quench probe. These cases are under ideal and realistic conditions respectively, and the configuration of this cycle enables for there to be more heat available for the superheating of the steam in the boiler. The power cycle for these cases is shown in **Figure 3-16**.

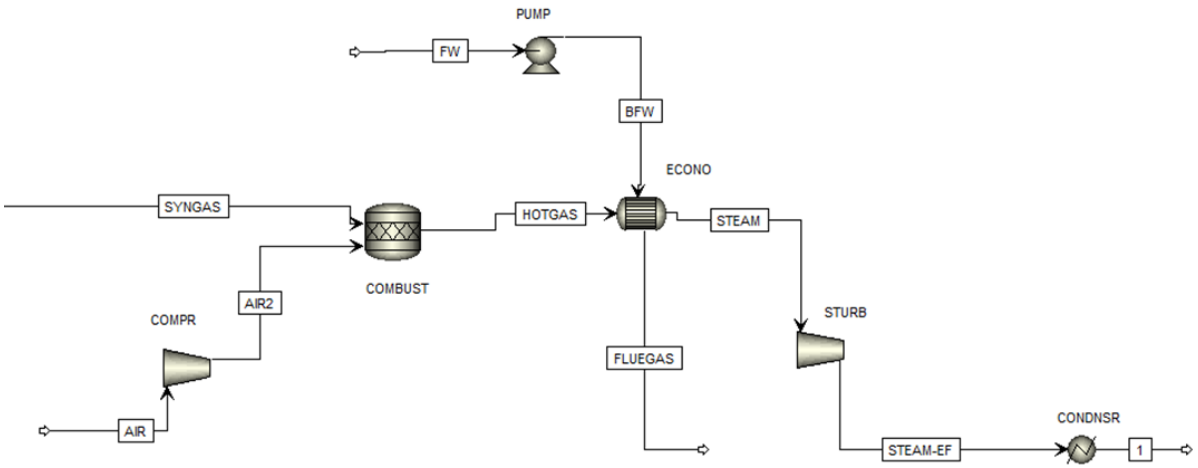


Figure 3-16: Direct Syngas Feeding Rankine Cycle Process Without Preparation Stages

Case 4e and **Case 4f** present the models for the reheated Rankine cycle process schematically depicted in **Figure 3-8** under ideal and real conditions. This process has been modified to just a two-stage steam turbine expansion system due to the efficient heat transfer occurring in the super-heater of the boiler and the high temperature exhaust of the first steam turbine. The update power cycle can be seen in **Figure 3-17**.

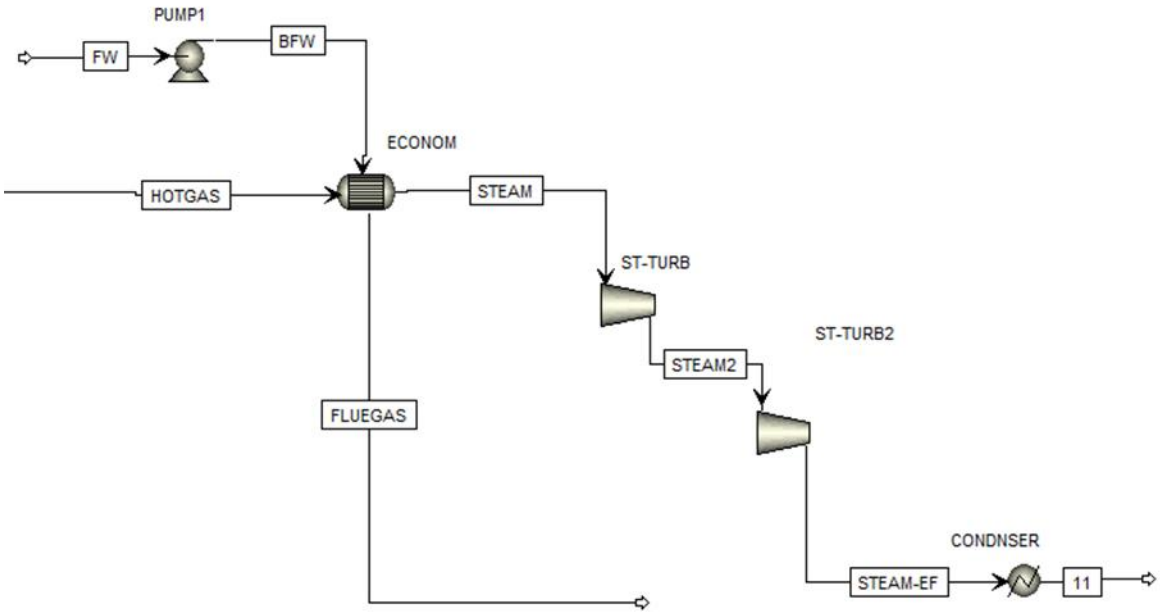


Figure 3-17: Two-stage Expansion Process

3.3.3.3 Combined Power Cycle

The models for the combined power cycle feature the single stage gas turbine cases shown in section 3.3.3.1, combined with a heat recovery system to direct heat into a bottom power cycle. The purpose of such combined cycles is to improve thermal efficiency. The expanded flue gas stream passes through a heat recovery steam generator block, modelled using a heat exchanger block for heating up the feed water in the Rankine cycle and connecting the top Brayton cycle with the bottom Rankine.

Table 3-5: Process Description for the Combined Power Cycle Cases

Case 5	Process Description
Case 5a	A standard ideal Combined cycle using an isentropic efficiency of 100%.
Case 5b	A standard real Combined cycle using an isentropic efficiency of 86%.
Case 5c	An ideal Combined cycle where the syngas is directly combusted in the combustion chamber without any prior compression. (Isentropic efficiency of 100%)
Case 5d	A real Combined cycle where the syngas is directly combusted in the combustion chamber without any prior compression. (Isentropic efficiency of 86%)
Case 5e	An ideal Combined cycle with a turbine expander to generate additional Power from the syngas effluent of the plasma gasifier, in addition to the power from the Brayton and Rankine cycle (Isentropic efficiency of 100%)
Case 5f	A real Combined cycle with a turbine expander to generate additional Power from the syngas effluent of the plasma gasifier, in addition to the power from the Brayton and Rankine cycle (Isentropic efficiency of 86%)

These power cycle models are developed based around some gas turbine models that have been reviewed in the previous sections with the addition of the steam Rankine cycle as the bottoming power cycle to recover waste heat from the exhaust of the gas turbine.

Case 5a and **Case 5b** focus on the development of a simple combined power cycle modelled under ideal and real process conditions. The topping Brayton cycle is based on **Case 3a** and **Case 3b**. The bottoming Rankine cycle heat recovery system is like **Figure 3-15**, with the HOTGAS stream being the flue gas effluent of the gas turbine, for this case as waste heat is being recovered from this stream. The development of these models will assess how the incorporation of the waste heat recovery system, through the combined power cycle improves the thermodynamic performance of this power cycle.

The models developed for **Case 5c** and **Case 5d** are based on the model for **Case 3c** as the topping cycle which involves the direct combustion of a pressurized synthesis gas product stream. A bottoming Rankine cycle model like **Figure 3-15** is coupled to this process through a heat recovery steam generator in the exhaust stream of the gas turbine. Compared to the simple combined cycle, these cases are assessing the impact of omitting the quench probe on

the thermal efficiency of the cycle. It can be expected that the available waste heat for these cases will be higher compared to the previous cases, due to the presence of two significant sensible heat streams.

The models for **Case 5e** and **Case 5f** are developed based on the turbine expander **Case 3d** model as the topping power cycle. The bottoming Rankine cycle model shown in **Figure 3-15** will be used as the heat recovery system coupled through the exhaust stream of the gas turbine power cycle model.

All the above cases of the combined power cycle are using the topping Brayton cycle as the main cycle of these power cycles. The bottoming Rankine cycle being used is a tool for heat recovery as the power that can be generated by this part of the cycle heavily relies on the heat value from the gas turbine effluent stream.

3.3.3.4 Model Specifications

This section presents the process parameters of the different cycles such as the temperatures (°C), Pressures (bar), Pressure ratios, mass flowrates (kg/hr) and the isentropic efficiencies (%).

Table 3-6: Process Operating Conditions

Gas Turbine	
Turbine Inlet Temperature (°C)	1000
Air Compressor Pressure (bar)	5
Gas Turbine Pressure Ratio	5
Air Inlet Temperature (°C)	25
Air Inlet Pressure (bar)	1
Compressor Isentropic efficiency	85%
Gas Turbine Isentropic Efficiency	85%
Mass flowrate of the wet syngas (kg/hr)	30.862
Mass flowrate of the dry syngas (kg/hr)	27.489

Reheat Gas Turbine	
Turbine 1 Exhaust Pressure (bar)	3
Turbine 2 Exhaust Pressure (bar)	1

Steam Turbine	
Combustion Chamber Product gas temperature (°C)	1650

Steam Turbine Inlet Temperature (°C)	800
Pump Outlet Pressure (bar)	30
Boiler Feed water Flowrate (kg/hr)	75
Feed water Temperature (°C)	25
Pump Isentropic efficiency (%)	86
Steam Turbine Isentropic efficiency (%)	86
Mass flowrate of the syngas (kg/hr)	30.86

Reheated Steam Turbine	
Steam Turbine Inlet Pressure (bar)	30
High Pressure Turbine Outlet Pressure (bar)	8

Combined Power Cycle	
Gas Turbine Inlet Temperature (°C)	1000
Gas Turbine Inlet Pressure (bar)	5
Gas Turbine Pressure Ratio	5
Gas Turbine Isentropic efficiency	85%
Steam Turbine Inlet Pressure (bar)	8
Steam Turbine Pressure Ratio	100
Steam Turbine Isentropic efficiency	86%
Feed water Flowrate (kg/hr)	68

3.4 Energy Analysis

The energy analysis of the process involved in this investigation can be separated into two sections i.e., plasma gasification reactor and the power cycles. The energy analysis for both these sections follows the 1st law of thermodynamics.

The efficiency of the plasma gasification reactor is found using the cold gas efficiency formula, which assesses the energy value of the synthesis gas leaving the plasma gasifier, with respect to the potential heat energy in the biomass inlet and the power of the plasma torch.

$$\eta_{CGE} = \frac{\dot{m}_{syngas} \cdot LHV_{syngas}}{\dot{m}_{biomass} \cdot LHV_{biomass} + W_{torch}} \cdot 100 \quad (3.3)$$

The cold gas efficiency gives an indication of the extent to which the energy input of the process goes towards reforming the biomass into synthesis gas.

For the power cycles, the first law of thermodynamics will be used in calculating the thermal efficiency of these power cycles.

$$\eta = \frac{W_{net}}{Q_{added\ to\ process}} \tag{3.4}$$

$$Q_{combustion} = \dot{m} \cdot C_p \cdot \Delta T \tag{3.5}$$

$$W_{net} = W_{turbines} - W_{compressors} - W_{pump} \tag{3.6}$$

The thermal efficiency for the different power cycles will be calculated using equation 3.4 which shows the percentage of the heat added into the process that goes towards the production of power. For the Brayton cycle, the heat added to the process is through the combustion of the synthesis gas in the presence of air, while for the steam Rankine cycle, the heat is added through the superheating process of the working fluid which is water. The thermal efficiency for the Brayton cycle and Rankine cycles is represented by equation 3.7 and 3.8 respectively:

$$\eta = \frac{(W_{turbine} - W_{blower} - W_{compressor})}{Q_{combustion}} \cdot 100 \tag{3.7}$$

$$\eta = \frac{(W_{turbine} - W_{compressor} - W_{pump})}{Q_{superheating}} \cdot 100 \tag{3.8}$$

The thermal efficiency for the Brayton cycle can also be expressed according to the lower heating value of the synthesis gas as shown by equation 3.9. The thermal efficiency shows the extent to which the heat present in the process is converted to work.

$$\eta_{LHV} = \frac{W_{net}}{\dot{m}_{syngas} \cdot LHV_{syngas}} \cdot 100 \tag{3.9}$$

In the case of the combined cycle the heat added into the process is through the combustion process in the Brayton cycle section so the equation for the thermal efficiency can be expressed as shown in equation 3.10:

$$\eta = \frac{(W_{turbine} - W_{compressor} - W_{blower} - W_{pump})}{Q_{combustion}} \cdot 100 \tag{3.10}$$

The thermal efficiency for the entire process involves the power used in the operation of the plasma torch, which means this must be accounted for and can be done according to equation 3.11.

$$\eta_{overall} = \frac{(W_{net} - W_{DC-ARC})}{m_{syngas} \cdot LHV_{syngas}} \cdot 100 \tag{3.11}$$

3.5 Exergy Analysis

There are four different components of exergy in a process i.e. 1) physical exergy, 2) chemical exergy, 3) kinetic exergy and 4) potential exergy. Only the physical and chemical exergy components are equivalent in the simulation of the power generation system and the plasma gasification reactor. The potential and kinetic exergy will be negligible as the assumption was made that the process operates under steady state conditions and fixed to the ground. Aspen Plus can only calculate the physical exergy component of a stream. The steady state equation for the calculation of the exergy destruction, E_d, for the different process units are found (Moran & Shapiro, 2006) in equation 3.12 and 3.13:

$$0 = \sum_j \left(1 - \frac{T_0}{T_j}\right) \cdot \dot{Q}_j - \dot{W}_{cv} + \dot{m} \cdot \left(e_{f1} - e_{f2}\right) - \dot{E}_d \quad (3.12)$$

$$e_{f1} - e_{f2} = (h_1 - h_2) - T_0 \cdot (s_1 - s_2) \quad (3.13)$$

The exergy analysis will be performed for the power cycles, over the various unit operations. For the studied Brayton cycle cases, **Case 3b** and **Case 3c** will be the focus of the exergy analysis and the analysis will be done over the following process units:

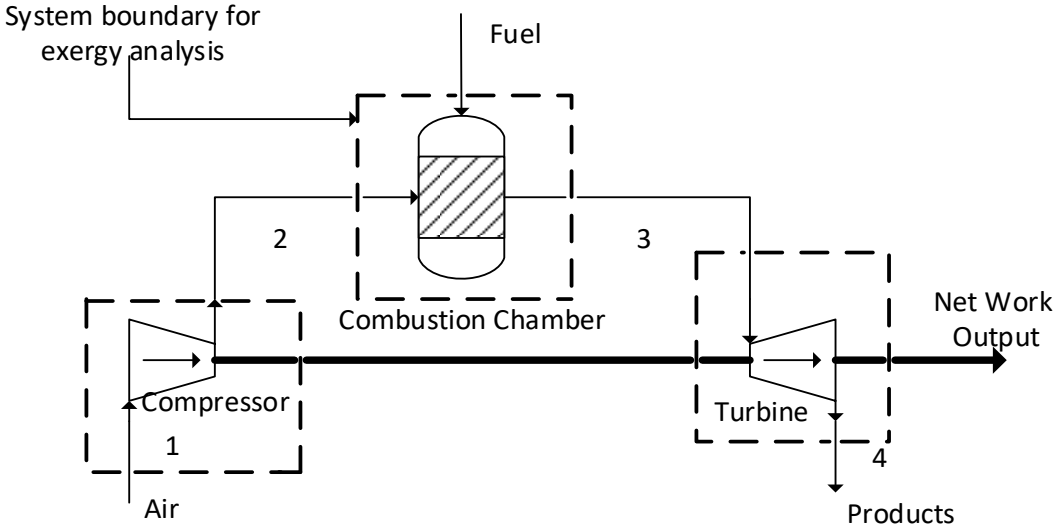


Figure 3-18: Exergy Analysis Process System Boundary for the Brayton Power Cycle

- Air Compressor
- Syngas Blower 1 and Syngas Blower 2
- Syngas Combustion chamber
- Quench probe for the cooling of syngas from the reactor

- The turbine for the expansion of the hot gas

For the studied Rankine cycle cases, **Case 4b** and **Case 4c** will be the focus of the exergy analysis and the analysis will be done over the following process units:

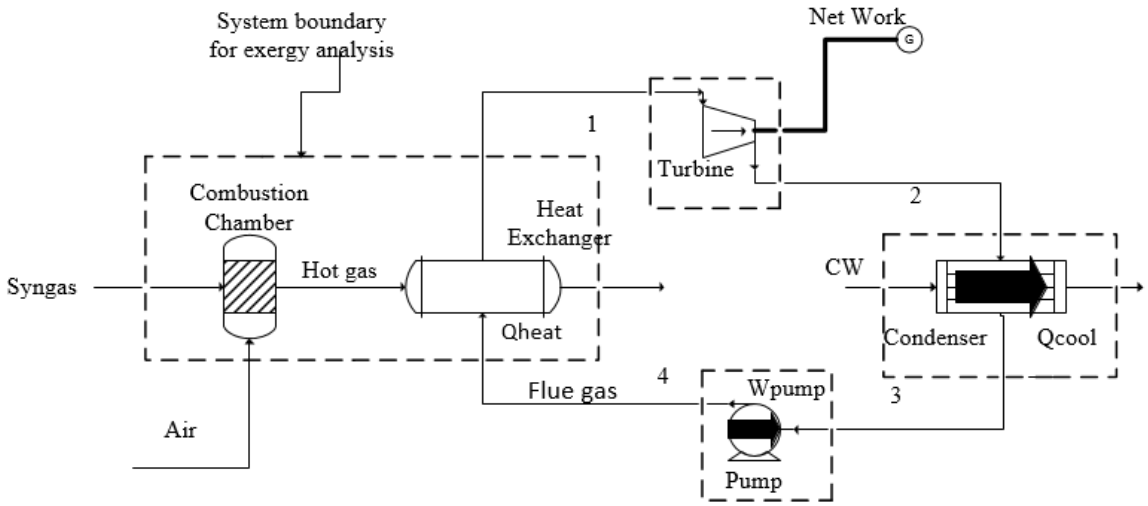


Figure 3-19: Exergy Analysis Process System Boundaries for the Rankine Power Cycle

- Air Compressor
- Syngas Blower
- Boiler for the firing of syngas and heating feed water
- Quench probe for the cooling of syngas from the reactor
- Feed water Pump
- Steam Turbine

The exergy analysis over the condenser has been neglected as this is not considered useful for the study, since there are no feasible means of recovering the heat lost over the condenser. The exergy analysis is done with the purpose of finding process units with thermal inefficiencies and possible means of addressing them.

For the studied combined cycle cases, **Case 5b** and **Case 5d** will be the focus of the exergy analysis and the analysis will be done over the following process units:

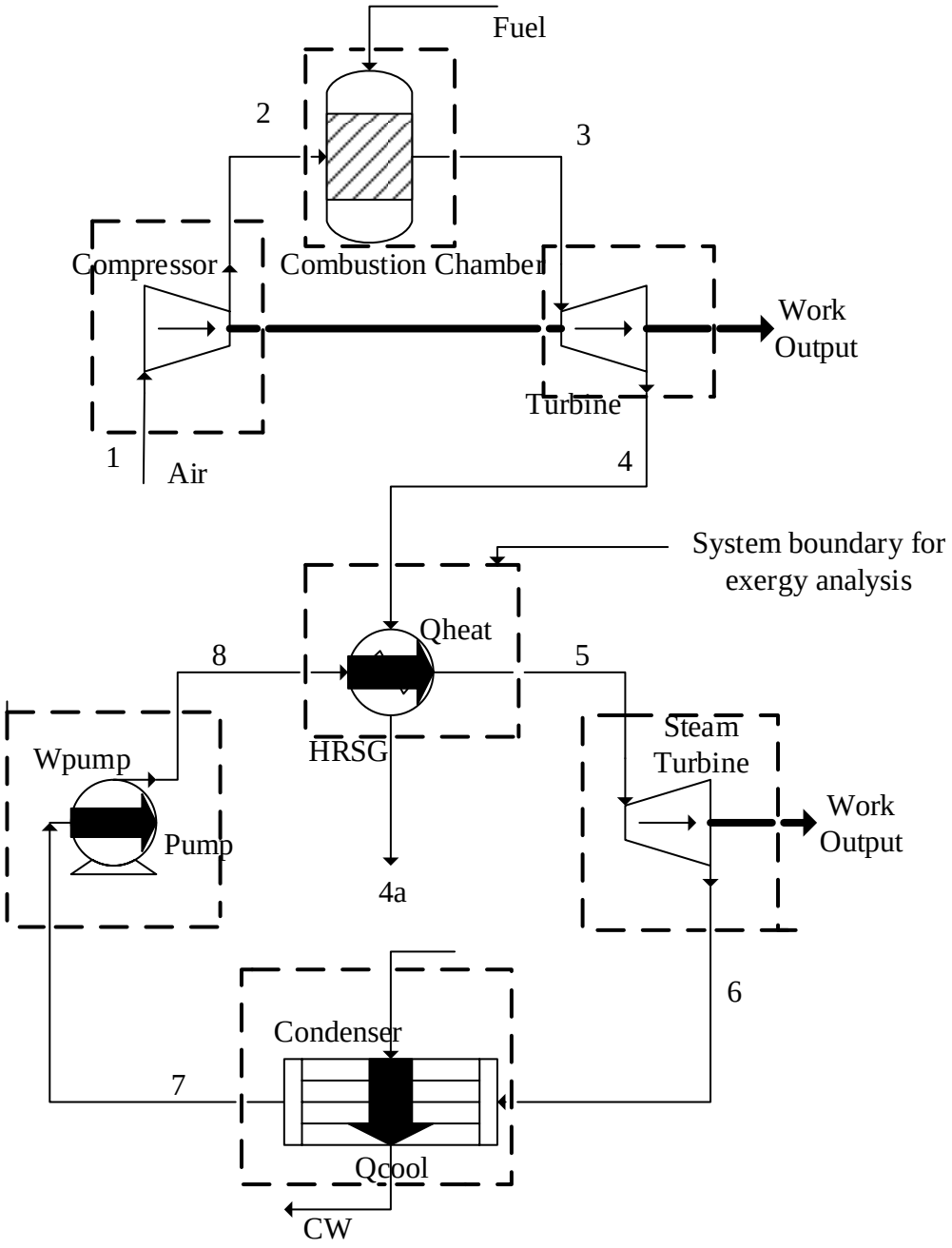


Figure 3-20: Exergy Analysis Process System Boundaries for the Combined Power Cycle

- Air Compressor
- Syngas Blower 1 and Syngas Blower 2
- Syngas Combustion chamber
- Quench probe for the cooling of syngas from the reactor
- The turbine for the expansion of the hot gas
- Heat Recovery Steam Generator
- Feed water pump

- Steam turbine

The process units shown in the different **Figure 3-18**, **Figure 3-19** and **Figure 3-20** can be classified according to their function which determines how equation 3.10 will be used i.e., the exergy destruction for pressure change units such as pumps, compressors, blowers and turbines can be calculated using equation 3.14:

$$\dot{E}_d = -W + \sum_i E_i - \sum_e E_e \quad (3.14)$$

While for heat exchanging process units such as the combustion chamber, boiler and quench probe, the exergy destruction can be calculated according to the equation 3.15:

$$\dot{E}_d = \sum_i E_i - \sum_e E_e \quad (3.15)$$

The other component of exergy which is chemical exergy will also be consider and this exergy accounts for the maximum possible potential energy available during the transient phase of the reaction (Gray, 2019). This form of exergy is mostly applicable for streams that have some fuel value and can thus be reacted to generate energy.

$$\varepsilon_i = -RT_0 \cdot Ln(x_{i,0}) \quad (3.16)$$

$$\varepsilon_{chem,i} = \varepsilon_i + RT_0 \cdot Ln(a_i) \quad (3.17)$$

$$E_{mix} = \sum_i n_i \cdot \varepsilon_{chem,i} = \sum_i n_i \cdot \varepsilon_i + RT_0 \cdot \sum_i n_i \cdot Ln(a_i) \quad (3.18)$$

$$E_{mix} = \sum_i x_i \cdot \varepsilon_{chem,i} = \sum_i x_i \cdot \varepsilon_i + RT_0 \cdot \sum_i x_i \cdot Ln(x_i) \quad (3.19)$$

$$E_d = \left(\sum_i E_{mix,i}\right)_{output} - \left(\sum_i E_{mix,i}\right)_{input} \quad (3.20)$$

Where n_i is molar flowrate of species i, ε_i is the specific chemical exergy of species i, a_i is the activity of species i, x_i is the molar fraction of species i, R is the universal gas constant, E_{mix} is the chemical exergy of a mixture and T is the temperature.

3.6 Economic Analysis

With a lot of the power generation systems being large scale commercial in nature, the exploration of smaller systems usually presents challenges such as thermodynamic limitations (previously highlighted in section 3.3) and financing challenges, as most supplier strive through large scale systems. After assessing the different behaviours and thermodynamic possibilities associated with these small-scale systems, the next goal will be the economic evaluation of these small-scale systems. The economic evaluation aims to find the costs associated with acquiring these small-scale systems and the costs of operating them continuously. The

following types of costs are the most relevant in the operation of not only power generation systems but other industrial operational systems (Greeff, 2004):

- The capital cost
- The operating costs e.g., maintenance and labour

This economic evaluation can be used to determine the economic potential in small scale power generation system when compared to the larger commercially available systems. This economic analysis will focus exclusively on the costs associated with small scale gas and steam turbines.

3.7 **References**

Babinszki, B. et al., 2021. Thermal decomposition of biomass wastes derived from palm oil production. *Journal of Analytical and Applied Pyrolysis,* Volume 155, p. 105069.

Cengel, Y. A. & Boles, M. A., 2015. *Thermodynamics: An Engineering Approach.* 8th ed. New York: McGraw Hill Education.

Gray, T. D., 2019. *An introduction to exergy and its evaluation using Aspen Plus,* Utah: University of Utah, Masters of Science Thesis Report.

Greeff, I. L., 2004. *Recovery of work from exothermic chemical reaction systems by means of turbine expansion,* Eindhoven: PhD of Engineering Thesis, Eindhoven University of Technology.

Minutillo, M., Perna, A. & Di Bona, D., 2009. Modelling and performance analysis of an integrated plasma gasification combined cycle (IPGCC) power plant. *Energy Conversion and Management,* 20 July, Volume 50, pp. 2837-2842.

Moran, M. J. & Shapiro, H. N., 2006. *Fundamentals of Engineering Therrmodynamics.* 5th ed. Chichester: John Wiley & Sons.

Motau, P. S. et al., 2017. *Process Description For the Sanedi Facility,* Pretoria: NECSA.

Ncwane, S., Greeff, I. L. & Van der Walt, I. J., 2021. *Energy recovery from solid waste via plasma gasification.* South Africa, South African Engineering Congress, September 2021.

Okoroigwe, E. C., Enibe, S. O. & Onyegegbu, S. O., 2016. Determination of oxidation characteristics and decomposition kinetics of some Nigerian biomass. *Journal of Energy in Southern Africa,* August, 27(3), pp. 39-49.

Rao Pala, L. P., Wang, Q., Kolb, G. & Hessel, V., 2017. Steam gasification of biomass with subsequent syngas adjustment using shift reaction for syngas production: An Aspen Plus model. *Renewable Energy*, Volume 101, pp. 484-492.

Saddawi, A., Jones, J. M., Williams, A. & Wojtowicz, M. A., 2010. Kinetics of the Thermal Decomposition of Biomass. *Energy Fuels*, Volume 24, pp. 1274-1282.

Sesotyo, P. A., Nur, M. & Suseno, J. E., 2019. *Plasma gasification modeling of municipal solid waste from Jatibarang Landfill in Semarang, Indonesia: analyzing its performance parameters for energy potential.* Semarang, EDP Sciences.

Chapter 4 Results and Discussion

4.1 Introduction

This chapter will demonstrate the feasibility of biomass to power generation systems using a plasma gasification reactor for the thermal reforming of biomass feedstocks. The results from the various simulation models presented in the previous chapter will be collected and analysed. The analysed results will be presented in graphical and tabular formats to highlight the distinctive behaviours of these processes. The energy analysis will be supplemented by a brief economic analysis of the key mechanical units such as the small-scale gas turbine and steam turbine. An exergy analysis of selected case studies of the power cycles will be explored, to find the process units with the highest inefficiencies.

4.2 Model Validation

The model validation process is done through a two-phase process, where a theoretical model is developed for the plasma gasification reactor according to literature. For the second stage, the model is consolidated to replicate the model NECSA used for their demonstration system.

Theoretical validation

In the validation of the plasma gasification Aspen Plus model, the fuel used in the study by Minutillo et al, (2009) was tested and the synthesis gas results obtained by the model were compared to those obtained within this study. The plasma gas used in the Minutillo et al, (2009) study is an oxygen enriched air stream with 40% wt. O_2 and 60% wt. N_2. The Proximate and Ultimate analysis of the refused derived fuel used can be found in **Table 3-1** of **Chapter 3.2.7**.

The main assumptions that were made can be found in **Table 4-1**. The results for the validation of the theoretical Aspen Plus model for the plasma gasification reactor can be found in **Table 4-2**.

Table 4-1: Plasma gasification model operational assumptions

Plasma gas type	**O_2 40% v, N_2 60% v**
Gasification pressure (bar)	1
HTR Temperature (°C)	2500
Output syngas temperature (°C)	1250
RDF input, LHV (kW)	12900
Plasma gas mass flow (kg/hr)	3600
RDF mass flow (kg/hr)	2314.8
Plasma Torch Temperature (°C)	4000

Source: (Minutillo, et al., 2009)

Table 4-2: Syngas model validation results

Mole fraction (%)	**Minutillo et al, 2009**	**The Model**	**Absolute Difference**
H_2	31.48	30.81	0.67
CO	38.73	37.42	1.31
CO_2	0	0.01	0.01
N_2	16.32	17.45	1.13
CH_4	0	0.02	0.02
H_2O	12.5	13.74	1.24
HCl	0.31	0.32	0.01
H_2S	0.22	0.22	0
COS	0.01	0.01	0

Table 4-2 highlights the synthesis gas product obtained by Minutillo et al, (2009) and the results generated from the model. Some slight variations can be noted for the synthesis gas results between these two models; however, they are within range of each other.

Validation using NECSA model data

Through some adjustments to the model for the plasma gasification reactor, it can be configured to produce a synthesis gas quality like what was obtained by the NECSA model of their demonstration plant. The comparison of the results between the two models can be seen in **Table 4-3**.

Table 4-3: Demonstration Model Results Validation

		Demonstration Plant Model Syngas Product Data	**Aspen Model Syngas Product Data**	**Absolute Difference**
Temperature	°C	1000	1000	0
Pressure	bar	0.84	0.84	0
Mass Flows	**kg/hr**	**30.864**	**32.468**	**1.604**
H_2	kg/hr	1.309	1.309	0
N_2	kg/hr	3.83	3.869	0.039
CO	kg/hr	18.31	19.19	0.88
CO_2	kg/hr	4.031	4.946	0.915
H_2O	kg/hr	3.373	3.141	0.232
H_2S	kg/hr	0.006	0.004	0.002
HCl	kg/hr	0.003	0.01	0.007

Table 4-3 highlights some slight differences between the synthesis gas products of these two models. These compositional differences are expected due to the number of assumptions made in the simulation. The assumption made in the development of the current model might differ from those made for the NECSA model.

In assessing the performance of a plasma gasification reactor in the conversion of biomass and other organic feedstock, the cold gas efficiency is used. The cold gas efficiency associates the performance of the process with the calorific values of the input and the output products. The different values involved in the calculation of the cold gas efficiency for the plasma gasification model are shown in **Table 4-4**. The calculation for the cold gas efficiency of the plasma gasification reactor can be found in **Table 4-4**.

Table 4-4: Cold Gas Efficiency

Mass flow syngas (kg/hr)	32.47
LHV syngas (kJ/kg)	10812.26
Mass flow biomass (kg/hr)	23.39
LHV biomass (kJ/kg)	19200
W_{torch} (kJ/s)	20.72
Cold Gas Efficiency (%)	**67.04**

Cold Gas Efficiency Calculation

$$\dot{m}_{syngas} \cdot LHV_{syngas} = 32.47 \frac{kg}{hr} \cdot \frac{10812.26kJ}{kg} \cdot \frac{1hr}{3600s} = 97.52 \frac{kJ}{s} = 97.52\ kW$$

$$\dot{m}_{biomass} \cdot LHV_{biomass} = 23.39 \frac{kg}{hr} \cdot \frac{19200kJ}{kg} \cdot \frac{1hr}{3600s} = \frac{124.75kJ}{s} = 124.75\ kW$$

$$\eta_{CGE} = \frac{97.52\ kW}{124.75\ kW + 20.72\ kW} \cdot 100 = 67.04\%$$

The obtained cold gas efficiency for the plasma gasification reactor model is 67% and previous studies of commercial scale gasification reactors have a proven typical cold gas efficiency of 65-80% (Luque & Speight, 2015). Even with the presence of the plasma torch which significantly reduces the thermal efficiency of the gasifier, the addition of oxygen in the plasma gas reduces the work potential for the plasma torch, due to the energy release during the combustion of the biomass constituent material (Muvhiiwa, et al., 2021). In the study by Muvhiiwa, et al. (2021), it was shown that the use of oxygen as a plasma gas has the added benefit of increasing the heat energy present in the gasification reactor. This is a result of the combustion of some of the synthesis gas components such as H_2 and CO. A better thermodynamic performance of the reactor is responsible for the calorific value of the produced synthesis gas, which in this case is high indicating that far more thermal value can be derived from this synthesis gas in downstream processes.

4.3 Energy Balance

4.3.1 Brayton Cycle

The power production results for the Brayton cycle system case studies can be seen in **Table 4-5**.

Table 4-5: Gas Turbine cases Energy Balances

Case 3b		Case 3c		Case 3d	
Power Production (kW)		**Power Production (kW)**		**Power Production (kW)**	
TURBINE	44.45	TURBINE	49.95	TURBINE	44.62
				TURB-EXP	5.74
Total	**44.45**	**Total**	**49.95**	**Total**	**50.36**
Power Consumption (kW)		**Power Consumption (kW)**		**Power Consumption (kW)**	
BLOWER	0.98	COMPR	22.9	BLOWER	1.03
		Plasma Gas			
BLOWER2	2.05	compressor	0.88	BLOWER2	2.16
COMPR	20.48	DC-ARC	20.72	COMPR	20.57
				PLASMA GAS	
DC-ARC	20.72			COMPRESSOR	0.88
				DC-ARC	20.72
Total	**44.23**	**Total**	**44.5**	**Total**	**45.36**
Backwork Ratio (Excl. DC-ARC)	**0.53**	**Backwork Ratio (Excl. DC-ARC)**	**0.48**	**Backwork Ratio (Excl. DC-ARC)**	**0.49**
Backwork Ratio (With DC-ARC)	**1.00**	**Backwork Ratio (With DC-ARC)**	**0.89**	**Backwork Ratio (With DC-ARC)**	**0.90**

Table 4-5 shows the energy production of the gas turbine for the different cases in this study. The analysis focuses on the mechanical units of the power cycle with the power consumption side and the power production side. The back work ratio for the power cycle is also included and this ratio is used to show the fraction of the power generated and used within the power cycle. In the power consumption side of the cycle, all the plants power consuming units are shown including the DC-ARC plasma torch and the compressor used to pressurize the plasma gasification reactor for the hypothetical case studies.

The air to fuel ratio affects the power production capacity of the system, and this can be seen through the power production for **Case 3c** of 49.95 kW while the other gas turbine power cycles produce power below 45 kW. In **Case 3c**, the synthesis gas enters the combustion chamber at temperatures far higher than for the other cases, this then requires more air to ensure a

temperature of 1000 °C is reached after combustion, which is why the mass flowrate of the hot gas is far higher than for the other cases. Even though the gas turbine in **Case 3c** produces the highest amount of power, the overall power produced in **Case 3d** is much higher due to the presence of a gas turbine expander which utilises the sensible heat in the synthesis gas product of the plasma reactor to produce **5.74 kW** of power. A higher air to fuel ratio indicates that more gas flowed through the gas turbine, resulting in more power being generated. As other influential factors in the operation of the gas turbine such as the temperature, pressure, pressure ratio and isentropic efficiency are constant, variations in the air to fuel ratios are going to have major influences on the gas turbine power output as seen through the power output for **Case 3c**.

The energy balances for the missing case studies can be found in **Appendix A.3.1**.

The air to fuel ratios for the gas turbine case studies can be seen in **Table 4-6** with **Case 3c** having the highest air to fuel ratio at 12.90.

Table 4-6: Air to Fuel Ratio for the Gas Turbine Case studies

	Case 3b	**Case 3c**	**Case 3d**	**Case 3e**
Air (kg/hr)	356.26	398.24	357.77	362.25
Fuel (kg/hr)	30.86	30.86	30.86	30.86
A-F Ratio	**11.54**	**12.90**	**11.59**	**11.74**

A simple case study of the Brayton cycle modelled through **Case 3b** has no surplus power generation capacity as all of the power produced accounts for the power consumed by the cycle. The troubling part about there being no surplus power in this system is the flue gas stream leaves the gas turbine at a temperature of 657 °C. A lot of sensible heat is lost as the gas turbine exhaust stream is discarded into the environment. Previous studies have shown that only about 30 to 40% of the potential heat from the fuel used in gas turbines is converted into mechanical work (Jadhao & Thombane, 2013). The change in temperature of the hot gas from 1000 °C to 657 °C as it is expanded in the gas turbine supports this statement. For a large system this might not be much of a stumbling block, however for such a small system the loss of this waste heat has major influences on the thermal efficiency that can be achieved for this power cycle.

For the scenario with the burning of synthesis gas without any prior treatment, modelled through **Case 3c**, there is a surplus in power generation of about **5.77 kW** which is 11.6% of the power production. For **Case 3d** and **Case 3e** the surpluses are 5.32 kW and 3.9 kW which accounts for 10.6% & 8.1% of the total power produced through these power cycles. These modified versions of the Brayton cycle have a higher potential for the generation of power, even with the loss of sensible heat through the exhaust gas flowing out of the gas turbines at high temperatures. The power generation capacity for **Case 3e** can be attributed to the two-stage expansion system and the inter-heater. The inter-heater increases the amount of sensible heat available for expansion in the second turbine resulting in more power being generated through this turbine. The inclusion of the inter-heater, however, means that more fuels will have to be combusted to supply the heat necessary to get the hot gas back to 1000°C. Incorporation of a heat recovery system is observed to drastically improve the power generation capabilities of these systems.

The backwork ratio can also be included in the energy analysis of gas power cycles to illustrate how much of the power generated is used within these power cycles. In gas power cycles typical backwork ratios range from 40% – 80% and with the exclusion of the DC-ARC plasma torch which is not a part of the gas power cycles, the backwork ratio for all the case studies can be noted to fall within the commercial limits. For the overall process, the backwork ratio can be noted to be near one for most of these case studies. This indicates that a lot of the power generated through this system is consumed by the mechanical units, with the air compressor and the DC-ARC plasma torch consuming most of the power generated.

This section investigates how much of the heat present in these Brayton cycle models is converted into mechanical work. The thermal efficiencies achieved in these different configurations are illustrated in **Figure 4-1**.

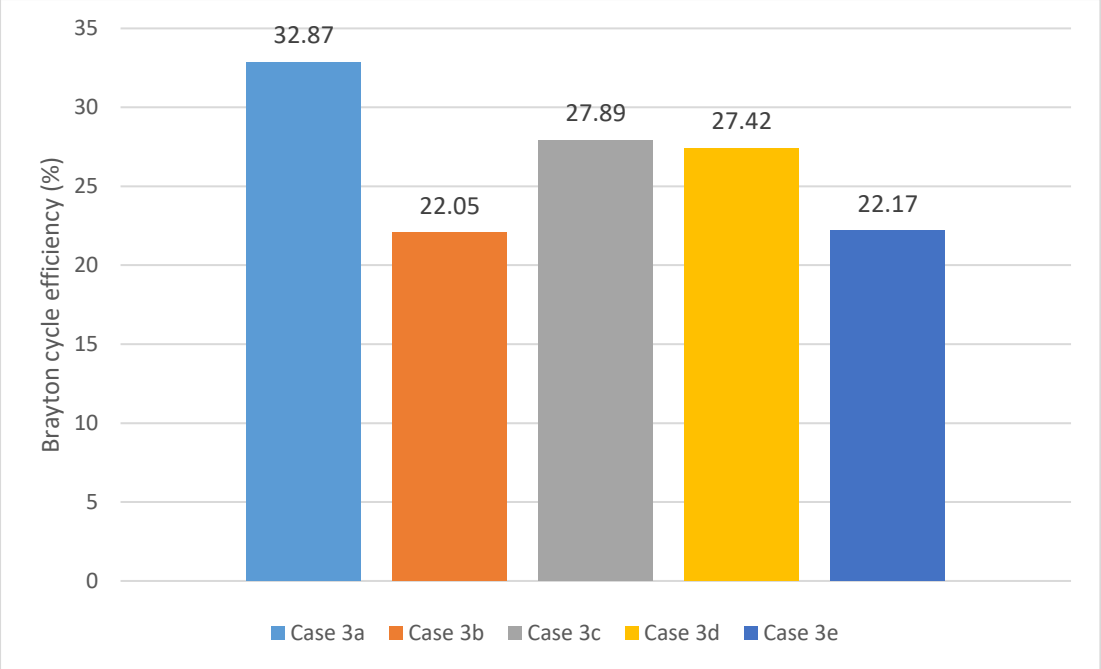


Figure 4-1: Brayton cycle thermal efficiencies for the various cases

Figure 4-1 shows the thermal efficiencies of the different Brayton cycle case studies. These include an ideal version of the simple Brayton cycle, **Case 3a** to highlight the effect of the isentropic efficiency on the thermal efficiency for the modelled simple Brayton cycle case studies. The ideal (isentropic efficiency=100%) modelled case for the simple Brayton cycle achieves a thermal efficiency of 32.87% while the real Brayton cycle at an isentropic efficiency of 85% achieves a thermal efficiency of 22.05%, resulting in a 10.82% difference between these two systems.

For the real Brayton cycle case studies which are operating at an isentropic efficiency of 85% for the compressor and turbines, **Case 3c** achieves the highest thermal efficiency of 27.89%. This is closely followed by **Case 3d** which achieves a thermal efficiency of 27.42%. The high efficiency achieved by these two case studies can be attributed to the absence of the quench probe which results in a sensible heat loss of 16.6 kW. The utilization of this heat energy from the plasma gasification reactor effluent into the Brayton cycle increases the amount of heat available towards the production of mechanical work. For **Case 3c** the flowrate of the air increases by more than 40 kg/hr compared to the other systems resulting in a higher air to fuel ratio. A higher air to fuel ratio results in a higher power production capacity. The synthesis gas for **Case 3b** and **Case 3c** have different LHV with the synthesis gas for **Case 3c** being crude. The higher feed temperature of the synthesis gas in **Case 3c** result in more air being required to reduce the temperature of the hot combustion gas to 1 000 °C.

The two-stage expansion gas turbine cycle shown by **Case 3e** does not have much of an improvement when compared to **Case 3b** which is the single gas turbine expansion system. For **Case 3e** the addition of more heat to the process does not have much of an influence on the power generated which results in the thermal efficiency being lower, as there is an excess of heat while there is not much of a difference with the power generated.

Although **Case 3c** and **Case 3d** results in thermal efficiencies that are higher than those for the other case studies, they are all below the typical efficiency of a Brayton cycle system in the range of 30% - 40% (Langston, 2020). Improving these thermal efficiencies can only be achieved through changes to the process, which is demonstrated by **Case 3c** and **Case 3d**. The utilization of the sensible heat from the hot synthesis gas has been proven to improve the thermal efficiency for the gas turbine.

Other possible means of improving the performance of the Brayton power cycle using synthesis gas involves increasing the scale and steam injection. The steam injection technique was investigated by (Renzi, et al., 2017), using a model for a 100 kW micro gas turbine using synthesis gas generated from biomass. A thermal efficiency of 27.2% is achieved by the gas turbine when using the steam injection improvement to the gas turbine cycle. In this model by (Renzi, et al., 2017), the gas turbine has a 145.656 kg/hr fuel consumption rate whilst for the current model there is a 30.864 kg/hr fuel consumption rate for all the case studies. The extent to which this change in the fuel consumption rate has on the thermal efficiency might determine the effectiveness of this technique in the improvement of the gas turbine performance.

4.3.2 Rankine Cycle

The Rankine cycle is an externally fired power cycle, and the thermal efficiency of externally fired systems are much lower than those of internally fired systems, due to the intermediate heat transfer system connecting the combustion system to the power cycle. This loss of heat quality can be seen through the lower power generation capacity in the Rankine cycle, when compared to the Brayton cycle and the power dynamics of the Rankine cycle case studies can be seen in **Table 4-7**.

Table 4-7: Steam Turbine cases energy balances

Case 4b		**Case 4c**		**Case 4f**	
Power Production (kW)		**Power Production (kW)**		**Power Production (kW)**	
ST-TURB	31.3	ST-TURB	35.48	STURB	10.64
				STURB2	21.75
Total	**31.3**	**Total**	**35.48**	**Total**	**32.39**
Power Consumption (kW)		**Power Consumption (kW)**		**Power Consumption (kW)**	
BLOWER	1.23	COMPR	1.98	BLOWER	1.23
COMPR	1.74	PUMP1	0.09	COMPR	1.74
PUMP1	0.08	DC-ARC	20.72	PUMP1	0.08
DC-ARC	20.72	PLASMA GAS COMPRESSOR	0.56	DC-ARC	20.72
Total	**23.77**	**Total**	**23.35**	**Total**	**23.77**
Evaporator (kW)		**Evaporator (kW)**		**Evaporator (kW)**	
Boiler	86.02	Boiler	97.49	Boiler	86.02

Case 4c which modelled the synthesis gas being directly combusted in the boiler without being quenched or cleaned has the highest power produced of 35.48 kW. This is closely followed by the two-stage expansion steam turbine system **Case 4f** at 32.39 kW and lastly the simple steam turbine power cycle **Case 4a** sees the lowest power produced of 31.3 kW. The Rankine cycle has a far higher conversion of heat into mechanical work compared to the Brayton cycle, as the steam can be expanded until it reaches a vapour fraction limit of 0.95 which occurs below temperatures of 100 °C.

All the cases generate a surplus of power with **Case 4c** producing the highest surplus at 12.13 kW which is 34.2% of the total power produced. **Case 4f** generates a surplus of 8.62 kW which is 26.6% of the total power. Lastly **Case 4b** produces the lowest net power output amongst the three case studies of 7.53 kW at 24.1% of the total power produced. A point of note for the Rankine cycle modelled case studies is that a positive net power output is obtained for all of the cases after accounting for all of the process units that consume mechanical power such as compressors, pumps and the DC-ARC plasma torch.

Compared to the power production capability of the Brayton cycle modelled cases shown in **Table 4-5**, the Rankine cycle produces power in smaller quantities but the demand of power within the process is smaller as modelled cases such as **Case 4c** produce power surpluses of

34.2% of the total power produced. The net power production surplus of 34.2% (12.13 kW) is higher than all the modelled Brayton cycle cases, as **Case 3c** produced the highest net power production surplus of 5.77 kW at 11.6% of the total power produced.

A similar analysis into the first law of thermodynamics is carried out for all the Rankine cycle models. The thermal efficiencies at which these steam turbine cycles operate can be found in **Figure 4-2**.

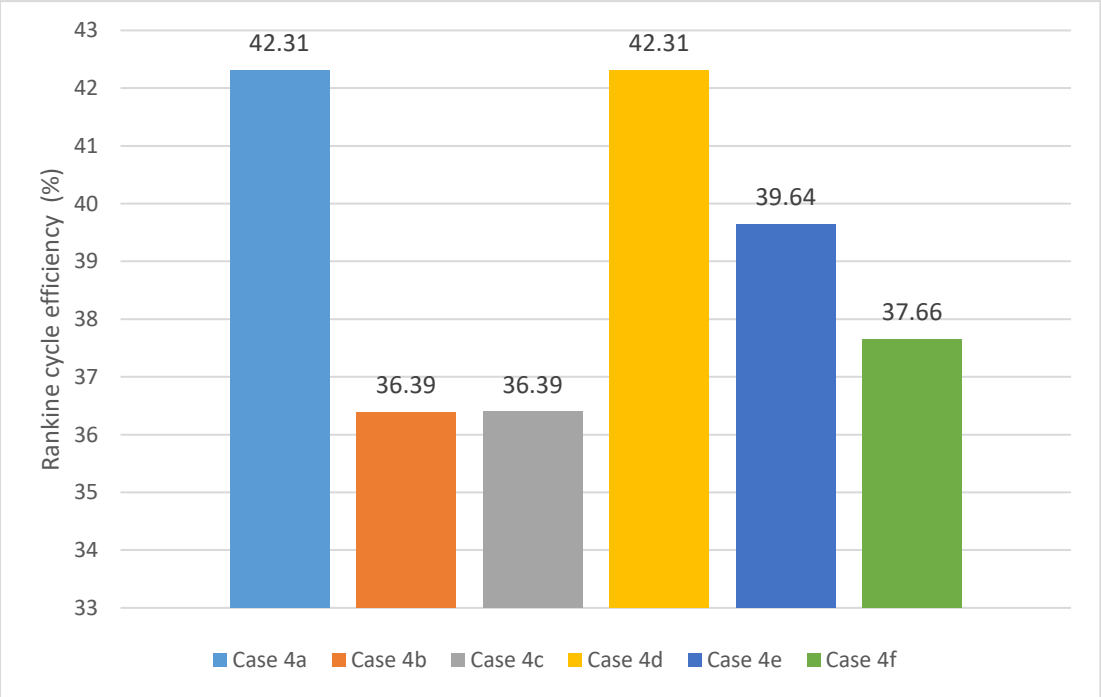


Figure 4-2: Rankine cycle thermal efficiency

The thermal efficiencies shown in **Figure 4.2** illustrate a direct contrast between the ideal and real versions of the three steam Rankine cycle cases. These are i) the simple steam Rankine cycle (case 4a & 4b), ii) a direct fired steam Rankine cycle (case 4c & 4d) and iii) a two-stage expansion steam Rankine cycle (case 4e & 4f).

The thermal efficiencies achieved by the steam Rankine cycle are all reasonable as they are all above 35%, and there are minor variations between the different cases with **Case 4f**, the two-stage steam expansion power cycle achieving the highest thermal efficiency of 37.66%. The expansion of the steam over two stages is a lot more efficient than a single stage, due to the irreversibility's that occur over a large temperature change in one stage compared to smaller temperature changes over numerous stages. In the two-stage expansion steam Rankine cycle, a high-pressure turbine and low pressure turbine system exists. This reduces the load on the

turbine system and turbines operating at lower loads and pressures are noted to be more efficiency and experience less heat loss (Blažević, et al., 2019).

The similarities in the thermal efficiencies for **Case 4b** and **Case 4c** can be explained using the temperature – entropy diagram. The temperature entropy diagram is a better illustration of the work done by the system or to the system and the heat added to the system or lost by the system. This can lead to a better understanding of the thermal efficiency achieved by the system in respect to how the temperature, pressure and entropy vary through the different stages associated with the power cycle.

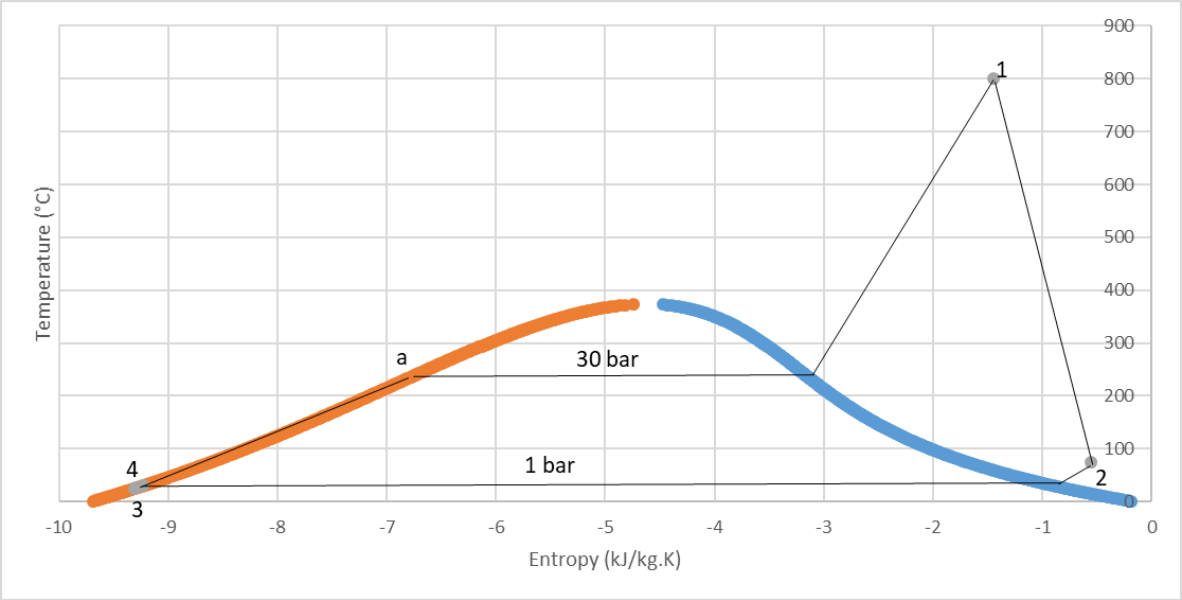


Figure 4-3: Temperature Entropy Diagram for Case 4b

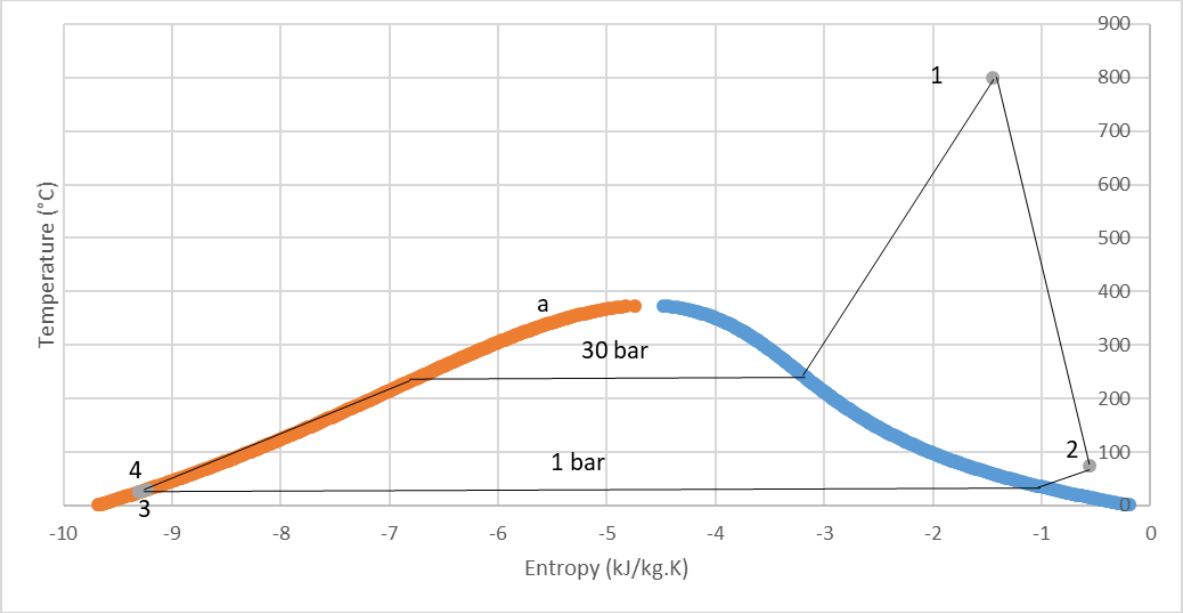


Figure 4-4: Temperature Entropy Diagram for Case 4c

The physical properties for **Case 4b** and **Case 4c** are similar leading to the T-s diagrams for both these case studies being similar as shown in **Figure 4-3** and **Figure 4-4**. Even with the variations in the power production capabilities of these two systems, the usage of the heat added during the superheating process of the working fluid leads to the same path and conclusion. Further analysis of the T-S diagram shows that the heat from the steam is not fully utilized as point 2, which is the turbine effluent is still in the superheat region. At point 2 though the pressure is low at 0.03bar and further expansion of this steam product might not be thermodynamically possible. The temperature-entropy diagrams for **Case 4b** and **Case 4c** shown in **Figure 4-3** and **Figure 4-4** support the similar thermal efficiencies achieved by these two cases as there is a similar behaviour with the temperature, pressure and entropy between these case studies.

Further analysis of **Case 4b** and **Case 4c** through the efficiency using the potential heat from the fuel source shows that **Case 4c** has a better efficiency. The efficiency calculated through the lower heating value formula gives an indication of how much of the potential heat from the fuel source is used to generate power. The comparison between the efficiencies between these two processes can be seen in **Table 4-8**.

Table 4-8: Lower Heating Value Efficiencies of Case 4b and Case 4c

	Case 4b	**Case 4c**
Efficiency (LHV) (%)	32.95	37.36

Table 4-8 shows a higher efficiency for **Case 4c** when compared to **Case 4b** and this can be attributed to more heat being available in **Case 4c**. The addition of the sensible heat in the synthesis gas stream directly to the boiler, increases the amount of heat present in the process and this in return increases the amount of power that can be generated. The temperature restrictions on the superheating of the water means that only a certain amount of this heat can be used to generate steam. A good amount of heat is lost through the flue gas stream in **Case 4c** and the only way to recover this heat would be the addition of more water.

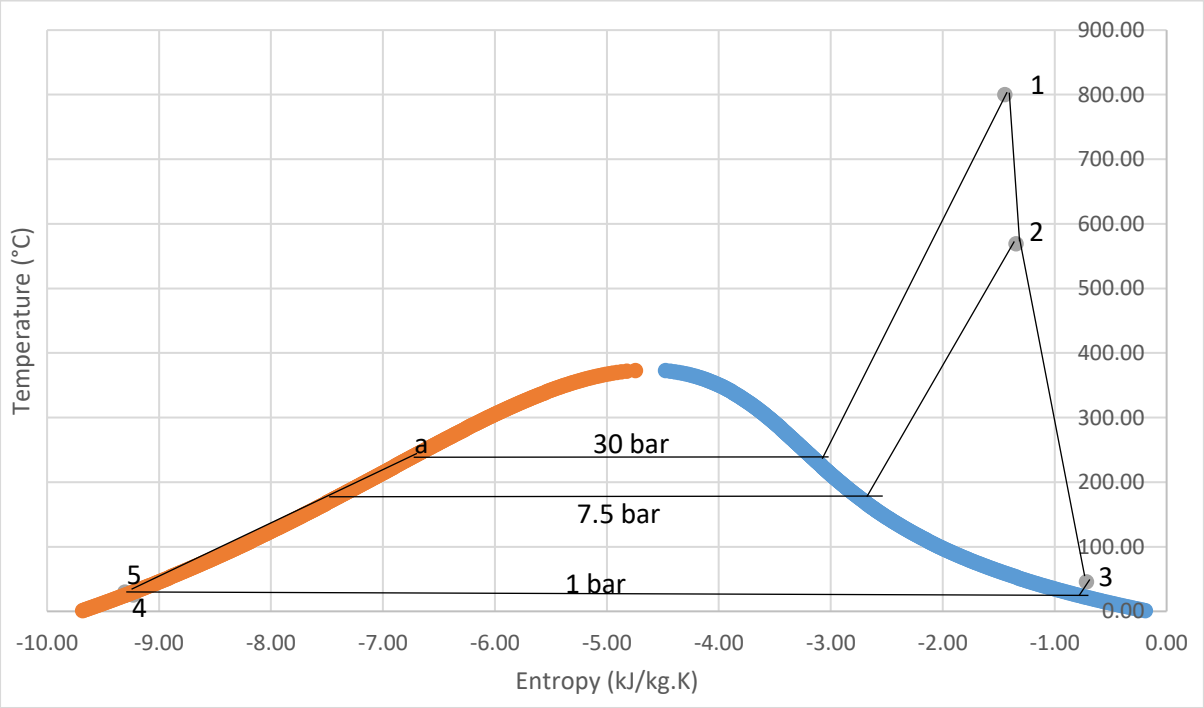


Figure 4-5: Temperature Entropy Diagram for Case 4f

For the two-stage steam turbine expansion power cycle, the T-s diagrams differs as can be seen in **Figure 4-5**, with the contributions of the two-stage gas turbine being noted through the division of the T-S diagram. The division in the expansion stage of the power cycles to two stages results in a steeper slope on T-S diagram as can be noted in the comparison of **Figure 4-5** and **Figure 4-3**. The steeper slope results in the area under the curve being greater, which means a higher thermal efficiency is achieved by the two-stage expansion power cycle.

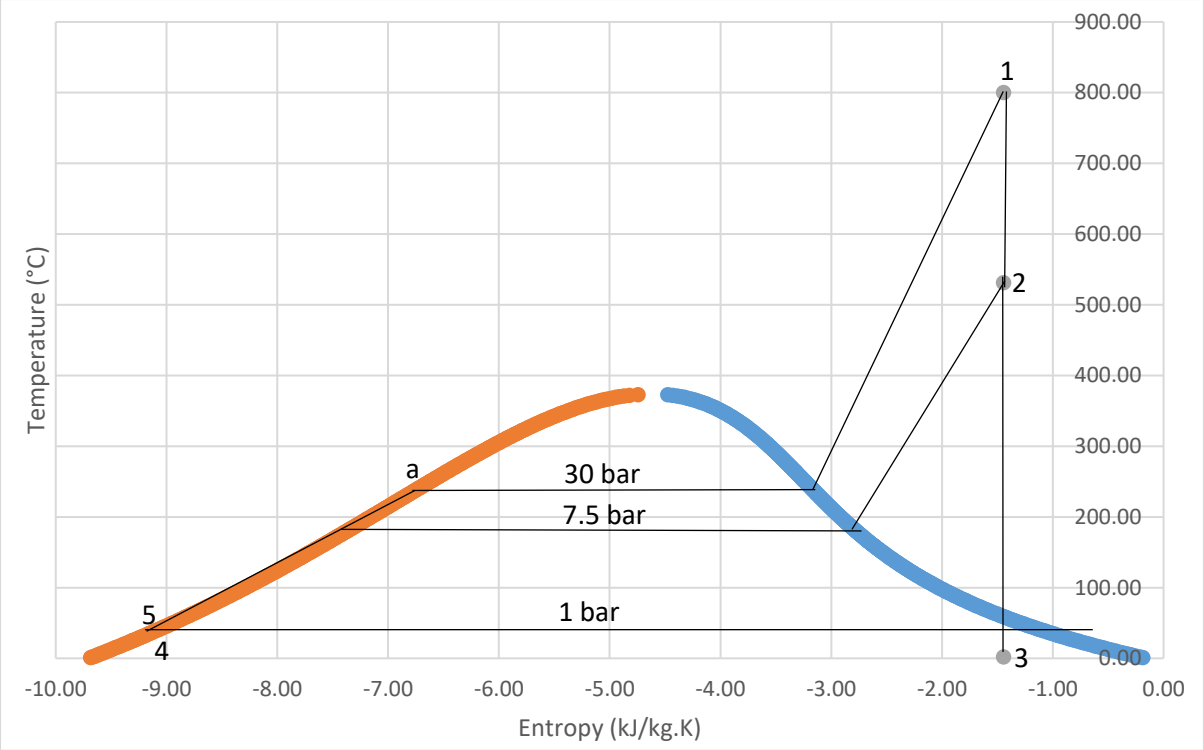


Figure 4-6: Temperature Entropy Diagram for Case 4e

A comparison of the ideal cycle and real cycle through the temperature entropy diagram can be done using **Figure 4.5** and **Figure 4.6**. A point to note is that in the ideal cycle the heat value in the steam is fully utilized, point 3 (the spent steam) is well within the saturation region.

The thermal efficiencies achieved for all of these Rankine cycle case studies show great promise as they are all above 30%. All of these simulated case studies are sub-critical as the pressure is below 22.1 MPa/221 bar, and typical fossil fuel based sub-critical Rankine cycle systems have a thermal efficiency of 36% - 40% (Salazar-Pereyra, et al., 2016). All of the simulated case studies through realistic isentropic conditions are within this thermal efficiency framework.

4.3.3 Combined Power Cycle

The Combined power cycle aims to account for the shortfalls of the Brayton cycle with regards to the waste heat being discarded to the environment. A secondary power cycle is added to the initial cycle with the aim of recovering heat from the gas turbine exhaust stream and this cycle is a steam Rankine cycle. These case studies are modelled and the results in terms of energy consumption and energy production for these modifications are shown in **Table 4-9**.

Table 4-9: Combined Power cycle cases energy balances

Case 5b		**Case 5d**		**Case 5f**	
Power Production (kW)		Power Production (kW)		Power Production (kW)	
TURBINE	44.43	TURBINE	47.68	TURBINE	44.43
ST-TURB	14.62	ST-TURB	14.62	TURB-EXP	5.74
				ST-TURB	14.62
Total	**59.05**	**Total**	**62.3**	**Total**	**64.79**
Power Consumption (kW)		**Power Consumption (kW)**		**Power Consumption (kW)**	
BLOWER	1.26	COMPR	20.36	BLOWER	1.26
BLOWER1	2.19	PUMP	0.02	BLOWER1	2.19
COMPR	20.36	PLASMA GAS COMPRESSOR	0.56	COMPR	20.36
PUMP	0.02	DC-ARC	20.72	PLASMA GAS COMPRESSOR	0.56
DC-ARC	20.72			PUMP1	0.02
				DC-ARC	20.72
Total	**44.55**	**Total**	**41.66**	**Total**	**45.11**
Heat Recovery (kW)		**Heat Recovery (kW)**		**Heat Recovery (kW)**	
HRSG	63.10	HRSG	63.10	HRSG	63.10

Table 4-9 shows the power production (kW), power consumption (kW) and the heat used by the HRSG (kW). The incorporation of the heat recovery system to the combined cycle can be seen to improve the power generation of the process when comparing **Table 4.9** to **Table 4.5**. The credibility of this investigation lies in the same amount of fuel being combusted for all the power cycles, however the differing configurations of the cycles, bring about changes to the amount of air that is required for the combustion of this fuel. In some of the configurations the synthesis gas fuel source is fed to the combustion chamber at different temperatures, which results in different amounts of air being required in the combustion of this fuel to ensure a turbine inlet temperature of 1 000 °C.

In terms of the net power output **Case 5d** which involves the direct combustion of the synthesis gas without any pre-treatment processes generates a power output of 62.3 kW. Case 5d consumes the least amount power at 41.66 kW resulting in a power surplus of 20.64 kW which is 33.1% of the total power produced by this cycle. The model for the combined cycle with a turbine expander prior to the cycle (**Case 5f)**, produces the highest power output of 64.79 kW and a surplus in power of 19.68 kW. The simple combined power cycle modelled as **Case 5b** produced the lowest amount of power between the three variations of the combined cycle of 59.05 kW and the lowest power surplus of 14.5 kW. The surplus power produced for all of

these cases is higher than 20% of the total power production for each case. The Brayton cycle is a major contributor to the power consumption especially the air compressor and the plasma torch which contributes over 90% of the total power consumption. An analysis of the thermal efficiency of these case studies will show the effectiveness these power cycles had in converting the heat to power.

The energy analysis for the combined power cycle through the 1st law of thermodynamics is shown in **Figure 4-7**.

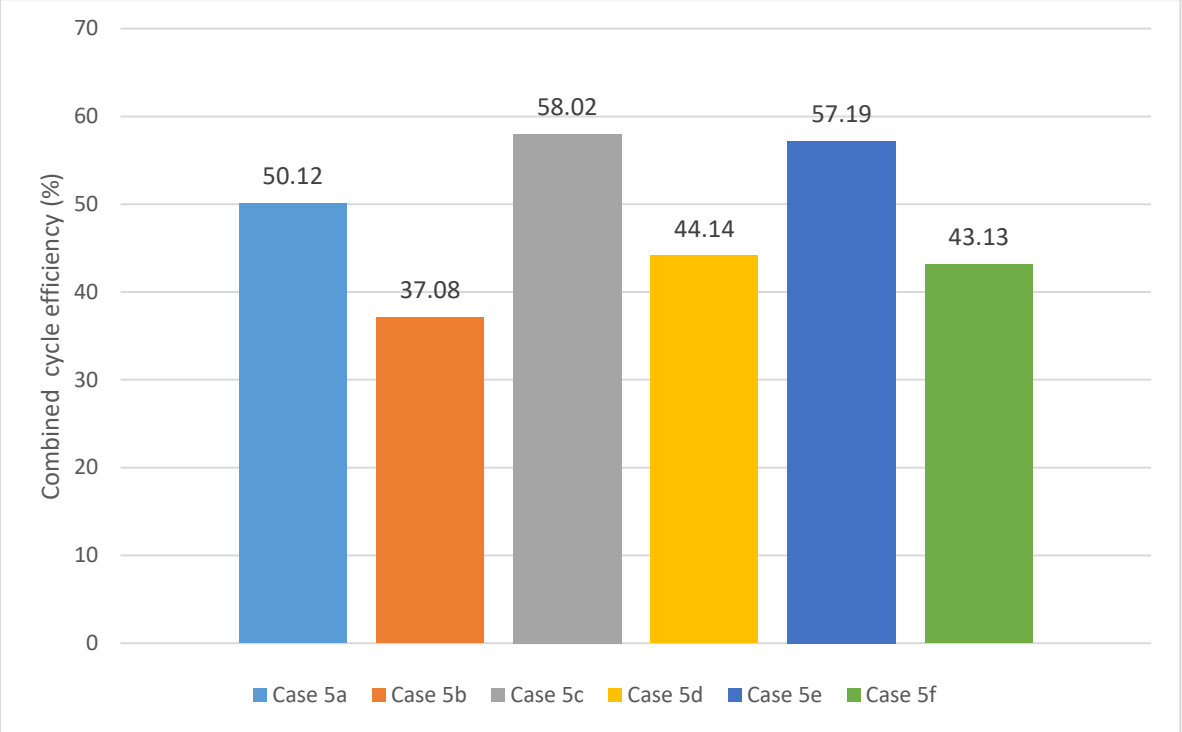


Figure 4-7: Combined cycle thermal efficiency

The thermal efficiencies shown in **Figure 4-7** illustrates a direct contrast between the ideal and real versions of the three combined power cycle case studies. These case studies are, i) the simple combined power cycle (**Case 5a** & **Case 5b**), ii) the combined power cycle with direct synthesis gas firing & no pre-treatment stage of the synthesis gas (**Case 5c** & **Case 5d**), and iii) the combined power cycle with a gas turbine expander present prior to the power cycle (**Case 5e** & **Case 5f**). The Brayton cycle section operates at an isentropic efficiency of 85% while the steam Rankine cycle section operates at an isentropic efficiency of 86%.

The thermal efficiencies of the cycles under ideal conditions are used as means of illustrating how different the thermodynamic performance of the cycle, would be if no irreversibility's were present in the system. The conditions necessary for these efficiencies to be achieved are

thus highly unrealistic. The idealized thermal efficiencies of these power cycles are included to show the effects of isentropic efficiency on the thermal efficiency and what could be achieved if idealized conditions were feasible. In the case of the actual version of these combined cycles, **Case 5d** achieves the best thermal efficiency of 44.14% closely followed by **Case 5f** with a thermal efficiency of 43.13%.

The simple combined cycle **Case 5b** achieves the lowest thermal efficiency amongst these three configurations of the combined cycle of 37.08%. When compared to the other simple power cycles such as the gas turbine and steam turbine, this is the best thermal efficiency. These results highlight the effectiveness of the employing a waste heat recovery system through the bottoming power cycle.

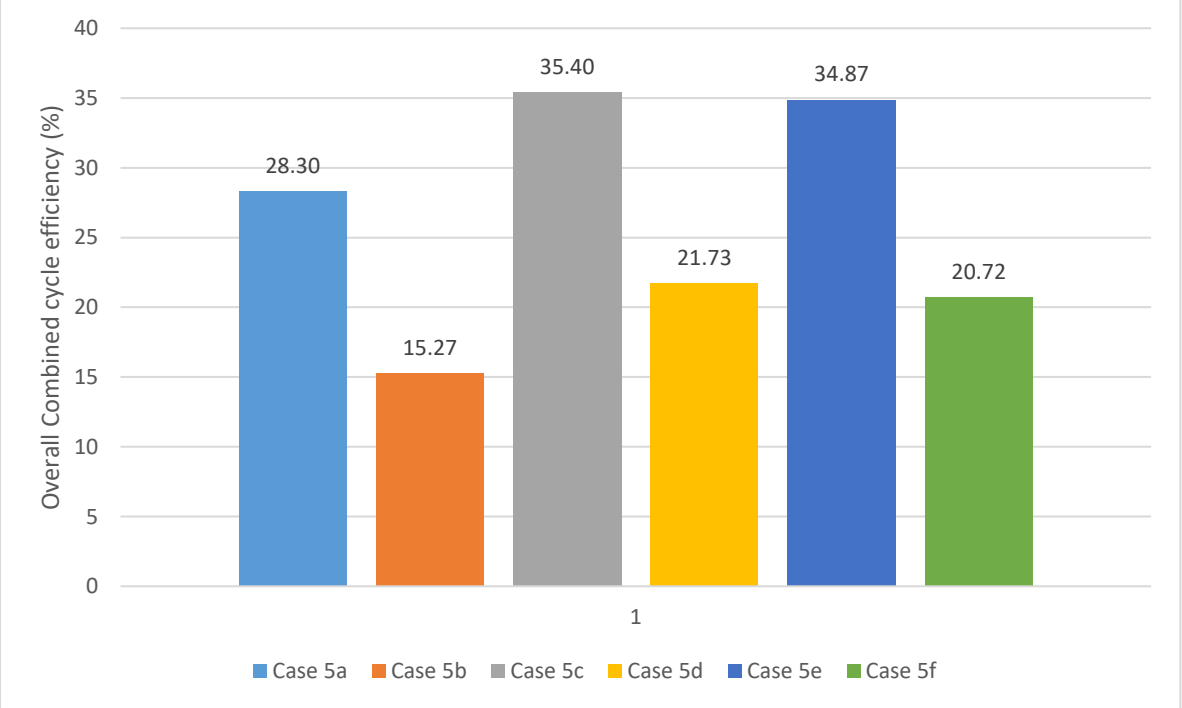


Figure 4-8: Overall integrated plasma gasification combined cycle thermal efficiency

Figure 4-8 shows the thermal efficiency of the overall process achieved with the inclusion of the power required by the plasma arc torch. The energy demanding nature of the DC-ARC plasma torch can be seen through the drastic drop in the thermal efficiencies of these various system. The efficiency for **Case 5b** decreases from 37.08% to 15.27%, for **Case 5d** there is a drop from 44.14% to 21.73% and lastly for **Case 5f** a decrease from 43.13% to 20.72%. The comparison of **Figure 4-7** and **Figure 4-8** suggests that even though the process attains a surplus in the net power produced, energy demanding process units such as the air compressor and DC-ARC plasma torch essentially affect the thermodynamic behaviour of the process.

There is also no feasible way of optimizing them as the process needs pressurized air for the combustion of the synthesis gas. The optimization of the smaller process units such as the quench probe do make a difference to the thermal efficiency but still not enough to have drastic impact on the process.

Typical combined power cycles are expected to have a thermal efficiency between 50% - 60% (Ramireddy, 2012), with underperforming power cycles having a thermal efficiency below this range. All of the combined power cycle case studies simulated under realistic isentropic efficiency conditions can be noted to be below the projected range, even **Case 5d** with the highest thermal efficiency at 44.14%. This performance is mostly due to the topping Brayton cycle which produced suboptimal results using synthesis gas. These performance ranges for all of these power cycles, were subject to the power cycles using a fossil fuel source and the shift to synthesis gas might be another attributing factor. Synthesis gas has been known to have LHVs which are lower than those of fossil-based fuel sources such as bituminous coal and natural gas. These fossil fuel sources have LHVs which are all above 20 000 kJ/kg as a minimum value, while the current wet synthesis gas used in this study has a lower heating value of 11 079 kJ/kg.

4.3.4 Real Synthesis Gas Composition from the NECSA Reactor

A synthesis gas product generated by the actual demonstration plasma gasification reactor has the composition shown in **Table 4-10**. This synthesis gas product is used on the gas turbine model to test the power generation capacity that can be attained from it compared to the synthesis gas generated by the plants model.

Table 4-10: Experimental synthesis gas composition

Syngas Composition	
Pressure (kPa)	34.9
Mole Fraction (%)	**100**
Acetylene	0.50
Carbon dioxide	8.70
Carbon Monoxide	44.80
Ethylene	0.04
Hydrogen	22.40
Methane	3.10
Nitrogen	19.50
Oxygen	0.43
Argon	0.53

Using the synthesis gas product shown in **Table 4-10** in the gas turbine model with the process conditions shown in **Table 3-6**, the power generation obtained is shown in **Table 4-11**.

Table 4-11: Energy Analysis of the gas turbine

Power Consumed (kW)	
BLOWER	4.22
COMPR	12.67
Total	**16.89**
Power Produced (kW)	
TURBINE	28.36
Net Power Output (kW)	**11.47**
LHV Syngas (kJ/kg)	9126.87
Mass flowrate of syngas (kg/hr)	**27.49**
Efficiency (LHV) (%)	**16.46**

The synthesis gas from the NECSA reactor has a lower LHV when compared to the synthesis gas generated by the model, leading to lower power production as less oxygen is required for the combustion of this synthesis gas. This effect in power production can be seen by comparing the power generation of the current model at **28.36 kW** with that of **Case 3b** at **44.45 kW**.

This is due to the differences in LHVs of the synthesis gas products, and consequently the air to fuel ratios shown in **Table 4-12**.

Table 4-12: Air to Fuel Ratio

	Case 3b	**Experimental**
Air (kg/hr)	356.26	220.35
Fuel (kg/hr)	30.86	30.86
A-F Ratio	**11.54**	**7.14**
LHV (kJ/hr)	**11079**	**9126.87**

The results for this experimental synthesis gas case study suggests that the use of this fuel for power generation is highly unfeasible as the system is unable to meet the internal power demand. After accounting for the DC-ARC plasma torch, there is a net power deficit of 9.25 kW meaning that the system requires an external power source to meet internal power demand. An increase to the temperature and pressure ratio could be an alternative to improving the power generation capacity and thermal efficiency of this power cycle.

4.4 Sensitivity Analysis of the Experimental Synthesis Gas Turbine

A sensitivity analysis is performed for the gas turbine using the real synthesis gas compositions from the experimental demonstration plant. This sensitivity analysis is performed to investigate the effects of pressure ratio and temperature on the power produced and the thermal efficiency.

For the pressure ratio sensitivity analysis, the pressure is varied at four intervals of 5, 8, 11 and 15 bar with a constant temperature of 1 000 °C. In the temperature sensitivity analysis, the temperature is varied at four intervals of 1 000 °C, 1 200 °C, 1 300 °C and 1 400 °C with a constant pressure ratio of 15 bar.

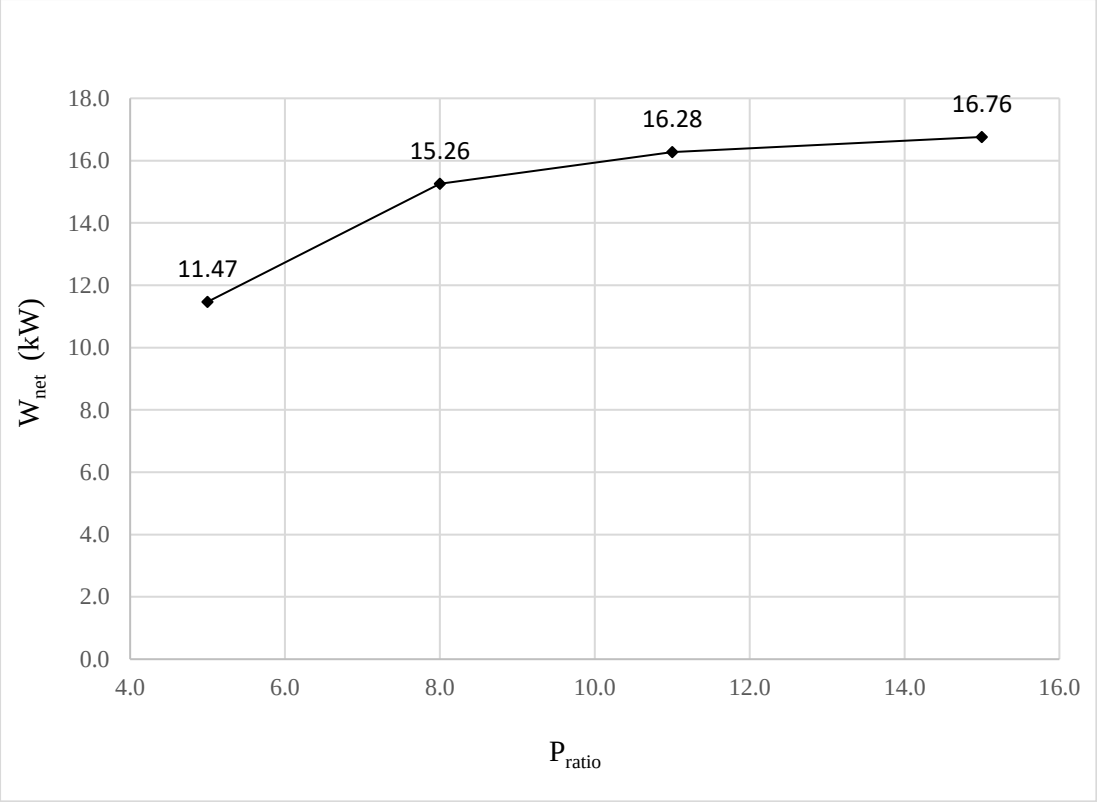


Figure 4-9: Pressure Ratio sensitivity analysis on the gas turbine at T=1 000 °C

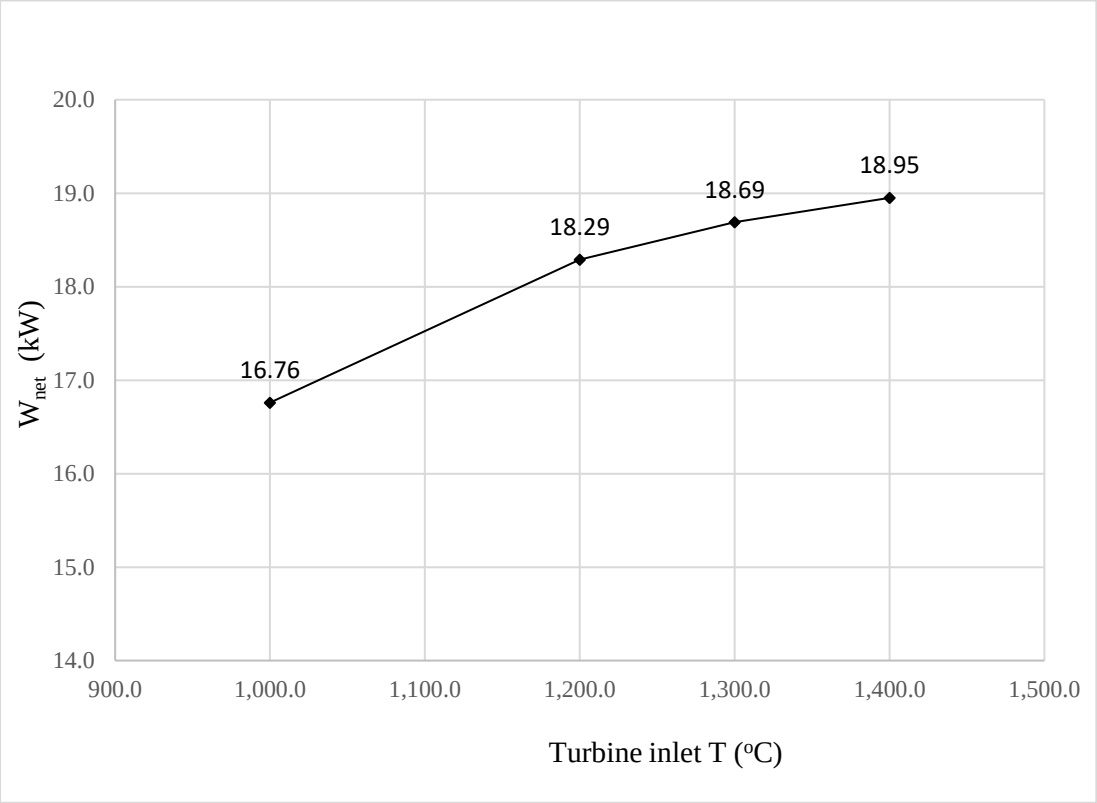


Figure 4-10: Temperature sensitivity analysis on the gas turbine at P_{ratio}=15

In this sensitivity analysis for the pressure ratio and the temperature with the results shown in **Figure 4-9** and **Figure 4-10**, a positive response can be noted for both with regards to the net power produced. Even with this positive response for both, the pressure ratio is noted to have a better response, with a W_{net} of 11.49 kW at P_{ratio}=5 bar and a W_{net} of 16.76 kW at P_{ratio}=15.

With the pressure ratio of 15 producing the best net power produced for a constant temperature of 1 000 °C, the secondary sensitivity analysis for the temperature at this constant pressure of 15 bar yields positive results. In this analysis the temperature of 1 000 °C yields a W_{net} of 16.76 kW while the temperature of 1 400 °C yields a W_{net} of 18.95 kW.

Changing the pressure and temperature from 5 bar & 1 000 °C to 15 bar & 1 400 °C can be noted to bring a change to the W_{net} from 11.47 kW to 18.95 kW. There is a change of 7.48 kW to the net power produced, however even with these changes to the operational parameters of the gas turbine, the internal power demand is still not met. Accounting for the DC-ARC plasma torch results in a power deficit of 1.77 kW meaning this must be provided through an external power supplier.

The use of the real synthesis gas on the gas turbine model shows that the fuel value derived is not sufficient to produce power.

4.5 Exergy Analysis

The exergy analysis is carried out over the individual process units of the power cycle models and aims to identify the process units with the highest inefficiencies. In doing so, solutions can be found to address them and improve the thermal efficiency of the process. The exergy analysis over selected modelled case studies of the Brayton, Rankine and combined power cycle have been done and the results are presented in **Table 4-13**, **Table 4-14** and **Table 4-15**.

Table 4-13: Brayton cycle exergy analysis for case 3b and case 3c

	Case 3b		Case 3c	
Components	**E_d (kW)**	**%Total**	**E_d (kW)**	**%Total**
Combustion Chamber	150.59	92.06	152.95	96.81
Compressor	1.88	1.15	2.11	1.34
Quenching system	8.21	5.02	0.00	0.00
Gas Turbine	2.60	1.59	2.92	1.85
Blower	0.12	0.07	0.00	0.00
Blower1	0.17	0.10	0.00	0.00
Total	**163.57**	**100.00**	**157.99**	**100.00**

The process unit with the highest destruction of exergy is the combustion chamber, which is a result of the drastic change in temperature with the combustion of the synthesis gas. The formation energy for the different products during the combustion process adds to the changes in temperature, during the transient phase of the reaction before equilibrium could reached. This high destruction of exergy is indicative that the combustion process is highly inefficient, which results in a lot of heat being lost through this stage of the cycle. The large changes in the temperature during the combustion process along with the breakdown of the molecular structures of some compounds can be attributed for the large exergy destruction. For the Rankine cycle, the highest exergy destruction rate comes from the boiler which is the equivalent of the combustion chamber in the Brayton cycle, and these results can be found in **Table 4-14**.

The boiler for the simple Rankine cycle case study has a lower exergy destruction than the combustion chamber in the simple Brayton cycle case study. This is indicating that there is a better combustion and heat transfer regimen in the boiler than the combustion in the chamber. This is evident of the better heat distribution and reaction rates in the Rankine cycle.

Table 4-14: Rankine cycle exergy analysis for case 4b and case 4c

	Case 4b		Case 4c	
Components	**E_d (kW)**	**%Total**	**E_d (kW)**	**%Total**
Boiler	134.87	90.6	149.24	95.8
Compressor	0.21	0.1	0.24	0.2
Quenching system	8.21	5.5	0.00	0.0
Steam Turbine	5.51	3.7	6.23	4.0
Blower	0.13	0.1	0.00	0.0
Pump	0.01	0.0	0.01	0.0
Total	**148.94**	**100.00**	**155.72**	**100.00**

The steam turbine unlike the gas turbine has a higher exergy destruction rate as the expansion process in the steam turbine is less efficient. This is a result drastic changes in temperature from 800 °C to temperatures below 100 °C, while for the Brayton cycle the expansion process causes a temperature change from 1 000 °C to temperatures below 650 °C.

Table 4-15: Combined Power cycle exergy analysis for Case 5b and Case 5d

	Case 5b		Case 5d	
Components	**E_d (kW)**	**%Total**	**E_d (kW)**	**%Total**
Combustion Chamber	150.88	84.51	154.61	86.07
Compressor	1.88	1.05	1.36	0.76
Quenching system	8.21	4.60		0.00
Gas Turbine	1.45	0.81	2.96	1.65
Blower	0.14	0.08		0.00
Blower1	0.18	0.10		0.00
HRSG	13.58	7.60	18.43	10.26
Steam Turbine	2.23	1.25	2.27	1.26
Pump	0.00	0.00	0.00	0.00
Total	**178.54**	**100.00**	**179.63**	**100.00**

The combined power cycle can be assumed to mimic the thermal performances of the individual power cycles in the Brayton cycle and the Rankine cycle. This can be seen by observing the exergy destruction of the gas turbine and the steam turbine, with the steam turbine

having a much higher exergy destruction rate even with a much lower mass flowing through it. The steam turbine has enables for a pressure change from 8 bar to 0.08 bar which causes exergy losses to occur, due to temperature changes and friction losses. The gas turbine on the other hand has a change in pressure from 5 bar to 1 bar which does not cause much frictional exergy losses.

The highest exergy destruction rates are accounted for by the combustion chamber and the heat recovery steam generator. With the combination of these two process units accounting for over 90% of the power cycles exergy destruction. A drastic amount of energy is required in the superheating of waste which causes a lot of frictional exergy losses in the steam generating heat exchanger.

The exergy behaviour of the Rankine cycle case studies can be supported by a study performed by (Ouadha, et al., 2007), who modelled the energy analysis of the steam Rankine cycle. The study found that the boiler and the turbine accounted for 85.80% and 12.65% of the exergy losses, respectively. This can be seen in **Table 4.14** for case 4b and case 4c where the boiler accounted for over 90% of the power cycles exergy losses while the turbine accounted for approximately 4% of the exergy loss. The difference in the exergy losses for the turbines can be attributed to the difference in the turbine stages, with a single stage turbine used in this study while a multiple stage turbine system is used by (Ouadha, et al., 2007).

The obtained results can be compared to other synthesis gas power cycle processes by Greeff, (2022), which uses synthesis gas to generate electricity in an externally fired combined power cycle. This is a process with a larger scale; however, a basis of comparison can still be formed for the exergy destruction of the different process units involved. Most importantly with regards to the contribution of these process units to the overall exergy losses of the power cycle.

Table 4-16: Exergy Analysis for an externally heated combined power cycle

	Case A	
	E_d (kW)	**%**
Syngas Cooling Heat Exchanger (SGCOOL)		0.00
Waste Heat Boiler (WHB)	112594	65.58
Reheater Exchanger (REHEAT)		0.00
Helium Steam Generator Heat Exchanger (HEST)	14919	8.69
Helium Compressor (HEC)	12025	7.00
Helium Turbine Expander (HET)	18813	10.96
Helium Turbine Expander (HET2)		0.00
Steam Turbine Expander (ST1)	2417	1.41
Steam Turbine Expander (ST2)	10925	6.36
E_d (total)	**171693**	**100.00**

Source: (Greeff, 2022)

A comparison of the exergy destruction rates obtained for the small-scale gas turbines and small-scale steam turbines in **Table 4-13** and **Table 4-14**, are in line with the results in **Table 4-16** (Greeff, 2022) where the boilers and combustion chambers have the highest destruction of exergy. The exergy destruction values in **Table 4-16** are higher than those shown in the current study, primarily due to the size difference between these two studies. The gas turbine denoted as HET in **Table 4-16** has an exergy destruction of 18 813 kW, while the steam turbines denoted as ST1 and ST2 have exergy destruction rates of 2 417 kW and 10 925 kW, respectively. The above demonstrates that turbine expanders have significantly lower activity than gas turbines due to the differences in the extent of expansion, along with the flow of mass between the two systems.

For all the simulated power cycle case studies from the Brayton cycle to the combined power cycle, there is a constant in the form of the quenching probe which has similar heat changes for all these studies. The quench probe has been noted to have the second highest exergy destruction rate for the Brayton cycle and the Rankine cycle. In the combined cycle analysis, it has the third highest exergy destruction rate. The exergy losses in the quench probe can be explored in further detail to identify the cause of these inefficiencies and possible means of

improving them. The quantitative values of the exergy destruction for the quench probe can thus be seen in **Table 4-17**.

Table 4-17: Quench Probe exergy analysis

Input	
Exergy input (syngas) (kJ/kg)	988.46
Mass flowrate (syngas) (kg/hr)	30.86
Exergy input (water) (kJ/kg)	0.00
Mass flowrate (water) (kg/hr)	1307.10
Exergy In (kJ/hr)	**30503.79**
Output	
Exergy output (syngas) (kJ/kg)	-0.74
Mass flowrate (syngas) (kg/hr)	30.86
Exergy output (Water) (kJ/kg)	0.74
Mass flowrate (water) (kg/hr)	1307.10
Exergy Out (kJ/hr)	**941.42**
Exergy Destruction (kW)	
E_d (kW)	**8.21**

Due to constant cooling of the synthesis gas for all the case studies, a detailed exergy analysis of the quench probe has been presented in **Table 4-17**. The quench probe destructs a high amount of exergy at 8.21 kW which is higher than the exergy destruction rate per unit mass for the gas turbines and steam turbines. A mass flowrate of 380 – 420 kg/hr flows through the gas turbine while for the quench probe a mass flowrate of 31 kg/hr, indicating the extent of inefficiency for the quench probe.

An improvement could be implemented on the process by using a quench probe that can recover, some of the heat present in the synthesis gas product stream from the plasma gasification reactor. The goal would not be to eliminate the quenching process as it has other functions such as reforming the composition of the synthesis gas with regards to tar formation. The quench probe can be designed to recover a certain quantity of the sensible heat destroyed during the cooling process. Quenching mechanisms such as the radiant quench process have been found to perform duties such as cooling of the synthesis gas, while recovering some of the heat present from the synthesis gas being cooled down (Liu, et al., 2010).

4.6 Economic Analysis

The economic evaluation is performed for only the small-scale gas turbines as there is not much information on the financing and commercial availability of small-scale steam turbines. In the performance of small-scale turbine systems, the power rating is a determining factor of the commercial availability of such systems. A trend can be noted between the simulated models to find an actual system within the power production range estimated by the simulations. The gas turbine models were found to have a power generation capacity in the range of 44–52 kW, while the steam turbine models have power generation capacities ranging from 31–36 kW. According to the above power rating results generated from these models, it would be desirable to find actual small-scale turbines with power ratings from 50 kW–80 kW.

Small scale gas turbine systems are widely available across many suppliers. Economic information was found from a study that averaged the prices of small-scale gas turbines from different suppliers. In this economic study from 2016 information of the operating parameters for a 61 kW power rated gas turbine is presented, and this was the selected option to represent an actual gas turbine system that can be used for this study. The capital cost including the installation cost from 2016 were converted using the cost price index from 2016 and 2021, thereafter the exchange rate is used to convert the costs from the U.S Dollar ($) to the South African Rand (R).

Table 4-18: Small scale gas turbine cost calculations

Small Scale Gas Turbine	
Capital Cost ($/kW)	3220
Turbine rating (kW)	61
Capital Cost ($) (2016)	196420
Capital Cost ($) (2021)	222118.28
Capital Cost (R) (2021)	**R3 258 475**

The cost price index for 2016 and 2021 can be found in **Table 4-19** as acquired from the Federal Reserve Bank of Minneapolis (Federal Reserve Bank of Minneapolis, 2021).

Table 4-19: United States CPI

U.S.A Consumer Price Index	
2016	240
2021	271.4

Source: (Federal Reserve Bank of Minneapolis, 2021)

The U.S Dollar ($) to South African Rand (R) exchange rate as acquired on the 22nd of September 2021 at 18:20 was $1:R14.67 (XE Currency Data API, 2021).

Table 4-18 shows an averaged capital cost of R3 258 475 for a small-scale gas turbine at a power rating of 61 kW. This is an estimated cost at which a small-scale gas turbine system with a power rating of 61 kW can be acquired and installed. After the installation of such a system, there are costs involved in its operation such as operational and maintenance costs which are consider in **Table 4-20**.

Table 4-20: Operational Maintenance Cost of Small-scale gas turbine

Small Scale Gas Turbines	
O & M costs (¢/kWh)	1.3
Turbine production (kWh)	396500
Operational Time (h)	6500
O & M costs (¢)	515450
O & M costs ($) (2016)	5154.50
O & M costs ($) (2021)	5828.88
O & M costs (R) (2021)	**R85 510**

Table 4-20 shows the operating and maintenance costs of the small-scale gas turbine system per kWh of the power produced.

Several research studies have been done considering the prospect of operating a steam turbine under small scale conditions. Steam turbines are traditionally large-scale systems, and they offer the best thermodynamic behaviour when they operate under large-scale conditions. This has resulted in a slow response in the design of small-scale steam turbines, and the low demand means that the costs of these systems will be high, and mostly likely will not provide a reasonable return. The constant changes in the research landscape of the small-scale turbine system will equate to commercial availability of these systems and eventually regulate the pricing system as more companies develop these turbines. For now, though there are some difficulties in finding commercially available small scale gas turbine systems.

4.7 Co-generation System Producing Steam for a Hospital

Another practical application for the plasma gasification technology would be through a hospital, with special regards to waste management. Rather than dispose of the waste generated

in the hospital through a third party or hospital incinerators which release a lot of toxic gases, it could be gasified, and the heat could be used in a co-generation cycle. The co-generation cycle would be centred on generating electricity, whilst providing low pressure steam to the hospital.

The co-generation cycle features a plasma gasification reactor, with a gas turbine power cycle model generating electricity and a steam generator using waste heat from the effluent of the gas turbine. The model of the gas turbine power cycle is like the previous simple Brayton cycle **Case 3b,** along with the heat recovery steam generator.

The plasma gasification reactor model section of the co-generation system is like the other plasma gasification reactor systems. The power generation side features the pre-treatment stage along with the open Brayton cycle system and waste heat recovery system through a steam generator as shown in **Figure 4-11**.

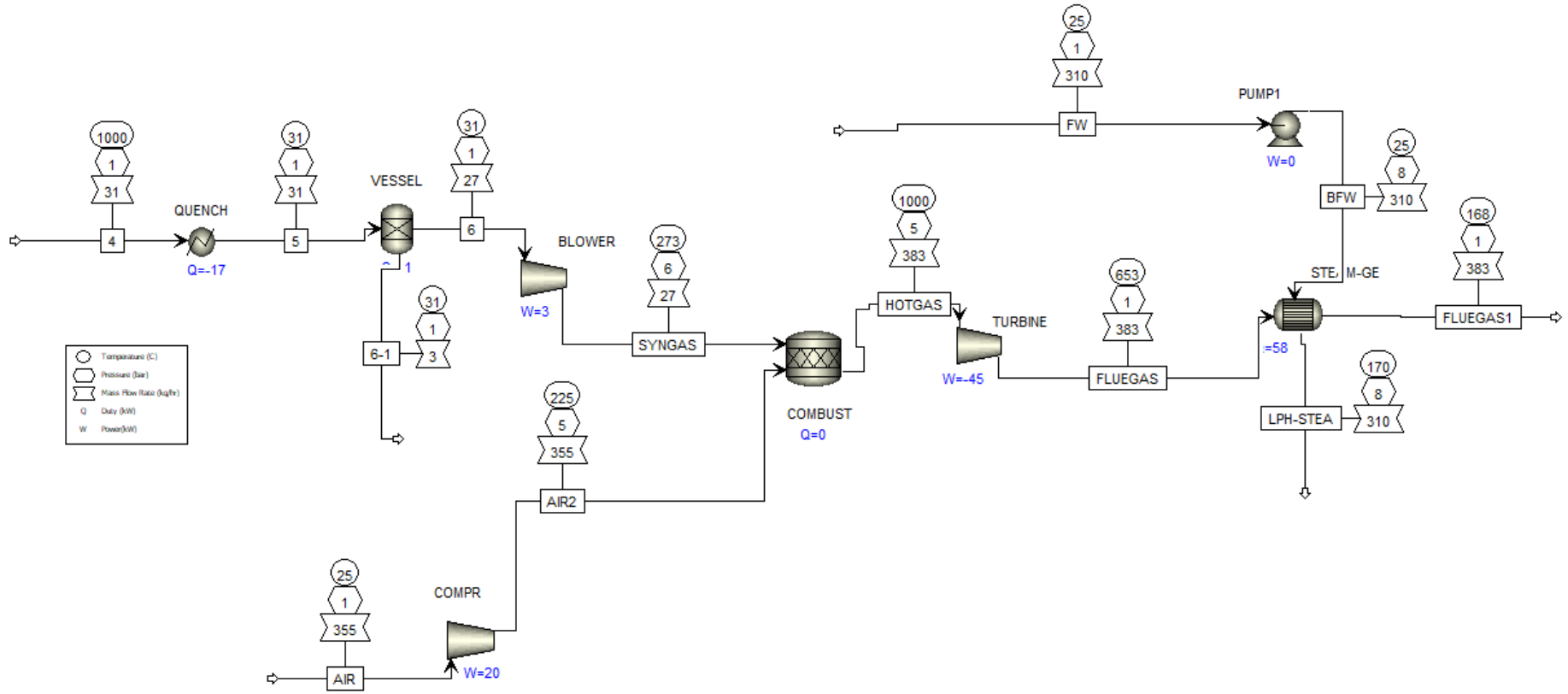


Figure 4-11: Brayton cycle and steam co-generation model

An analysis of this system shows potential of being able to generate 310 kg/hr of low-pressure steam at a temperature of 170 °C and a pressure of 8 bar, while meeting the power requirement of operation.

Table 4-21: Power balance for the co-generation cycle

Co-generation system	**kW**
Gas Turbine	44.87
Blower	-3.1
COMPR	-20.2
Pump	-0.07
Plasma Arc	-20.72
Net Power	**0.78**

Table 4-21 shows that the model for the co-generation cycle produced enough power to account for the power consumption requirement of the system, and a small fraction of net power is produced. In this case study of the co-generation cycle, power is produced to drive equipment such as the DC-ARC plasma torch, compressors and pumps. Without this production of power, an externally electricity source would have to acquired. Acquiring electricity from an external source would increase the costs associated with this project. **Table 4-21** shows a small amount of power is left at **0.78 kW** and this power can be used for lighting and other activities that require small amounts of electricity, thus reducing the electricity bill of the hospital.

These activities thus severely impact the amount of heat available for generating the steam. Only low-pressure steam can be generated and a small amount of excess electricity for low duty activities.

High pressure and low-pressure steam are required for several reasons in a hospital such as provision of heat and steam for ventilators and humidifiers. The low-pressure steam generated in this scenario at 170 °C and 8 bar can be applied for several different purposes such as those mentioned above. A study by Fraile et al, (2014) on a 600-bed hospital shows that hot water is typically supplied at a maximum temperature of 83 °C. The low-pressure steam generated by this process could be downgraded to supply the hot water. The downgrading of the steam to hot water does however beat the point of generating the low-pressure steam in the first place. The downgrading of steam is a lot more costly than just generating the hot water in the first

place, however this is just to point out the different processes through which the low-pressure steam could be used.

A more practical approach would be the direct use of low-pressure steam in processes requiring it, such as humidified room for patients having breathing problems. The flow of the steam could be controlled through valves to ensure it is supplied at desired conditions. Steam also plays a major role in the sterilization of surgical rooms and tools found within those rooms.

4.8 References

Blažević, S., Mrzljak, V., Anđelić, N. & Car, Z., 2019. Comparison of energy flow stream and isentropic method for steam turbine energy analysis. *Acta Polytechnica*, 59(02), pp. 109-125.

Federal Reserve Bank of Minneapolis, 2021. *Minneapolisfed.* [Online]
Available at: https://www.minneapolisfed.org/about-us/monetary-policy/inflation-calculator/consumer-price-index-1913-
[Accessed 22 September 2021].

Fraile, J.-C., San-José, J. & González-Alonso, A., 2014. A Boiler Room in a 600-Bed Hospital Complex: Study, Analysis, and Implementation of Energy Efficiency Improvements. *Energies*, Volume 7, pp. 3282-3303.

Greeff, I., 2022. Using synthesis gas heat to produce work via an externally fired gas power cycle. *Energy*, 239(122132).

Jadhao, J. S. & Thombane, D. G., 2013. Review on Exhaust Gas Heat Recovery for I.C. Engine. *International Journal of Engineering and Innovative Technology*, 2(12), pp. 93-100.

Langston, L. S., 2020. Aspects of Gas Turbine Thermal Efficiency. *Mechanical Engineering*, 142(09), pp. 54-55.

Liu, Y. H., Chen, W., Che, D. F. & Cao, Z. D., 2010. *Comparisons of four quench methods for high temperature Syngas-Exergy Analyses.* China, AIP Publishing, pp. 674-679.

Luque, R. & Speight, J. G., 2015. *Gasification for Synthesis Fuel Production: Fundamentals, Processes and Applications.* 1st ed. Cambridge: Woodhead Publishing.

Minutillo, M., Perna, A. & Di Bona, D., 2009. Modelling and performance analysis of an integrated plasma gasification combined cycle (IPGCC) power plant. *Energy Conversion and Management*, 20 July, Volume 50, pp. 2837-2842.

Muvhiiwa, R., Sempuga, B. & Hildebrandt, D., 2021. Using the G-H space to show heat and work efficiencies associated with nitrogen plasma gasification of wood. *Chemical Engineering Science 243 (2021) 116793,* 2021(116793), pp. 1-16 (Online).

Ouadha, A., En-nacer, M. & Imine, O., 2007. *Modelling and Exergy Analysis of Steam Turbine Cycles.* Evora, Portugal, Proceedings of 3rd International Energy, Exergy and Environment Symposium.

Ramireddy, V., 2012. An Overview of Combined Cycle Power Plant. *Electrical Engineering Portal*, 25 August, p. Online.

Renzi, M., Patuzzi, F. & Baratieri, M., 2017. Syngas feed of micro gas turbines with steam injection: Effects on performance, combustion and pollutants formation. *Applied Energy*, Volume 206, pp. 697-707.

Salazar-Pereyra, M., Lugo-Leyte, R., Bonilla-Blancas, A. E. & Lugo-Méndez, H. D., 2016. *THERMODYNAMIC ANALYSIS OF SUPERCRITICAL AND SUBCRITICAL RANKINE CYCLES.* Seoul, South Korea, ASME.

XE Currency Data API, 2021. *Xe.* [Online]
Available at:
https://www.xe.com/currencyconverter/convert/?Amount=1&From=USD&To=ZAR
[Accessed 22 September 2021].

Chapter 5 Recommendations and Conclusion

5.1 Recommendations

A lot of the difficulties encountered in the development of the models for the power cycles and the plasma gasification reactor have been noted in the body of the report. The following changes are recommended to improve the performance of the system:

- The quenching process should be a radiant quench system which can recover a portion of the heat found in the plasma gasification reactor.
- There should be other means of recovering the heat present in the hot synthesis gas from the plasma gasification reactor, without the need to quench such as feeding the synthesis gas to an externally fired power cycle. This process has already been proven effective by Greeff, (2022).
- The open Brayton power cycle should feature a recuperating system to recover the heat from the effluent of this gas turbine system.
- The sensitivity analysis performed in this study showed that operating the gas turbine at higher pressure and temperatures i.e., 15 kW & 1 000 °C, improves the power produced.
- Other means of utilizing the synthesis gas can be explored such as generating biofuels.

5.2 Conclusion

In this work through modelling using the flowsheet simulator Aspen Plus, a plasma gasification reactor model aimed at producing synthesis gas was presented. This plasma gasification reactor was further coupled to various power cycles for the generation of electricity. An energy analysis is done on the plasma gasification reactor to assess the effectiveness of the reactor model in reforming the biomass to synthesis gas. In the analysis of the plasma gasification reactor, a cold gas efficiency of 67.04% is obtained, and this is found to be within the range of commercial gasification reactors. Conventional thermal gasification reactors tend to have higher cold gas efficiencies, than plasma gasification reactors due to the absence of the plasma torch. The plasma torch uses a significant amount of electricity which tends to reduce the thermal efficiency of the plasma gasification reactor.

The synthesis gas generated from this small-scale plasma gasification reactor system thereafter is combusted in a various number of power cycles, and their different configurations to assess

the power cycle model which can offer the best power production capabilities and thermal efficiency. For the Brayton cycle different configurations are considered and **Case 3c** involving a power cycle with synthesis gas directly fired in the gas turbine from a hypothetical pressurized plasma gasification reactor achieves the best thermal efficiency of 27.89 %. A restricting factor for the performance of these gas turbine system is the capacity which is low, and small-scale gas turbine systems tend to be highly inefficient and this is usually corrected through the incorporation of a waste recovery system.

The steam Rankine cycle systems considered by this study generated lower amount of power compared to their gas turbine counterpart, however the steam Rankine cycle case studies achieved better thermal efficiencies all above 30 %. **Case 4f** which is a two-stage expansion steam turbine system achieves the best thermal efficiency of 37.66 %. The operational dynamics of the steam Rankine cycle enable for better usage of heat in the cycle compared to the Brayton cycle which sees the exhaust gas being discarded to the environment at high temperatures leading to a significant loss of heat.

Adding the heat recovery system to the Brayton cycle through the combined power cycle drastically improves the performance of the cycle as the thermal efficiencies are far higher. The case study which achieves the best thermal efficiency for the combined cycle is **Case 5d** involving a Brayton cycle model as in case 3c coupled with a steam turbine cycle to recovery the heat from the exhaust of the gas turbine and the model for this case achieves an efficiency of 44.14 %.

A synthesis gas product generated through the actual plasma gasification reactor was found to have a lower LHV, which lead to a power produced of 28.36 kW. This was lower than the power produced for **Case 3b** which used the synthesis gas product generated by the model of the demonstration plant. In the case of the experimental synthesis gas product, the lower LHV leads to a lower air to fuel ratio which severely affects the amount of power that can be generated through this cycle. A sensitivity analysis performed on the gas turbine model using this experimental synthesis gas product, shows that the power produced increases with increases to the pressure ratio. If the gas turbines can be designed to operate at higher pressures, the power produced can be much higher.

An exergy analysis performed for the various power cycles shows that the combustion chamber and the boiler have the highest exergy destruction rates. This is expected as the combustion process is a highly exothermic process which comes with a lot of inefficient operation. The

HRSG in the combined power cycle is found to have the second highest thermal efficiency, as the superheating of water has been noted to be highly inefficient. The quench probe has the second highest thermal efficiency in the gas and vapour power cycle of **8.21 kW**. The operation of the quench probe is shown to be less efficient than the steam turbine and gas turbine combined.

A co-generation cycle is explored as an alternative means of deriving the energy value found in the synthesis gas. This cycle generated low pressure steam at a temperature and pressure of 170 °C and 8 bar, respectively. This steam can be used for several different processes in a hospital.

5.3 References

Greeff, I., 2022. Using synthesis gas heat to produce work via an externally fired gas power cycle. *Energy*, 239(122132).

Appendix

Appendix A.1 Plasma Gasification Reactor

The setup for the model of the demonstration plasma gasification plant can be found in **Figure A-1**, along with the mass balance for this model in **Table A-1**.

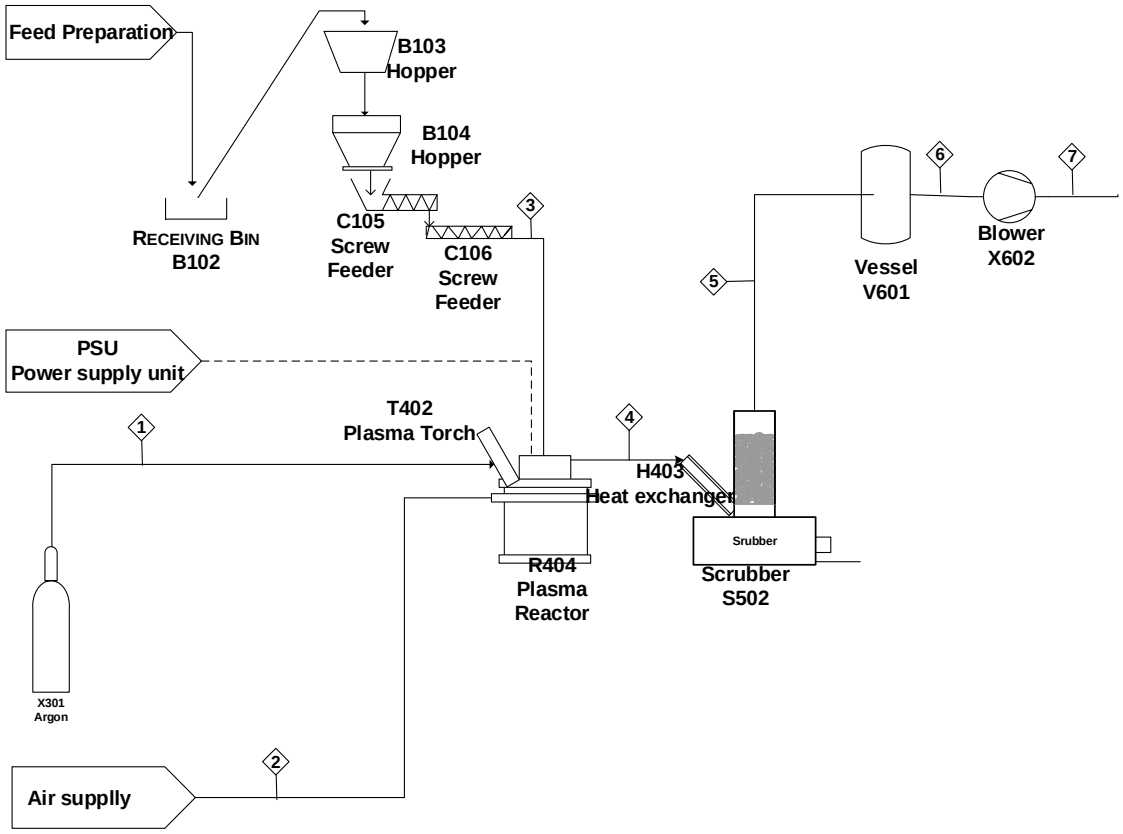


Figure A-1: NECSA Demonstration Plasma Gasification Reactor Plant Model

Table A-1: Mass Balance for the demonstration plasma gasification plant model

Stream		1	2	3	4	5	6	7
Process Pressure	kPa(a)	87.5	87.5	84.5	84	83	84	200
Temperature	Deg C	Amb	Amb	Amb	1000	42	36	153
Component	kg/h							
wood chips excluding ash and H_20				20				
Ash				0.02				
O_2								
N_2			3.832		3.832	3.832	3.832	3.832
Ar		4.00						
CO					18.31	18.31	18.31	18.31
CO_2					4.031	4.031	4.031	4.031
H_2					1.309	1.309	1.309	1.309
H_2O				3.37	3.373	3.373	3.373	
H_2S					0.006	0.006	0.006	
HCl					0.003	0.003	0.003	
LPG								
TOTAL		**4**	**3.832**	**23.39**	**30.864**	**30.864**	**30.864**	**27.482**

Calculation of the yield proportion in the decomposition of the biomass

The compositions in the RYIELD Reactor were calculated using the ultimate and proximate analysis of the biomass feedstock type as follows with FACT representing the dry mass fraction of the biomass.

FACT = (100 - MOISTURE) / 100

H_2O = MOISTURE / 100

ASH = ULT (1) / 100 * FACT

C = ULT (C) / 100 * FACT

H_2 = ULT (H) / 100 * FACT

N_2 = ULT (N) / 100 * FACT

O_2 = ULT (O) / 100 * FACT

S = ULT (S) / 100 * FACT

Cl_2 = ULT (CL) / 100 * FACT

Theoretical Model Validation

The Aspen Plus model for the theoretical model of the plasma gasification reactor can be seen in **Figure A-2** along with the mass balance in **Table A-2**.

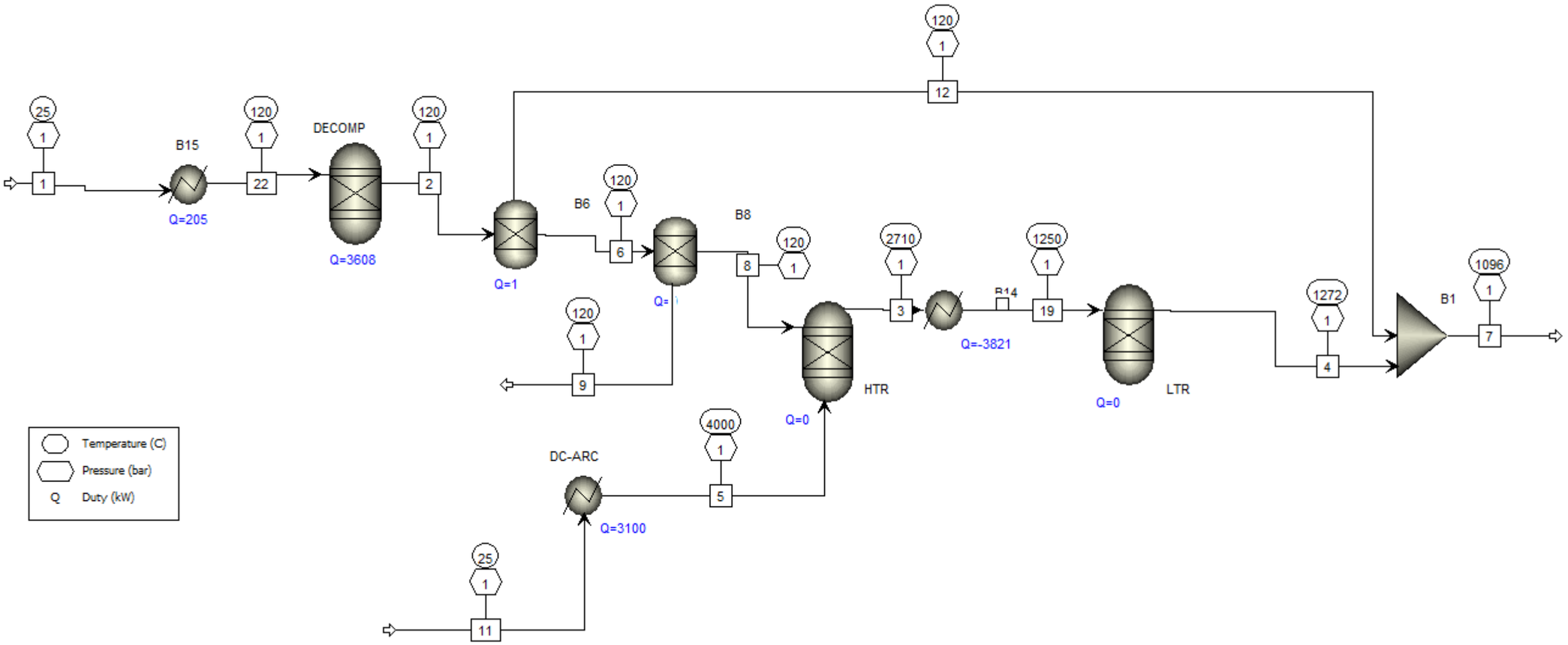


Figure A-2: Aspen Plus model flow diagram for the Minutillo (2009) reactor validation case

Table A-2: Mass Balance for the Minutillo (2009) reactor validation case

	Units	1	2	3	4	5	6	7	8	9	11	12	19	22
Temperature	C	25.00	120.00	2709.53	1272.24	4000.00	120.00	1096.32	120.00	120.00	25.00	120.00	1250.00	120.00
Pressure	bar	1.00	1.00	1.00	1.00	1.00	1.00	1.00	1.00	1.00	1.00	1.00	1.00	1.00
Mass Vapor Fraction		0.00	0.50	0.98	0.98	1.00	0.37	0.99	0.43	0.00	1.00	1.00	0.98	0.00
Mass Liquid Fraction		0.00	0.01	0.00	0.00	0.00	0.01	0.00	0.01	0.00	0.00	0.00	0.00	0.00
Mass Solid Fraction		1.00	0.50	0.02	0.02	0.00	0.62	0.01	0.56	1.00	0.00	0.00	0.02	1.00
Mass Enthalpy	kJ/kg	-6385.88	-2573.37	2444.47	-423.34	4820.97	96.24	-2097.02	228.31	-728.00	-0.29	-13248.08	-423.34	-6180.90
Mass Density	kg/cum	1305.22	0.70	0.08	0.15	0.08	0.74	0.17	0.64	3486.88	1.19	0.56	0.15	1305.22
Enthalpy Flow	kW	-6385.88	-2573.37	3257.31	-564.10	3099.88	76.99	-3213.72	157.42	-80.43	-0.18	-2649.62	-564.10	-6180.90
Mass Flows	**kg/hr**	**3600.00**	**3600.00**	**4797.07**	**4797.07**	**2314.80**	**2880.00**	**5517.07**	**2482.27**	**397.73**	**2314.80**	**720.00**	**4797.07**	**3600.00**
H_2	kg/hr	0.00	183.46	182.35	180.89	0.00	183.46	180.89	183.46	0.00	0.00	0.00	182.35	0.00
O_2	kg/hr	0.00	820.22	0.00	0.00	925.92	820.22	0.00	820.22	0.00	925.92	0.00	0.00	0.00
N_2	kg/hr	0.00	35.14	1424.01	1424.00	1388.88	35.14	1424.00	35.14	0.00	1388.88	0.00	1424.01	0.00
Cl_2	kg/hr	0.00	32.54	0.00	0.00	0.00	32.54	0.00	32.54	0.00	0.00	0.00	0.00	0.00
NO_2	kg/hr	0.00	0.00	0.00	0.00	0.00	0.00	0.00	0.00	0.00	0.00	0.00	0.00	0.00
CO	kg/hr	0.00	0.00	3056.79	3052.58	0.00	0.00	3052.58	0.00	0.00	0.00	0.00	3056.79	0.00
CO_2	kg/hr	0.00	0.00	0.01	1.27	0.00	0.00	1.27	0.00	0.00	0.00	0.00	0.01	0.00
H_2O	kg/hr	0.00	720.00	0.03	1.17	0.00	0.00	721.17	0.00	0.00	0.00	720.00	0.03	0.00
CH_4	kg/hr	0.00	0.00	0.01	0.78	0.00	0.00	0.78	0.00	0.00	0.00	0.00	0.01	0.00
C_2H_4	kg/hr	0.00	0.00	0.00	0.00	0.00	0.00	0.00	0.00	0.00	0.00	0.00	0.00	0.00
C_2H_6	kg/hr	0.00	0.00	0.00	0.00	0.00	0.00	0.00	0.00	0.00	0.00	0.00	0.00	0.00
N_2O	kg/hr	0.00	0.00	0.00	0.00	0.00	0.00	0.00	0.00	0.00	0.00	0.00	0.00	0.00
H_2S	kg/hr	0.00	0.00	3.03	22.07	0.00	0.00	22.07	0.00	0.00	0.00	0.00	3.03	0.00
HCl	kg/hr	0.00	0.00	33.47	33.47	0.00	0.00	33.47	0.00	0.00	0.00	0.00	33.47	0.00
NH_3	kg/hr	0.00	0.00	0.00	0.02	0.00	0.00	0.02	0.00	0.00	0.00	0.00	0.00	0.00
FEED	kg/hr	3600.00	0.00	0.00	0.00	0.00	0.00	0.00	0.00	0.00	0.00	0.00	0.00	3600.00
C	kg/hr	0.00	1389.02	78.18	78.71	0.00	1389.02	78.71	1389.02	0.00	0.00	0.00	78.18	0.00
S	kg/hr	0.00	21.89	18.87	0.00	0.00	21.89	0.00	21.89	0.00	0.00	0.00	18.87	0.00
ASH	kg/hr	0.00	397.73	0.00	0.00	0.00	397.73	0.00	0.00	397.73	0.00	0.00	0.00	0.00

Experimental Model Validation

Plasma Gasification Reactor Aspen Plus Model

The model for the plasma gasification reactor correlated with the model for the demonstration plant plasma gasification reactor can be found in **Figure A-3** along with the mass balance in **Table A-3**.

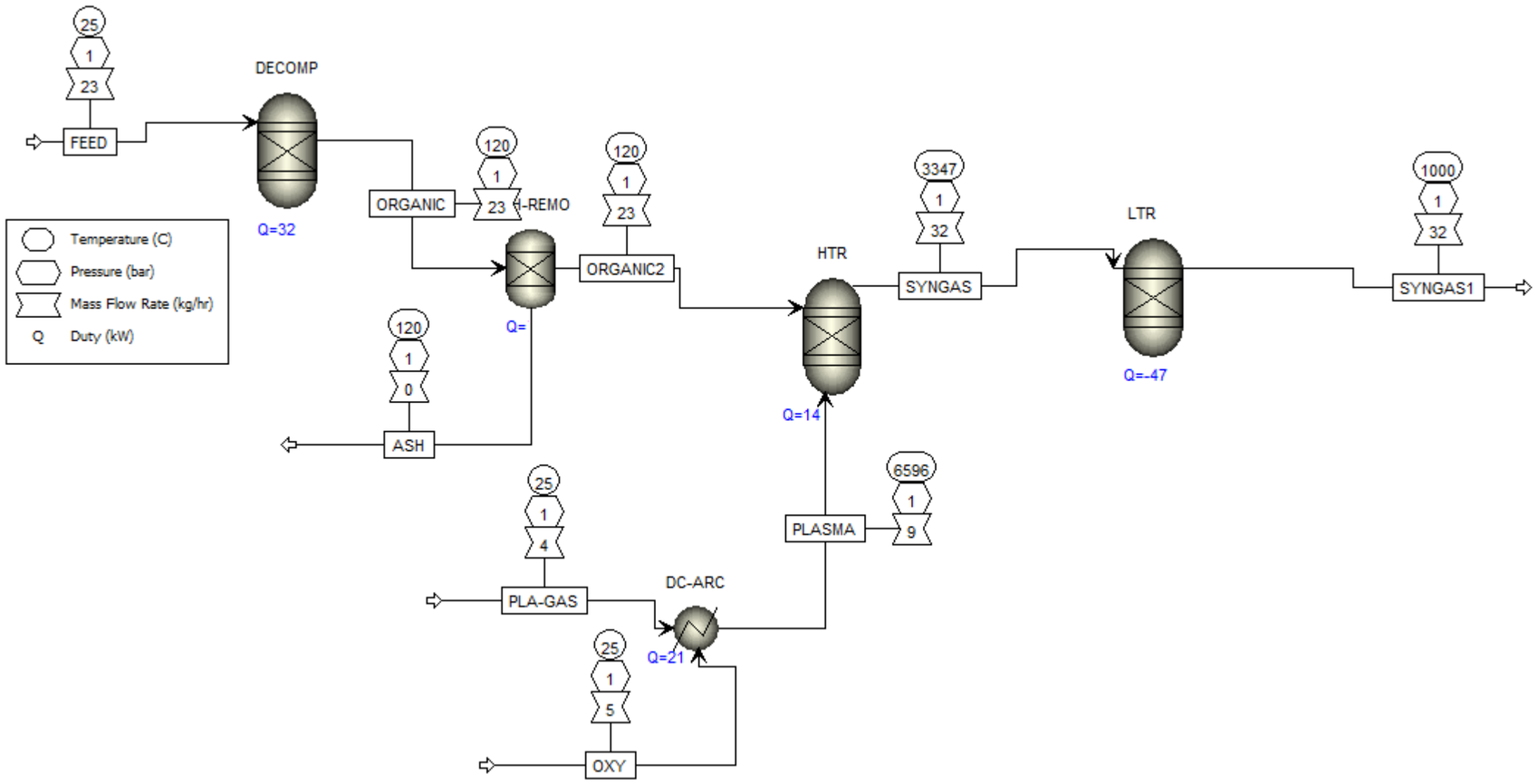


Figure A-3: Plasma Gasification Reactor Model

Table A-3: Mass balance for the plasma gasification Reactor Model

	Units	FEED	ORGANIC	ASH	ORGANIC2	PLA-GAS	OXY	PLASMA	SYNGAS	SYNGAS1
Temperature	C	25	120	120	120	25	25	6596.08	3347.37	1000
Pressure	bar	0.845	0.845	0.845	0.845	0.875	1	0.875	0.84	0.84
Mass Vapor Fraction		0	0.58	0	0.59	1	1	1	1	1
Mass Liquid Fraction		0	0	0	0	0	0	0	0	0
Mass Solid Fraction		1	0.42	1	0.41	0	0	0	0	0
Mass Enthalpy	kJ/kg	-7446.01	-2526.71	-728	-2543.56	-0.24	-0.3	8023.8	1997.59	-3257.91
Mass Density	kg/cum	1268.99	0.57	3486.88	0.56	0.99	1.29	0.05	0.05	0.15
Enthalpy Flow	kW	-48.38	-16.42	-0.04	-16.37	0	0	20.72	18.02	-29.38
Mass Flows	**kg/hr**	**23.39**	**23.39**	**0.22**	**23.17**	**3.83**	**5.46**	**9.3**	**32.47**	**32.47**
H_2	kg/hr	0	1.14	0	1.14	0	0	0	1.22	1.31
O_2	kg/hr	0	7.73	0	7.73	0	5.46	5.46	0.56	0
N_2	kg/hr	0	0.04	0	0.04	3.83	0	3.83	3.87	3.87
Cl_2	kg/hr	0	0.01	0	0.01	0	0	0	0	0
NO_2	kg/hr	0	0	0	0	0	0	0	0	0
CO	kg/hr	0	0	0	0	0	0	0	21.4	19.19
CO_2	kg/hr	0	0	0	0	0	0	0	1.47	4.95
H_2O	kg/hr	0	4.68	0	4.68	0	0	0	3.93	3.14
CH_4	kg/hr	0	0	0	0	0	0	0	0	0
C_2H_4	kg/hr	0	0	0	0	0	0	0	0	0
C_2H_6	kg/hr	0	0	0	0	0	0	0	0	0
N_2O	kg/hr	0	0	0	0	0	0	0	0	0
H_2S	kg/hr	0	0	0	0	0	0	0	0	0
HCl	kg/hr	0	0	0	0	0	0	0	0.01	0.01
NH_3	kg/hr	0	0	0	0	0	0	0	0	0
FEED	kg/hr	23.39	0	0	0	0	0	0	0	0
C	kg/hr	0	9.58	0	9.58	0	0	0	0	0
S	kg/hr	0	0	0	0	0	0	0	0	0
ASH	kg/hr	0	0.22	0.22	0	0	0	0	0	0

Appendix A.2 Power cycle Models and Mass Balance

Appendix A.2.1 Brayton cycle Mass Balance

The models for the different configurations of the Brayton cycle case studies explored in this research study can be found in the annotations for each case study along with the accompanying mass balance.

Case 3a

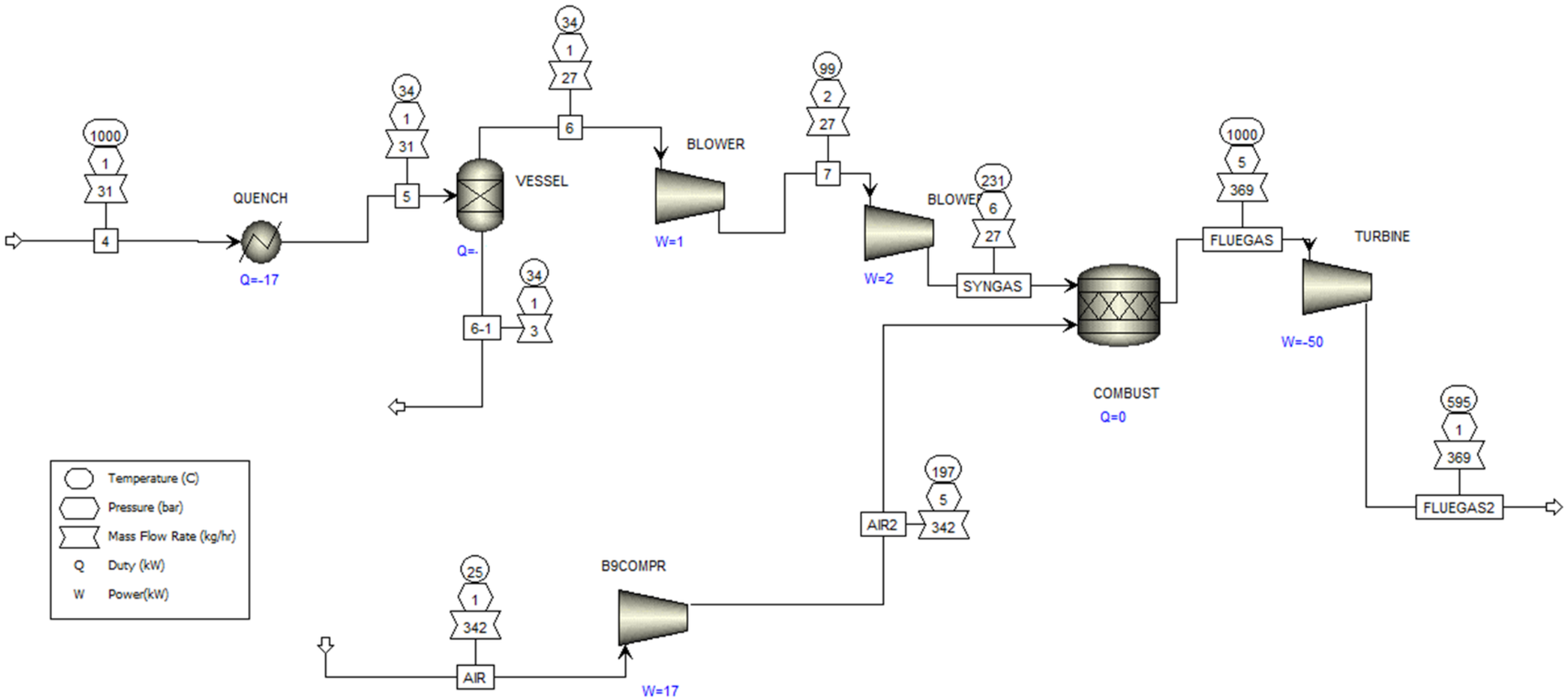


Figure A-4: Aspen Plus model flow diagram for Case 3a

Table A-4: Mass balance for Case 3a

	Units	4	5	6	6-1	7	AIR	AIR2	SYNGAS	FLUEGAS	FLUEGAS2
Temperature	C	1000.00	33.70	33.70	33.70	99.45	25.00	197.26	231.29	1000.00	595.21
Pressure	bar	0.84	1.00	1.00	1.00	2.00	1.00	5.00	6.00	5.00	1.00
Mass Vapor Fraction		1.00	0.93	1.00	0.00	1.00	1.00	1.00	1.00	1.00	1.00
Mass Liquid Fraction		0.00	0.07	0.00	1.00	0.00	0.00	0.00	0.00	0.00	0.00
Mass Solid Fraction		0.00	0.00	0.00	0.00	0.00	0.00	0.00	0.00	0.00	0.00
Mass Enthalpy	kJ/kg	-3200.34	-5130.64	-3925.95	-15923.01	-3817.17	-0.28	175.66	-3595.34	-104.94	-595.54
Mass Density	kg/cum	0.14	0.75	0.70	843.74	1.16	1.16	3.67	2.56	1.37	0.40
Enthalpy Flow	kW	-27.44	-43.98	-29.98	-14.92	-29.15	-0.03	16.68	-27.45	-10.77	-61.11
Mass Flows	**kg/hr**	**30.86**	**30.86**	**27.49**	**3.37**	**27.49**	**341.94**	**341.94**	**27.49**	**369.43**	**369.43**
H_2	kg/hr	1.31	1.31	1.31	0.00	1.31	0.00	0.00	1.31	0.00	0.00
O_2	kg/hr	0.00	0.00	0.00	0.00	0.00	71.81	71.81	0.00	50.96	50.96
N_2	kg/hr	3.83	3.83	3.83	0.00	3.83	270.13	270.13	3.83	273.96	273.96
Cl_2	kg/hr	0.00	0.00	0.00	0.00	0.00	0.00	0.00	0.00	0.00	0.00
NO_2	kg/hr	0.00	0.00	0.00	0.00	0.00	0.00	0.00	0.00	0.00	0.00
CO	kg/hr	18.31	18.31	18.31	0.00	18.31	0.00	0.00	18.31	0.00	0.00
CO_2	kg/hr	4.03	4.03	4.03	0.00	4.03	0.00	0.00	4.03	32.80	32.80
H_2O	kg/hr	3.37	3.37	0.00	3.37	0.00	0.00	0.00	0.00	11.70	11.70
CH_4	kg/hr	0.00	0.00	0.00	0.00	0.00	0.00	0.00	0.00	0.00	0.00
C_2H_4	kg/hr	0.00	0.00	0.00	0.00	0.00	0.00	0.00	0.00	0.00	0.00
C_2H_6	kg/hr	0.00	0.00	0.00	0.00	0.00	0.00	0.00	0.00	0.00	0.00
N_2O	kg/hr	0.00	0.00	0.00	0.00	0.00	0.00	0.00	0.00	0.00	0.00
H_2S	kg/hr	0.01	0.01	0.01	0.00	0.01	0.00	0.00	0.01	0.01	0.01
HCl	kg/hr	0.00	0.00	0.00	0.00	0.00	0.00	0.00	0.00	0.00	0.00

Case 3b

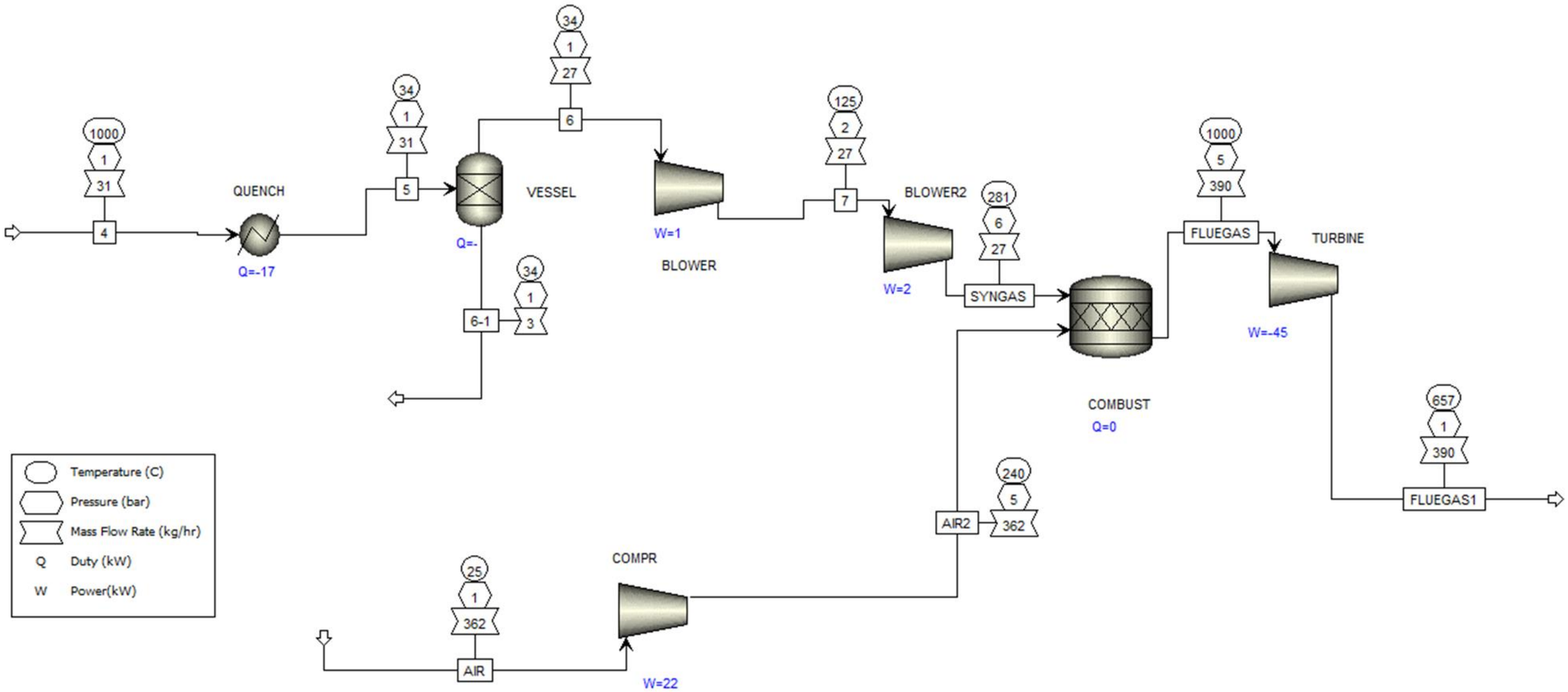


Figure A-5: Aspen Plus model flow diagram for Case 3b

Table A-5: Mass balance for Case 3b

	Units	4	5	6	6-1	7	AIR	AIR2	FLUEGAS	FLUEGAS1	SYNGAS
Temperature	C	1000.00	33.70	33.70	33.70	110.95	25.00	227.15	1000.00	657.38	270.14
Pressure	bar	0.84	1.00	1.00	1.00	2.00	1.00	5.00	5.00	1.00	6.00
Mass Vapor Fraction		1.00	0.93	1.00	0.00	1.00	1.00	1.00	1.00	1.00	1.00
Mass Liquid Fraction		0.00	0.07	0.00	1.00	0.00	0.00	0.00	0.00	0.00	0.00
Mass Solid Fraction		0.00	0.00	0.00	0.00	0.00	0.00	0.00	0.00	0.00	0.00
Mass Enthalpy	kJ/kg	-3200.34	-5130.64	-3925.95	-15923.01	-3797.97	-0.28	206.70	-60.89	-477.87	-3529.01
Mass Density	kg/cum	0.14	0.75	0.70	843.74	1.12	1.16	3.45	1.36	0.37	2.38
Enthalpy Flow	kW	-27.44	-43.98	-29.98	-14.92	-29.00	-0.03	20.46	-6.49	-50.94	-26.95
Mass Flows	**kg/hr**	**30.86**	**30.86**	**27.49**	**3.37**	**27.49**	**356.26**	**356.26**	**383.75**	**383.75**	**27.49**
H_2	kg/hr	1.31	1.31	1.31	0.00	1.31	0.00	0.00	0.00	0.00	1.31
O_2	kg/hr	0.00	0.00	0.00	0.00	0.00	74.81	74.81	53.97	53.97	0.00
N_2	kg/hr	3.83	3.83	3.83	0.00	3.83	281.45	281.45	285.28	285.28	3.83
Cl_2	kg/hr	0.00	0.00	0.00	0.00	0.00	0.00	0.00	0.00	0.00	0.00
NO_2	kg/hr	0.00	0.00	0.00	0.00	0.00	0.00	0.00	0.00	0.00	0.00
CO	kg/hr	18.31	18.31	18.31	0.00	18.31	0.00	0.00	0.00	0.00	18.31
CO_2	kg/hr	4.03	4.03	4.03	0.00	4.03	0.00	0.00	32.80	32.80	4.03
H_2O	kg/hr	3.37	3.37	0.00	3.37	0.00	0.00	0.00	11.70	11.70	0.00
CH_4	kg/hr	0.00	0.00	0.00	0.00	0.00	0.00	0.00	0.00	0.00	0.00
C_2H_4	kg/hr	0.00	0.00	0.00	0.00	0.00	0.00	0.00	0.00	0.00	0.00
C_2H_6	kg/hr	0.00	0.00	0.00	0.00	0.00	0.00	0.00	0.00	0.00	0.00
N_2O	kg/hr	0.00	0.00	0.00	0.00	0.00	0.00	0.00	0.00	0.00	0.00
H_2S	kg/hr	0.01	0.01	0.01	0.00	0.01	0.00	0.00	0.01	0.01	0.01
HCl	kg/hr	0.00	0.00	0.00	0.00	0.00	0.00	0.00	0.00	0.00	0.00

Case 3c

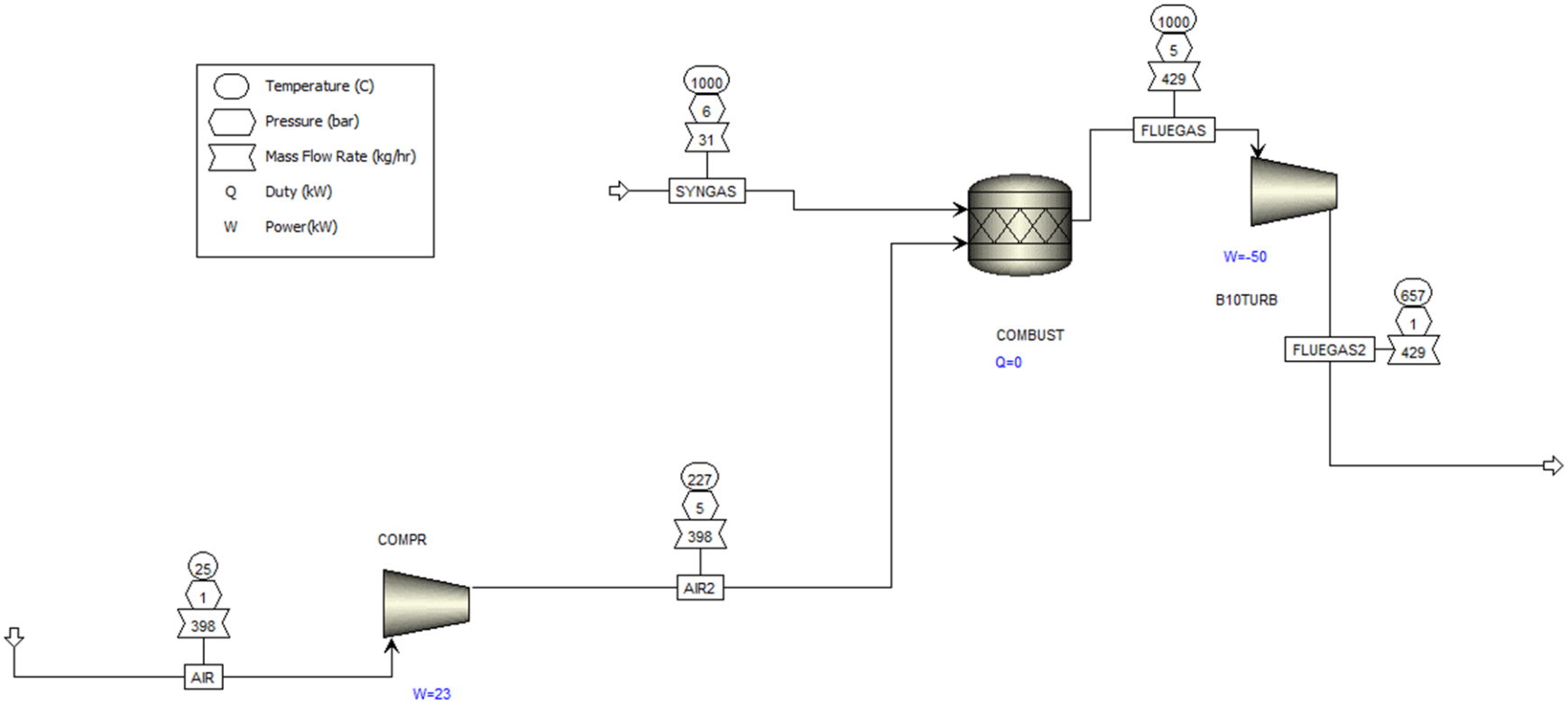


Figure A-6: Aspen Plus model flow diagram for Case 3c

Table A-6: Mass balance for Case 3c

	Units	AIR	AIR2	FLUEGAS	FLUEGAS2	SYNGAS
Temperature	C	25.00	227.15	1000.00	656.87	1000.00
Pressure	bar	1.00	5.00	5.00	1.00	5.50
Mass Vapor Fraction		1.00	1.00	1.00	1.00	1.00
Mass Liquid Fraction		0.00	0.00	0.00	0.00	0.00
Mass Solid Fraction		0.00	0.00	0.00	0.00	0.00
Mass Enthalpy	kJ/kg	-0.28	206.70	-38.31	-457.37	-3199.92
Mass Density	kg/cum	1.16	3.45	1.36	0.37	0.93
Enthalpy Flow	kW	-0.03	22.87	-4.57	-54.52	-27.43
Mass Flows	**kg/hr**	**398.24**	**398.24**	**429.10**	**429.10**	**30.86**
H_2	kg/hr	0.00	0.00	0.00	0.00	1.31
O_2	kg/hr	83.63	83.63	62.78	62.78	0.00
N_2	kg/hr	314.61	314.61	318.44	318.44	3.83
Cl_2	kg/hr	0.00	0.00	0.00	0.00	0.00
NO_2	kg/hr	0.00	0.00	0.00	0.00	0.00
CO	kg/hr	0.00	0.00	0.00	0.00	18.31
CO_2	kg/hr	0.00	0.00	32.80	32.80	4.03
H_2O	kg/hr	0.00	0.00	15.07	15.07	3.37
CH_4	kg/hr	0.00	0.00	0.00	0.00	0.00
H_2S	kg/hr	0.00	0.00	0.01	0.01	0.01
HCl	kg/hr	0.00	0.00	0.00	0.00	0.00

Case 3d

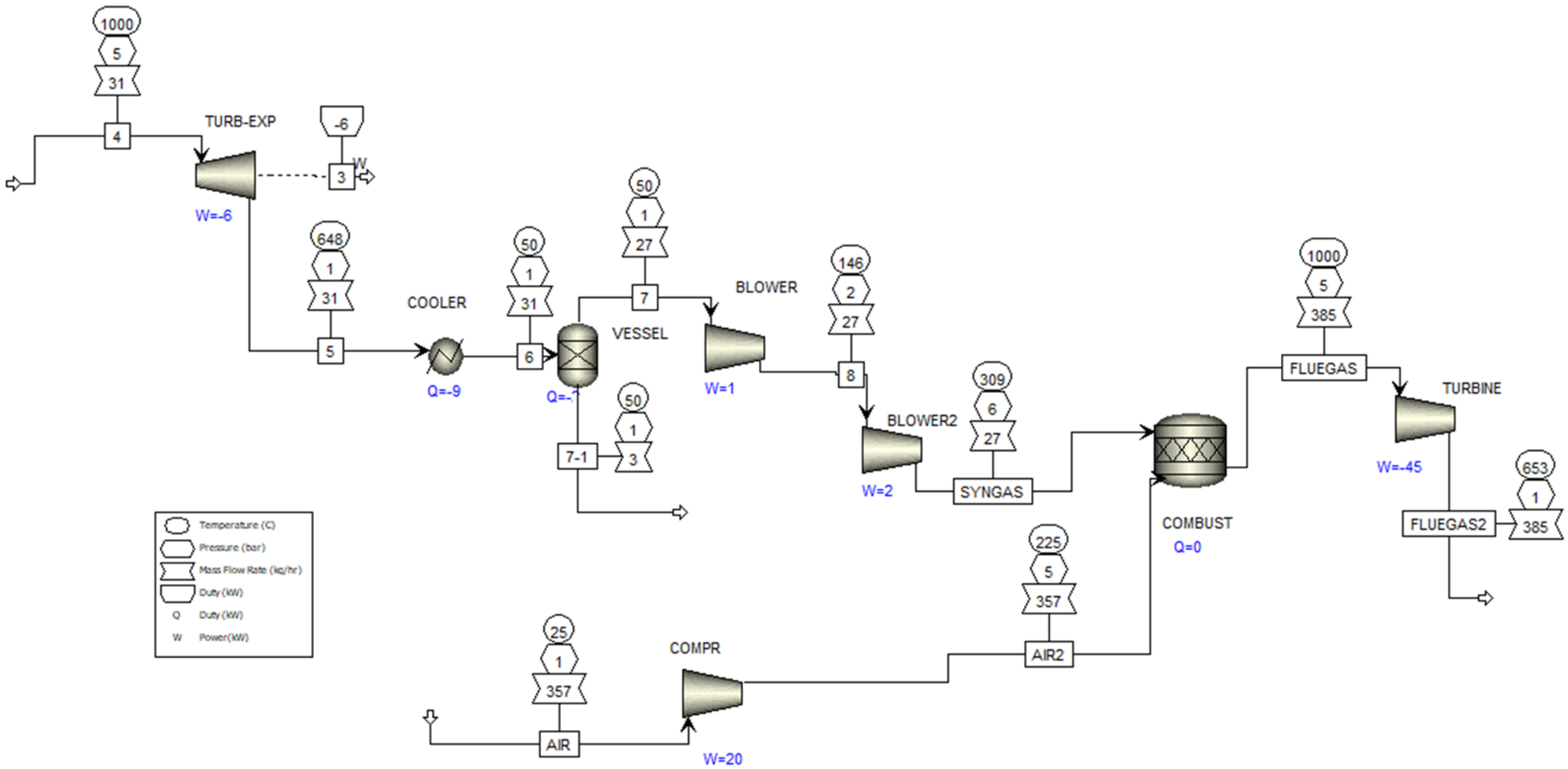


Figure A-7: Aspen Plus model flow diagram for Case 3d

Table A-7: Mass balance for Case 3d

	Units	4	5	6	7	7-1	8	AIR	AIR2	FLUEGAS	FLUEGAS2	SYNGAS
Temperature	C	1000.00	652.61	50.00	50.00	50.00	131.07	25.00	227.15	1000.00	657.33	297.90
Pressure	bar	5.00	1.00	1.00	1.00	1.00	2.00	1.00	5.00	5.00	1.00	6.00
Mass Vapor Fraction		1.00	1.00	1.00	1.00	0.00	1.00	1.00	1.00	1.00	1.00	1.00
Mass Liquid Fraction		0.00	0.00	0.00	0.00	1.00	0.00	0.00	0.00	0.00	0.00	0.00
Mass Solid Fraction		0.00	0.00	0.00	0.00	0.00	0.00	0.00	0.00	0.00	0.00	0.00
Mass Enthalpy	kJ/kg	-3199.97	-3869.75	-4935.11	-3899.05	-15849.51	-3764.31	-0.28	206.70	-56.45	-473.42	-3481.41
Mass Density	kg/cum	0.85	0.23	0.67	0.67	834.12	1.07	1.16	3.45	1.36	0.37	2.26
Enthalpy Flow	kW	-27.43	-33.17	-42.31	-29.77	-14.85	-28.74	-0.03	20.54	-6.04	-50.66	-26.58
Mass Flows	**kg/hr**	**30.86**	**30.86**	**30.86**	**27.49**	**3.37**	**27.49**	**357.77**	**357.77**	**385.26**	**385.26**	**27.49**
H_2	kg/hr	1.31	1.31	1.31	1.31	0.00	1.31	0.00	0.00	0.00	0.00	1.31
O_2	kg/hr	0.00	0.00	0.00	0.00	0.00	0.00	75.13	75.13	54.28	54.28	0.00
N_2	kg/hr	3.83	3.83	3.83	3.83	0.00	3.83	282.64	282.64	286.47	286.47	3.83
Cl_2	kg/hr	0.00	0.00	0.00	0.00	0.00	0.00	0.00	0.00	0.00	0.00	0.00
NO_2	kg/hr	0.00	0.00	0.00	0.00	0.00	0.00	0.00	0.00	0.00	0.00	0.00
CO	kg/hr	18.31	18.31	18.31	18.31	0.00	18.31	0.00	0.00	0.00	0.00	18.31
CO_2	kg/hr	4.03	4.03	4.03	4.03	0.00	4.03	0.00	0.00	32.80	32.80	4.03
H_2O	kg/hr	3.37	3.37	3.37	0.00	3.37	0.00	0.00	0.00	11.70	11.70	0.00
CH_4	kg/hr	0.00	0.00	0.00	0.00	0.00	0.00	0.00	0.00	0.00	0.00	0.00
C_2H_4	kg/hr	0.00	0.00	0.00	0.00	0.00	0.00	0.00	0.00	0.00	0.00	0.00
C_2H_6	kg/hr	0.00	0.00	0.00	0.00	0.00	0.00	0.00	0.00	0.00	0.00	0.00
N_2O	kg/hr	0.00	0.00	0.00	0.00	0.00	0.00	0.00	0.00	0.00	0.00	0.00
H_2S	kg/hr	0.01	0.01	0.01	0.01	0.00	0.01	0.00	0.00	0.01	0.01	0.01
HCl	kg/hr	0.00	0.00	0.00	0.00	0.00	0.00	0.00	0.00	0.00	0.00	0.00

Case 3e

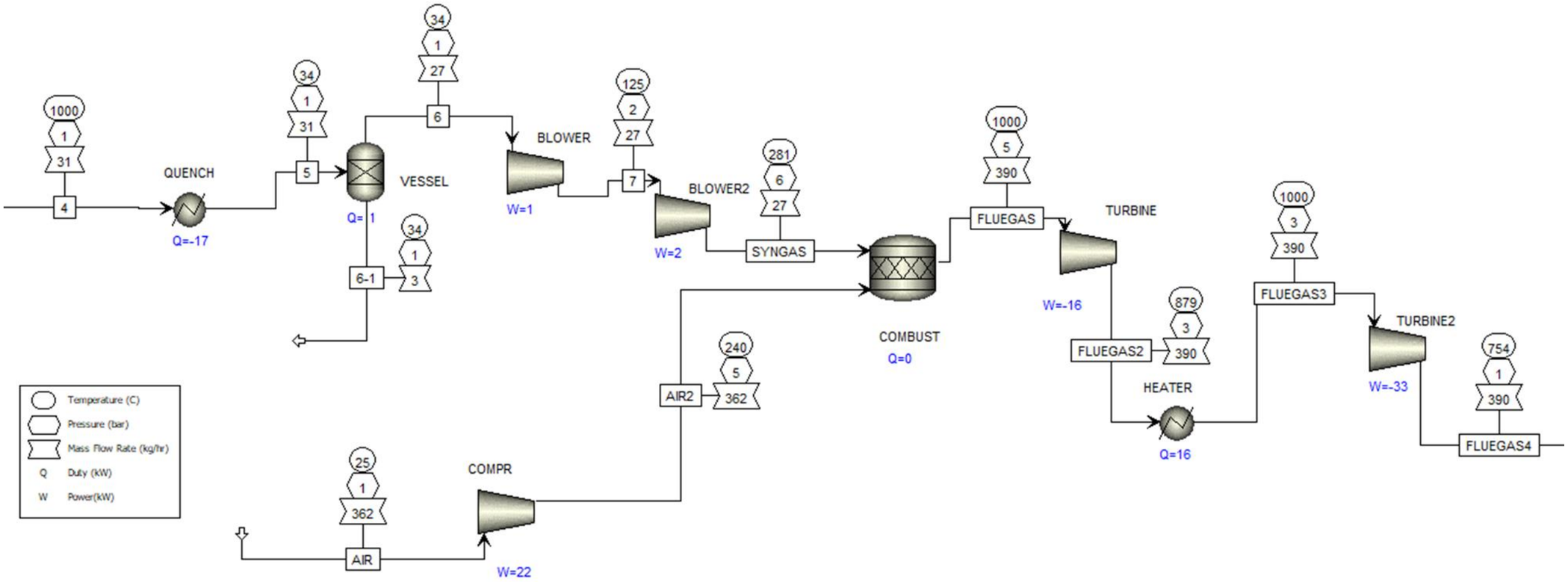


Figure A-8: Aspen Plus Flow diagram for Case 3e

Table A-8: Mass balance for Case 3e

	Units	4	5	6	6-1	7	AIR	AIR2	FLUEGAS	FLUEGAS2	FLUEGAS3	FLUEGAS4	SYNGAS
Temperature	C	1000.00	33.70	33.70	33.70	125.40	25.00	239.56	1000.00	878.86	1000.00	754.04	281.05
Pressure	bar	0.84	1.00	1.00	1.00	2.00	1.00	5.00	5.00	3.00	3.00	1.00	6.00
Mass Vapor Fraction		1.00	0.93	1.00	0.00	1.00	1.00	1.00	1.00	1.00	1.00	1.00	1.00
Mass Liquid Fraction		0.00	0.07	0.00	1.00	0.00	0.00	0.00	0.00	0.00	0.00	0.00	0.00
Mass Solid Fraction		0.00	0.00	0.00	0.00	0.00	0.00	0.00	0.00	0.00	0.00	0.00	0.00
Mass Enthalpy	kJ/kg	-3200.34	-5130.64	-3925.95	-15923.01	-3773.81	-0.28	219.64	-43.44	-193.41	-43.59	-345.08	-3510.33
Mass Density	kg/cum	0.14	0.75	0.70	843.74	1.08	1.16	3.37	1.36	0.91	0.82	0.34	2.33
Enthalpy Flow	kW	-27.44	-43.98	-29.98	-14.92	-28.82	-0.03	22.10	-4.70	-20.94	-4.72	-37.36	-26.80
Mass Flows	**kg/hr**	**30.86**	**30.86**	**27.49**	**3.37**	**27.49**	**362.25**	**362.25**	**389.74**	**389.74**	**389.74**	**389.74**	**27.49**
H_2	kg/hr	1.31	1.31	1.31	0.00	1.31	0.00	0.00	0.00	0.00	0.00	0.00	1.31
O_2	kg/hr	0.00	0.00	0.00	0.00	0.00	76.07	76.07	55.22	55.22	55.22	55.22	0.00
N_2	kg/hr	3.83	3.83	3.83	0.00	3.83	286.18	286.18	290.01	290.01	290.01	290.01	3.83
Cl_2	kg/hr	0.00	0.00	0.00	0.00	0.00	0.00	0.00	0.00	0.00	0.00	0.00	0.00
NO_2	kg/hr	0.00	0.00	0.00	0.00	0.00	0.00	0.00	0.00	0.00	0.00	0.00	0.00
CO	kg/hr	18.31	18.31	18.31	0.00	18.31	0.00	0.00	0.00	0.00	0.00	0.00	18.31
CO_2	kg/hr	4.03	4.03	4.03	0.00	4.03	0.00	0.00	32.80	32.80	32.80	32.80	4.03
H_2O	kg/hr	3.37	3.37	0.00	3.37	0.00	0.00	0.00	11.70	11.70	11.70	11.70	0.00
CH_4	kg/hr	0.00	0.00	0.00	0.00	0.00	0.00	0.00	0.00	0.00	0.00	0.00	0.00
C_2H_4	kg/hr	0.00	0.00	0.00	0.00	0.00	0.00	0.00	0.00	0.00	0.00	0.00	0.00
C_2H_6	kg/hr	0.00	0.00	0.00	0.00	0.00	0.00	0.00	0.00	0.00	0.00	0.00	0.00
N_2O	kg/hr	0.00	0.00	0.00	0.00	0.00	0.00	0.00	0.00	0.00	0.00	0.00	0.00
H_2S	kg/hr	0.01	0.01	0.01	0.00	0.01	0.00	0.00	0.01	0.01	0.01	0.01	0.01
HCl	kg/hr	0.00	0.00	0.00	0.00	0.00	0.00	0.00	0.00	0.00	0.00	0.00	0.00

Case 3f

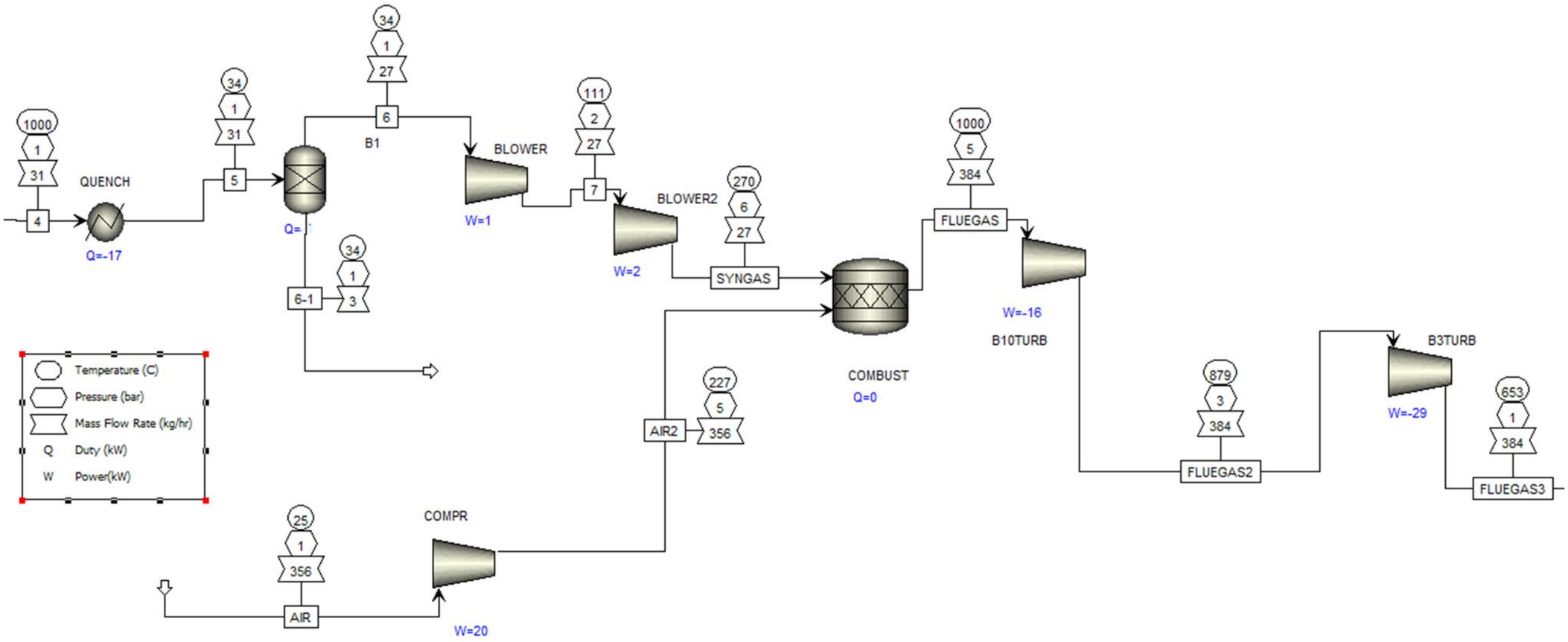


Figure A-9: Aspen Plus Flow diagram for Case 3f

Table A-9: Mass balance for Case 3f

	Units	4	5	6	6-1	7	AIR	AIR2	FLUEGAS	FLUEGAS2	FLUEGAS3	SYNGAS
Temperature	C	1000.00	33.70	33.70	33.70	110.95	25.00	227.15	1000.00	878.94	652.95	270.14
Pressure	bar	0.84	1.00	1.00	1.00	2.00	1.00	5.00	5.00	3.00	1.00	6.00
Mass Vapor Fraction		1.00	0.93	1.00	0.00	1.00	1.00	1.00	1.00	1.00	1.00	1.00
Mass Liquid Fraction		0.00	0.07	0.00	1.00	0.00	0.00	0.00	0.00	0.00	0.00	0.00
Mass Solid Fraction		0.00	0.00	0.00	0.00	0.00	0.00	0.00	0.00	0.00	0.00	0.00
Mass Enthalpy	kJ/kg	-3200.34	-5130.64	-3925.95	-15923.01	-3797.97	-0.28	206.70	-60.89	-210.86	-483.09	-3529.01
Mass Density	kg/cum	0.14	0.75	0.70	843.74	1.12	1.16	3.45	1.36	0.91	0.38	2.38
Enthalpy Flow	kW	-27.44	-43.98	-29.98	-14.92	-29.00	-0.03	20.46	-6.49	-22.48	-51.50	-26.95
Mass Flows	**kg/hr**	**30.86**	**30.86**	**27.49**	**3.37**	**27.49**	**356.26**	**356.26**	**383.75**	**383.75**	**383.75**	**27.49**
H_2	kg/hr	1.31	1.31	1.31	0.00	1.31	0.00	0.00	0.00	0.00	0.00	1.31
O_2	kg/hr	0.00	0.00	0.00	0.00	0.00	74.81	74.81	53.97	53.97	53.97	0.00
N_2	kg/hr	3.83	3.83	3.83	0.00	3.83	281.45	281.45	285.28	285.28	285.28	3.83
Cl_2	kg/hr	0.00	0.00	0.00	0.00	0.00	0.00	0.00	0.00	0.00	0.00	0.00
NO_2	kg/hr	0.00	0.00	0.00	0.00	0.00	0.00	0.00	0.00	0.00	0.00	0.00
CO	kg/hr	18.31	18.31	18.31	0.00	18.31	0.00	0.00	0.00	0.00	0.00	18.31
CO_2	kg/hr	4.03	4.03	4.03	0.00	4.03	0.00	0.00	32.80	32.80	32.80	4.03
H_2O	kg/hr	3.37	3.37	0.00	3.37	0.00	0.00	0.00	11.70	11.70	11.70	0.00
CH_4	kg/hr	0.00	0.00	0.00	0.00	0.00	0.00	0.00	0.00	0.00	0.00	0.00
C_2H_4	kg/hr	0.00	0.00	0.00	0.00	0.00	0.00	0.00	0.00	0.00	0.00	0.00
C_2H_6	kg/hr	0.00	0.00	0.00	0.00	0.00	0.00	0.00	0.00	0.00	0.00	0.00
N_2O	kg/hr	0.00	0.00	0.00	0.00	0.00	0.00	0.00	0.00	0.00	0.00	0.00
H_2S	kg/hr	0.01	0.01	0.01	0.00	0.01	0.00	0.00	0.01	0.01	0.01	0.01

Appendix A.2.2 Rankine cycle Mass Balance

The models for the different configurations of the Rankine cycle case studies explored in this research study can be found in the annotations for each case study along with the accompanying mass balance.

Case 4a

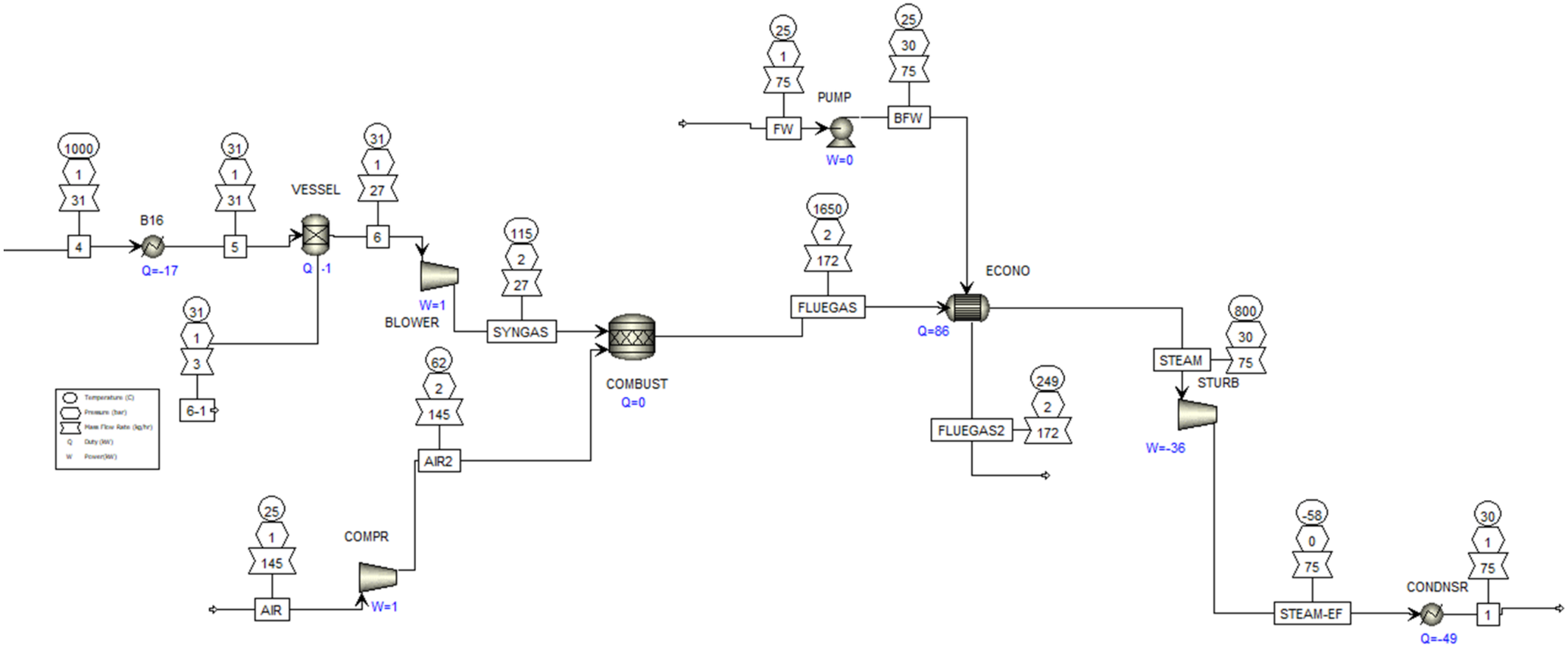


Figure A-10: Aspen Plus model flow diagram for Case 4a

Table A-10: Mass Balance for Case 4a

	Units	1	4	5	6	6-1	AIR	AIR2	SYNGAS	FLUEGAS	FLUEGAS2	STEAM	STEAM-EF	FW	BFW
Temperature	C	30.00	1000.00	31.37	31.37	31.37	25.00	61.52	115.02	1650.00	249.28	800.00	-57.60	25.00	25.15
Pressure	bar	1.00	0.85	0.84	0.84	0.84	1.00	1.50	2.00	1.50	1.50	30.00	0.03	1.00	30.00
Mass Vapor Fraction		0.00	1.00	0.93	1.00	0.00	1.00	1.00	1.00	1.00	1.00	1.00	1.00	0.00	0.00
Mass Liquid Fraction		1.00	0.00	0.07	0.00	1.00	0.00	0.00	0.00	0.00	0.00	0.00	0.00	1.00	1.00
Mass Solid Fraction		0.00	0.00	0.00	0.00	0.00	0.00	0.00	0.00	0.00	0.00	0.00	0.00	0.00	0.00
Mass Enthalpy	kJ/kg	-15939.67	-3200.34	-5130.64	-3929.74	-15933.53	-0.28	36.75	-3791.17	-574.33	-2372.87	-11829.42	-13576.58	-15962.21	-15958.79
Mass Density	kg/cum	845.85	0.14	0.64	0.60	845.07	1.16	1.55	1.11	0.27	1.01	6.09	0.03	848.65	848.87
Enthalpy Flow	kW	-332.08	-27.44	-43.98	-30.01	-14.93	-0.01	1.48	-28.95	-27.47	-113.50	-246.45	-282.85	-332.55	-332.47
Mass Flows	**kg/hr**	**75.00**	**30.86**	**30.86**	**27.49**	**3.37**	**144.71**	**144.71**	**27.49**	**172.20**	**172.20**	**75.00**	**75.00**	**75.00**	**75.00**
H_2	kg/hr	0.00	1.31	1.31	1.31	0.00	0.00	0.00	1.31	0.00	0.00	0.00	0.00	0.00	0.00
O_2	kg/hr	0.00	0.00	0.00	0.00	0.00	30.39	30.39	0.00	9.54	9.54	0.00	0.00	0.00	0.00
N_2	kg/hr	0.00	3.83	3.83	3.83	0.00	114.32	114.32	3.83	118.15	118.15	0.00	0.00	0.00	0.00
Cl_2	kg/hr	0.00	0.00	0.00	0.00	0.00	0.00	0.00	0.00	0.00	0.00	0.00	0.00	0.00	0.00
NO_2	kg/hr	0.00	0.00	0.00	0.00	0.00	0.00	0.00	0.00	0.00	0.00	0.00	0.00	0.00	0.00
CO	kg/hr	0.00	18.31	18.31	18.31	0.00	0.00	0.00	18.31	0.00	0.00	0.00	0.00	0.00	0.00
CO_2	kg/hr	0.00	4.03	4.03	4.03	0.00	0.00	0.00	4.03	32.80	32.80	0.00	0.00	0.00	0.00
H_2O	kg/hr	75.00	3.37	3.37	0.00	3.37	0.00	0.00	0.00	11.70	11.70	75.00	75.00	75.00	75.00
CH_4	kg/hr	0.00	0.00	0.00	0.00	0.00	0.00	0.00	0.00	0.00	0.00	0.00	0.00	0.00	0.00
C_2H_4	kg/hr	0.00	0.00	0.00	0.00	0.00	0.00	0.00	0.00	0.00	0.00	0.00	0.00	0.00	0.00
C_2H_6	kg/hr	0.00	0.00	0.00	0.00	0.00	0.00	0.00	0.00	0.00	0.00	0.00	0.00	0.00	0.00
N_2O	kg/hr	0.00	0.00	0.00	0.00	0.00	0.00	0.00	0.00	0.00	0.00	0.00	0.00	0.00	0.00
H_2S	kg/hr	0.00	0.01	0.01	0.01	0.00	0.00	0.00	0.01	0.01	0.01	0.00	0.00	0.00	0.00
HCl	kg/hr	0.00	0.00	0.00	0.00	0.00	0.00	0.00	0.00	0.00	0.00	0.00	0.00	0.00	0.00

Case 4b

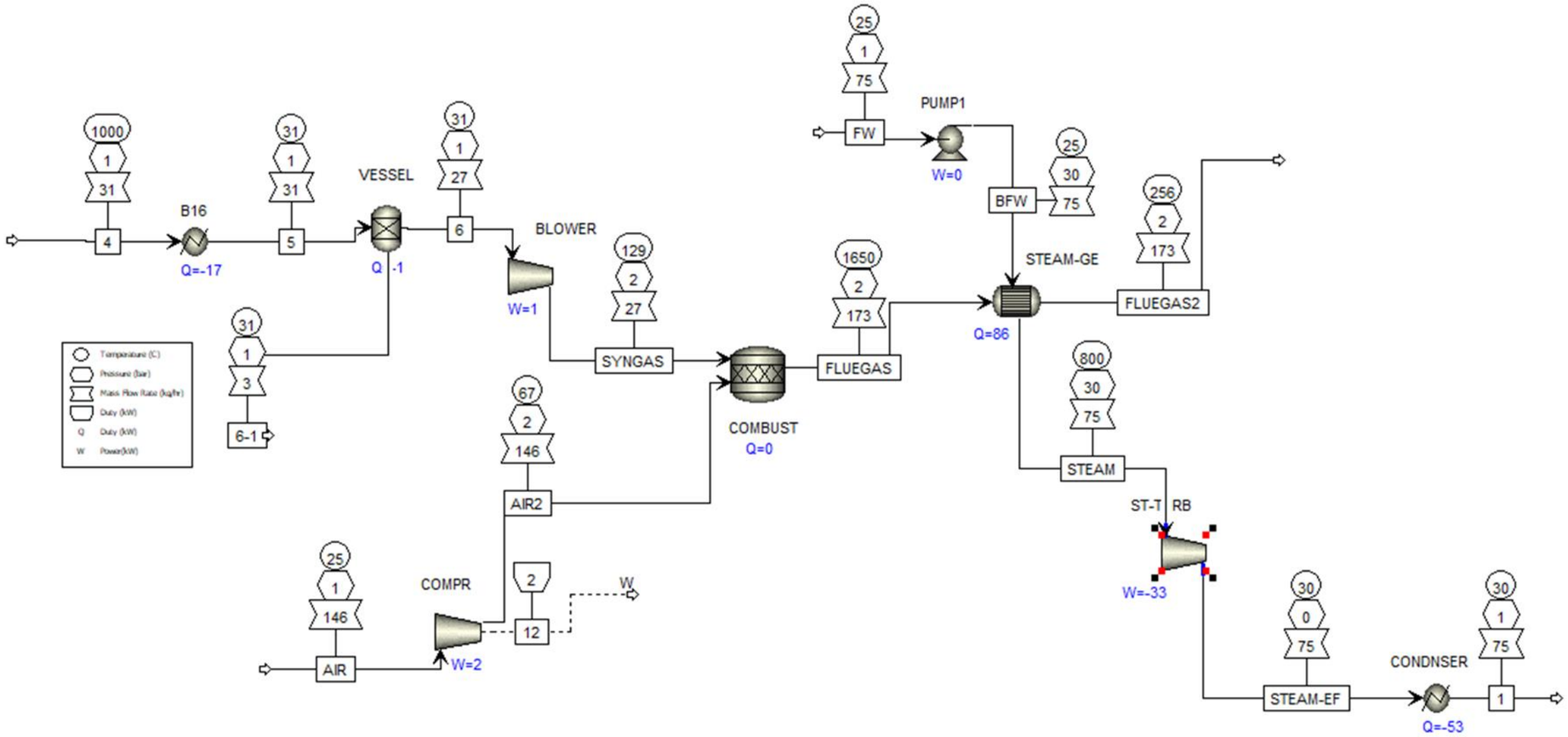


Figure A-11: Aspen Plus model flow diagram for Case 4b

Table A-11: Mass balance for Case 4b

	Units	1	4	5	6	6-1	AIR	AIR2	FLUEGAS	FLUEGAS2	STEAM	STEAM-EF	FW	BFW	SYNGAS
Temperature	C	30.00	1000.00	31.37	31.37	31.37	25.00	67.44	1650.00	256.45	800.00	73.69	25.00	25.27	128.50
Pressure	bar	1.00	0.85	0.84	0.84	0.84	1.00	1.50	1.50	1.50	30.00	0.03	1.00	30.00	2.00
Mass Vapor Fraction		0.00	1.00	0.93	1.00	0.00	1.00	1.00	1.00	1.00	1.00	1.00	0.00	0.00	1.00
Mass Liquid Fraction		1.00	0.00	0.07	0.00	1.00	0.00	0.00	0.00	0.00	0.00	0.00	1.00	1.00	0.00
Mass Solid Fraction		0.00	0.00	0.00	0.00	0.00	0.00	0.00	0.00	0.00	0.00	0.00	0.00	0.00	0.00
Mass Enthalpy	kJ/kg	-15939.67	-3200.34	-5130.64	-3929.74	-15933.53	-0.28	42.78	-562.79	-2352.63	-11829.42	-13331.98	-15962.21	-15958.23	-3768.61
Mass Density	kg/cum	845.85	0.14	0.64	0.60	845.07	1.16	1.52	0.27	0.99	6.09	0.02	848.65	848.80	1.07
Enthalpy Flow	kW	-332.08	-27.44	-43.98	-30.01	-14.93	-0.01	1.73	-27.05	-113.06	-246.45	-277.75	-332.55	-332.46	-28.78
Mass Flows	**kg/hr**	**75.00**	**30.86**	**30.86**	**27.49**	**3.37**	**145.52**	**145.52**	**173.01**	**173.01**	**75.00**	**75.00**	**75.00**	**75.00**	**27.49**
H_2	kg/hr	0.00	1.31	1.31	1.31	0.00	0.00	0.00	0.00	0.00	0.00	0.00	0.00	0.00	1.31
O_2	kg/hr	0.00	0.00	0.00	0.00	0.00	30.56	30.56	9.71	9.71	0.00	0.00	0.00	0.00	0.00
N_2	kg/hr	0.00	3.83	3.83	3.83	0.00	114.96	114.96	118.79	118.79	0.00	0.00	0.00	0.00	3.83
Cl_2	kg/hr	0.00	0.00	0.00	0.00	0.00	0.00	0.00	0.00	0.00	0.00	0.00	0.00	0.00	0.00
NO_2	kg/hr	0.00	0.00	0.00	0.00	0.00	0.00	0.00	0.00	0.00	0.00	0.00	0.00	0.00	0.00
CO	kg/hr	0.00	18.31	18.31	18.31	0.00	0.00	0.00	0.00	0.00	0.00	0.00	0.00	0.00	18.31
CO_2	kg/hr	0.00	4.03	4.03	4.03	0.00	0.00	0.00	32.80	32.80	0.00	0.00	0.00	0.00	4.03
H_2O	kg/hr	75.00	3.37	3.37	0.00	3.37	0.00	0.00	11.70	11.70	75.00	75.00	75.00	75.00	0.00
CH_4	kg/hr	0.00	0.00	0.00	0.00	0.00	0.00	0.00	0.00	0.00	0.00	0.00	0.00	0.00	0.00
C_2H_4	kg/hr	0.00	0.00	0.00	0.00	0.00	0.00	0.00	0.00	0.00	0.00	0.00	0.00	0.00	0.00
C_2H_6	kg/hr	0.00	0.00	0.00	0.00	0.00	0.00	0.00	0.00	0.00	0.00	0.00	0.00	0.00	0.00
N_2O	kg/hr	0.00	0.00	0.00	0.00	0.00	0.00	0.00	0.00	0.00	0.00	0.00	0.00	0.00	0.00
H_2S	kg/hr	0.00	0.01	0.01	0.01	0.00	0.00	0.00	0.01	0.01	0.00	0.00	0.00	0.00	0.01
HCl	kg/hr	0.00	0.00	0.00	0.00	0.00	0.00	0.00	0.00	0.00	0.00	0.00	0.00	0.00	0.00

Case 4c

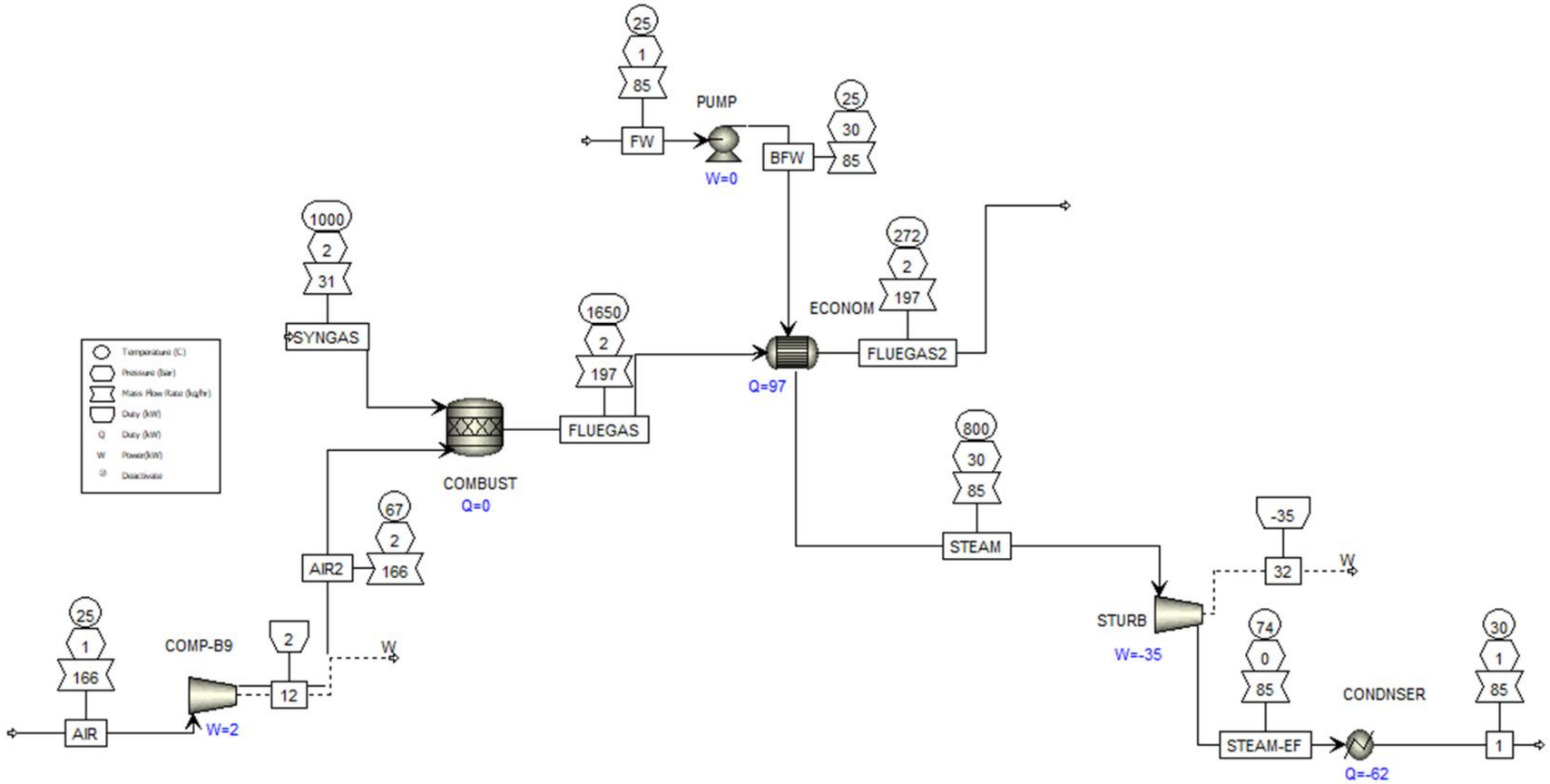


Figure A-12: Aspen Plus model Flow diagram for Case 4c

Table A-12: Mass balance for Case 4c

	Units	1	AIR	AIR2	FLUEGAS	FLUEGAS2	STEAM	STEAM-EF	FW	BFW	SYNGAS
Temperature	C	30.00	25.00	67.44	1650.00	271.73	800.00	73.69	25.00	25.27	1000.00
Pressure	bar	1.00	1.00	1.50	1.50	1.50	30.00	0.03	1.00	30.00	2.00
Mass Vapor Fraction		0.00	1.00	1.00	1.00	1.00	1.00	1.00	0.00	0.00	1.00
Mass Liquid Fraction		1.00	0.00	0.00	0.00	0.00	0.00	0.00	1.00	1.00	0.00
Mass Solid Fraction		0.00	0.00	0.00	0.00	0.00	0.00	0.00	0.00	0.00	0.00
Mass Enthalpy	kJ/kg	-15939.67	-0.28	42.78	-466.04	-2250.22	-11829.42	-13331.98	-15962.21	-15958.23	-3200.24
Mass Density	kg/cum	845.85	1.16	1.52	0.27	0.95	6.09	0.02	848.65	848.80	0.34
Enthalpy Flow	kW	-376.35	-0.01	1.97	-25.46	-122.95	-279.31	-314.78	-376.89	-376.79	-27.43
Mass Flows	**kg/hr**	**85.00**	**165.84**	**165.84**	**196.70**	**196.70**	**85.00**	**85.00**	**85.00**	**85.00**	**30.86**
H_2	kg/hr	0.00	0.00	0.00	0.00	0.00	0.00	0.00	0.00	0.00	1.31
O_2	kg/hr	0.00	34.83	34.83	13.98	13.98	0.00	0.00	0.00	0.00	0.00
N_2	kg/hr	0.00	131.01	131.01	134.84	134.84	0.00	0.00	0.00	0.00	3.83
Cl_2	kg/hr	0.00	0.00	0.00	0.00	0.00	0.00	0.00	0.00	0.00	0.00
NO_2	kg/hr	0.00	0.00	0.00	0.00	0.00	0.00	0.00	0.00	0.00	0.00
CO	kg/hr	0.00	0.00	0.00	0.00	0.00	0.00	0.00	0.00	0.00	18.31
CO_2	kg/hr	0.00	0.00	0.00	32.80	32.80	0.00	0.00	0.00	0.00	4.03
H_2O	kg/hr	85.00	0.00	0.00	15.07	15.07	85.00	85.00	85.00	85.00	3.37
CH_4	kg/hr	0.00	0.00	0.00	0.00	0.00	0.00	0.00	0.00	0.00	0.00
C_2H_4	kg/hr	0.00	0.00	0.00	0.00	0.00	0.00	0.00	0.00	0.00	0.00
C_2H_6	kg/hr	0.00	0.00	0.00	0.00	0.00	0.00	0.00	0.00	0.00	0.00
N_2O	kg/hr	0.00	0.00	0.00	0.00	0.00	0.00	0.00	0.00	0.00	0.00
H_2S	kg/hr	0.00	0.00	0.00	0.01	0.01	0.00	0.00	0.00	0.00	0.01

Case 4d

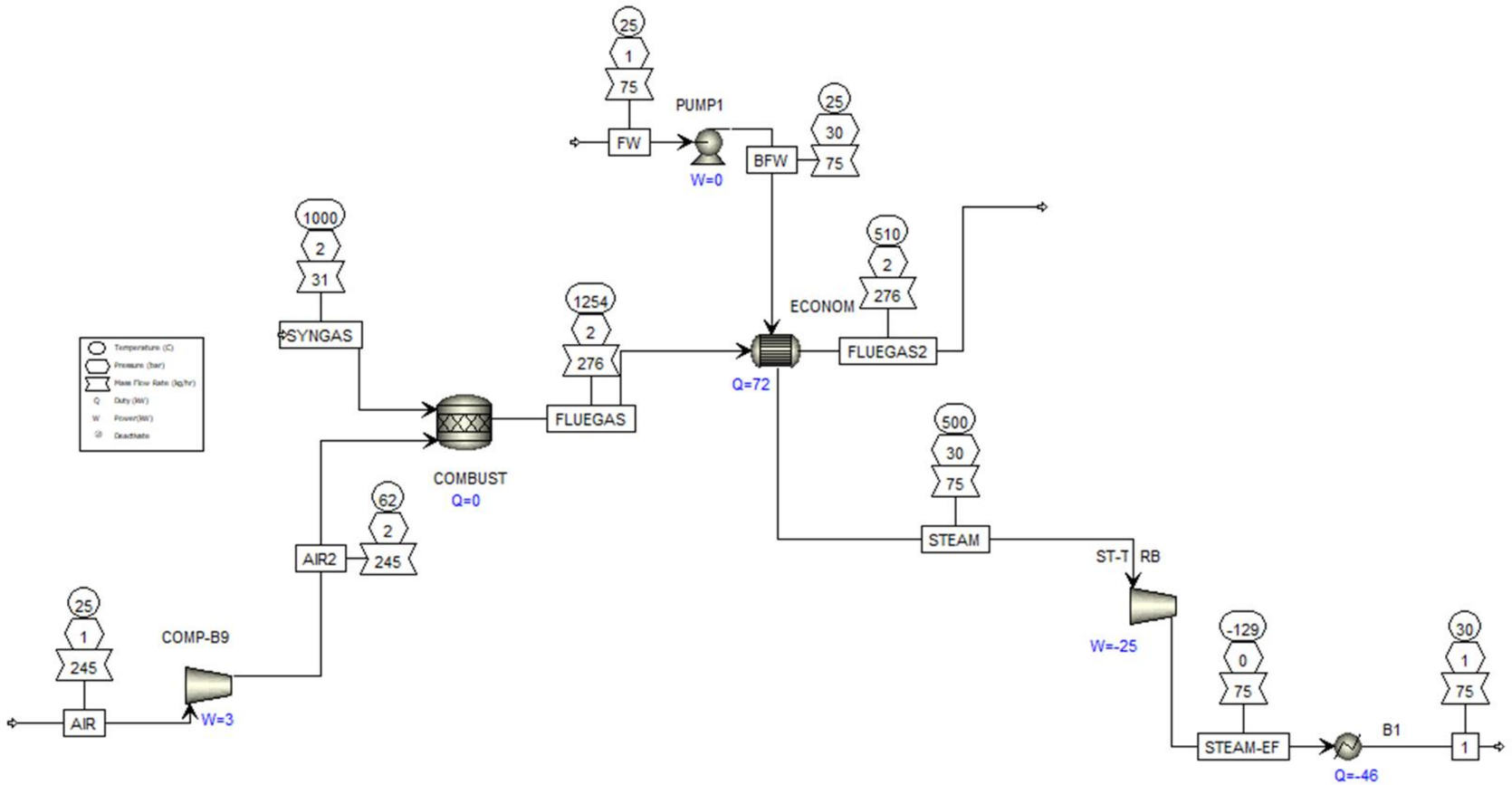


Figure A-13: Aspen Plus model flow diagram for Case 4d

Table A-13: Mass Balance for Case 4d

	Units	SYNGAS	AIR	AIR2	FLUEGAS	FLUEGAS2	STEAM	STEAM-EF	FW	BFW	1
Temperature	C	1000.00	25.00	61.52	1253.87	510.01	500.00	-129.49	25.00	25.15	30.00
Pressure	bar	2.00	1.00	1.50	1.50	1.50	30.00	0.03	1.00	30.00	1.00
Mass Vapor Fraction		1.00	1.00	1.00	1.00	1.00	1.00	1.00	0.00	0.00	0.00
Mass Liquid Fraction		0.00	0.00	0.00	0.00	0.00	0.00	0.00	1.00	1.00	1.00
Mass Solid Fraction		0.00	0.00	0.00	0.00	0.00	0.00	0.00	0.00	0.00	0.00
Mass Enthalpy	kJ/kg	-3200.24	-0.28	36.75	-325.13	-1259.59	-12519.25	-13709.90	-15962.21	-15958.79	-15939.67
Mass Density	kg/cum	0.34	1.16	1.55	0.34	0.66	8.65	0.05	848.65	848.87	845.85
Enthalpy Flow	kW	-27.43	-0.02	2.50	-24.93	-96.59	-260.82	-285.62	-332.55	-332.47	-332.08
Mass Flows	**kg/hr**	**30.86**	**245.20**	**245.20**	**276.06**	**276.06**	**75.00**	**75.00**	**75.00**	**75.00**	**75.00**
H_2	kg/hr	1.31	0.00	0.00	0.00	0.00	0.00	0.00	0.00	0.00	0.00
O_2	kg/hr	0.00	51.49	51.49	30.64	30.64	0.00	0.00	0.00	0.00	0.00
N_2	kg/hr	3.83	193.70	193.70	197.53	197.53	0.00	0.00	0.00	0.00	0.00
Cl_2	kg/hr	0.00	0.00	0.00	0.00	0.00	0.00	0.00	0.00	0.00	0.00
NO_2	kg/hr	0.00	0.00	0.00	0.00	0.00	0.00	0.00	0.00	0.00	0.00
CO	kg/hr	18.31	0.00	0.00	0.00	0.00	0.00	0.00	0.00	0.00	0.00
CO_2	kg/hr	4.03	0.00	0.00	32.80	32.80	0.00	0.00	0.00	0.00	0.00
H_2O	kg/hr	3.37	0.00	0.00	15.07	15.07	75.00	75.00	75.00	75.00	75.00
CH_4	kg/hr	0.00	0.00	0.00	0.00	0.00	0.00	0.00	0.00	0.00	0.00
C_2H_4	kg/hr	0.00	0.00	0.00	0.00	0.00	0.00	0.00	0.00	0.00	0.00
C_2H_6	kg/hr	0.00	0.00	0.00	0.00	0.00	0.00	0.00	0.00	0.00	0.00
N_2O	kg/hr	0.00	0.00	0.00	0.00	0.00	0.00	0.00	0.00	0.00	0.00
H_2S	kg/hr	0.01	0.00	0.00	0.01	0.01	0.00	0.00	0.00	0.00	0.00
HCl	kg/hr	0.00	0.00	0.00	0.00	0.00	0.00	0.00	0.00	0.00	0.00

Case 4e

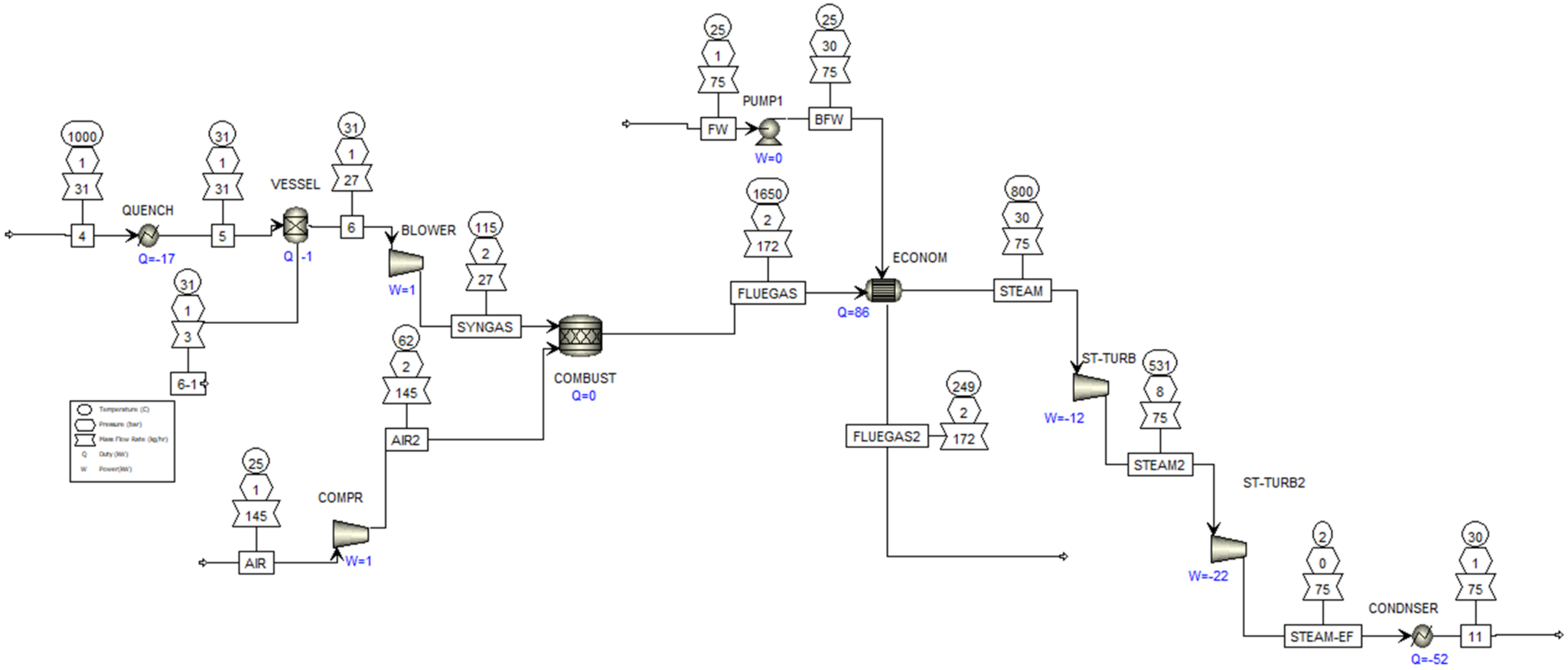


Figure A-14: Aspen Plus model flow diagram for Case 4e

Table A-14: Mass balance for Case 4e

	Units	4	5	6	6-1	11	AIR	AIR2	SYNGAS	FLUEGAS	FLUEGAS2	STEAM	STEAM2	STEAM-EF	FW	BFW
Temperature	C	1000.00	31.37	31.37	31.37	30.00	25.00	61.52	115.02	1650.00	249.28	800.00	531.05	2.01	25.00	25.15
Pressure	bar	0.85	0.84	0.84	0.84	1.00	1.00	1.50	2.00	1.50	1.50	30.00	7.50	0.08	1.00	30.00
Mass Vapor Fraction		1.00	0.93	1.00	0.00	0.00	1.00	1.00	1.00	1.00	1.00	1.00	1.00	1.00	0.00	0.00
Mass Liquid Fraction		0.00	0.07	0.00	1.00	1.00	0.00	0.00	0.00	0.00	0.00	0.00	0.00	0.00	1.00	1.00
Mass Solid Fraction		0.00	0.00	0.00	0.00	0.00	0.00	0.00	0.00	0.00	0.00	0.00	0.00	0.00	0.00	0.00
Mass Enthalpy	kJ/kg	-3200.34	-5130.64	-3929.74	-15933.53	-15939.67	-0.28	36.75	-3791.17	-574.33	-2372.87	-11829.42	-12423.43	-13466.20	-15962.21	-15958.79
Mass Density	kg/cum	0.14	0.64	0.60	845.07	845.85	1.16	1.55	1.11	0.27	1.01	6.09	2.03	0.06	848.65	848.87
Enthalpy Flow	kW	-27.44	-43.98	-30.01	-14.93	-332.08	-0.01	1.48	-28.95	-27.47	-113.50	-246.45	-258.82	-280.55	-332.55	-332.47
Mass Flows	**kg/hr**	**30.86**	**30.86**	**27.49**	**3.37**	**75.00**	**144.71**	**144.71**	**27.49**	**172.20**	**172.20**	**75.00**	**75.00**	**75.00**	**75.00**	**75.00**
H_2	kg/hr	1.31	1.31	1.31	0.00	0.00	0.00	0.00	1.31	0.00	0.00	0.00	0.00	0.00	0.00	0.00
O_2	kg/hr	0.00	0.00	0.00	0.00	0.00	30.39	30.39	0.00	9.54	9.54	0.00	0.00	0.00	0.00	0.00
N_2	kg/hr	3.83	3.83	3.83	0.00	0.00	114.32	114.32	3.83	118.15	118.15	0.00	0.00	0.00	0.00	0.00
Cl_2	kg/hr	0.00	0.00	0.00	0.00	0.00	0.00	0.00	0.00	0.00	0.00	0.00	0.00	0.00	0.00	0.00
NO_2	kg/hr	0.00	0.00	0.00	0.00	0.00	0.00	0.00	0.00	0.00	0.00	0.00	0.00	0.00	0.00	0.00
CO	kg/hr	18.31	18.31	18.31	0.00	0.00	0.00	0.00	18.31	0.00	0.00	0.00	0.00	0.00	0.00	0.00
CO_2	kg/hr	4.03	4.03	4.03	0.00	0.00	0.00	0.00	4.03	32.80	32.80	0.00	0.00	0.00	0.00	0.00
H_2O	kg/hr	3.37	3.37	0.00	3.37	75.00	0.00	0.00	0.00	11.70	11.70	75.00	75.00	75.00	75.00	75.00
CH_4	kg/hr	0.00	0.00	0.00	0.00	0.00	0.00	0.00	0.00	0.00	0.00	0.00	0.00	0.00	0.00	0.00
C_2H_4	kg/hr	0.00	0.00	0.00	0.00	0.00	0.00	0.00	0.00	0.00	0.00	0.00	0.00	0.00	0.00	0.00
C_2H_6	kg/hr	0.00	0.00	0.00	0.00	0.00	0.00	0.00	0.00	0.00	0.00	0.00	0.00	0.00	0.00	0.00
N_2O	kg/hr	0.00	0.00	0.00	0.00	0.00	0.00	0.00	0.00	0.00	0.00	0.00	0.00	0.00	0.00	0.00
H_2S	kg/hr	0.01	0.01	0.01	0.00	0.00	0.00	0.00	0.01	0.01	0.01	0.00	0.00	0.00	0.00	0.00
HCl	kg/hr	0.00	0.00	0.00	0.00	0.00	0.00	0.00	0.00	0.00	0.00	0.00	0.00	0.00	0.00	0.00

Case 4f

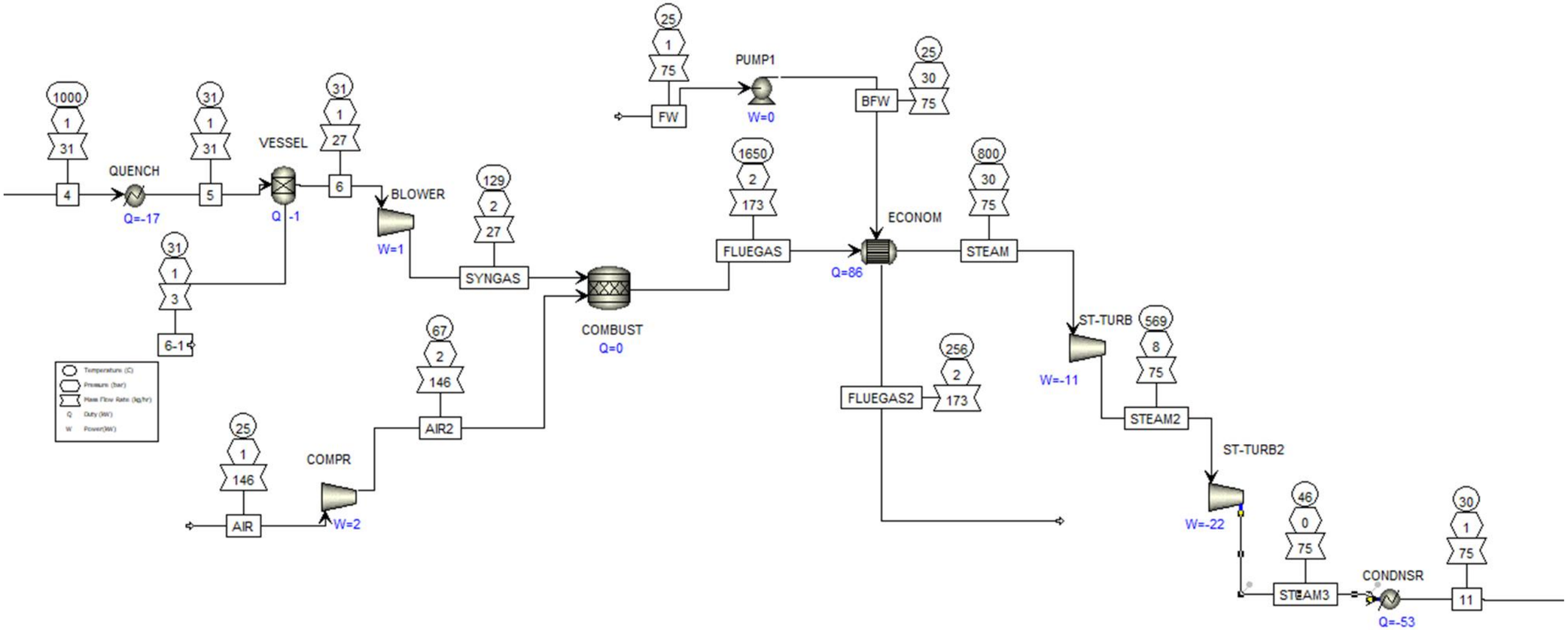


Figure A-15: Aspen Plus model flow diagram for Case 4f

Table A-15: Mass balance for Case 4f

	Units	4	5	6	6-1	SYNGAS	AIR	AIR2	FLUEGAS	FLUEGAS2	STEAM	STEAM2	STEAM3	FW	BFW	11
Temperature	C	1000.00	31.37	31.37	31.37	128.50	25.00	67.44	1650.00	256.45	800.00	569.12	45.81	25.00	25.27	30.00
Pressure	bar	0.85	0.84	0.84	0.84	2.00	1.00	1.50	1.50	1.50	30.00	7.50	0.03	1.00	30.00	1.00
Mass Vapor Fraction		1.00	0.93	1.00	0.00	1.00	1.00	1.00	1.00	1.00	1.00	1.00	1.00	0.00	0.00	0.00
Mass Liquid Fraction		0.00	0.07	0.00	1.00	0.00	0.00	0.00	0.00	0.00	0.00	0.00	0.00	1.00	1.00	1.00
Mass Solid Fraction		0.00	0.00	0.00	0.00	0.00	0.00	0.00	0.00	0.00	0.00	0.00	0.00	0.00	0.00	0.00
Mass Enthalpy	kJ/kg	-3200.34	-5130.64	-3929.74	-15933.53	-3768.61	-0.28	42.78	-562.79	-2352.63	-11829.42	-12340.27	-13384.25	-15962.21	-15958.23	-15939.67
Mass Density	kg/cum	0.14	0.64	0.60	845.07	1.07	1.16	1.52	0.27	0.99	6.09	1.94	0.02	848.65	848.80	845.85
Enthalpy Flow	kW	-27.44	-43.98	-30.01	-14.93	-28.78	-0.01	1.73	-27.05	-113.06	-246.45	-257.09	-278.84	-332.55	-332.46	-332.08
Mass Flows	**kg/hr**	**30.86**	**30.86**	**27.49**	**3.37**	**27.49**	**145.52**	**145.52**	**173.01**	**173.01**	**75.00**	**75.00**	**75.00**	**75.00**	**75.00**	**75.00**
H_2	kg/hr	1.31	1.31	1.31	0.00	1.31	0.00	0.00	0.00	0.00	0.00	0.00	0.00	0.00	0.00	0.00
O_2	kg/hr	0.00	0.00	0.00	0.00	0.00	30.56	30.56	9.71	9.71	0.00	0.00	0.00	0.00	0.00	0.00
N_2	kg/hr	3.83	3.83	3.83	0.00	3.83	114.96	114.96	118.79	118.79	0.00	0.00	0.00	0.00	0.00	0.00
Cl_2	kg/hr	0.00	0.00	0.00	0.00	0.00	0.00	0.00	0.00	0.00	0.00	0.00	0.00	0.00	0.00	0.00
NO_2	kg/hr	0.00	0.00	0.00	0.00	0.00	0.00	0.00	0.00	0.00	0.00	0.00	0.00	0.00	0.00	0.00
CO	kg/hr	18.31	18.31	18.31	0.00	18.31	0.00	0.00	0.00	0.00	0.00	0.00	0.00	0.00	0.00	0.00
CO_2	kg/hr	4.03	4.03	4.03	0.00	4.03	0.00	0.00	32.80	32.80	0.00	0.00	0.00	0.00	0.00	0.00
H_2O	kg/hr	3.37	3.37	0.00	3.37	0.00	0.00	0.00	11.70	11.70	75.00	75.00	75.00	75.00	75.00	75.00
CH_4	kg/hr	0.00	0.00	0.00	0.00	0.00	0.00	0.00	0.00	0.00	0.00	0.00	0.00	0.00	0.00	0.00
C_2H_4	kg/hr	0.00	0.00	0.00	0.00	0.00	0.00	0.00	0.00	0.00	0.00	0.00	0.00	0.00	0.00	0.00
C_2H_6	kg/hr	0.00	0.00	0.00	0.00	0.00	0.00	0.00	0.00	0.00	0.00	0.00	0.00	0.00	0.00	0.00
N_2O	kg/hr	0.00	0.00	0.00	0.00	0.00	0.00	0.00	0.00	0.00	0.00	0.00	0.00	0.00	0.00	0.00
H_2S	kg/hr	0.01	0.01	0.01	0.00	0.01	0.00	0.00	0.01	0.01	0.00	0.00	0.00	0.00	0.00	0.00
HCl	kg/hr	0.00	0.00	0.00	0.00	0.00	0.00	0.00	0.00	0.00	0.00	0.00	0.00	0.00	0.00	0.00

Appendix A.2.3 Combined power cycle Mass balance

The models for the different configurations of the combined power cycle case studies explored in this research study can be found in the annotations for each case study along with the accompanying mass balance.

Case 5a

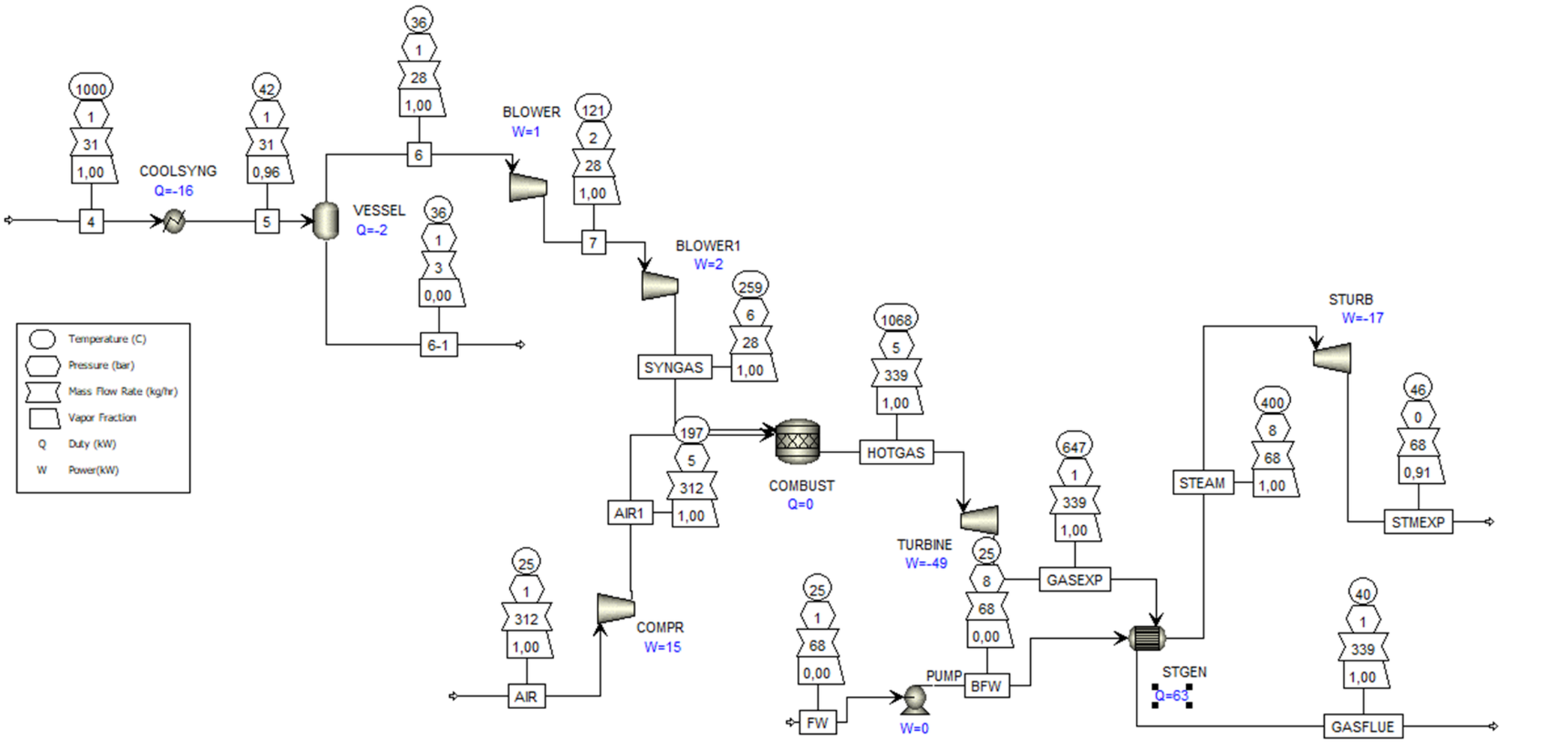


Figure A-16: Aspen Plus model flow diagram for Case 5a

Table A-16: Mass balance for Case 5a

	Units	4	5	6	6-1	7	AIR	AIR1	HOTGAS	GASEXP	GASFLUE	STEAM	STMEXP	FW	BFW	SYNGAS
Temperature	C	1000.00	42.00	36.00	36.00	120.80	25.00	197.16	1068.00	646.93	39.86	400.00	46.30	25.00	24.99	259.49
Pressure	bar	0.85	0.83	0.84	0.84	2.00	1.00	5.00	5.00	1.00	1.00	8.00	0.08	1.00	8.00	6.00
Molar Vapor Fraction		1.00	0.96	1.00	0.00	1.00	1.00	1.00	1.00	1.00	1.00	1.00	0.91	0.00	0.00	1.00
Molar Liquid Fraction		0.00	0.04	0.00	1.00	0.00	0.00	0.00	0.00	0.00	0.00	0.00	0.09	1.00	1.00	0.00
Molar Solid Fraction		0.00	0.00	0.00	0.00	0.00	0.00	0.00	0.00	0.00	0.00	0.00	0.00	0.00	0.00	0.00
Mass Vapor Fraction		1.00	0.96	1.00	0.00	1.00	1.00	1.00	1.00	1.00	1.00	1.00	0.91	0.00	0.00	1.00
Mass Liquid Fraction		0.00	0.04	0.00	1.00	0.00	0.00	0.00	0.00	0.00	0.00	0.00	0.09	1.00	1.00	0.00
Molar Enthalpy	kJ/kmol	-57466.11	-90486.28	-70524.42	-285000.13	-67998.82	-6.62	5055.47	-3694.65	-18689.04	-38135.92	-228848.65	-245067.15	-289046.50	-289033.81	-63788.94
Mass Enthalpy	kJ/kg	-3200.90	-5040.15	-3929.91	-15819.91	-3789.17	-0.23	175.23	-127.28	-643.81	-1313.73	-12703.03	-13603.29	-16044.52	-16043.81	-3554.58
Mass Entropy	kJ/kg-K	4.92	2.15	2.79	-8.91	2.79	0.15	0.15	1.39	1.39	0.21	-1.85	-1.85	-9.51	-9.51	2.79
Mass Density	kg/cum	0.14	0.59	0.59	993.77	1.09	1.16	3.68	1.30	0.38	1.12	2.60	0.06	993.96	993.96	2.42
Enthalpy Flow	kW	-27.43	-43.20	-30.02	-14.73	-28.95	-0.02	15.17	-11.99	-60.64	-123.75	-239.95	-256.95	-303.06	-303.05	-27.16
Average MW		17.95	17.95	17.95	18.02	17.95	28.85	28.85	29.03	29.03	29.03	18.02	18.02	18.02	18.02	17.95
Mass Flows	**kg/hr**	**30.86**	**30.86**	**27.50**	**3.35**	**27.50**	**311.60**	**311.60**	**339.11**	**339.11**	**339.11**	**68.00**	**68.00**	**68.00**	**68.00**	**27.50**
H_2O	kg/hr	3.37	3.37	0.02	3.35	0.02	0.00	0.00	11.72	11.72	11.72	68.00	68.00	68.00	68.00	0.02
H_2	kg/hr	1.31	1.31	1.31	0.00	1.31	0.00	0.00	0.00	0.00	0.00	0.00	0.00	0.00	0.00	1.31
CO	kg/hr	18.31	18.31	18.31	0.00	18.31	0.00	0.00	0.00	0.00	0.00	0.00	0.00	0.00	0.00	18.31
CO_2	kg/hr	4.03	4.03	4.03	0.00	4.03	0.00	0.00	32.80	32.80	32.80	0.00	0.00	0.00	0.00	4.03
AR	kg/hr	0.00	0.00	0.00	0.00	0.00	0.00	0.00	0.00	0.00	0.00	0.00	0.00	0.00	0.00	0.00
CH_4	kg/hr	0.00	0.00	0.00	0.00	0.00	0.00	0.00	0.00	0.00	0.00	0.00	0.00	0.00	0.00	0.00
N_2	kg/hr	3.83	3.83	3.83	0.00	3.83	239.03	239.03	242.86	242.86	242.86	0.00	0.00	0.00	0.00	3.83
HCl	kg/hr	0.00	0.00	0.00	0.00	0.00	0.00	0.00	0.00	0.00	0.00	0.00	0.00	0.00	0.00	0.00
H_2S	kg/hr	0.00	0.00	0.00	0.00	0.00	0.00	0.00	0.00	0.00	0.00	0.00	0.00	0.00	0.00	0.00
O_2	kg/hr	0.00	0.00	0.00	0.00	0.00	72.58	72.58	51.73	51.73	51.73	0.00	0.00	0.00	0.00	0.00

Case 5b

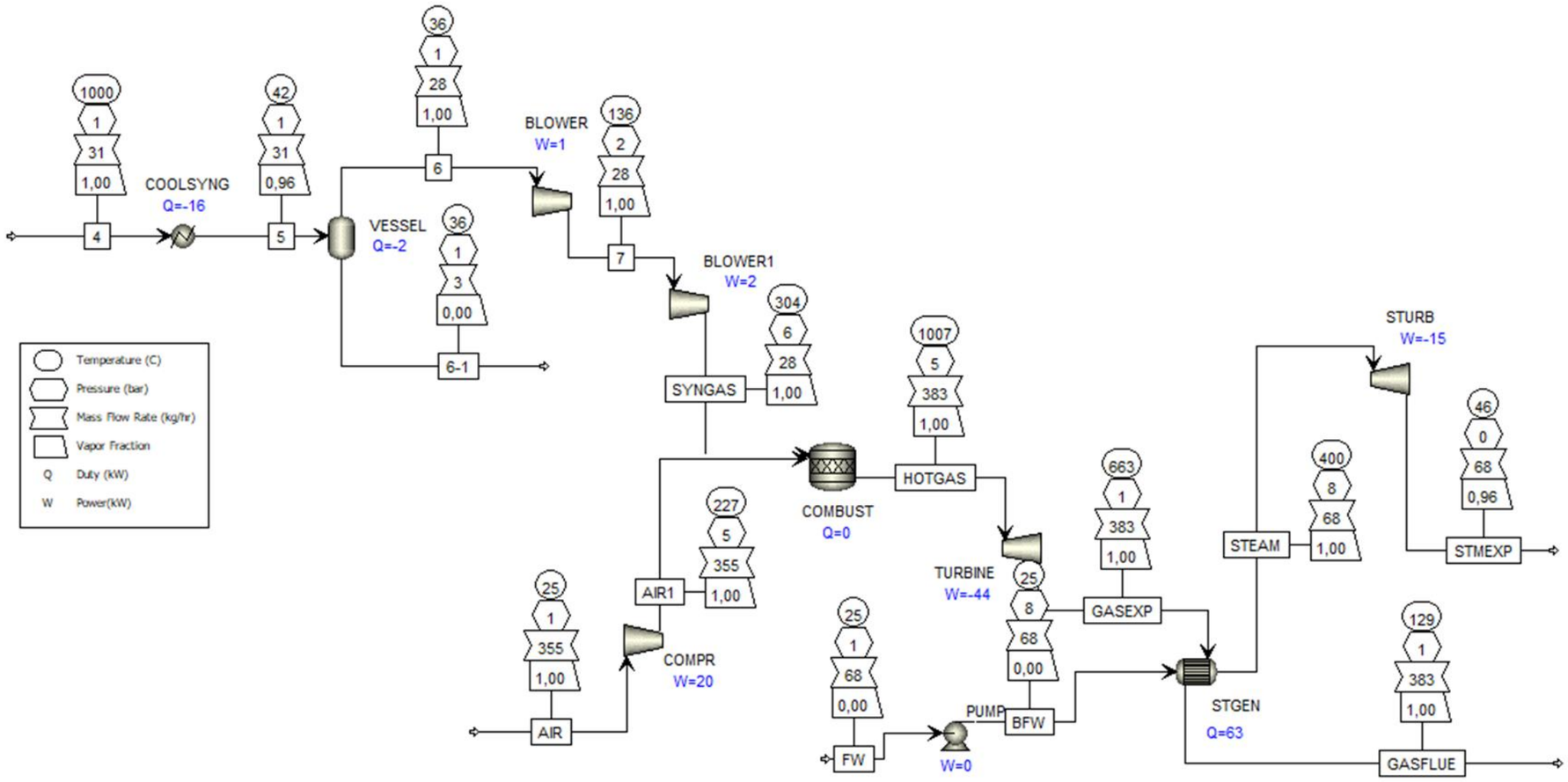


Figure A-17: Aspen Plus model flow diagram for Case 5b

Table A-17: Mass balance for Case 5b

	Units	4	5	6	6-1	7	AIR	AIR1	HOTGAS	GASEXP	GASFLUE	STEAM	STMEXP	FW	BFW
Temperature	C	1000.00	42.00	36.00	36.00	135.63	25.00	227.03	1006.53	662.87	128.55	400.00	46.30	25.00	25.02
Pressure	bar	0.85	0.83	0.84	0.84	2.00	1.00	5.00	5.00	1.00	1.00	8.00	0.08	1.00	8.00
Molar Vapor Fraction		1.00	0.96	1.00	0.00	1.00	1.00	1.00	1.00	1.00	1.00	1.00	0.96	0.00	0.00
Molar Liquid Fraction		0.00	0.04	0.00	1.00	0.00	0.00	0.00	0.00	0.00	0.00	0.00	0.04	1.00	1.00
Molar Solid Fraction		0.00	0.00	0.00	0.00	0.00	0.00	0.00	0.00	0.00	0.00	0.00	0.00	0.00	0.00
Mass Vapor Fraction		1.00	0.96	1.00	0.00	1.00	1.00	1.00	1.00	1.00	1.00	1.00	0.96	0.00	0.00
Mass Liquid Fraction		0.00	0.04	0.00	1.00	0.00	0.00	0.00	0.00	0.00	0.00	0.00	0.04	1.00	1.00
Molar Enthalpy	kJ/kmol	-57466.11	-90486.28	-70524.42	-285000.13	-67553.12	-6.62	5948.78	-1703.28	-13834.41	-31062.28	-228848.65	-242796.56	-289046.50	-289031.75
Mass Enthalpy	kJ/kg	-3200.90	-5040.15	-3929.91	-15819.91	-3764.34	-0.23	206.19	-58.72	-476.91	-1070.80	-12703.03	-13477.26	-16044.52	-16043.70
Molar Entropy	J/kmol-K	88380.79	38542.29	50124.11	-160491.62	51234.67	4361.64	6203.11	38434.17	40801.63	13761.47	-33402.56	-26294.77	-171283.83	-171290.19
Mass Entropy	kJ/kg-K	4.92	2.15	2.79	-8.91	2.86	0.15	0.22	1.32	1.41	0.47	-1.85	-1.46	-9.51	-9.51
Molar Density	kmol/cum	0.01	0.03	0.03	55.16	0.06	0.04	0.12	0.05	0.01	0.03	0.14	0.00	55.17	55.17
Mass Density	kg/cum	0.14	0.59	0.59	993.77	1.05	1.16	3.46	1.36	0.37	0.87	2.60	0.06	993.96	993.94
Enthalpy Flow	kW	-27.43	-43.20	-30.02	-14.73	-28.76	-0.02	20.33	-6.24	-50.67	-113.77	-239.95	-254.57	-303.06	-303.05
Average MW		17.95	17.95	17.95	18.02	17.95	28.85	28.85	29.01	29.01	29.01	18.02	18.02	18.02	18.02
Mole Fractions															
Mass Flows	**kg/hr**	**30.86**	**30.86**	**27.50**	**3.35**	**27.50**	**355.00**	**355.00**	**382.50**	**382.50**	**382.50**	**68.00**	**68.00**	**68.00**	**68.00**
H_2O	kg/hr	3.37	3.37	0.02	3.35	0.02	0.00	0.00	11.72	11.72	11.72	68.00	68.00	68.00	68.00
H_2	kg/hr	1.31	1.31	1.31	0.00	1.31	0.00	0.00	0.00	0.00	0.00	0.00	0.00	0.00	0.00
CO	kg/hr	18.31	18.31	18.31	0.00	18.31	0.00	0.00	0.00	0.00	0.00	0.00	0.00	0.00	0.00
CO_2	kg/hr	4.03	4.03	4.03	0.00	4.03	0.00	0.00	32.80	32.80	32.80	0.00	0.00	0.00	0.00
AR	kg/hr	0.00	0.00	0.00	0.00	0.00	0.00	0.00	0.00	0.00	0.00	0.00	0.00	0.00	0.00
CH_4	kg/hr	0.00	0.00	0.00	0.00	0.00	0.00	0.00	0.00	0.00	0.00	0.00	0.00	0.00	0.00
N_2	kg/hr	3.83	3.83	3.83	0.00	3.83	272.31	272.31	276.15	276.15	276.15	0.00	0.00	0.00	0.00
HCl	kg/hr	0.00	0.00	0.00	0.00	0.00	0.00	0.00	0.00	0.00	0.00	0.00	0.00	0.00	0.00
H_2S	kg/hr	0.00	0.00	0.00	0.00	0.00	0.00	0.00	0.00	0.00	0.00	0.00	0.00	0.00	0.00
O_2	kg/hr	0.00	0.00	0.00	0.00	0.00	82.69	82.69	61.84	61.84	61.84	0.00	0.00	0.00	0.00

Case 5c

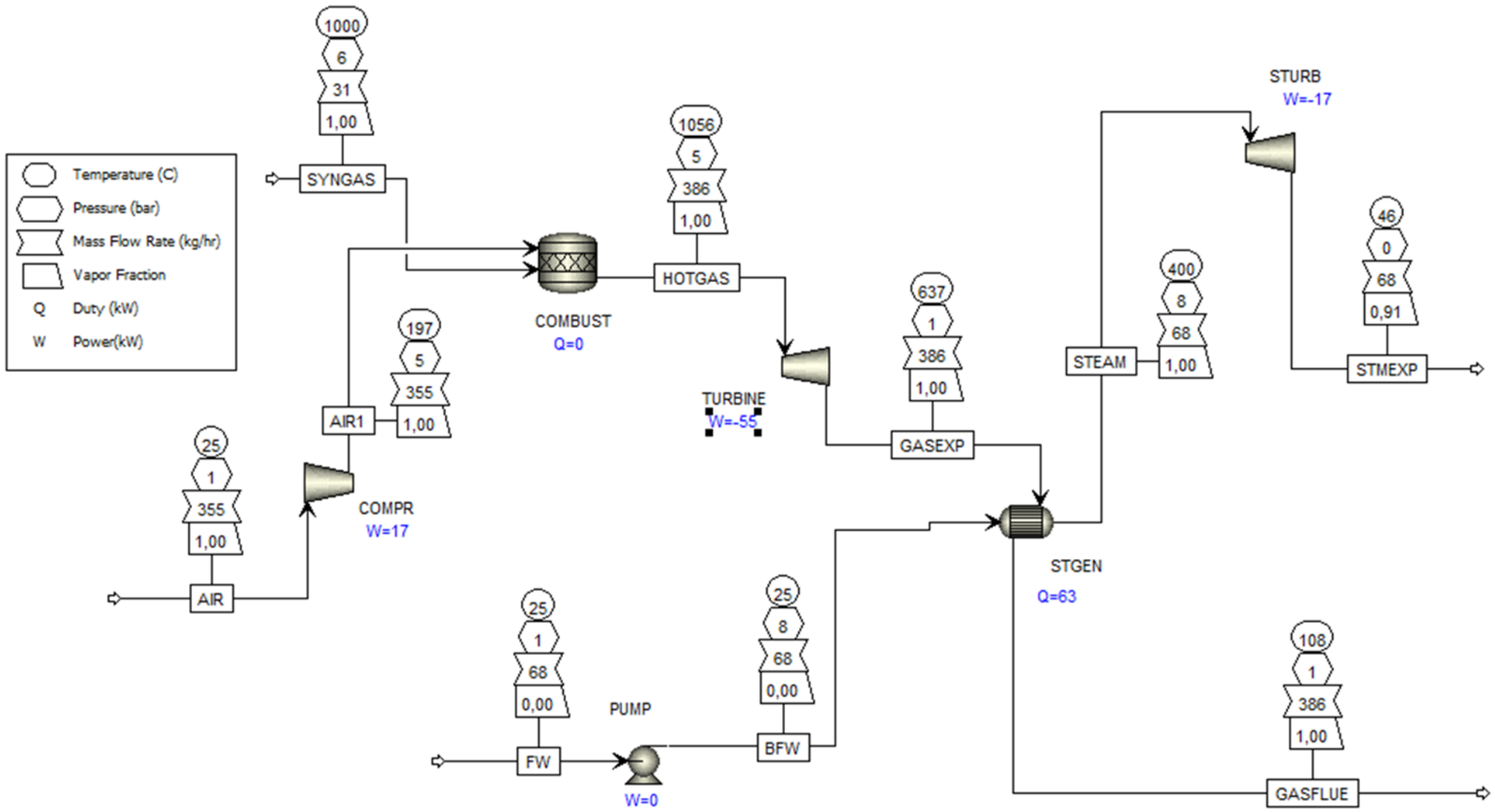


Figure A-18: Aspen Plus model flow diagram for Case 5c

Table A-18: Mass balance for Case 5c

	Units	SYNGAS	AIR	AIR1	HOTGAS	GASEXP	GASFLUE	STEAM	STMEXP	FW	BFW
Temperature	C	1000.00	25.00	197.16	1055.50	636.75	108.23	400.00	46.30	25.00	25.02
Pressure	bar	5.50	1.00	5.00	5.00	1.00	1.00	8.00	0.08	1.00	8.00
Molar Vapor Fraction		1.00	1.00	1.00	1.00	1.00	1.00	1.00	0.91	0.00	0.00
Molar Liquid Fraction		0.00	0.00	0.00	0.00	0.00	0.00	0.00	0.09	1.00	1.00
Molar Solid Fraction		0.00	0.00	0.00	0.00	0.00	0.00	0.00	0.00	0.00	0.00
Mass Vapor Fraction		1.00	1.00	1.00	1.00	1.00	1.00	1.00	0.91	0.00	0.00
Mass Liquid Fraction		0.00	0.00	0.00	0.00	0.00	0.00	0.00	0.09	1.00	1.00
Mass Solid Fraction		0.00	0.00	0.00	0.00	0.00	0.00	0.00	0.00	0.00	0.00
Molar Enthalpy	kJ/kmol	-57454.11	-6.62	5055.47	-2732.31	-17575.26	-34563.42	-228848.65	-245067.15	-289046.50	-289031.75
Mass Enthalpy	kJ/kg	-3200.23	-0.23	175.23	-94.69	-609.08	-1197.81	-12703.03	-13603.29	-16044.52	-16043.70
Molar Entropy	J/kmol-K	72808.11	4361.64	4361.64	39555.47	39555.47	11850.38	-33402.56	-33402.56	-171283.83	-171290.19
Mass Entropy	kJ/kg-K	4.06	0.15	0.15	1.37	1.37	0.41	-1.85	-1.85	-9.51	-9.51
Molar Density	kmol/cum	0.05	0.04	0.13	0.05	0.01	0.03	0.14	0.00	55.17	55.17
Mass Density	kg/cum	0.93	1.16	3.68	1.30	0.38	0.91	2.60	0.06	993.96	993.94
Enthalpy Flow	kW	-27.43	-0.02	17.28	-10.15	-65.28	-128.38	-239.95	-256.95	-303.06	-303.05
Average MW		17.95	28.85	28.85	28.86	28.86	28.86	18.02	18.02	18.02	18.02
Mass Flows	**kg/hr**	**30.86**	**355.00**	**355.00**	**385.86**	**385.86**	**385.86**	**68.00**	**68.00**	**68.00**	**68.00**
H_2O	kg/hr	3.37	0.00	0.00	15.07	15.07	15.07	68.00	68.00	68.00	68.00
H_2	kg/hr	1.31	0.00	0.00	0.00	0.00	0.00	0.00	0.00	0.00	0.00
CO	kg/hr	18.31	0.00	0.00	0.00	0.00	0.00	0.00	0.00	0.00	0.00
CO_2	kg/hr	4.03	0.00	0.00	32.80	32.80	32.80	0.00	0.00	0.00	0.00
AR	kg/hr	0.00	0.00	0.00	0.00	0.00	0.00	0.00	0.00	0.00	0.00
CH_4	kg/hr	0.00	0.00	0.00	0.00	0.00	0.00	0.00	0.00	0.00	0.00
N_2	kg/hr	3.83	272.31	272.31	276.15	276.15	276.15	0.00	0.00	0.00	0.00
HCl	kg/hr	0.00	0.00	0.00	0.00	0.00	0.00	0.00	0.00	0.00	0.00
H_2S	kg/hr	0.00	0.00	0.00	0.00	0.00	0.00	0.00	0.00	0.00	0.00
O_2	kg/hr	0.00	82.69	82.69	61.84	61.84	61.84	0.00	0.00	0.00	0.00

Case 5d

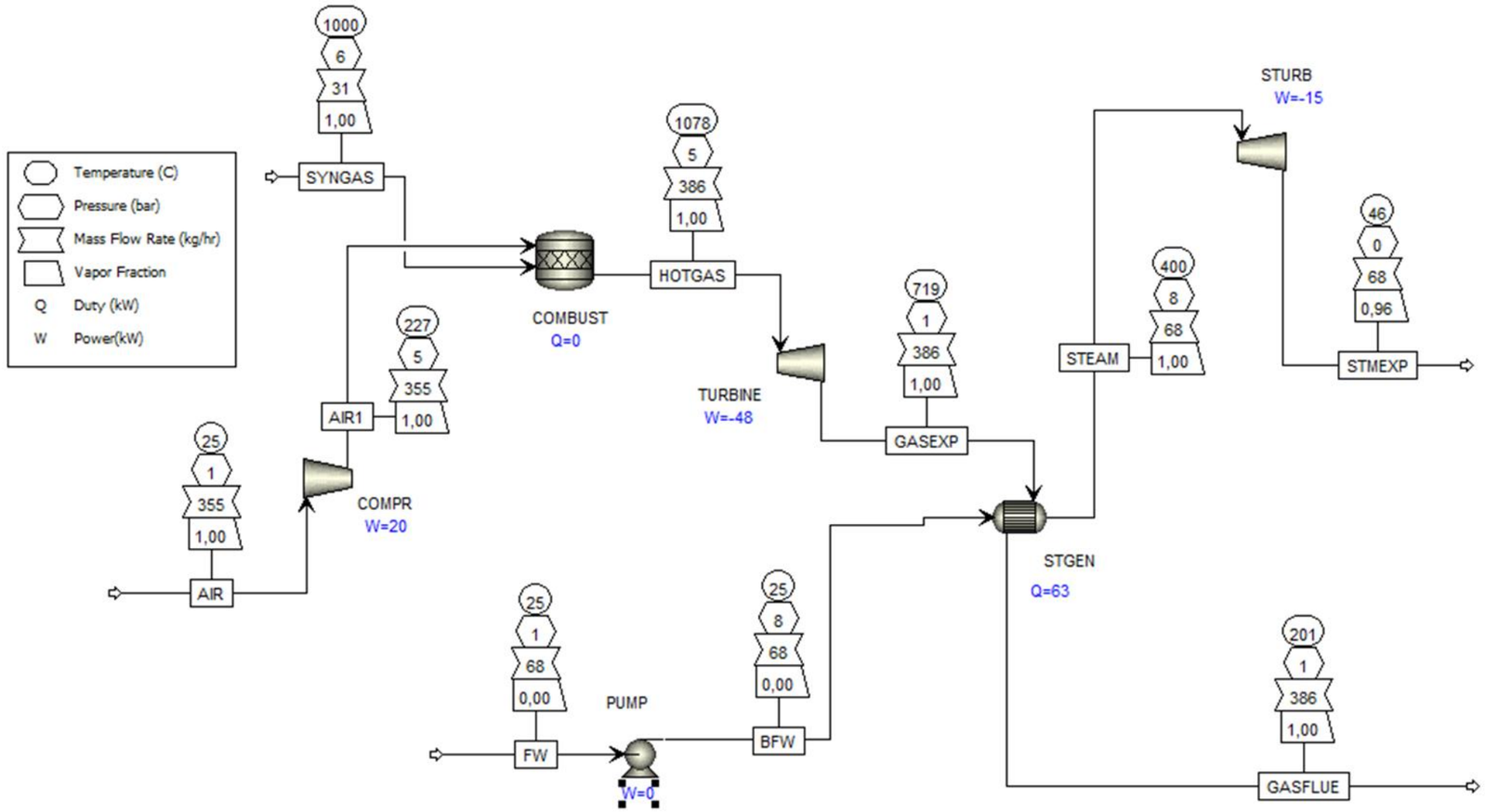


Figure A-19: Aspen Plus model flow diagram for Case 5d

Table A-19: Mass balance for Case 5d

	Units	SYNGAS	AIR	AIR1	HOTGAS	GASEXP	GASFLUE	STEAM	STMEXP	FW	BFW
Temperature	C	1000.00	25.00	227.03	1077.99	718.93	200.76	400.00	46.30	25.00	25.02
Pressure	bar	5.50	1.00	5.00	5.00	1.00	1.00	8.00	0.08	1.00	8.00
Molar Vapor Fraction		1.00	1.00	1.00	1.00	1.00	1.00	1.00	0.96	0.00	0.00
Molar Liquid Fraction		0.00	0.00	0.00	0.00	0.00	0.00	0.00	0.04	1.00	1.00
Molar Solid Fraction		0.00	0.00	0.00	0.00	0.00	0.00	0.00	0.00	0.00	0.00
Mass Vapor Fraction		1.00	1.00	1.00	1.00	1.00	1.00	1.00	0.96	0.00	0.00
Mass Liquid Fraction		0.00	0.00	0.00	0.00	0.00	0.00	0.00	0.04	1.00	1.00
Mass Solid Fraction		0.00	0.00	0.00	0.00	0.00	0.00	0.00	0.00	0.00	0.00
Molar Enthalpy	kJ/kmol	-57454.11	-6.62	5948.78	-1910.29	-14746.73	-31734.90	-228848.65	-242796.56	-289046.50	-289031.75
Mass Enthalpy	kJ/kg	-3200.23	-0.23	206.19	-66.20	-511.05	-1099.79	-12703.03	-13477.26	-16044.52	-16043.70
Molar Entropy	J/kmol-K	72808.11	4361.64	6203.11	40168.98	42531.28	18488.50	-33402.56	-26294.77	-171283.83	-171290.19
Mass Entropy	kJ/kg-K	4.06	0.15	0.22	1.39	1.47	0.64	-1.85	-1.46	-9.51	-9.51
Molar Density	kmol/cum	0.05	0.04	0.12	0.04	0.01	0.03	0.14	0.00	55.17	55.17
Mass Density	kg/cum	0.93	1.16	3.46	1.28	0.35	0.73	2.60	0.06	993.96	993.94
Enthalpy Flow	kW	-27.43	-0.02	20.33	-7.10	-54.78	-117.88	-239.95	-254.57	-303.06	-303.05
Average MW		17.95	28.85	28.85	28.86	28.86	28.86	18.02	18.02	18.02	18.02
Mole Fractions											
Mass Flows	**kg/hr**	**30.86**	**355.00**	**355.00**	**385.86**	**385.86**	**385.86**	**68.00**	**68.00**	**68.00**	**68.00**
H_2O	kg/hr	3.37	0.00	0.00	15.07	15.07	15.07	68.00	68.00	68.00	68.00
H_2	kg/hr	1.31	0.00	0.00	0.00	0.00	0.00	0.00	0.00	0.00	0.00
CO	kg/hr	18.31	0.00	0.00	0.00	0.00	0.00	0.00	0.00	0.00	0.00
CO_2	kg/hr	4.03	0.00	0.00	32.80	32.80	32.80	0.00	0.00	0.00	0.00
AR	kg/hr	0.00	0.00	0.00	0.00	0.00	0.00	0.00	0.00	0.00	0.00
CH_4	kg/hr	0.00	0.00	0.00	0.00	0.00	0.00	0.00	0.00	0.00	0.00
N_2	kg/hr	3.83	272.31	272.31	276.15	276.15	276.15	0.00	0.00	0.00	0.00
HCl	kg/hr	0.00	0.00	0.00	0.00	0.00	0.00	0.00	0.00	0.00	0.00
H_2S	kg/hr	0.00	0.00	0.00	0.00	0.00	0.00	0.00	0.00	0.00	0.00
O_2	kg/hr	0.00	82.69	82.69	61.84	61.84	61.84	0.00	0.00	0.00	0.00

Case 5e

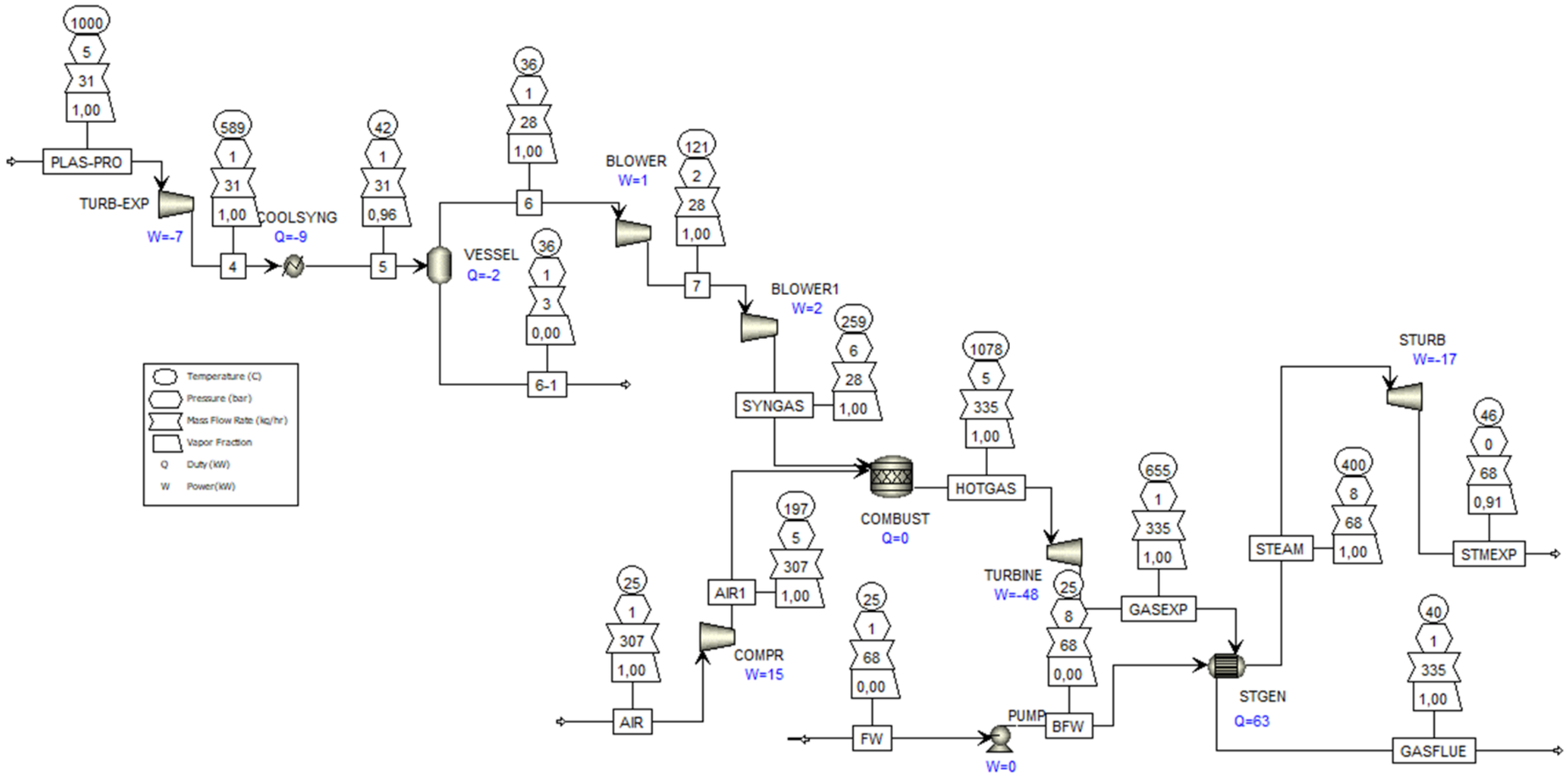


Figure A-20: Aspen Plus model flow diagram for case 5e

Table A-20: Mass balance for Case 5e

	Units	PLAS-PRO	4	5	6	6-1	7	SYNGAS	AIR	AIR1	HOTGAS	GASEXP	GASFLUE	STEAM	STMEXP	FW	BFW
Temperature	C	1000.00	589.03	42.00	36.00	36.00	120.80	259.49	25.00	197.16	1078.00	654.50	40.45	400.00	46.30	25.00	24.99
Pressure	bar	5.00	1.00	0.83	0.84	0.84	2.00	6.00	1.00	5.00	5.00	1.00	1.00	8.00	0.08	1.00	8.00
Molar Vapor Fraction		1.00	1.00	0.96	1.00	0.00	1.00	1.00	1.00	1.00	1.00	1.00	1.00	1.00	0.91	0.00	0.00
Molar Liquid Fraction		0.00	0.00	0.04	0.00	1.00	0.00	0.00	0.00	0.00	0.00	0.00	0.00	0.00	0.09	1.00	1.00
Molar Enthalpy	kJ/kmol	-57455.40	-71605.40	-90486.28	-70524.42	-285000.13	-67998.82	-63788.94	-6.62	5055.47	-3808.27	-18919.59	-38618.99	-228848.65	-245067.15	-289046.50	-289033.81
Mass Enthalpy	kJ/kg	-3200.30	-3988.47	-5040.15	-3929.91	-15819.91	-3789.17	-3554.58	-0.23	175.23	-131.18	-651.70	-1330.26	-12703.03	-13603.29	-16044.52	-16043.81
Molar Entropy	J/kmol-K	73600.39	73600.39	38542.29	50124.11	-160491.62	50124.11	50124.11	4361.64	4361.64	40575.77	40575.77	6209.53	-33402.56	-33402.56	-171283.83	-171297.10
Mass Entropy	kJ/kg-K	4.10	4.10	2.15	2.79	-8.91	2.79	2.79	0.15	0.15	1.40	1.40	0.21	-1.85	-1.85	-9.51	-9.51
Mass Density	kg/cum	0.85	0.25	0.59	0.59	993.77	1.09	2.42	1.16	3.68	1.29	0.38	1.11	2.60	0.06	993.96	993.96
Enthalpy Flow	kW	-27.43	-34.18	-43.20	-30.02	-14.73	-28.95	-27.16	-0.02	14.96	-12.20	-60.61	-123.71	-239.95	-256.95	-303.06	-303.05
Average MW		17.95	17.95	17.95	17.95	18.02	17.95	17.95	28.85	28.85	29.03	29.03	29.03	18.02	18.02	18.02	18.02
Mass Flows	**kg/hr**	**30.86**	**30.86**	**30.86**	**27.50**	**3.35**	**27.50**	**27.50**	**307.28**	**307.28**	**334.79**	**334.79**	**334.79**	**68.00**	**68.00**	**68.00**	**68.00**
H_2O	kg/hr	3.37	3.37	3.37	0.02	3.35	0.02	0.02	0.00	0.00	11.72	11.72	11.72	68.00	68.00	68.00	68.00
H_2	kg/hr	1.31	1.31	1.31	1.31	0.00	1.31	1.31	0.00	0.00	0.00	0.00	0.00	0.00	0.00	0.00	0.00
CO	kg/hr	18.31	18.31	18.31	18.31	0.00	18.31	18.31	0.00	0.00	0.00	0.00	0.00	0.00	0.00	0.00	0.00
CO_2	kg/hr	4.03	4.03	4.03	4.03	0.00	4.03	4.03	0.00	0.00	32.80	32.80	32.80	0.00	0.00	0.00	0.00
AR	kg/hr	0.00	0.00	0.00	0.00	0.00	0.00	0.00	0.00	0.00	0.00	0.00	0.00	0.00	0.00	0.00	0.00
CH_4	kg/hr	0.00	0.00	0.00	0.00	0.00	0.00	0.00	0.00	0.00	0.00	0.00	0.00	0.00	0.00	0.00	0.00
N_2	kg/hr	3.83	3.83	3.83	3.83	0.00	3.83	3.83	235.71	235.71	239.54	239.54	239.54	0.00	0.00	0.00	0.00
HCl	kg/hr	0.00	0.00	0.00	0.00	0.00	0.00	0.00	0.00	0.00	0.00	0.00	0.00	0.00	0.00	0.00	0.00
H_2S	kg/hr	0.00	0.00	0.00	0.00	0.00	0.00	0.00	0.00	0.00	0.00	0.00	0.00	0.00	0.00	0.00	0.00
O_2	kg/hr	0.00	0.00	0.00	0.00	0.00	0.00	0.00	71.57	71.57	50.72	50.72	50.72	0.00	0.00	0.00	0.00

Case 5f

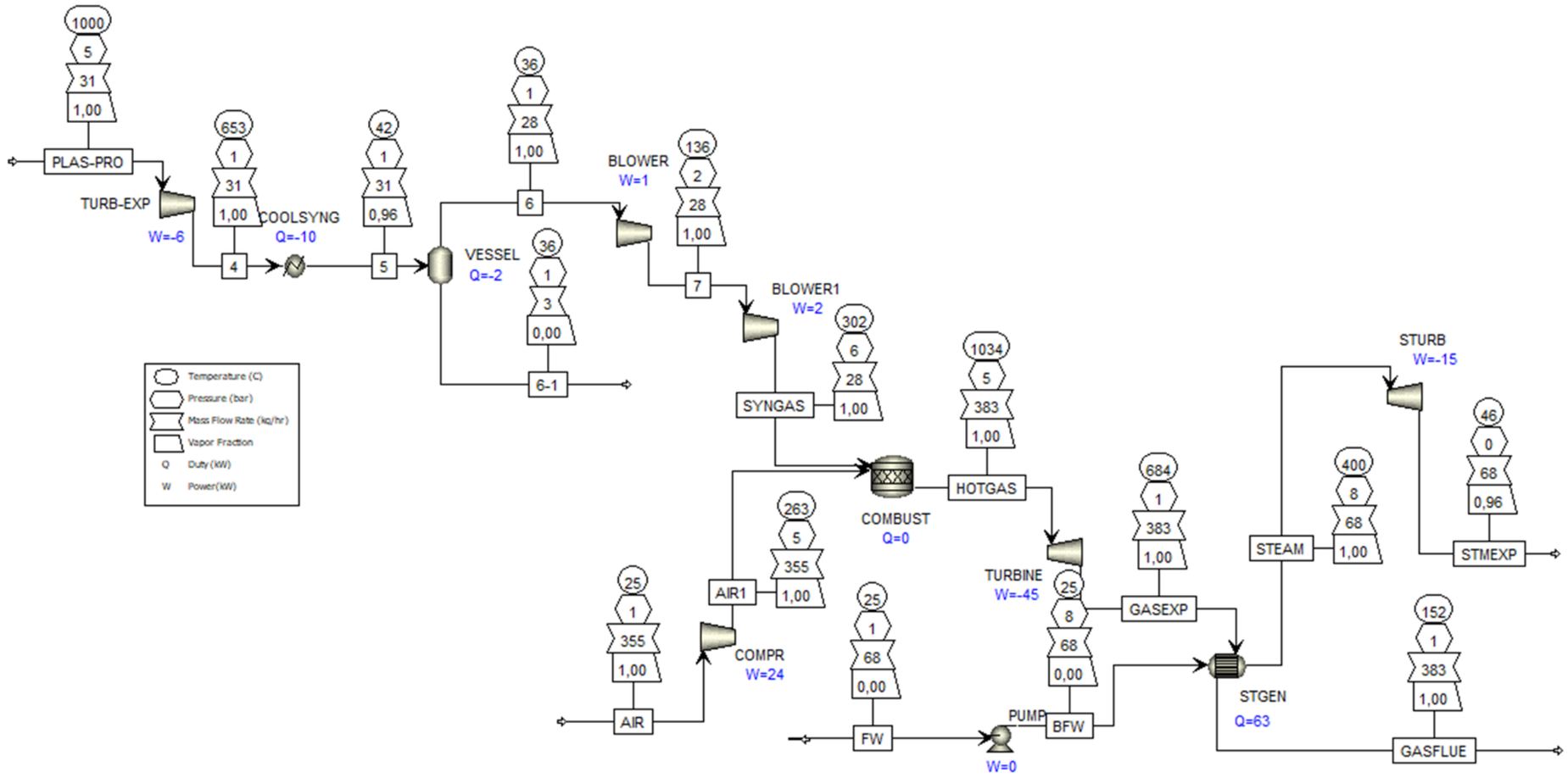


Figure A-21: Aspen Plus model flow diagram for Case 5f

Table A-21: Mass balance for Case 5f

	Units	PLAS-PRO	4	5	6	6-1	7	SYNGAS	AIR	AIR1	HOTGAS	GASEXP	GASFLUE	STEAM	STMEXP	FW	BFW
Temperature	C	1000.00	652.66	42.00	36.00	36.00	135.63	304.12	25.00	227.03	1006.53	662.87	128.55	400.00	46.30	25.00	25.02
Pressure	bar	5.00	1.00	0.83	0.84	0.84	2.00	6.00	1.00	5.00	5.00	1.00	1.00	8.00	0.08	1.00	8.00
Molar Vapor Fraction		1.00	1.00	0.96	1.00	0.00	1.00	1.00	1.00	1.00	1.00	1.00	1.00	1.00	0.96	0.00	0.00
Molar Liquid Fraction		0.00	0.00	0.04	0.00	1.00	0.00	0.00	0.00	0.00	0.00	0.00	0.00	0.00	0.04	1.00	1.00
Mass Enthalpy	kJ/kg	-3200.30	-3870.24	-5040.15	-3929.91	-15819.91	-3764.34	-3478.08	-0.23	206.19	-58.72	-476.91	-1070.80	-12703.03	-13477.26	-16044.52	-16043.70
Molar Entropy	J/kmol-K	73600.39	75975.39	38542.29	50124.11	-160491.62	51234.67	52599.30	4361.64	6203.11	38434.17	40801.63	13761.47	-33402.56	-26294.77	-171283.83	-171290.19
Mass Entropy	kJ/kg-K	4.10	4.23	2.15	2.79	-8.91	2.86	2.93	0.15	0.22	1.32	1.41	0.47	-1.85	-1.46	-9.51	-9.51
Mass Density	kg/cum	0.85	0.23	0.59	0.59	993.77	1.05	2.24	1.16	3.46	1.36	0.37	0.87	2.60	0.06	993.96	993.94
Enthalpy Flow	kW	-27.43	-33.17	-43.20	-30.02	-14.73	-28.76	-26.57	-0.02	20.33	-6.24	-50.67	-113.77	-239.95	-254.57	-303.06	-303.05
Average MW		17.95	17.95	17.95	17.95	18.02	17.95	17.95	28.85	28.85	29.01	29.01	29.01	18.02	18.02	18.02	18.02
Mass Flows	**kg/hr**	**30.86**	**30.86**	**30.86**	**27.50**	**3.35**	**27.50**	**27.50**	**355.00**	**355.00**	**382.50**	**382.50**	**382.50**	**68.00**	**68.00**	**68.00**	**68.00**
H_2O	kg/hr	3.37	3.37	3.37	0.02	3.35	0.02	0.02	0.00	0.00	11.72	11.72	11.72	68.00	68.00	68.00	68.00
H_2	kg/hr	1.31	1.31	1.31	1.31	0.00	1.31	1.31	0.00	0.00	0.00	0.00	0.00	0.00	0.00	0.00	0.00
CO	kg/hr	18.31	18.31	18.31	18.31	0.00	18.31	18.31	0.00	0.00	0.00	0.00	0.00	0.00	0.00	0.00	0.00
CO_2	kg/hr	4.03	4.03	4.03	4.03	0.00	4.03	4.03	0.00	0.00	32.80	32.80	32.80	0.00	0.00	0.00	0.00
CH_4	kg/hr	0.00	0.00	0.00	0.00	0.00	0.00	0.00	0.00	0.00	0.00	0.00	0.00	0.00	0.00	0.00	0.00
N_2	kg/hr	3.83	3.83	3.83	3.83	0.00	3.83	3.83	272.31	272.31	276.15	276.15	276.15	0.00	0.00	0.00	0.00
H_2S	kg/hr	0.00	0.00	0.00	0.00	0.00	0.00	0.00	0.00	0.00	0.00	0.00	0.00	0.00	0.00	0.00	0.00
O_2	kg/hr	0.00	0.00	0.00	0.00	0.00	0.00	0.00	82.69	82.69	61.84	61.84	61.84	0.00	0.00	0.00	0.00

Appendix A.2.4 Brayton cycle for the experimental synthesis gas results

The mass balance for the case study involving the experimental synthesis gas product from the NECSA reactor demonstration plant can be found in **Table A-22,** along with the flowsheet for this gas turbine model shown in **Figure A-22**.

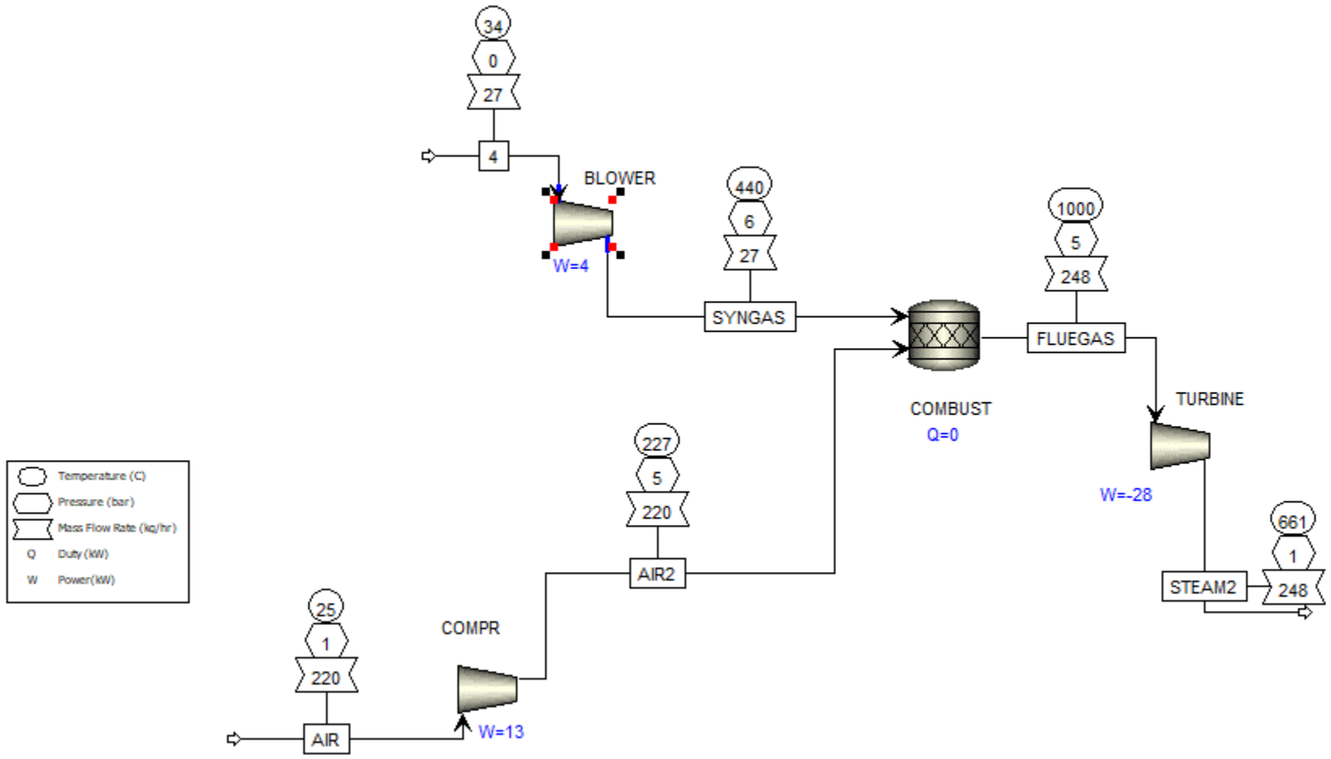


Figure A-22: Brayton cycle model processing the experimental synthesis gas from the demonstration plant

Table A-22: Mass balance for the Brayton cycle model processing the experimental synthesis gas product

	Units	**4**	**AIR**	**AIR2**	**GASEXP**	**HOTGAS**	**SYNGAS**
Phase		Vapor Phase	Vapor Phase	Vapor Phase	Vapor Phase	Vapor Phase	Vapor Phase
Temperature	C	34.00	25.00	227.15	661.04	1000.00	439.81
Pressure	bar	0.35	1.00	5.00	1.00	5.00	6.00
Molar Vapor Fraction		1.00	1.00	1.00	1.00	1.00	1.00
Molar Liquid Fraction		0.00	0.00	0.00	0.00	0.00	0.00
Molar Solid Fraction		0.00	0.00	0.00	0.00	0.00	0.00
Mass Vapor Fraction		1.00	1.00	1.00	1.00	1.00	1.00
Mass Liquid Fraction		0.00	0.00	0.00	0.00	0.00	0.00
Mass Solid Fraction		0.00	0.00	0.00	0.00	0.00	0.00
Molar Enthalpy	kJ/kmol	-84634.37	-8.02	5946.04	-16734.40	-4643.70	-71778.20
Mass Enthalpy	kJ/kg	-3635.47	-0.28	206.70	-570.16	-158.22	-3083.23
Molar Entropy	kJ/mol-K	0.06	0.00	0.01	0.04	0.04	0.06
Mass Entropy	kJ/kg-K	2.56	0.14	0.21	1.41	1.33	2.68
Molar Density	kmol/cum	0.01	0.04	0.12	0.01	0.05	0.10
Mass Density	kg/cum	0.32	1.16	3.45	0.38	1.38	2.35
Enthalpy Flow	kW	-27.76	-0.02	12.65	-39.25	-10.89	-23.54
Average MW		23.28	28.77	28.77	29.35	29.35	23.28
Mass Flows	**kg/hr**	**27.49**	**220.35**	**220.35**	**247.84**	**247.84**	**27.49**
H_2	kg/hr	0.53	0.00	0.00	0.00	0.00	0.53
O_2	kg/hr	0.16	46.27	46.27	33.74	33.74	0.16
N_2	kg/hr	6.45	174.07	174.07	180.52	180.52	6.45
Cl_2	kg/hr	0.00	0.00	0.00	0.00	0.00	0.00
CO	kg/hr	14.82	0.00	0.00	0.00	0.00	14.82
CO_2	kg/hr	4.52	0.00	0.00	27.80	27.80	4.52
H_2O	kg/hr	0.00	0.00	0.00	4.77	4.77	0.00
CH_4	kg/hr	0.59	0.00	0.00	0.59	0.59	0.59
H_2S	kg/hr	0.00	0.00	0.00	0.00	0.00	0.00
HCl	kg/hr	0.00	0.00	0.00	0.00	0.00	0.00
AR	kg/hr	0.25	0.00	0.00	0.25	0.25	0.25
ACETYLEN	kg/hr	0.15	0.00	0.00	0.15	0.15	0.15
ETHYLENE	kg/hr	0.01	0.00	0.00	0.01	0.01	0.01

Appendix A.3 Energy Analysis

Appendix A.3.1 Brayton cycle Energy Balance

The energy balances of the various case studies for the Brayton power cycle can be found in **Table A-23**.

Table A-23: Brayton cycle energy balance for the various case studies

Case 3a		**Case 3b**		**Case 3c**		**Case 3d**		**Case 3e**		**Case 3f**	
Power Production (kW)		**Power Production (kW)**		**Power Production (kW)**		**Power Production (kW)**		**Power Production (kW)**		**Power Production (kW)**	
TURBINE	50.28	TURBINE	44.45	TURBINE	49.95	TURBINE	44.62	TURBINE	15.99	TURBINE	15.99
						TURB-EXP	5.74	TURBINE2	32.14	TURBINE2	29.02
Total	**50.28**	**Total**	**44.45**	**Total**	**49.95**	**Total**	**50.36**	**Total**	**48.13**	**Total**	**45.01**
Power Consumption (kW)		**Power Consumption (kW)**		**Power Consumption (kW)**		**Power Consumption (kW)**		**Power Consumption (kW)**		**Power Consumption (kW)**	
BLOWER	16.69	BLOWER	0.98	COMPR	22.9	BLOWER	1.03	BLOWER	0.98	BLOWER	0.98
BLOWER2	2.37	BLOWER2	2.05	Plasma Gas compressor	0.88	BLOWER2	2.16	BLOWER2	2.05	BLOWER2	2.05
COMPR	20.72	COMPR	20.48	DC-ARC	20.72	COMPR	20.57	COMPR	20.48	COMPR	20.48
DC-ARC		DC-ARC	20.72			PLASMA GAS COMPRESSOR	0.88	DC-ARC	20.72	DC-ARC	20.72
						DC-ARC	20.72				
Total	**39.78**	**Total**	**44.23**	**Total**	**44.5**	**Total**	**45.36**	**Total**	**44.23**	**Total**	**44.23**
Backwork Ratio	**0.38**	**Backwork Ratio**	**0.53**	**Backwork Ratio**	**0.48**	**Backwork Ratio**	**0.49**	**Backwork Ratio**	**0.49**	**Backwork Ratio**	**0.52**
Brayton cycle efficiency (%)	**29.27**	**Brayton cycle efficiency (%)**	**21.91**	**Brayton cycle efficiency (%)**	**27.73**	**Brayton cycle efficiency (%)**	**27.25**	**Brayton cycle efficiency (%)**	**22.06**	**Brayton cycle efficiency (%)**	**22.50**
Brayton cycle Efficiency (LHV) (%)	**32.87**	**Brayton cycle Efficiency (LHV) (%)**	**22.05**	**Brayton cycle Efficiency (LHV) (%)**	**27.89**	**Brayton cycle Efficiency (LHV) (%)**	**27.42**	**Brayton cycle Efficiency (LHV) (%)**	**22.17**	**Brayton cycle Efficiency (LHV) (%)**	**22.64**
Overall Process thermal efficiency (%)	**10.98**	**Overall Process thermal efficiency (%)**	**0.23**	**Overall Process thermal efficiency (%)**	**6.04**	**Overall Process thermal efficiency (%)**	**5.57**	**Overall Process thermal efficiency (%)**	**3.49**	**Overall Process thermal efficiency (%)**	**0.82**

Appendix A.3.2 Rankine cycle Energy balance

The energy balances of the various case studies for the Rankine power cycle can be found in **Table A-24.**

Table A-24: Rankine cycle energy balance for the various case studies

Case 4a		**Case 4b**		**Case 4c**		**Case 4d**		**Case 4e**		**Case 4f**	
Power Production (kW)		**Power Production (kW)**		**Power Production (kW)**		**Power Production (kW)**		**Power Production (kW)**		**Power Production (kW)**	
ST-TURB	36.4	ST-TURB	31.3	ST-TURB	35.48	ST-TURB	41.25	ST-TURB	12.38	STURB	10.64
								ST-TURB2	21.72	STURB2	21.75
Total	**36.4**	**Total**	**31.3**	**Total**	**35.48**	**Total**	**41.25**	**Total**	**34.1**	**Total**	**32.39**
Power Consumption (kW)		**Power Consumption (kW)**		**Power Consumption (kW)**		**Power Consumption (kW)**		**Power Consumption (kW)**		**Power Consumption (kW)**	
BLOWER	1.06	BLOWER	1.23	COMPR	1.98	COMPR	1.7	BLOWER	1.06	BLOWER	1.23
COMPR	1.49	COMPR	1.74	PUMP1	0.09	PUMP	0.08	COMPR	1.49	COMPR	1.74
PUMP	0.07	PUMP1	0.08	DC-ARC	20.72	DC-ARC	20.72	PUMP	0.07	PUMP1	0.08
DC-ARC	20.72	DC-ARC	20.72	PLASMA GAS COMPRESSOR	0.56	PLASMA GAS COMPRESSOR	0.48	DC-ARC	20.72	DC-ARC	20.72
Total	**23.34**	**Total**	**23.77**	**Total**	**23.35**	**Total**	**22.98**	**Total**	**23.34**	**Total**	**23.77**
Backwork Ratio	**0.64**	**Backwork Ratio**	**0.76**	**Backwork Ratio**	**0.66**	**Backwork Ratio**	**0.56**	**Backwork Ratio**	**0.68**	**Backwork Ratio**	**0.73**
Rankine cycle efficiency (Work out) (%)	**42.31**	**Rankine cycle efficiency (Work out) (%)**	**36.39**	**Rankine cycle efficiency (Work out) (%)**	**36.39**	**Rankine cycle efficiency (Work out) (%)**	**42.31**	**Rankine cycle efficiency (Work out) (%)**	**39.64**	**Rankine cycle efficiency (Work out) (%)**	**37.66**
Rankine cycle efficiency (net work) (%)	**39.27**	**Rankine cycle efficiency (net work) (%)**	**32.84**	**Rankine cycle efficiency (net work) (%)**	**33.70**	**Rankine cycle efficiency (net work) (%)**	**39.99**	**Rankine cycle efficiency (net work) (%)**	**36.59**	**Rankine cycle efficiency (net work) (%)**	**34.11**
Overall Process efficiency (%)	**15.18**	**Overall Process efficiency (%)**	**8.75**	**Overall Process efficiency (%)**	**12.44**	**Overall Process efficiency (%)**	**18.74**	**Overall Process efficiency (%)**	**12.51**	**Overall Process efficiency (%)**	**10.02**

Appendix A.3.3 Combined power cycle energy balance

The energy balances of the various case studies for the combined power cycle can be found in **Table A-25**.

Table A-25: Combined power cycle energy balance for the various case studies

Case 5a		**Case 5b**		**Case 5c**		**Case 5d**		**Case 5e**		**Case 5f**	
Power Production (kW)		**Power Production (kW)**		**Power Production (kW)**		**Power Production (kW)**		**Power Production (kW)**		**Power Production (kW)**	
TURBINE	48.66	TURBINE	44.43	TURBINE	55.13	TURBINE	47.68	TURBINE	48.41	TURBINE	44.43
ST-TURB	17.01	ST-TURB	14.62	ST-TURB	17.3	ST-TURB	14.62	TURB-EXP	6.76	TURB-EXP	5.74
								ST-TURB	17.01	ST-TURB	14.62
Total	**65.67**	**Total**	**59.05**	**Total**	**72.43**	**Total**	**62.3**	**Total**	**72.18**	**Total**	**64.79**
Power Consumption (kW)		**Power Consumption (kW)**		**Power Consumption (kW)**		**Power Consumption (kW)**		**Power Consumption (kW)**		**Power Consumption (kW)**	
BLOWER	1.08	BLOWER	1.26	COMPR	17.3	COMPR	20.36	BLOWER	1.08	BLOWER	1.26
BLOWER1	1.79	BLOWER1	2.19	PUMP	0.02	PUMP	0.02	BLOWER1	1.79	BLOWER1	2.19
COMPR	15.19	COMPR	20.36	DC-ARC	20.72	PLASMA GAS COMPRESSOR	0.56	COMPR	14.98	COMPR	20.36
PUMP	0.01	PUMP	0.02	PLASMA GAS COMPRESSOR	0.48	DC-ARC	20.72	PLASMA GAS COMPRESSOR	0.48	PLASMA GAS COMPRESSOR	0.56
DC-ARC	20.72	DC-ARC	20.72					PUMP1	0.01	PUMP1	0.02
								DC-ARC	20.72	DC-ARC	20.72
Total	**38.79**	**Total**	**44.55**	**Total**	**38.52**	**Total**	**41.66**	**Total**	**39.06**	**Total**	**45.11**
Backwork Ratio	**0.59**	**Backwork Ratio**	**0.75**	**Backwork Ratio**	**0.53**	**Backwork Ratio**	**0.67**	**Backwork Ratio**	**0.54**	**Backwork Ratio**	**0.70**
Brayton cycle efficiency (LHV) (%)	**32.22**	**Brayton cycle efficiency (LHV) (%)**	**21.71**	**Brayton cycle efficiency (LHV) (%)**	**41.70**	**Brayton cycle efficiency (LHV) (%)**	**28.76**	**Brayton cycle efficiency (LHV) (%)**	**39.29**	**Brayton cycle efficiency (LHV) (%)**	**27.75**
Rankine cycle efficiency (%)	**26.96**	**Rankine cycle efficiency (%)**	**23.17**	**Rankine cycle efficiency (%)**	**27.42**	**Rankine cycle efficiency (%)**	**23.17**	**Rankine cycle efficiency (%)**	**26.94**	**Rankine cycle efficiency (%)**	**23.17**
Combined cycle efficiency (%)	**50.12**	**Combined cycle efficiency (%)**	**37.08**	**Combined cycle efficiency (%)**	**58.02**	**Combined cycle efficiency (%)**	**44.14**	**Combined cycle efficiency (%)**	**57.19**	**Combined cycle efficiency (%)**	**43.13**
Overall Process efficiency (%)	**28.30**	**Overall Process efficiency (%)**	**15.27**	**Overall Process efficiency (%)**	**35.40**	**Overall Process efficiency (%)**	**21.73**	**Overall Process efficiency (%)**	**34.87**	**Overall Process efficiency (%)**	**20.72**

Appendix A.3.4 Brayton cycle for the experimental synthesis gas product

The energy balance for the case study involving the experimental synthesis gas product from the NECSA reactor demonstration plant can be found in **Table A-26**.

Table A-26: Energy balance for the Brayton cycle processing the experimental synthesis gas product

Power Consumed (kW)	
BLOWER	4.22
COMPR	12.67
Total	**16.89**

Power Produced (kW)	
TURBINE	**28.36**
Net Power Output (kW)	**11.47**
LHV Syngas (kJ/kg)	**9126.87**
Mass flowrate of syngas (kg/hr)	**27.49**
Efficiency (LHV) (%)	**16.46**

Appendix A.4 Exergy Analysis

Elemental Chemical Exergy

The specific chemical exergy values for the compounds involved in these processes in atmospheric conditions can be found in **Table A-27**.

Table A-27: Atmospheric Specific molar exergy values

Specific chemical exergy		
Chem ex		
kJ/kmol		
9500	gas	H_2O
236100		H_2
275100		CO
19870		CO_2
831650		CH_4
720		N_2
812000		H_2S
3970		O_2

Brayton Power Cycle

The exergy analysis for the Brayton power cycle is carried over the system boundaries in the process units shown in **Figure A-23.** The exergy analysis is carried over in **Case 3b** and **Case 3c** as highlighted in the main body of the report.

Case 3b

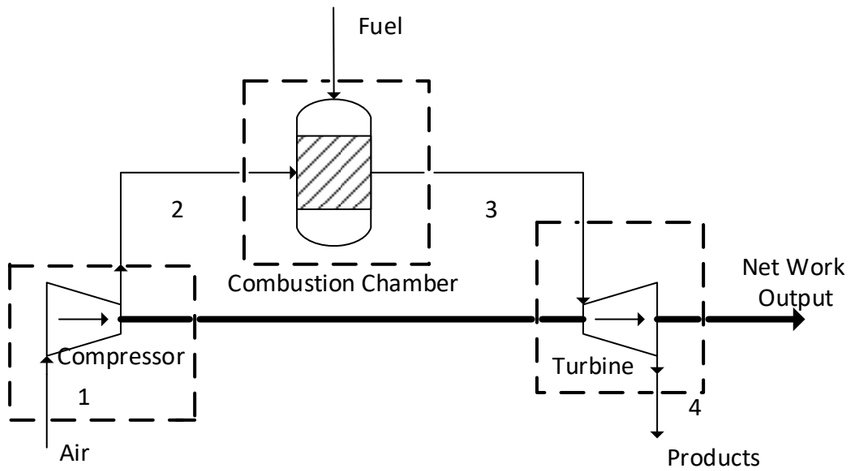


Figure A-23: Exergy analysis boundary for the gas turbine

Table A-28: Exergy Analysis for the Model of Case 3b

Combustion Chamber		**Turbine**		**Blower**		**Blower1**		**COMPR**	
Mass Flowrate		Mass Flowrate		Mass Flowrate		Mass Flowrate		Mass Flowrate	
(kg/hr)	383.75	(kg/hr)	383.75	(kg/hr)	27.49	(kg/hr)	27.49	(kg/hr)	356.26
Exergy inlet		Exergy inlet		Exergy inlet		Exergy inlet		Exergy inlet	
(kJ/kg)	197.09	(kJ/kg)	768.18	(kJ/kg)	-1.61	(kJ/kg)	111.23	(kJ/kg)	-1.13
Exergy outlet		Exergy outlet		Exergy outlet		Exergy outlet		Exergy outlet	
(kJ/kg)	768.18	(kJ/kg)	326.80	(kJ/kg)	111.23	(kJ/kg)	357.56	(kJ/kg)	186.77
E_d (kW) (P.E)	60.88	**E_d (kW)**	**2.60**	**E_d (kW)**	**0.12**	**E_d (kW)**	**0.17**	**E_d (kW)**	**1.88**
E_d(kW) (C.E)	89.71								
Ed(kW) (T.E)	**150.59**								

Table A-29: Exergy Analysis for the synthesis gas quench probe

Input	
Exergy input (syngas) (kJ/kg)	988.46
Mass flowrate (syngas) (kg/hr)	30.86
Exergy input (water) (kJ/kg)	0.00
Mass flowrate (water) (kg/hr)	1307.10
Exergy In (kJ/hr)	**30503.79**
Output	
Exergy output (syngas) (kJ/kg)	-0.74
Mass flowrate (syngas) (kg/hr)	30.86
Exergy output (Water) (kJ/s)	0.74
Mass flowrate (water) (kg/hr)	1307.10
Exergy Out (kJ/hr)	**941.42**
Exergy Destruction (kW)	
E_d	8.21

Table A-30: Combustion chamber chemical exergy analysis for Case 3b

	SYNGAS	**AIR2**	**FLUEGAS**	**SYNGAS**	**AIR2**	**FLUEGAS**	**SYNGAS**	**AIR2**	**FLUEGAS**	**Total E_d**	
				xi*LN (xi)	**xi*LN (xi)**	**xi*LN (xi)**	**Emix (kJ/kmol)**	**Emix (kJ/kmol)**	**Emix (kJ/kmol)**	**Ed (kJ/kmol)**	**Ed (kW)**
Molar Fraction	**1.00**	**1.00**	**1.00**	-1.11	-0.48	-0.77	216089.96	129.38	723.75	215495.60	89.71
H_2	0.42	0.00	0.00	-0.36							
O_2	0.00	0.19	0.13		-0.31	-0.26					
N_2	0.09	0.81	0.77	-0.22	-0.17	-0.20					
Cl_2	0.00	0.00	0.00								
CO	0.43	0.00	0.00	-0.36							
CO_2	0.06	0.00	0.06	-0.17		-0.16					
H_2O	0.00	0.00	0.05			-0.15					
CH_4	0.00	0.00	0.00								
H2S	0.00	0.00	0.00	0.00		0.00					
HCl	0.00	0.00	0.00	0.00		0.00					

Case 3c

Table A-31: Exergy Analysis for the model of Case 3c

Combustion Chamber		**Turbine**		**Compressors**	
Mass Flowrate		Mass Flowrate		Mass Flowrate	
(kg/hr)	429.10	(kg/hr)	429.10	(kg/hr)	398.24
Exergy inlet		Exergy inlet		Exergy inlet	
(kJ/kg)	241.87	(kJ/kg)	771.62	(kJ/kg)	-1.13
Exergy outlet		Exergy outlet		Exergy outlet	
(kJ/kg)	771.62	(kJ/kg)	328.01	(kJ/kg)	186.77
E_d (kW) (P.E)	63.14	**E_d (kW)**	**2.924**	**E_d (kW)**	**2.11**
E_d (kW) (C.E)	89.80				
E_d (kW) (T.E)	**152.95**				

Table A-32: Combustion chamber chemical exergy analysis for Case 3c

	SYNGAS	**AIR2**	**FLUEGAS**	**SYNGAS**	**AIR2**	**FLUEGAS**	**SYNGAS**	**AIR2**	**FLUEGAS**	**Total E_d**	
				xi*LN (xi)	**xi*LN (xi)**	**xi*LN (xi)**	**Emix (kJ/kmol)**	**Emix (kJ/kmol)**	**Emix (kJ/kmol)**	**Ed (kJ/kmol)**	**Ed (kW)**
Molar Fraction	**1.00**	**1.00**	**1.00**	-1.11	-0.48	-0.77	216089.96	129.38	723.75	215495.60	89.71
H_2	0.42	0.00	0.00	-0.36							
O_2	0.00	0.19	0.13		-0.31	-0.26					
N_2	0.09	0.81	0.77	-0.22	-0.17	-0.20					
Cl_2	0.00	0.00	0.00								
CO	0.43	0.00	0.00	-0.36							
CO_2	0.06	0.00	0.06	-0.17		-0.16					
H_2O	0.00	0.00	0.05			-0.15					
CH_4	0.00	0.00	0.00								
H_2S	0.00	0.00	0.00	0.00		0.00					
HCl	0.00	0.00	0.00	0.00		0.00					

Rankine Power Cycle

The exergy analysis for the Rankine power cycle is carried over the system boundaries in the process units shown in **Figure A-24.** The exergy analysis is carried over in **Case 4b** and **Case 4c** as highlighted in the main body of the report.

Case 4b

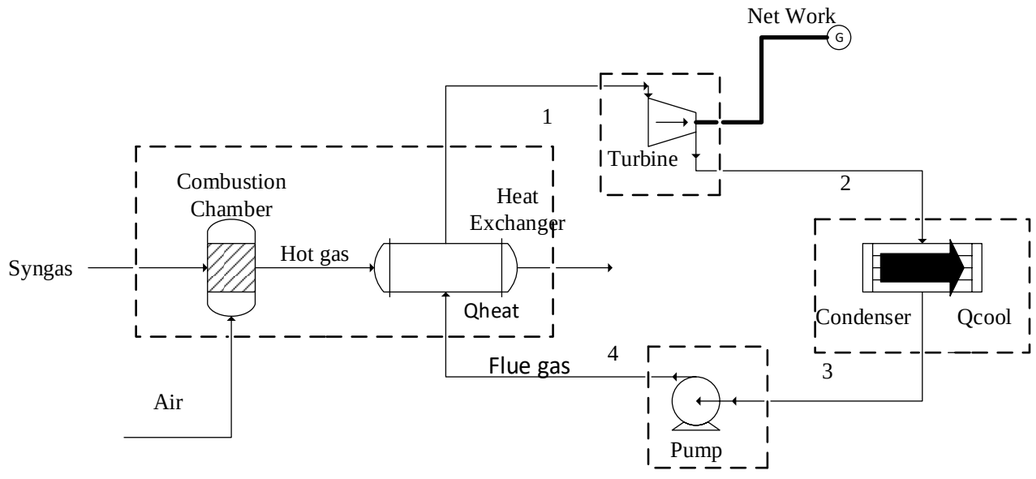


Figure A-24: Exergy analysis boundary for the steam turbine

Table A-33: Exergy analysis for the model of Case 4b

Turbine		**Blower**		**COMPR**		**Pump**	
Mass Flowrate (kg/hr)	75.00	Mass Flowrate (kg/hr)	27.49	Mass Flowrate (kg/hr)	145.52	Mass Flowrate (kg/hr)	75.00
Exergy inlet (kJ/kg)	1789.30	Exergy inlet (kJ/kg)	-25.79	Exergy inlet (kJ/kg)	-1.13	Exergy inlet (kJ/kg)	0.00
Exergy outlet (kJ/kg)	22.65	Exergy outlet (kJ/kg)	118.31	Exergy outlet (kJ/kg)	36.60	Exergy outlet (kJ/kg)	3.42
E_d (kW)	**5.51**	**E_d (kW)**	**0.13**	**E_d (kW)**	**0.21**	**E_d (kW)**	**0.01**

Table A-34: Boiler exergy analysis for the model of Case 4b

Boiler Heat Input (kJ/s)	86.02
Boiler Heat Input (kJ/hr)	**309661.21**

Input	
Exergy input (fuel) (kJ/kg)	118.31
Mass flowrate (fuel) (kg/hr)	27.49
Exergy input (air) (kJ/kg)	36.60
Mass flowrate (air) (kg/hr)	145.52
Exergy input (Water) (kJ/kg)	3.42
Mass flowrate (water) (kg/hr)	75.00
Exergy In (kJ/hr)	**8834.82**

Output	
Exergy output (flue gas) (kJ/kg)	105.43
Mass flowrate (flue gas) (kg/hr)	173.01
Exergy output (Water) (kJ/s)	1789.30
Mass flowrate (water) (kg/hr)	75.00
Exergy Out (kJ/hr)	**152438.36**

Exergy Destruction (kW)	
E_d (kW) (P.E)	46.13
E_d (kW) (C.E)	88.74
E_d (kW) (T.E)	**134.87**

Table A-35: Combustion chamber chemical exergy analysis for Case 4b

	SYNGAS	AIR2	FLUEGAS	SYNGAS	AIR2	FLUEGAS	SYNGAS	AIR2	FLUEGAS	Total E_d	
				xi*LN (xi)	xi*LN (xi)	xi*LN (xi)	Emix (kJ/kmol)	Emix (kJ/kmol)	Emix (kJ/kmol)	Ed (kJ/kmol)	Ed (kJ/hr)
Molar Fraction	**1.00**	**1.00**	**1.00**	-1.11	-0.48	-0.90	216089.96	129.38	2047.59	214171.75	88.74
H_2	0.42	0.00	0.00	-0.36							
O_2	0.00	0.19	0.05		-0.31	-0.15					
N_2	0.09	0.81	0.71	-0.22	-0.17	-0.24					
Cl_2	0.00	0.00	0.00								
CO	0.43	0.00	0.00	-0.36							
CO_2	0.06	0.00	0.13	-0.17		-0.26					
H_2O	0.00	0.00	0.11			-0.24					
CH_4	0.00	0.00	0.00								
H_2S	0.00	0.00	0.00	0.00		0.00					
HCl	0.00	0.00	0.00	0.00		0.00					

Case 4c

Table A-36: Exergy analysis for the model of Case 4c

Turbine		**COMPR**		**Pump**	
Mass Flowrate		Mass Flowrate		Mass Flowrate	
(kg/hr)	85.00	(kg/hr)	165.84	(kg/hr)	85.00
Exergy inlet		Exergy inlet		Exergy inlet	
(kJ/kg)	1789.30	(kJ/kg)	-1.13	(kJ/kg)	0.00
Exergy outlet		Exergy outlet		Exergy outlet	
(kJ/kg)	22.65	(kJ/kg)	36.60	(kJ/kg)	3.42
E_d (kW)	**6.23**	**E_d (kW)**	**0.24**	**E_d (kW)**	**0.01**

Table A-37: Boiler exergy analysis for the model of Case 4c

Boiler Heat Input (kJ/s)	97.49
Boiler Heat Input (kJ/hr)	**350949.37**
Input	
Exergy input (fuel) (kJ/kg)	1108.34
Mass flowrate (fuel) (kg/hr)	30.86
Exergy input (air) (kJ/kg)	36.60
Mass flowrate (air) (kg/hr)	165.84
Exergy input (Water) (kJ/s)	3.42
Mass flowrate (water) (kg/hr)	85.00
Exergy In (kJ/hr)	**40565.97**
Output	
Exergy output (flue gas) (kJ/kg)	115.80
Mass flowrate (flue gas) (kg/hr)	196.70
Exergy output (Water) (kJ/s)	1789.30
Mass flowrate (water) (kg/hr)	85.00
Exergy Out (kJ/hr)	**174869.43**
Exergy Destruction (kW)	
E_d (kW) (P.E)	60.18
Ed (kW) (C.E)	89.06
Ed (kW) (T.E)	**149.24**

Table A-38: Combustion chamber chemical exergy analysis for Case 4c

	SYNGAS	AIR2	FLUEGAS	SYNGAS	AIR2	FLUEGAS	SYNGAS	AIR2	FLUEGAS	Total E_d	
							Emix	Emix	Emix	Ed	
				xi*LN (xi)	xi*LN (xi)	xi*LN (xi)	(kJ/kmol)	(kJ/kmol)	(kJ/kmol)	(kJ/kmol)	Ed (kJ/hr)
Molar Fraction	**1.00**	**1.00**	**1.00**	-1.09	-0.48	-0.92	193330.96	129.38	1821.32	191639.02	89.06
H_2	0.38	0.00	0.00	-0.37							
O_2	0.00	0.19	0.06		-0.31	-0.18					
N_2	0.08	0.81	0.70	-0.20	-0.17	-0.25					
Cl_2	0.00	0.00	0.00								
CO	0.38	0.00	0.00	-0.37							
CO_2	0.05	0.00	0.11	-0.16		-0.24					
H_2O	0.11	0.00	0.12			-0.26					
CH_4	0.00	0.00	0.00								
H_2S	0.00	0.00	0.00	0.00		0.00					
HCl	0.00	0.00	0.00	0.00		0.00					

Combined Power Cycle

The exergy balance for the combined power cycle is carried over the system boundaries in the process units shown in **Figure A-25.** The exergy analysis is carried over in **Case 5b** and **Case 5d** as highlighted in the main body of the report.

Case 5b

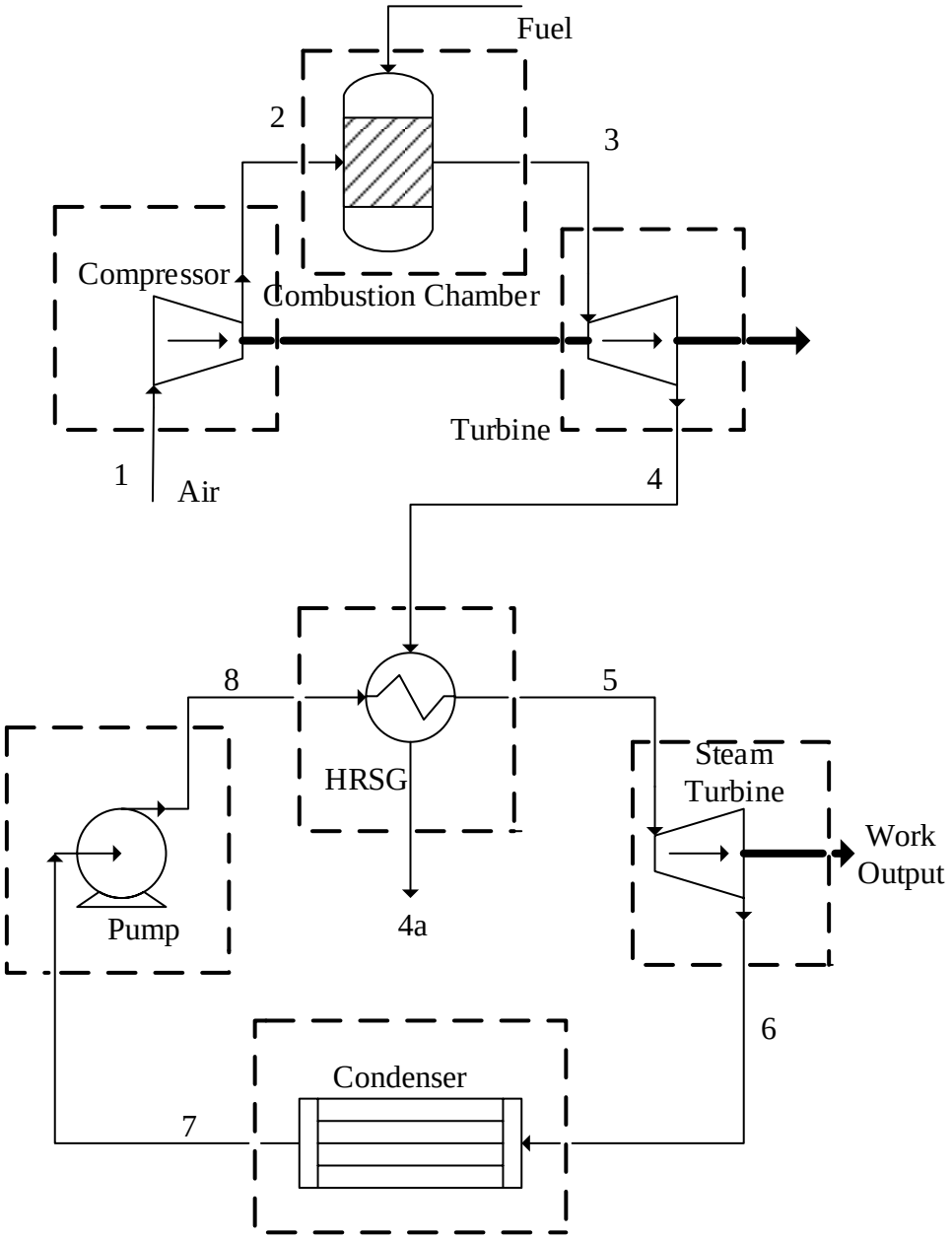


Figure A-25: Exergy analysis boundary for the combined power cycle

Table A-39: Exergy analysis for Case 5b

Combustion Chamber		**Turbine**		**Compressors**		**Blower**		**Blower1**		**Steam turbine**	
Mass Flowrate (kg/hr)	382.50	Mass Flowrate (kg/hr)	388.96	Mass Flowrate (kg/hr)	355.00	Mass Flowrate (kg/hr)	27.50	Mass Flowrate (kg/hr)	27.50	Mass Flowrate (kg/hr)	68.00
Exergy inlet (kJ/kg)	198.40	Exergy inlet (kJ/kg)	767.85	Exergy inlet (kJ/kg)	-1.13	Exergy inlet (kJ/kg)	-25.58	Exergy inlet (kJ/kg)	121.54	Exergy inlet (kJ/kg)	1059.57
Exergy outlet (kJ/kg)	773.67	Exergy outlet (kJ/kg)	343.24	Exergy outlet (kJ/kg)	186.26	Exergy outlet (kJ/kg)	121.54	Exergy outlet (kJ/kg)	385.13	Exergy outlet (kJ/kg)	167.71
E_d (kW)	**61.12**	**E_d (kW)**	**1.45**	**E_d (kW)**	**1.88**	**E_d (kW)**	**0.14**	**E_d (kW)**	**0.18**	**E_d (kW)**	**2.23**

Table A-40: Exergy Analysis for the pump of Case 5b

Pump	
Mass Flowrate (kg/hr)	68.00
Exergy inlet (kJ/kg)	0.00
Exergy outlet (kJ/kg)	0.92
Ed (kW)	**0.00**

Table A-41: Exergy Analysis for the HRSG of Case 5b

Input	
Exergy input (bfw) (kJ/kg)	0.92
Mass flowrate (bfw) (kg/hr)	68
Exergy output (gasexp) (kJ/kg)	331.15
Mass flowrate (gasexp) (kg/hr)	382.50
Exergy In (kJ/hr)	**126727.22**

Output	
Exergy input (steam) (kJ/kg)	1059.57
Mass flowrate (steam) (kg/hr)	68
Exergy output (gasflue) (kJ/s)	15.17
Mass flowrate (gasflue) (kg/hr)	382.50
Exergy Out (kJ/hr)	**77855.31**

Exergy Destruction (kW)	
E_d (kW)	**13.58**

Table A-42: Combustion chamber chemical exergy analysis for Case 5b

	SYNGAS	AIR2	FLUEGAS	SYNGAS	AIR2	FLUEGAS	SYNGAS	AIR2	FLUEGAS	Total E_d	
							Emix	Emix	Emix	Ed	
				xi*LN(xi)	xi*LN(xi)	xi*LN(xi)	(kJ/kmol)	(kJ/kmol)	(kJ/kmol)	(kJ/kmol)	Ed (kJ/hr)
Molar											
Fraction	**1.00**	**1.00**	**1.00**	-1.12	-0.51	-0.81	215852.99	125.00	699.08	215278.91	89.76
H_2O	0.00	0.00	0.05	-0.01		-0.15					
H_2	0.42	0.00	0.00	-0.36							
CO	0.43	0.00	0.00	-0.36							
CO_2	0.06	0.00	0.06	-0.17		-0.16					
AR	0.00	0.00	0.00								
CH_4	0.00	0.00	0.00								
N_2	0.09	0.79	0.75	-0.22	-0.19	-0.22					
HCl	0.00	0.00	0.00								
H_2S	0.00	0.00	0.00								
O_2	0.00	0.21	0.15		-0.33	-0.28					

Table A-43: Exergy Analysis for the combustion chamber of Case 5b

Combustion Chamber	
Mass Flowrate	
(kg/hr)	382.50
Exergy inlet	
(kJ/kg)	198.40
Exergy outlet	
(kJ/kg)	773.67
E_d (P.E) (kW)	61.12
E_d (C.E) (kW)	89.76
E_d (T.E) (kW)	**150.88**

Case 5d

Table A-44: Exergy Analysis for Case 5d

Combustion Chamber		**Turbine**		**Compressors**		**Turbine**		**Pump**	
Mass Flowrate (kg/hr)	385.86	Mass Flowrate (kg/hr)	385.86	Mass Flowrate (kg/hr)	355.00	Mass Flowrate (kg/hr)	68.00	Mass Flowrate (kg/hr)	68.00
Exergy inlet (kJ/kg)	254.18	Exergy inlet (kJ/kg)	859.52	Exergy inlet (kJ/kg)	-1.13	Exergy inlet (kJ/kg)	1059.57	Exergy inlet (kJ/kg)	0.00
Exergy outlet (kJ/kg)	859.52	Exergy outlet (kJ/kg)	387.09	Exergy outlet (kJ/kg)	191.57	Exergy outlet (kJ/kg)	165.31	Exergy outlet (kJ/kg)	0.92
E_d (P.E)(kJ/hr)	64.88	**E_d (kJ/hr)**	**2.96**	**E_d (kJ/hr)**	**1.36**	**Ed (kJ/hr)**	**2.27**	**Ed (kJ/hr)**	**0.00**
E_d (C.E)(kJ/hr)	89.73								
E_d (T.E)(kJ/hr)	**154.61**								

Table A-45: Exergy Analysis for the HRSG of Case 5d

Input	
Exergy input (hot) (kJ/kg)	344.49
Mass flowrate (hot) (kg/hr)	435.22
Exergy In (kJ/hr)	**126457.30**

Output	
Exergy input (cold) (kJ/kg)	0.47
Mass flowrate (Cold) (kg/hr)	75.00
Exergy output (cold) (kJ/s)	801.98
Mass flowrate (cold) (kg/hr)	75.00
Exergy Out (kJ/hr)	**60113.44**

Exergy Destruction (kW)	
E_d (kW)	**18.43**

Table A-46: Combustion chamber chemical exergy analysis for Case 5d

	SYNGAS	AIR2	FLUEGAS	SYNGAS	AIR2	FLUEGAS	SYNGAS	AIR2	FLUEGAS	Total E_d	
							Emix	Emix	Emix	Ed	
				xi*LN(xi)	xi*LN(xi)	xi*LN(xi)	(kJ/kmol)	(kJ/kmol)	(kJ/kmol)	(kJ/kmol)	Ed (kJ/hr)
Molar											
Fraction	**1.00**	**1.00**	**1.00**	-1.33	-0.51	-0.84	192672.13	125.00	721.75	192075.38	89.73
H_2O	0.11	0.00	0.06	-0.24		-0.17					
H_2	0.38	0.00	0.00	-0.37							
CO	0.38	0.00	0.00	-0.37							
CO_2	0.05	0.00	0.06	-0.16		-0.16					
AR	0.00	0.00	0.00								
CH_4	0.00	0.00	0.00								
N_2	0.08	0.79	0.74	-0.20	-0.19	-0.22					
HCl	0.00	0.00	0.00								
H_2S	0.00	0.00	0.00								
O_2	0.00	0.21	0.14		-0.33	-0.28					

Appendix A.5 Alternative Power cycles

The flowsheet for the model of the co-generation cycle can be seen in **Figure A-26** and the mass balance for this power cycle is found in **Table A-47**.

Appendix A.5.1 co-generation cycle

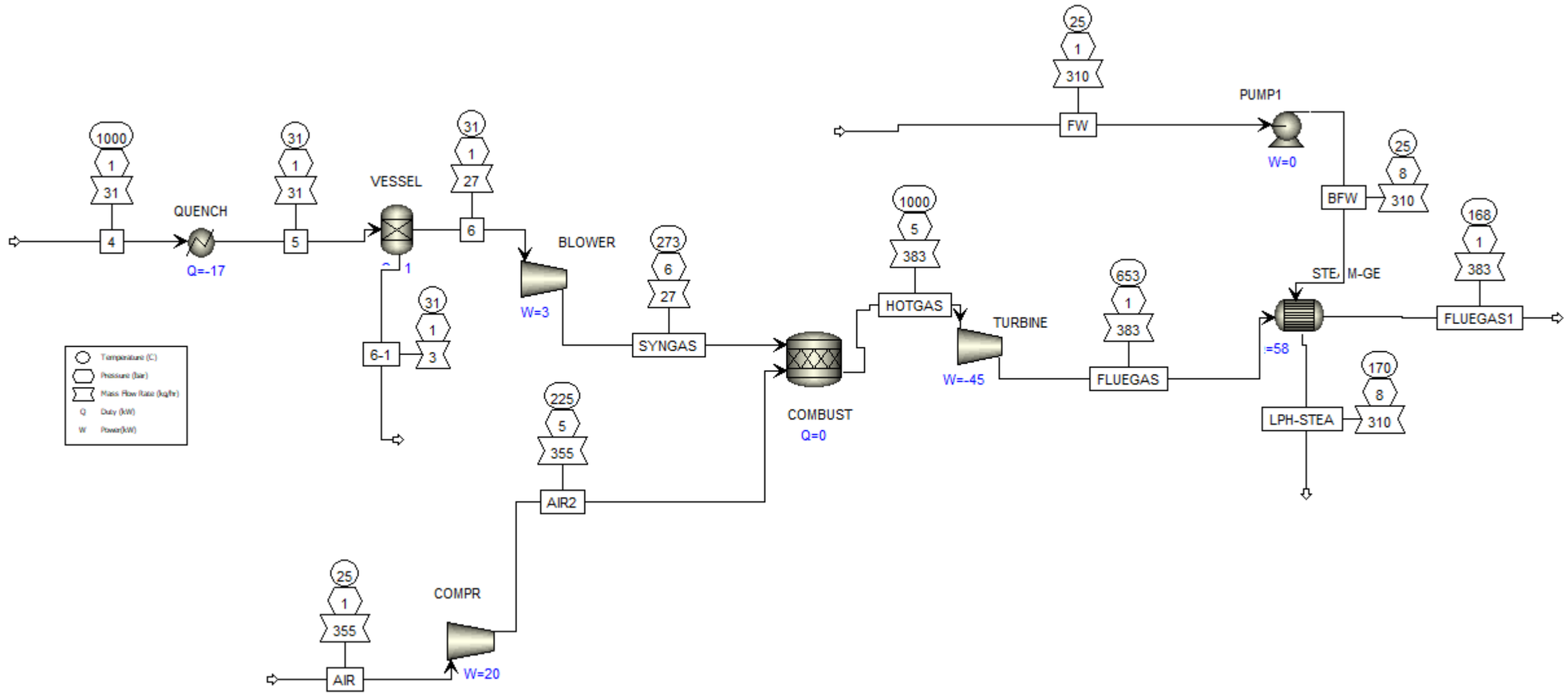


Figure A-26: Aspen Plus Model Flow Diagram for the co-generation cycle

Table A-47: Mass balance for the co-generation power cycle

	Units	4	5	6	6-1	AIR	AIR2	BFW	FLUEGAS	FLUEGAS1	FW	HOTGAS	LPH-STEA	SYNGAS
Temperature	C	1000.00	31.37	31.37	31.37	25.00	224.84	25.07	653.25	168.25	25.00	1000.00	170.00	272.86
Pressure	bar	0.85	0.84	0.84	0.84	1.00	5.00	8.00	1.00	1.00	1.00	5.00	8.00	5.50
Molar Vapor Fraction		1.00	0.93	1.00	0.00	1.00	1.00	0.00	1.00	1.00	0.00	1.00	0.00	1.00
Molar Liquid Fraction		0.00	0.07	0.00	1.00	0.00	0.00	1.00	0.00	0.00	1.00	0.00	1.00	0.00
Molar Solid Fraction		0.00	0.00	0.00	0.00	0.00	0.00	0.00	0.00	0.00	0.00	0.00	0.00	0.00
Mass Vapor Fraction		1.00	0.93	1.00	0.00	1.00	1.00	0.00	1.00	1.00	0.00	1.00	0.00	1.00
Mass Liquid Fraction		0.00	0.07	0.00	1.00	0.00	0.00	1.00	0.00	0.00	1.00	0.00	1.00	0.00
Mass Solid Fraction		0.00	0.00	0.00	0.00	0.00	0.00	0.00	0.00	0.00	0.00	0.00	0.00	0.00
Molar Enthalpy	kJ/kmol	-57462.85	-92121.75	-70530.49	-287046.95	-8.02	5876.80	-287546.32	-14038.59	-29706.02	-287563.59	-1833.57	-275495.16	-63254.77
Mass Enthalpy	kJ/kg	-3200.34	-5130.64	-3929.74	-15933.53	-0.28	204.30	-15961.25	-485.26	-1026.82	-15962.21	-63.38	-15292.31	-3524.36
Molar Entropy	kJ/mol-K	0.09	0.03	0.05	-0.17	0.00	0.01	-0.17	0.04	0.02	-0.17	0.04	-0.13	0.05
Mass Entropy	kJ/kg-K	4.92	1.84	2.77	-9.21	0.14	0.20	-9.30	1.39	0.57	-9.30	1.31	-7.48	2.88
Molar Density	kmol/cum	0.01	0.04	0.03	46.91	0.04	0.12	47.11	0.01	0.03	47.11	0.05	41.12	0.12
Mass Density	kg/cum	0.14	0.64	0.60	845.07	1.16	3.47	848.69	0.38	0.79	848.65	1.37	740.84	2.17
Enthalpy Flow	kW	-27.44	-43.98	-30.01	-14.93	-0.03	20.17	-1374.44	-51.61	-109.22	-1374.52	-6.74	-1316.84	-26.91
Average MW		17.96	17.96	17.95	18.02	28.77	28.77	18.02	28.93	28.93	18.02	28.93	18.02	17.95
Mass Flows	**kg/hr**	**30.86**	**30.86**	**27.49**	**3.37**	**355.42**	**355.42**	**310.00**	**382.91**	**382.91**	**310.00**	**382.91**	**310.00**	**27.49**
H_2	kg/hr	1.31	1.31	1.31	0.00	0.00	0.00	0.00	0.00	0.00	0.00	0.00	0.00	1.31
O_2	kg/hr	0.00	0.00	0.00	0.00	74.64	74.64	0.00	53.79	53.79	0.00	53.79	0.00	0.00
N_2	kg/hr	3.83	3.83	3.83	0.00	280.78	280.78	0.00	284.61	284.61	0.00	284.61	0.00	3.83
Cl_2	kg/hr	0.00	0.00	0.00	0.00	0.00	0.00	0.00	0.00	0.00	0.00	0.00	0.00	0.00
NO_2	kg/hr	0.00	0.00	0.00	0.00	0.00	0.00	0.00	0.00	0.00	0.00	0.00	0.00	0.00
CO	kg/hr	18.31	18.31	18.31	0.00	0.00	0.00	0.00	0.00	0.00	0.00	0.00	0.00	18.31
CO_2	kg/hr	4.03	4.03	4.03	0.00	0.00	0.00	0.00	32.80	32.80	0.00	32.80	0.00	4.03
H_2O	kg/hr	3.37	3.37	0.00	3.37	0.00	0.00	310.00	11.70	11.70	310.00	11.70	310.00	0.00
CH_4	kg/hr	0.00	0.00	0.00	0.00	0.00	0.00	0.00	0.00	0.00	0.00	0.00	0.00	0.00
C_2H_4	kg/hr	0.00	0.00	0.00	0.00	0.00	0.00	0.00	0.00	0.00	0.00	0.00	0.00	0.00
C_2H_6	kg/hr	0.00	0.00	0.00	0.00	0.00	0.00	0.00	0.00	0.00	0.00	0.00	0.00	0.00
N_2O	kg/hr	0.00	0.00	0.00	0.00	0.00	0.00	0.00	0.00	0.00	0.00	0.00	0.00	0.00
H_2S	kg/hr	0.01	0.01	0.01	0.00	0.00	0.00	0.00	0.01	0.01	0.00	0.01	0.00	0.01